Thiosemicarbazone complexes of transition metals: Synthesis, characterization and study of reactivity

Thesis submitted in partial fulfillment of the requirements for the degree of

Doctor of Philosophy

by

Saswati

Under the guidance of

Dr. Rupam Dinda

Department of Chemistry
National Institute of Technology, Rourkela
Rourkela-769008, Odisha, India

CERTIFICATE

This is to certify that the thesis entitled **"Thiosemicarbazone complexes of transition metals: Synthesis, characterization and study of reactivity"** submitted by **Saswati** of the Department of Chemistry, National Institute of Technology, Rourkela, India, for the degree of **Doctor of Philosophy** is a record of bona fide research work carried out by her under my guidance and supervision. I am satisfied that the thesis has reached the standard fulfilling the requirements of the regulations relating to the nature of the degree. To the best of my knowledge, the matter embodied in the thesis has not been submitted to any other University/Institute for the award of any degree or diploma.

Place: Rourkela
Date:

Supervisor,
Dr. Rupam Dinda,
Associate Professor,
Department of Chemistry,
National Institute of Technology,
Rourkela-769008, Odisha,
India

ACKNOWLEDGEMENTS

Achievement is a word which always sounds great. It is truly a joy to see the accomplishment of this thesis. I take this opportunity to offer my gratitude to every person who has been a part of this project.

I would like to express my sincere gratitude to my supervisor Dr. Rupam Dinda, Associate Professor, Department of Chemistry, National Institute of Technology, Rourkela for providing me with his well-needed guidance, provocative discussions, helpful advice and constructive criticisms. I would like to thank him for patiently scrutinizing the preparation of this thesis and making my work a successful and meaningful endeavor. I am privileged to work under his guidance.

I am thankful to the Prof. S. K. Sarangi, Director, National Institute of Technology, Rourkela for providing the essential infrastructural facilities. I would also like to extend my gratitude to Prof. N. Panda, HOD, Department of Chemistry for granting me the various laboratory and instrumental facilities during my Ph.D. work.

I sincerely thank my DSC members, Prof. R. K. Singh, Department of Chemical Engineering, Prof. S. Chatterjee and Prof. Sabita Patel, Department of Chemistry, NIT Rourkela for their valuable comments and evaluation of progress reports and seminars during the Ph. D. program. I am thankful to all the faculty members and staff of the Department of Chemistry for their constant help. Guidance received from Prof. S. Chatterjee and Prof. D. Sarkar deserves special mention.

I am thankful to Prof. S. K. Chattopadhyay, Department of Chemistry, IIEST, Shibpur, for his generous help in electrochemical studies and Prof. M. R. Maurya, Department of Chemistry, IIT Roorkee for the catalytic study and his valuable suggestions during manuscript preparation. I would like to acknowledge Prof. Ashis Biswas, School of Basic Sciences, IIT, Bhubaneswar, Prof. Surajit Das and Prof. S. K. Bhutia, Department of Life Science, NIT Rourkela and Prof. Bimba N. Joshi, Agharkar Research Institute for the biological studies and Prof. B. Mondal, IIT Guwahati for EPR analysis.

I am grateful to Prof. Ekkehard Sinn, Department of Chemistry, Western Michigan University, Kalamazoo, Aurélien Crochet, Fribourg Center for Nanomaterials, Department of Chemistry, University of Fribourg, Switzerland, Prof. Helen Stoeckli-Evans, Institute of Physics, University of Neuchâtel, Switzerland and Prof. M. Nethaji, Department of IPC, IISc. Bangalore for their kind cooperation in determining the X-ray structures of synthesized complexes.

Financial assistance received from the Department of Science and Technology, New Delhi [Grant No. SR/FT/CS-016/2008] & [Grant No. SR/FT/CS-010/2009], the Council of Scientific and Industrial Research, New Delhi [Grant No. 01(2735)/13/EMR-II] is gratefully acknowledged. I am thankful to the Council of Scientific and Industrial Research, New Delhi [Grant No. 9/983(0012)2k13-EMR-I] for the award of a senior research fellowship.

Active cooperation of the members of our research group, Sagarika Pasayat, Subhashree P. Dash, Satabdi Roy and Sudarshana Majumder is greatly acknowledged. I am genuinely appreciative to my friends Subhraseema Das and Prakash Malik for their suggestions and moral support during my work.

Last but not the least; it would not have been possible to complete this project without the love and support of my parents whose unflinching faith in my abilities helped me to overcome many obstacles and march ahead in spite of failures. I would like to dedicate this project to my family.

Date: Saswati

ABSTRACT

Thiosemicarbazone complexes of transition metals: Synthesis, characterization and study of reactivity

Saswati

Department of Chemistry, National Institute of Technology, Rourkela-769008, Odisha, India

---

Chapter 1: In this chapter the scope of the present investigation is delineated briefly along with the aim of the work.

Chapter 2: The syntheses and characterization of some new mixed-ligand nickel(II) complexes {[Ni(L^1)(PPh_3)] (**1**); [Ni(L^1)(Py)] (**2**); [Ni(L^2)(PPh_3)]·DMSO (**3**); [Ni(L^2)(Imz)] (**4**), [Ni(L^3)(4–pic)] (**5**) and [{Ni(L^3)}$_2$(μ–4,4′–byp)]·2DMSO (**6**)} of the selected three thiosemicarbazones {4–(*p*–X–phenyl)thiosemicarbazone of salicylaldehyde} ($H_2L^{1–3}$) are described in the present chapter, differing in the inductive effect of the substituent X (X = F, Br and OCH_3), in order to observe their influence, if any, on the redox potentials and biological activity of the complexes. All the synthesized ligands and the metal complexes are successfully characterized by elemental analysis, IR, UV–Vis, NMR spectroscopy and cyclic voltammetry. Molecular structures of four mononuclear (**1**–**3** and **5**) and one dinuclear (**6**) Ni(II) complexes have been determined by X–ray crystallography. The complexes have been screened for their antibacterial activity against *Escherichia coli and Bacillus*. Minimum inhibitory concentration of these complexes indicates compound **4** as the potential lead molecule for drug designing.

Chapter 3: 4–(*p*–X–phenyl)thiosemicarbazone of napthaldehyde {where, X = Cl (HL^1) and X = Br (HL^2)}, thiosemicarbazone of quinoline–2–carbaldehyde (HL^3) and 4–(*p*–fluorophenyl)thiosemicarbazone of salicylaldehyde (H_2L^4) and their copper(I), {[Cu(HL^1)(PPh_3)$_2$Br]·CH_3CN (**1**) and [Cu(HL^2)(PPh_3)$_2$Cl]·DMSO (**2**)} and copper(II), {[($Cu_2L^3{}_2Cl$)$_2$(μ–Cl)$_2$]·$2H_2O$ (**3**) and [Cu(L^4)(Py)] (**4**)} complexes are reported herein. The synthesized ligands and their copper complexes were successfully characterized by elemental analysis, cyclic voltammetry, NMR, ESI–MS, IR and UV–Vis spectroscopy. Molecular

structures of all the Cu(I) and Cu(II) complexes have been determined by X–ray crystallography. All the complexes (**1**–**4**) were tested for their ability to exhibit DNA-binding and -cleavage activity. The complexes effectively interact with CT–DNA possibly by groove binding mode, with binding constants ranging from $10^4 - 10^5$ M^{-1}. Among the complexes, **3** show highest chemical (60%) as well as photo-induced (80%) DNA cleavage activity against pUC19 DNA. Finally, the *in vitro* antiproliferative activity of all the complexes was assayed against the HeLa cell line. Some of the complexes have proved to be as active as the clinical referred drugs, and the greater potency of **3** may be correlated with its aqueous solubility and the presence of quinonoidal group in the thiosemicarbazone ligand coordinated to the metal.

Chapter 4: Oxygen atom transfer (OAT) reactivity of dioxidomolybdenum(VI) complexes $[Mo^{(VI)}O_2L^{1-6}]$ (**1**–**6**) {4–(*p*–bromophenyl)thiosemicarbazone of salicylaldehyde (H_2L^1), 4–(*p*–X–phenyl)thiosemicarbazone of *o*–vanillin {where, X = F (H_2L^2) and X = Cl (H_2L^3) and X = OMe (H_2L^4)}, 4–(*p*–bromophenyl)thiosemicarbazone of 5–bromosalicylaldehyde (H_2L^5), and 4–(*p*–chlorophenyl)thiosemicarbazone of *o*–hydroxynaphthaldehyde (H_2L^6)} with PPh_3 have been investigated. The OAT reactions proceed through the formation of $OPPh_3$, which have been characterized by ^{31}P NMR. Dioxidomolybdenum(VI) complexes $[Mo^{(VI)}O_2L^{1/5/6}(DMSO)]$ (**1a, 5a** & **6a**), $[Mo^{(VI)}O_2L^{2/4}(H_2O)]$ (**2a** & **4a**), and $[Mo^{(VI)}O_2L^3(DMSO)]_4{\cdot}2DMSO$ (**3a**) and monooxidomolybdenum(IV) complexes $[Mo^{(IV)}OL^{1-6}(N–N)]$ (**7**–**12**) {where, N–N = 2,2'–bipyridyl or 1,10–phenanthroline} are reported as the product of substrate binding and oxygen atom transfer reactivity of dioxidomolybdenum(VI) complexes $[Mo^{(VI)}O_2L^{1-6}]$ (**1**–**6**) respectively. All the complexes have been spectroscopically characterized. Molecular structures of some of the Mo(VI) (**1a**–**4a**) and Mo(IV) complexes (**7** and **9**–**11**) have been determined by single crystal X–ray crystallography. The catalytic activity of $Mo^{(VI)}$ complexes (**1a**–**6a**) have also been studied.

Chapter 5: The synthesis and characterization of an oxidovanadium(IV) $[V^{IV}O(L)(acac)]$ (**1**) and two dioxidovanadium(V) $[V^{V}O_2(L')]$ (**2**) and $[V^{V}O_2(L)]$ (**2a**) complexes of {(4–(*p*–fluorophenyl)thiosemicarbazone) of pyridine–2–aldehyde} (HL) is described in the present study. The oxidovanadium(IV) species $[V^{IV}O(L)(acac)]$ (**1**) was synthesized in usual way by the reaction of metal precursor $VO(acac)_2$ with thiosemicarbazone ligand (HL) in refluxing ethanol. The recrystallization of $[V^{IV}O(L)(acac)]$ (**1**) in DMF, CH_3CN or EtOH gave the same

product *i.e.* dioxidovanadium(V) complex $[V^{V}O_2(L)]$ (**2a**), whereas $[V^{V}O_2(L')]$ (**2**) was synthesized during recrystallization of $[V^{IV}O(L)(acac)]$ (**1**) in DMSO where the original ligand (HL) is transformed to a rearranged new ligand (HL'). The ligand in complex **1** is found to undergo methylation at the carbon centre attached to imine nitrogen in presence of DMSO and transformed to the corresponding dioxidovanadium(V) species through *in situ* reaction. The synthesized ligand and the metal complexes were characterized by elemental analysis, IR, UV–Vis, NMR and EPR spectroscopy. Molecular structures of complex **1** $[V^{IV}O(L)(acac)]$ and complex **2** $[V^{V}O_2(L')]$ have been determined by single crystal X–ray crystallography. Complexes **1** & **2** show *in vitro* insulin mimetic activity against insulin responsive L6 myoblast cells, with complex **1** being more potent, is comparable to insulin at 100 μM concentration, while complex **2** has considerable insulin mimetic activity. In addition, the *in vitro* antiproliferative activity of the complexes **1** & **2** against the MCF–7 and Vero cell lines were also assayed.

Chapter 6: 4–(*p*–methoxyphenyl)thiosemicarbazone of *o*–hydroxynapthaldehyde (H_2L^1), 4–(*p*–methoxyphenyl)thiosemicarbazone of benzoyl pyridine (HL^2) and 4–(*p*–chlorophenyl)thiosemicarbazone of *o*–vanillin (H_2L^3) and their dimeric Zn(II) complexes $[\{ZnL^1(DMSO)\}_2]\cdot 3DMSO$ (**1**), $[\{ZnL^2Cl\}_2]$ (**2**), and a novel tetrameric Zn(II) complex $[(Zn_2L^3)_2(\mu\text{–}OAc)_2(\mu_3\text{–}O)_2]$ (**3**) are reported. The synthesized ligands and their zinc complexes were characterized by elemental analysis, NMR, IR and UV–Vis spectroscopy. Molecular structures of all the complexes (**1**–**3**) have been determined by single crystal X–ray crystallography.

Keywords: Thiosemicarbazone / X-ray crystal structure / Pharmacological (Cytotoxic, Antibacterial, Insulin mimetic, DNA binding and cleaving) activity / Oxygen atom transfer (OAT) reactivity / Catalytic oxidation.

Table of Contents

Preface

The present dissertation describes the design, synthesis, full characterization and the exploration of chemical, electrochemical properties and the study of catalytic and biological activities of a series of variable valence transition metal (Ni, Cu, Mo, V & Zn) complexes of some selected multidentate ONS, NNS and monodentate S donor thiosemicabazone (TSC) ligands. Structures of twenty two important transition metal (Ni, Cu, Mo, V & Zn) complexes are determined by single crystal X-ray analysis. Structure-reactivity relations are discussed and implications of structure determination on the design of new complexes using the structurally characterized compounds as precursors are elaborated. All the complexes described in this dissertation are characterized by various physicochemical techniques such as elemental analysis, and by various spectroscopic techniques (UV-Vis, IR, NMR, EPR and ESI-MS). Electrochemical characteristics of the complexes were studied by cyclic voltammetry and, as pointed out before, single crystal X-ray crystallography were used to find out crystal and molecular structure of the compounds. Biological activities particularly antimicrobial, antiproliferative, insulin mimetic, DNA binding and cleavage activity and catalytic activities of some of the above complexes particularly oxidation of styrene and oxidation of cyclohexene were also studied. The subject matter of this dissertation is divided into six chapters containing the chemistry of transition metals (Ni, Cu, Mo, V & Zn) ligated to TSC ligands and a *brief resume* of the work embodied in this dissertation and *concluding remarks*.

Chapter 1 is a general introduction to the entire work described in the present dissertation and spells out the objectives of the thesis. The objectives of the works are placed at the end of the general introduction. The entire subject matter of this dissertation is organized as follows:

Chapter 2 deals with the syntheses and characterization of some mixed-ligand nickel(II) complexes {[Ni(L^1)(PPh_3)] (**1**); [Ni(L^1)(Py)] (**2**); [Ni(L^2)(PPh_3)]·DMSO (**3**); [Ni(L^2)(Imz)] (**4**), [Ni(L^3)(4–pic)] (**5**) and [{Ni(L^3)}$_2$(μ–4,4′–byp)]·2DMSO (**6**)} of the selected three thiosemicarbazones {4–(*p*–X–phenyl)thiosemicarbazone of salicylaldehyde} ($H_2L^{1–3}$), differing in the inductive effect of the substituent X (X = F, Br and OCH_3), in order to observe their influence, if any, on the redox potentials and biological activity of the complexes. All the synthesized ligands and the metal complexes were successfully characterized by elemental

analysis, IR, UV–Vis, NMR spectroscopy and cyclic voltammetry. Molecular structures of four mononuclear (**1**–**3** and **5**) and one dinuclear (**6**) Ni(II) complexes have been determined by X–ray crystallography. The complexes have been screened for their antibacterial activity against *Escherichia coli and Bacillus*. Minimum inhibitory concentration of these complexes indicates compound **4** as the potential lead molecule for drug designing.

In ***Chapter 3*** 4–(*p*–X–phenyl)thiosemicarbazone of napthaldehyde {where, X = Cl (HL^1) and X = Br (HL^2)}, thiosemicarbazone of quinoline–2–carbaldehyde (HL^3) and 4–(*p*–fluorophenyl)thiosemicarbazone of salicylaldehyde (H_2L^4) and their copper(I), {$[Cu(HL^1)(PPh_3)_2Br]\cdot CH_3CN$ (**1**) and $[Cu(HL^2)(PPh_3)_2Cl]\cdot DMSO$ (**2**)} and copper(II), {$[(Cu_2L^3{}_2Cl)_2(\mu\text{–}Cl)_2]\cdot 2H_2O$ (**3**) and $[Cu(L^4)(Py)]$ (**4**)} complexes are reported. The synthesized ligands and their copper complexes were successfully characterized by elemental analysis, cyclic voltammetry, NMR, ESI–MS, IR and UV–Vis spectroscopy. Molecular structures of all the Cu(I) and Cu(II) complexes have been determined by X–ray crystallography. All the complexes (**1**–**4**) were tested for their ability to exhibit DNA binding and cleavage activity. The complexes effectively interact with CT–DNA possibly by groove binding mode, with binding constants ranging from 10^4–10^5 M^{-1}. Among the complexes, **3** show highest chemical (60%) as well as photo-induced (80%) DNA cleavage activity against pUC19 DNA. Finally, the *in vitro* antiproliferative activity of all the complexes were assayed against the HeLa cell line. Some of the complexes proved to be as active as the clinically referred drugs, and the greater potency of **3** may be correlated with its aqueous solubility and the presence of quinonoidal group in the thiosemicarbazone ligand coordinated to the metal.

Chapter 4 describes oxygen atom transfer (OAT) reactivity of dioxidomolybdenum(VI) complexes $[Mo^{(VI)}O_2L^{1–6}]$ (**1**–**6**) {4–(*p*–bromophenyl)thiosemicarbazone of salicylaldehyde (H_2L^1), 4–(*p*–X–phenyl)thiosemicarbazone of *o*–vanillin {where, X = F (H_2L^2) and X = Cl (H_2L^3) and X = OMe (H_2L^4)}, 4–(*p*–bromophenyl)thiosemicarbazone of 5–bromosalicylaldehyde (H_2L^5), and 4–(*p*–chlorophenyl)thiosemicarbazone of *o*–hydroxynaphthaldehyde (H_2L^6)} with PPh_3. The OAT reactions proceed through the formation of $OPPh_3$, which have been characterized by ^{31}P NMR. Dioxidomolybdenum(VI) complexes $[Mo^{(VI)}O_2L^{1/5/6}(DMSO)]$ (**1a, 5a** & **6a**), $[Mo^{(VI)}O_2L^{2/4}(H_2O)]$ (**2a** & **4a**), and $[Mo^{(VI)}O_2L^3(DMSO)]_4\cdot 2DMSO$ (**3a**) and monooxidomolybdenum(IV) complexes

$[Mo^{(IV)}OL^{1-6}(N–N)]$ (**7**–**12**) {where, N–N = 2,2'–bipyridyl or 1,10–phenanthroline} are reported as the product of substrate binding and oxygen atom transfer reactivity of dioxidomolybdenum(VI) complexes $[Mo^{(VI)}O_2L^{1-6}]$ (**1**–**6**) respectively. All the complexes have been spectroscopically characterized. Molecular structures of some of the Mo(VI) (**1a**–**4a**) and Mo(IV) complexes (**7** and **9**–**11**) have been determined by single crystal X–ray crystallography. The catalytic activity of $Mo^{(VI)}$ complexes (**1a**–**6a**) have also been studied.

In ***chapter 5*** the synthesis and characterization of an oxidovanadium(IV) $[V^{IV}O(L)(acac)]$ (**1**) and two dioxidovanadium(V) $[V^{V}O_2(L')]$ (**2**) and $[V^{V}O_2(L)]$ (**2a**) complexes of {(4–(*p*–fluorophenyl)thiosemicarbazone) of pyridine–2–aldehyde} (HL) is described in the. The oxidovanadium(IV) species $[V^{IV}O(L)(acac)]$ (**1**) was synthesized in usual way by the reaction of metal precursor $VO(acac)_2$ with thiosemicarbazone ligand (HL) in refluxing ethanol. The recrystallization of $[V^{IV}O(L)(acac)]$ (**1**) in DMF, CH_3CN or EtOH gave the same product *i.e.* dioxidovanadium(V) complex $[V^{V}O_2(L)]$ (**2a**), whereas $[V^{V}O_2(L')]$ (**2**) was synthesized during recrystallization of $[V^{IV}O(L)(acac)]$ (**1**) in DMSO where the original ligand (HL) is transformed to a rearranged new ligand (HL'). The ligand in complex **1** is found to undergo methylation at the carbon centre attached to imine nitrogen in presence of DMSO and transformed to the corresponding dioxidovanadium(V) species through *in situ* reaction. The synthesized ligand and the metal complexes were characterized by elemental analysis, IR, UV–Vis, NMR and EPR spectroscopy. Molecular structures of complex **1** $[V^{IV}O(L)(acac)]$ and complex **2** $[V^{V}O_2(L')]$ have been determined by single crystal X–ray crystallography. Complexes **1** & **2** show *in vitro* insulin mimetic activity against insulin responsive L6 myoblast cells, with complex **1** being more potent, is comparable to insulin at 100 μM concentration, while complex **2** has considerable insulin mimetic activity. In addition, the *in vitro* antiproliferative activity of the complexes **1** & **2** against the MCF–7 and Vero cell lines were also assayed.

In ***chapter 6*** 4–(*p*–methoxyphenyl)thiosemicarbazone of *o*–hydroxynapthaldehyde (H_2L^1), 4–(*p*–methoxyphenyl)thiosemicarbazone of benzoyl pyridine (HL^2) and 4–(*p*–chlorophenyl)thiosemicarbazone of *o*–vanillin (H_2L^3) and their dimeric Zn(II) complexes $[\{ZnL^1(DMSO)\}_2]\cdot 3DMSO$ (**1**), $[\{ZnL^2Cl\}_2]$ (**2**), and a novel tetrameric Zn(II) complex $[(Zn_2L^3)_2(\mu\text{–}OAc)_2(\mu_3\text{–}O)_2]$ (**3**) are reported. The synthesized ligands and their zinc complexes were characterized by elemental analysis, NMR, IR and UV–Vis spectroscopy. Molecular

structures of all the complexes (**1**–**3**) have been determined by single crystal X–ray crystallography.

Chapter 1

Scope of the Present Investigation

Chapter 1

Scope of the present investigation

ABSTRACT

In this chapter the scope of the present investigation is delineated briefly along with the aim of the work.

1.1. REVIEWS ON TRANSITION METAL COMPLEXES OF THIOSEMICARBAZONE LIGANDS

The studies described in the present dissertation involve coordination complexes of various transition metals (Ni, Cu, Mo, V & Zn) with thiosemicarbazone (TSC) ligands, in relation to their biological and catalytic activities. TSCs are known to exhibit thione–thiol tautomerism (**Scheme 1.1**). It possesses several donor atoms, and generally behaves as an ONS/NNS tridentate chelate (**I**),[1] or as a monoanionic bidentate N,S–donor forming five–membered (**II**)[2] or a rather uncommon four membered chelate ring (**III**)[3] towards metal ions. It also behaves as a monodentate neutral S–donor ligand (**IV**).[4]

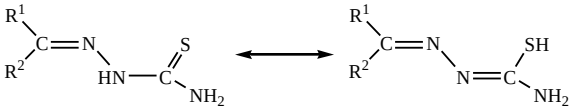

Thione-thiol tautomerism of TSC

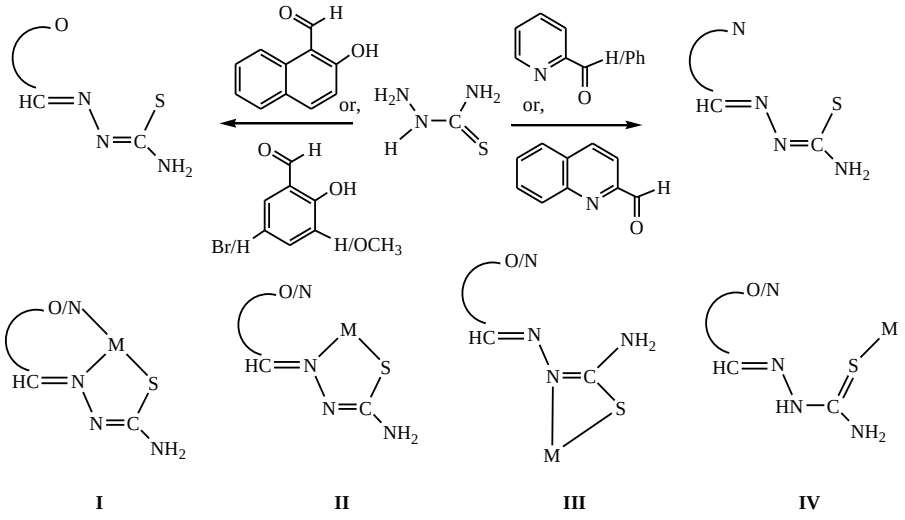

Scheme 1.1.

TSCs are a class of Schiff bases which are considered as one of the most important scaffolds and are embedded in many biologically active compounds. Brockman et al. first reported that 2–formylpyridine TSC possesses antileukemic activity in mice.[5] TSC complexes of transition metals have also demonstrated significant activity as antitumor, antiviral, antimicrobial, anti–amoebic and anti–inflammatory agents.[6] The coordination chemistry of various transition metal (Ni, Cu, Mo, V, & Zn) complexes with TSC ligands assumed special importance due to the following reasons:

1. Nickel(II) complexes with N and S donor ligands are highly interesting because several hydrogenases and carbon monoxide dehydrogenases[7] contain such nickel complexes as their active site.

2. Copper complexes have been extensively utilized in metal ion mediated DNA cleavage through the hydrogen ion abstraction by activated oxygen species.[8] Many Cu complexes of TSCs have demonstrated efficient antitumor potential.[9]

3. Several enzymes like DMSO reductase, xanthine oxidase and other oxotransferases in their prosthetic groups contain Mo(IV), Mo(V) or Mo(VI) ions coordinated by nitrogen, oxygen or sulfur donor atoms of a macromolecular ligand system.[10]

4. Vanadium is one of the trace bio–elements existing in the human body; its complexes have been found to exhibit antibacterial, antitumor, insulin–enhancing and antiparasitic effects.[11] Thio coordination to vanadium is additionally of interest with respect to the insulin–mimetic potential of vanadyl dithiocarbamates.[12]

5. Zn(II) ions, as a cofactor are part of over 300 enzymes like carbonic anhydrases, zinc proteinases, histone deacetylases, alkaline phosphatases, alcohol dehydrogenases, aminopeptidases, etc. Zn(II) complexes of thiosemicarbazone have been considered as agents with antitumor activity against MCF–7 and T24 human cancer cell lines.[13]

In this context, role of coordination environment around the central metal ion is most important. The chemistry of various transition metal complexes with thiosemicarbazone ligands has been of significant importance. Review on some of the recent reports of these metals with TSC environments which are drawing much interest as are highlighted below.

1.1.1. Nickel complexes of thiosemicarbazone: Nickel(II)–TSC complexes gained attention in the past few years. The reasons for this are the versatile coordination geometry preferences of this metal ion (square–planar, octahedral, tetrahedral), the formation of monomeric and dimeric complexes, and its ability to mimic platinum(II) to some extent, which is of great importance in chemotherapy.[14] Some salicylaldehyde TSC–based nickel(II) complexes exhibited similar cytotoxicity, under identical conditions on human lung cancer cells (A549) and liver cancer cells (HepG2) as compared to cis–diamminedichloridoplatinum(II).[15]

K. Natarajan et al. have reported several nickel thiosemicarbazone complexes with biological importance in the recent times.[16] In 2014 they have reported a series of novel nickel(II) thiosemicarbazone complexes and characterized them by various spectral, analytical techniques and X–ray crystallography. Their efficacy to interact with CT–DNA/BSA was explored. From the binding studies, it is inferred that one of the complexes [Ni(Msal–ptsc)(PPh_3)] (**Figure 1.1**) is more active than the other complexes. The complexes were bound with CT–DNA by intercalation mode. The complexes were also tested for their in vitro cytotoxicity against human lung adenocarcinoma (A549) cell line.

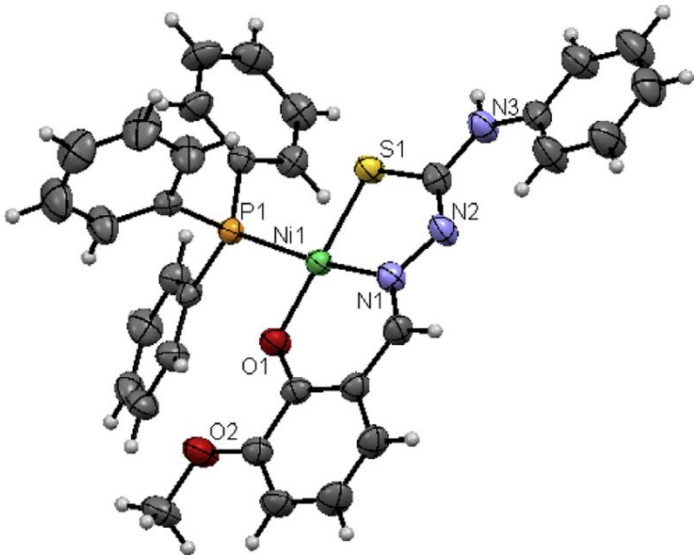

Figure 1.1.

In 2013 the same group reported the synthesis (**Scheme 1.2**), characterization and structure of some water soluble Ni(II) complexes of 4N–substituted thiosemicarbazones of 2–oxo–1,2–dihydroquinoline–3–carbaldehyde and their biological properties such as the binding properties with calf thymus DNA (CT–DNA), competitive binding studies with ethidium bromide (EB), antioxidant and cytotoxic activities.[14d]

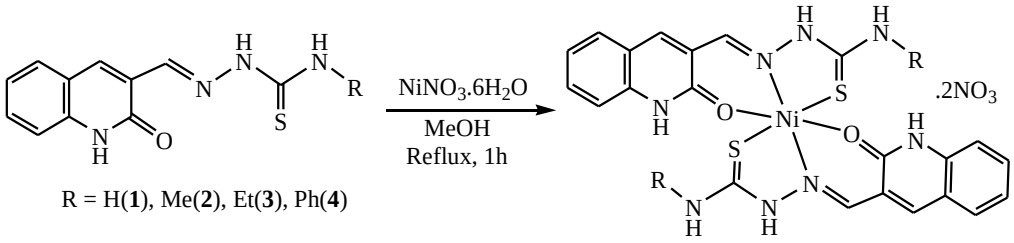

R = H(**1**), Me(**2**), Et(**3**), Ph(**4**)

The synthetic route of nickel(II) complexes

Scheme 1.2.

T. S. Lobana et al. have reported the study of the bonding patterns (**Scheme 1.3**), geometry, and fluorescence properties of some nickel(II) complexes with salicylaldehyde–based thiosemicarbazones [(2–OH–5–R^1–C_6H_3)C(R^2)=NNHC(=S)NHR^3, LH_2] by invoking the effect of substituents at the C–2 and N–1 atoms of the thio ligands and by using bipyridines/phenanthrolines as auxiliary ligands.[17]

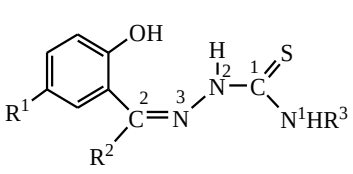

R^1 =	H,	H,	H,	Me,	NO_2,	NO_2,	H
R^2 =	H,	H,	H,	H,	H,	H,	Me
R^3 =	H,	Me,	Et,	Me,	Me,	Et,	Et
Abbrev.	L^1H_2,	L^2H_2,	L^3H_2,	L^4H_2,	L^5H_2,	L^6H_2,	L^7H_2

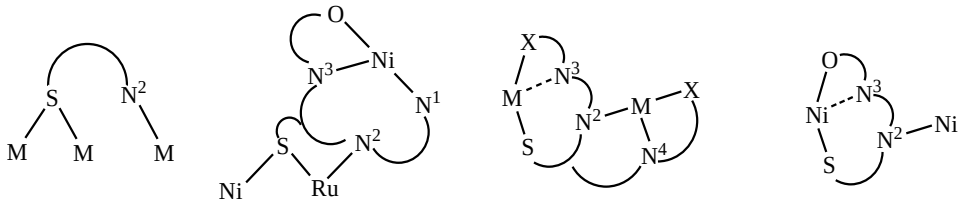

Type I Type II Type III Type IV

X = O, $N_{pyridyl}$

Scheme 1.3.

In 2012 D. M. Eichhorn et al. have reported synthesis and characterization of dinuclear Ni(II) complex of a thiosemicarbazone ligand synthesized by the condensation of 2,2´–dithiodibenzaldehyde (DTDB) with phenylthiosemicarbazide (**Figure 1.2**), and is the first example of a dinuclear bis(thiolate)-bridged Ni(II) complex with NS_3 coordination involving a thiosemicarbazide moiety. They also reported a mononuclear Ni(II) complex of TSC ligand derived from pyridine carboxaldehyde and phenylthiosemicarbazide.[18]

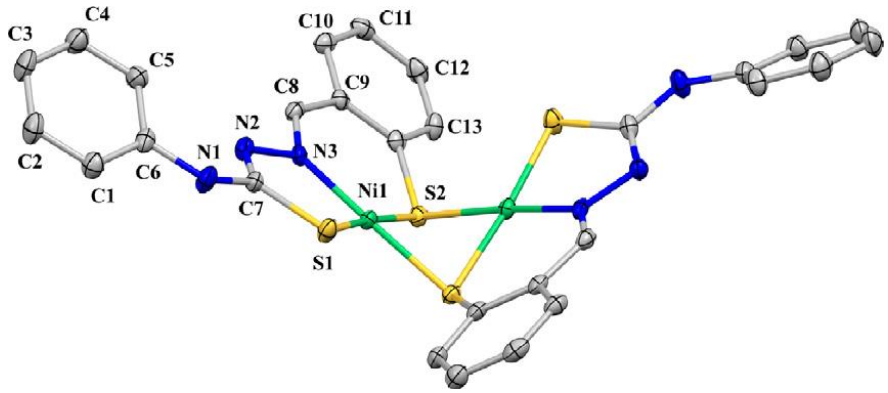

Figure 1.2.

S. Bhattacharya et al. have reported the synthesis, characterization, structure and catalytic activity of nickel complexes of thiosemicarbazones of salicylaldehyde (H_2L^1), 2–hydroxyacetophenone (H_2L^2) and 2–hydroxynaphthaldehyde (H_2L^3) (**Figure 1.3**). The complexes were found to show efficient catalytic activity for Suzuki cross–coupling reactions.[19]

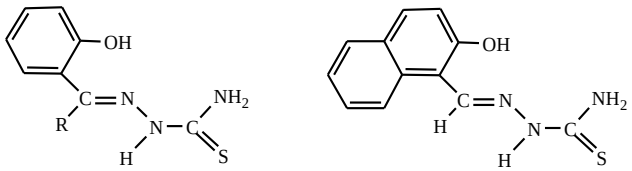

H_2L^1 (R = H)
H_2L^2 (R = CH_3)

H_2L^3

Figure 1.3.

1.1.2. Copper complexes of thiosemicarbazone: Copper is an essential element for most aerobic organisms, employed as a structural and catalytic cofactor, and consequently it is involved in many biological pathways.[20] The antitumor activity of copper−TSCs has been reported as early as 1960s,[21] and developments are still in progress.[22]

A. A. Kumbhar et al. in 2014 have reported the synthesis (**Scheme 1.4**) and characterization of copper(II) complexes of thiosemicarbazone derivative of anthracene; their DNA and protein–binding ability and DNA–cleavage properties were also studied. Their cellular uptake was monitored by fluorescence microscopy, and their anticancer efficacy on cervical cancer cells (HeLa cells) was correlated with their redox potential.[9a]

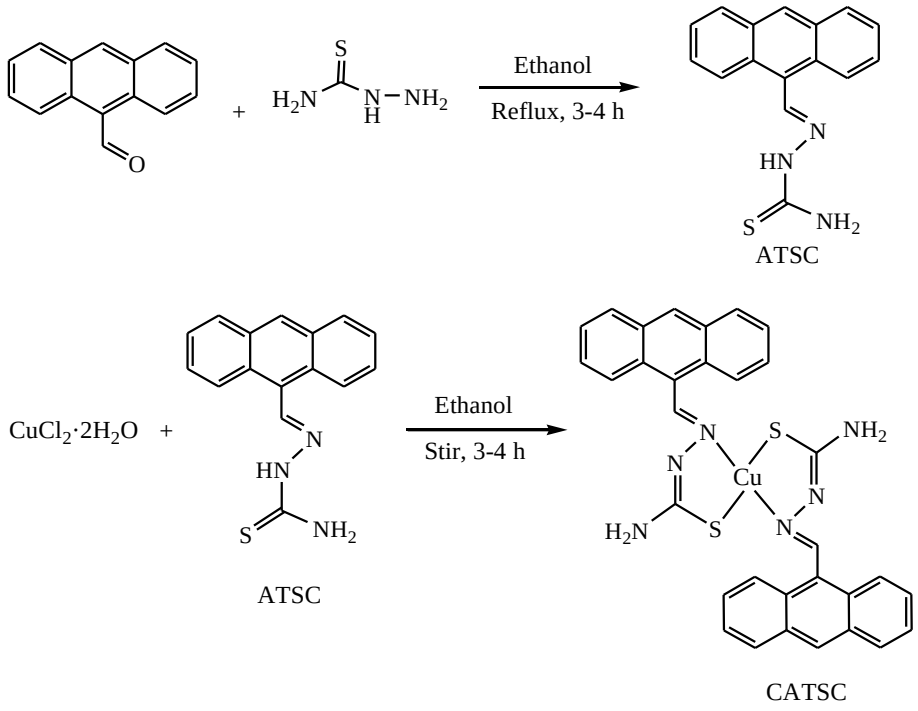

Scheme 1.4.

In the year 2013 V. B. Arion et al. have reported synthesis, spectroscopic characterization, and evaluation of the biological activity of two enantiomerically pure $_{L-}$ and $_{D-}$proline–2–formylpyridine thiosemicarbazone (FTSC), with excellent aqueous solubility, namely, 3–methyl–(*S*)–pyrrolidine–2–carboxylate–2–formylpyridine thiosemicarbazone [$_{L-}$Pro–FTSC or (*S*)–H_2L] and 3–methyl–(*R*)–pyrrolidine–2–carboxylate–2–formylpyridine thiosemicarbazone [$_{D-}$Pro–FTSC or (*R*)–H_2L]. The complexes [Cu(S,R)–L] and [Cu(R,S)–L] have been synthesized by the reaction of copper(II) acetate with (*S*)–H_2L and (*R*)–H_2L in water and comprehensively

characterized. An X–ray diffraction study of [Cu(*S*,*R*)–L] showed the formation of a square–pyramidal complex (**Figure 1.4**). Their antiproliferative activity was studied against CH1 ovarian carcinoma cells, and Topoisomerase IIα inhibition was evaluated in a DNA plasmid relaxation assay.[23]

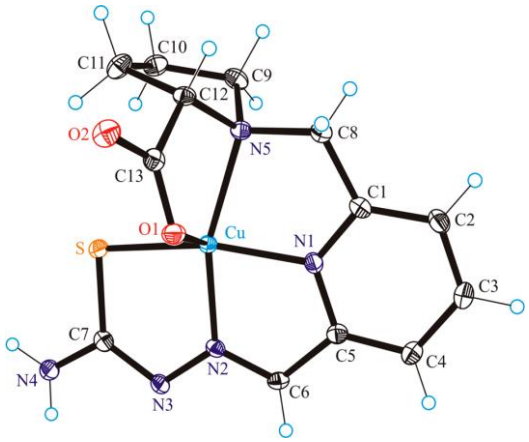

Figure 1.4.

J. S. Lewis et al. reported the evaluation of the Topo–IIα inhibition activity of a series of α–heterocyclic Cu(II)–thiosemicarbazonato complexes and their corresponding thiosemicarbazone ligands. **Scheme 1.5** showing the schematic representation of the ligands and synthetic pathways of their corresponding Cu(II) complexes. The ability of the metal complexes to inhibit the proliferation of two breast cancer cell lines, SK–BR–3 and MCF–7, which have been shown to express high and low levels of Topo–IIα, respectively.[24]

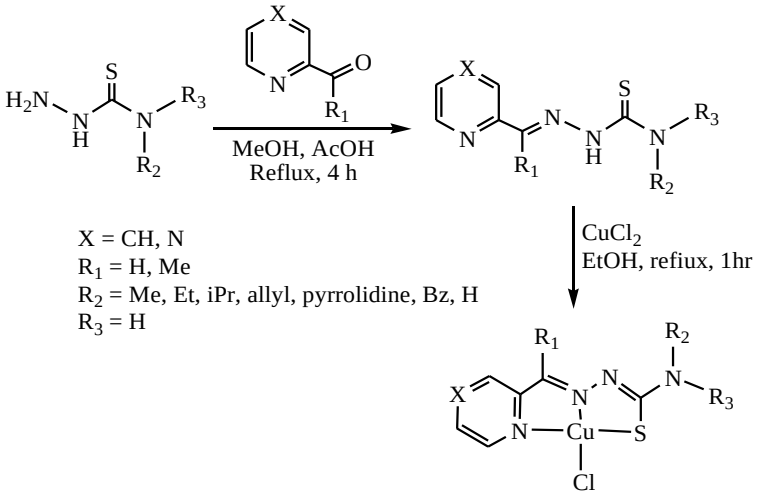

Scheme 1.5.

D. R. Richardson et al. have reported the structure activity relationships of novel copper(II) complexes of chelators 2–acetylpyridine–4,4–dimethyl–3–thiosemicarbazone (HAp44mT) (**Figure 1.5**) and di–2–pyridylketone–4,4–dimethyl–3–thiosemicarbazone (HDp44mT) with pronounced antitumor activity.[9d]

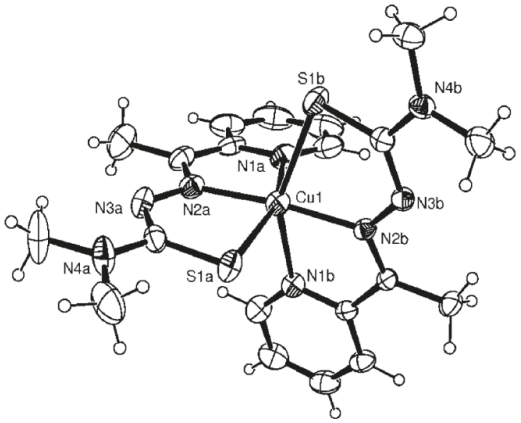

Figure 1.5.

S. Padhye et al. have reported the synthesis of quinoline–2–carboxaldehyde TSC (**Figure 1.6 (a)**) and its copper(II) complex (**Figure 1.6 (b)**) showing dose–dependent antiproliferative, and proapoptotic activity in PC–3 and LNCaP prostate cancer cells (**Figure 1.6 (c)**).[25]

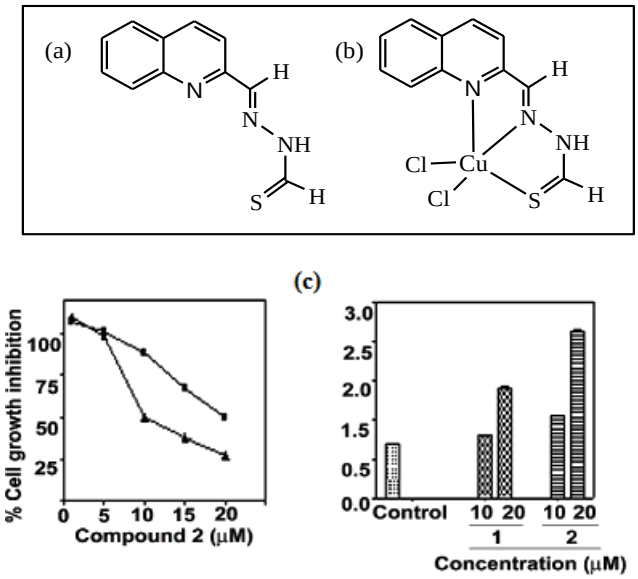

Figure 1.6.

1.1.3. Molybdenum complexes of thiosemicarbazone: Dioxidomolybdenum(VI) complexes have a long standing and successful history in mimicking active sites of molybdenum containing enzymes, especially of the sulfite oxidase family.[26–31] It has been known that the presence of sulfur atoms coordinated to molybdenum is favourable for complexes of molybdenum to have oxotransfer activity, and many model compounds that mimic such oxotransferases have been studied.[32–35]

M. R. Maurya et al. in 2014 have reported the synthesis and characterization of Schiff bases, H_3dfmp(sbdt)$_2$, H_3dfmp(smdt)$_2$ and H_3dfmp(tsc)$_2$ {derived from the condensation of 2,6–diformyl–4–methylphenol (dfmp) with *S*–benzyldithiocarbazate (sbdt), *S*–methyldithiocarbazate (smdt) and thiosemicarbazide (tsc)} and their dioxidomolybdenum(VI) complexes [$Mo^{VI}O_2${Hdfmp(sbdt)$_2$}(H_2O)], [$Mo^{VI}O_2${Hdfmp(smdt)$_2$}(H_2O)] and [$Mo^{VI}O_2${Hdfmp(tsc)$_2$}(MeOH)] (**Figure 1.7**). These molybdenum complexes catalyse the oxidation of styrene and cyclohexene using 30% H_2O_2 as oxidant in the presence of sodium bicarbonate.[36]

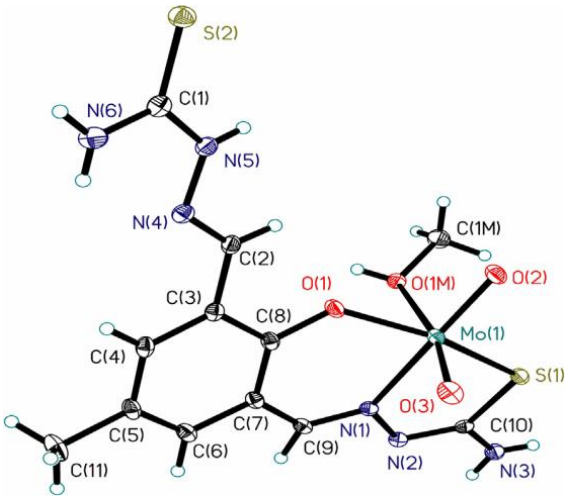

Figure 1.7.

M. Cindrić et al. have reported the chemistry of some dioxidomolybdenum(VI) complexes with thiosemicarbazone ligands derived from 3–thiosemicarbazide and 4–(diethylamino)salicylaldehyde (H_2L^1), 2–hydroxy–3–methoxybenzaldehyde (H_2L^2) (**Figure 1.8**)

and 2–hydroxy–1–naphthaldehyde (H_2L^3). The complexes were tested for their antiproliferative ability against selected human tumour cell lines.[37]

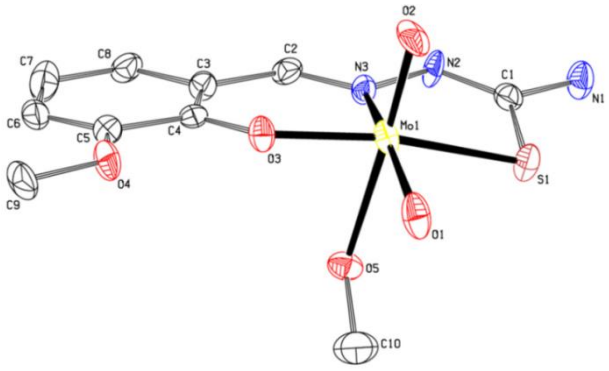

Figure 1.8.

In 2009 B. Krebs et al. have reported a series of homologous mononuclear dioxidomolybdenum complexes {[MoO_2(L)(dmf)] (**Figure 1.9**), [MoO_2(LF)(dmf)], [MoO_2(LCl)(MeOH)], [MoO_2(LBr)(dmf)], [MoO_2(LI)(dmf)], [MoO_2(LMe)(dmf)]·0.5Et_2O, [MoO_2(LOMe)(dmf)], [MoO_2(LNO_2)(MeOH)], [MoO_2(L_3OMe)(dmf)], [MoO_2(LCl_2)(dmf)], and [MoO_2(LBrCl)(dmf)] with 2–hydroxybenzaldehyde–4–triphenylmethylthiosemicarbazone (H_2L) ligand, supplying a tridentate O,N,S donor set to the central metal atom. The functional properties of these biomimetic model complexes for molybdenum–containing oxotransferases were described.[38]

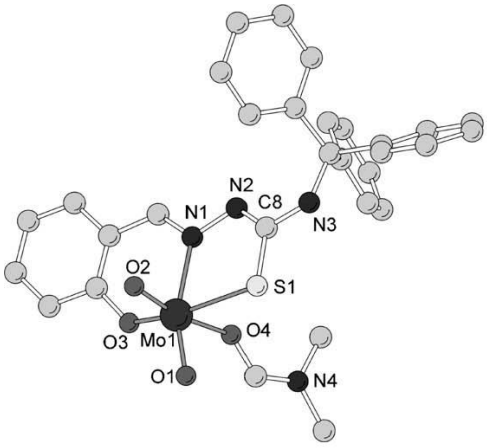

Figure 1.9.

1.1.4. Vanadium complexes of thiosemicarbazone: The coordination chemistry of vanadium attracts increasing interest because of the use of many vanadium complexes as models for the biological functions,[39–42] such as haloperoxidation,[43] phosphorylation,[44] insulin mimicking,[45–49] nitrogen fixation,[50] tumour growth inhibition and prophylaxis against carcinogenesis.[51]

In 2012 A. A. Holder et al. have reported the synthesis (**Scheme 1.6**) and chemical characterization of a series of vanadium(IV) complexes with thiosemicarbazones as ligands. The biological study of these compounds against several colorectal cancer cell lines was done, in order to evaluate their potential as chemotherapeutic candidates.[52]

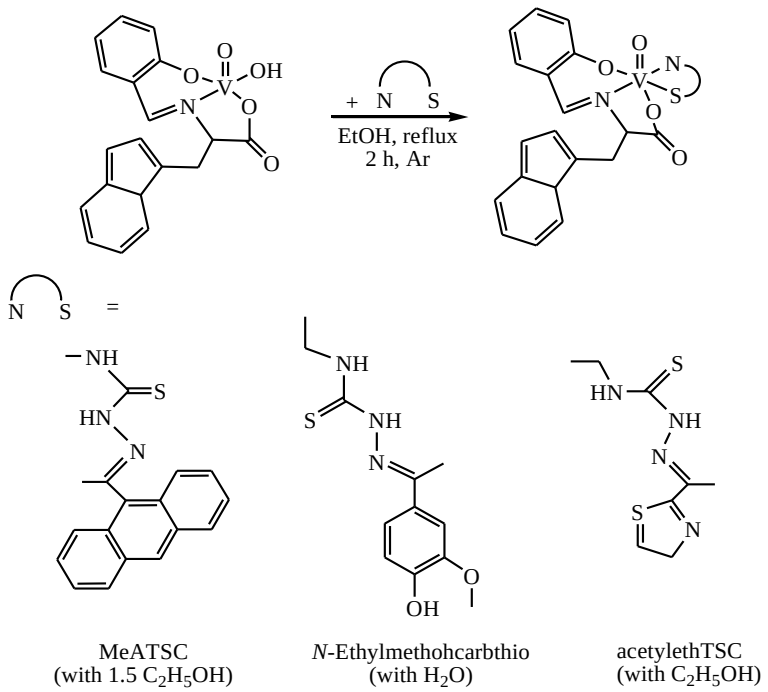

Scheme 1.6.

In the same year J. Lu et al. have reported the synthesis (**Scheme 1.7**) and characterization of four oxidovanadium complexes, [VO(hntdtsc)(phen)], [VO(hntdtsc)(bpy)] (hntdtsc = 2–hydroxy–1–naphthaldehyde thiosemicarbazone, phen = 1,10–phenanthroline), [VO(satsc)(phen)] and [VO(satsc)(bpy)] (satsc = salicylaldehyde thiosemicarbazone, bpy = 2,2′–bipyridine). The interactions of these four complexes with calf–thymus DNA (CT–DNA) were investigated using UV–Vis absorption titration, fluorescence spectra, viscosity measurements and thermal denaturation. Their photo cleavage reactions with pBR322 supercoiled plasmid DNA were

investigated by gel electrophoresis. In addition, the cytotoxicity of these four complexes against the Myeloma cell (Ag8.653) and Gliomas cell (U251) was also assessed by MTT assay.[11d]

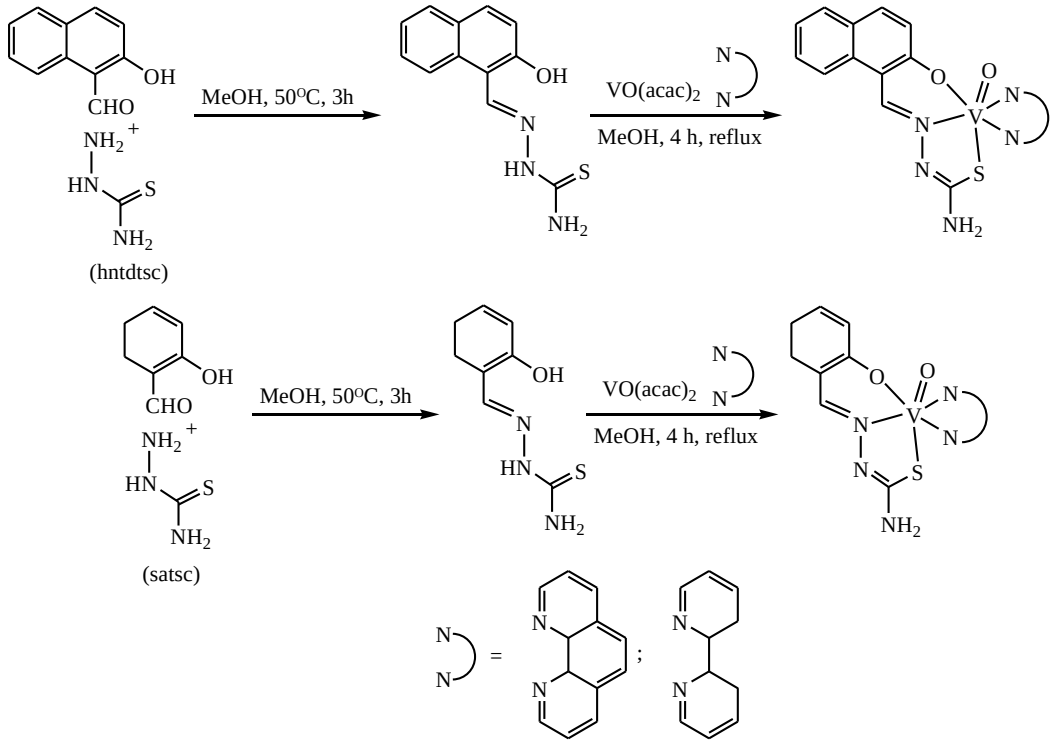

Scheme 1.7.

M. Cindrić et al. have reported the reactions of salicylaldehyde 4–phenylthiosemicarbazone (H_2L), with different vanadium precursors. They have investigated several synthetic strategies, structural and spectroscopic characterizations, as well as the reactivity of two different types of vanadium(V) complexes: (a) mononuclear alkoxido [VOL(OR)]; (b) dinuclear dialkoxido $[V_2O_3(L_{cycl})_2(OR)_2]$ (**Figure 1.10**), where L_{cycl} is the thiadiazole ligand formed by oxidative cyclization of H_2L.[53]

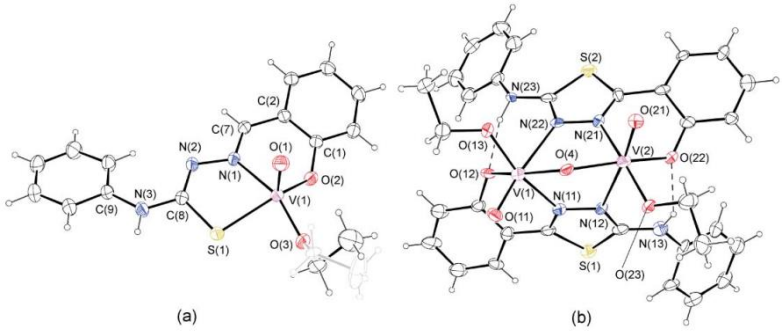

Figure 1.10.

R. Yanardag et al. have reported the synthesis and characterization of oxidovanadium(IV) chelate [VOL] (**Figure 1.11**) (L = N^1–2,4–dihydroxybenzylidene–N^4–2–hydroxybenzylidene–S–methyl–TSC); the biochemical and immunohistochemical effects of the administration of VOL to the pancreas of normal and streptozotocin–induced diabetic rats was also investigated.[54]

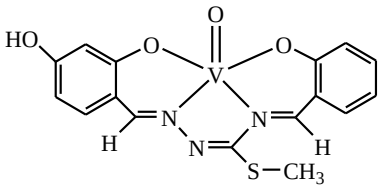

Figure 1.11.

In 2009 V. M. Deflon et al. have reported the preparation and structural characterization both in solution and in the solid state, of some oxidovanadium(IV) and the cis–dioxidovanadium(V) complexes (**Figure 1.12**) with different thiosemicarbazone derivatives {2–acetylpyridine–thiosemicarbazone (Haptsc), 2–acetylpyridine–N(4)–methylthiosemicarbazone (Hapmtsc) and 2–acetylpyridine–N(4)–phenylthiosemicarbazone (Happtsc)}. The activity of complexes, free ligands and common vanadium salts against *M. tuberculosis* H*37*Rv ATCC 27294 was evaluated. The vanadium compounds show comparable or larger anti– *M. tuberculosis* activities than the free thiosemicarbazone ligands, with MIC values within 62.5–1.56 (μg/mL).[55]

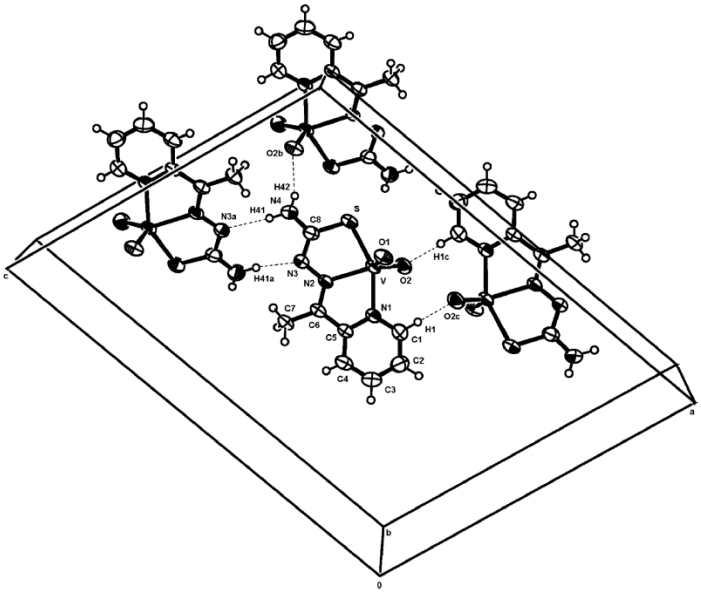

Figure 1.12.

1.1.5. Zinc complexes of thiosemicarbazone: Zn(II) is an essential metal ion because of its presence in certain metalloenzymes. Zn(II) is present in the human body and plays a significant role in a variety of fundamental physiological processes.[56] Moreover Zn(II) ion has structural and catalytic role in several proteins.[57] Zinc complex also exhibited significant antitumor activity against lung cancer A549 cell lines.[58]

In 2013 A. G. Samuelson et al. have reported the synthesis (**Scheme 1.8**) and characterization of dinuclear zinc bis(thiosemicarbazone) complexes. The cytotoxicity of the complexes has been evaluated in five cancer cell lines of different tissue origin. The cellular uptake was investigated by estimating the amount of accumulation of zinc in two cell lines using ICP–OES. The ability of zinc complexes to fluoresce within HepG2 cells has been examined by flow cytometry. Effects of these complexes on DNA binding and DNA cleavage have also been investigated.[59]

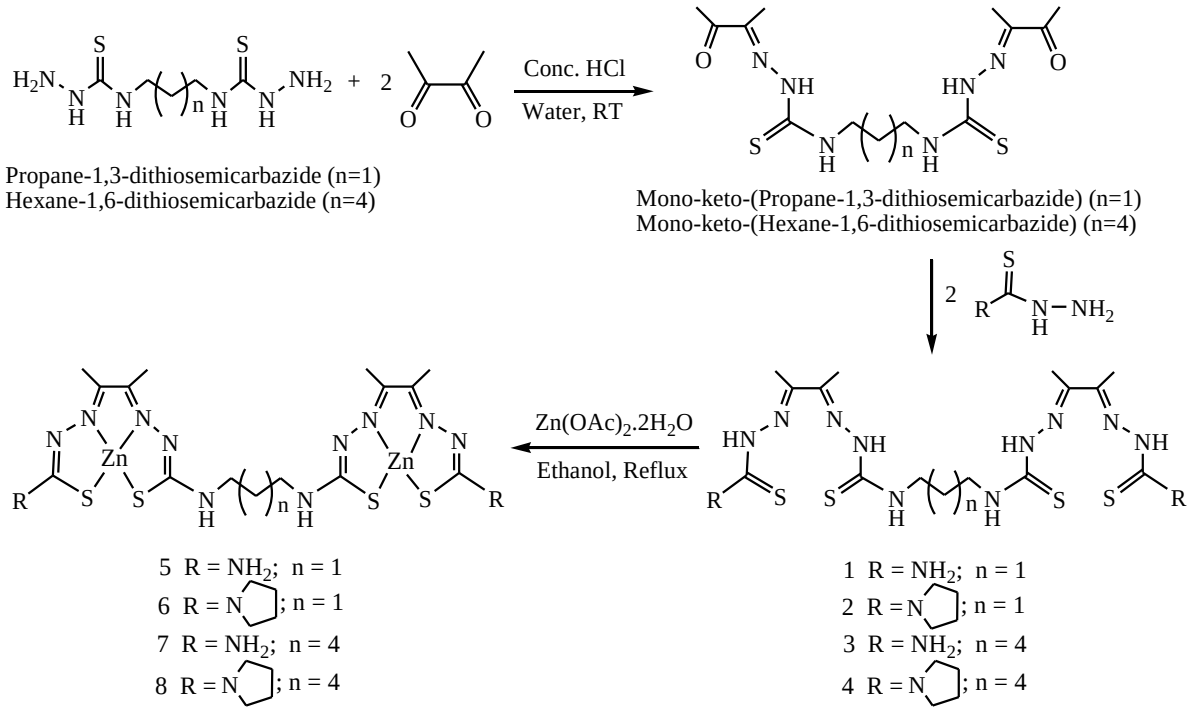

Scheme 1.8.

D. Kovala–Demertzi et al. have reported the synthesis and characterization of zinc(II) complexes $[Zn(AcPipPheF)_2]$ and $[Zn(OAc)(AcPip–PheF)]_2$ (**Figure 1.13**) of 2–acetyl pyridine 1–(4–fluorophenyl)–piperazinyl thiosemicarbazone (HAcPipPheF). The compounds were tested for

their antiproliferative activity in vitro against the cells of four human cancer cell lines: HeLa (cervix adenocarcinoma cell line), K562 (chronic myelogenous leukaemia), MDA–MB–361 and MDA–MB–453 (breast cancer cell lines).[60]

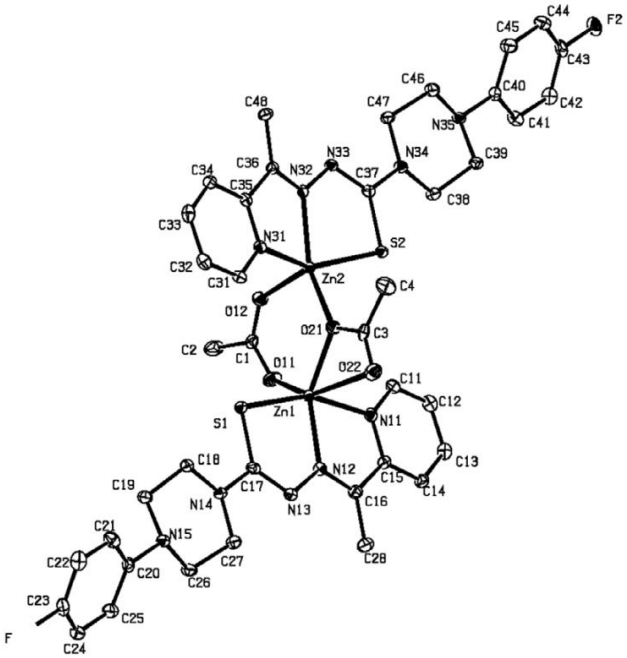

Figure 1.13.

S. I. Pascu et al. in 2008 have reported the synthesis and characterization of a highly fluorescent, zinc complex of bis(thiosemicarbazone) ligand incorporating extended aromatic backbones which where cytotoxic against A431 cell line (**Figure 1.14(a)**) and IGROV cell line (**Figure 1.14(b)**) at levels comparable to cisplatin; cellular fluorescence imaging studies suggested that these cause cell death by disruption of mitochondria.[61]

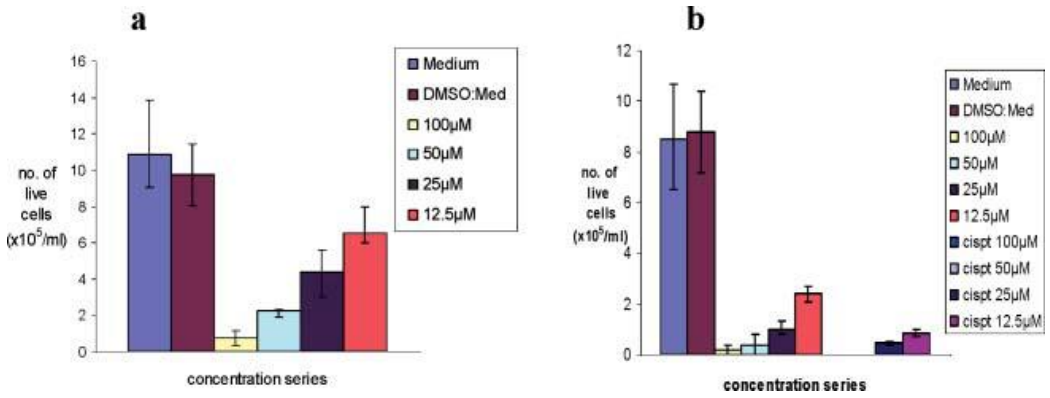

Figure 1.14.

J. R. Dilworth et al. have reported the synthesis and characterization of zinc bis(thiosemicarbazone) complexes and the use of their intrinsic fluorescence to track their uptake in a range of human cancer cell types, studied by fluorescence microscopy and the cellular distribution.[62] ORTEP representation of the structure of [ZnCl(ATSpyrH)] {ATSpyrH = diacetylbis(4–pyrrolidinyl–3–thiosemicarbazone)} is shown in **Figure 1.15**.

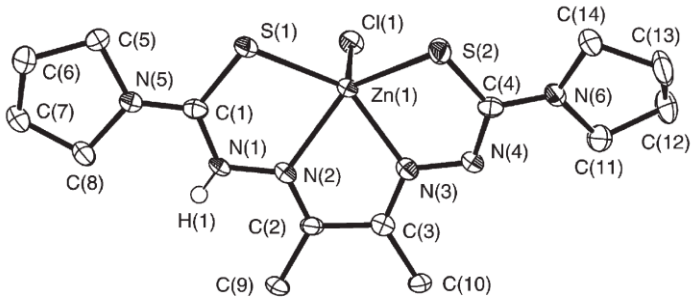

Figure 1.15.

In 2005 M. B. Ferrari have reported synthesis and characterization of cyclic α–ketoglutaric acid thiosemicarbazone (H_3ct) and their zinc complexes, with the aim to compare the biological effects of these compounds with the properties of the corresponding linear forms and their complexes. These molecules interact with DNA and, from the comparison of the K_b values of the cyclic and the open chain forms, it can be observed that the cyclic form binds nucleic acid more strongly.[63] The X–ray structures of ligands Me–H_2ctC, Allyl–H_2ctc and of complex [Zn(Me–$Hct_C)_2(OH_2)_2]\cdot 2H_2O$ (**Figure 1.16**) have also been determined.

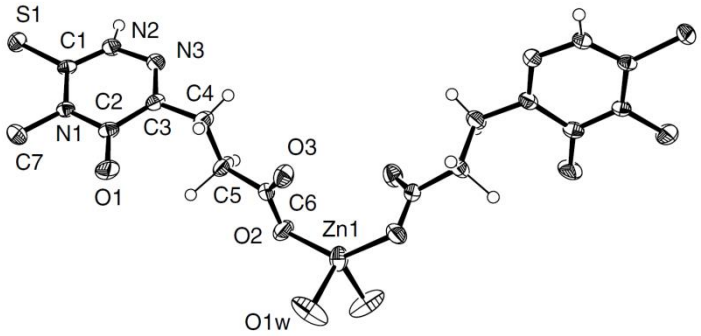

Figure 1.16.

1.2. AIM OF THE PRESENT WORK

The aim of the present work has been to study the chemistry of variable valence transition metal (Ni, Cu, Mo, V & Zn) complexes with thiosemicarbazone ligand systems. All the ligand systems and their synthesized metal complexes are collectively summarized below:

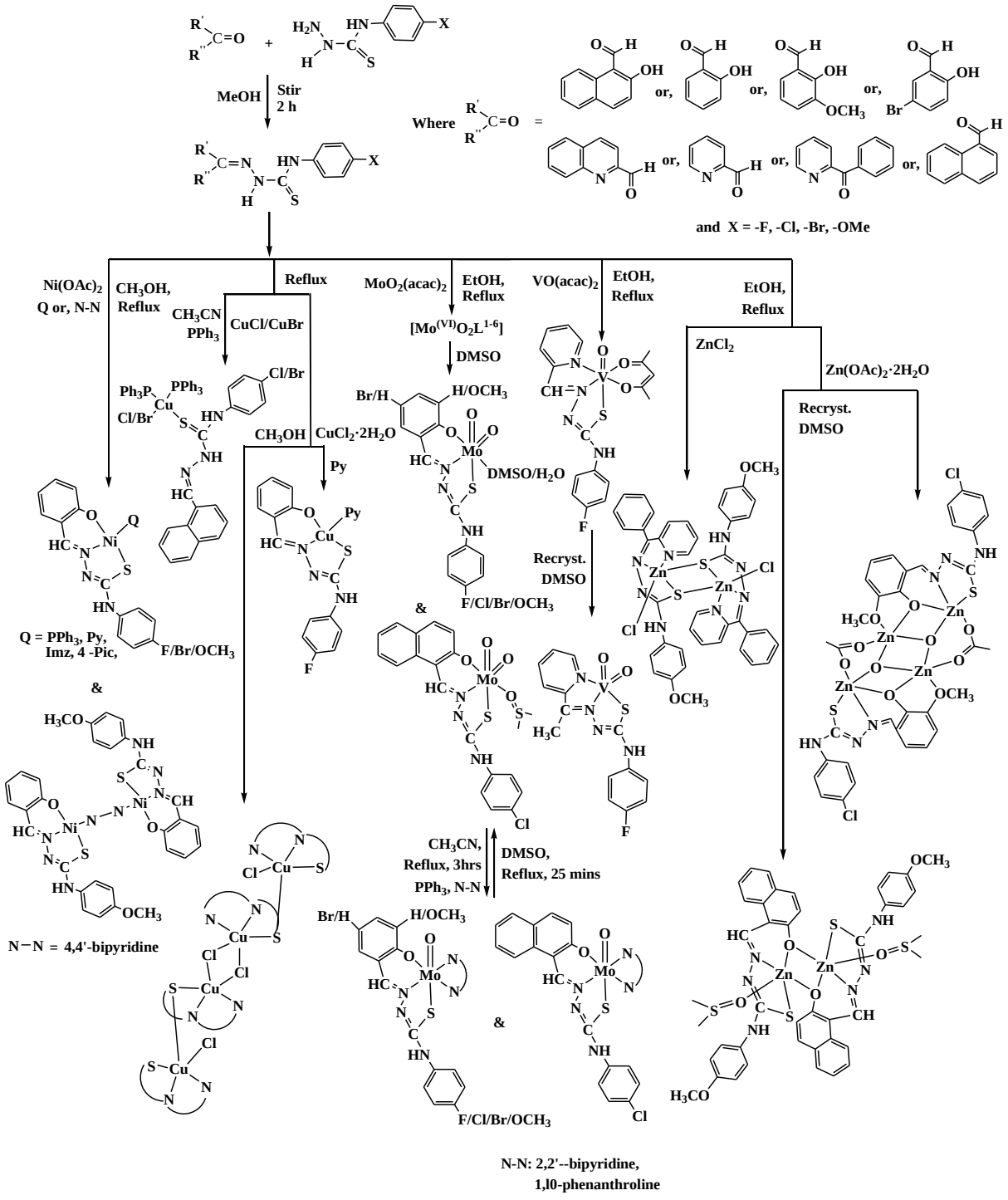

1.3. THE MAIN OBJECTIVES OF THE PRESENT STUDY

1. To develop some ONS, NNS and S donor thiosemicarbazone ligand systems, inspired by the paradigm of biologically and catalytically important transition metal–TSC complexes.

2. To develop versatile variable valence transition metal (Ni, Cu, Mo, V & Zn) complexes of the synthesized thiosemicarbazone ligands, for use as reagent in some bio– and catalytic reactions and as model complex for few metalloenzymes. This work uses synthetic and analytical approaches to generate and study the metal complexes, relying upon current mechanistic understanding of their mode of action.

3. Study of spectral, magnetic and redox behavior of these metal complexes, and solve their X–ray structure and develop the structure–reactivity correlation.

4. Exploration of pharmacological studies such as antimicrobial, DNA binding and cleavage, insulin mimetic and antiproliferative activity.

5. Study of catalytic activities particularly oxidation of styrene and oxidation of cyclohexene using the synthesized metal complexes.

1.4. REFERENCES

(1) Lobana, T. S.; Kumari, P.; Hundal, G.; Butcher, R. J. *Polyhedron* **2010**, *29*, 1130.

(2) (a) Campbell, M. J. M. *Coord. Chem. Rev.* **1975**, *15*, 279. (b) Padhye, S. B.; Kauffman, G. B. *Coord. Chem. Rev.* **1985**, *63*, 127. (c) Haiduc, I.; Silvestru, C. *Coord. Chem. Rev.* **1990**, *99*, 253.

(3) (a) Basuli, F.; Peng, S. M.; Bhattacharya, S. *Inorg. Chem.* **1997**, *36*, 5645. (b) Basuli, F.; Ruf, M.; Pierpont, C. G.; Bhattacharya, S. *Inorg. Chem.* **1998**, *37*, 6113.

(4) Lobana, T. S.; Rekha; Butcher, R. J.; Castineiras, A.; Bermejo, E.; Bharatam, P. V. *Inorg. Chem.* **2006**, *45*, 1535.

(5) Brockman, R. W.; Thomson, J. R.; Bell M. J.; Skipper, H. E. *Cancer Res.* **1956**, *16*, 167.

(6) (a) West, D. X.; Liberta, A. E.; Padhye, S. B.; Chikate, R. C.; Sonawane, P. B.; Kumbhar, A. S.; Yerande, R. G. *Coord. Chem. Rev*. **1993**, *123*, 49. (b) Beraldo, H.; Gambino, D. *Mini–Rev. Med. Chem.* **2004**, *4*, 31. (c) Afrasiabi, Z.; Sinn, E.; Padhye, S.; Dutta, S.; Padhye, S.; Newton, C.; Anson, C. E.; Powell, A. K. *J. Inorg. Biochem.* **2003**, *95*, 306. (d) Byrnes, R. W.; Mohan, M.; Antholine, W. E.; Xu, R. X.; Petering, D. H. *Biochemistry* **1990**, *29*, 7046. (e) Kolocouris, A.; Dimas, K.; Pannecouque, C.; Witvrouw, M.; Foscolos, G. B.; Stamatiou, G.; Fytas, G.; Zoidis, G.; Kolocouris, N.; Andrei, G.; Snoeck, R.; De Clercq, E. *Bioorg. Med. Chem.* **2002**, *12*, 723. (f) Hall, I. H.; Chen, S. Y.; Barners, B. J.; West, D. X. *Met.–Based Drugs* **1999**, *6*, 143. (g) Kelly, P. F.; Slawin, A. M. Z.; Soriano–Rama, A. *J. Chem. Soc., Dalton Trans.* **1996**, 53. (h) Klayman, D. L.; Bartosovich, J. F.; Griffin, T. S.; Mason, C. J.; Scovill, J. P. *J. Med. Chem.* **1979**, *22*, 855. (i) Bermejo, E.; Carballo, R.; Castineiras, A.; Dominguez, R.; Liberta, A. E.; Maichle–Mossmer, C.; West, D. X. *Z. Naturforsch.* **1999**, *B54*, 777. (j) Lakovidou, Z.; Papageorgiou, A.; Demertzis, M. A.; Mioglou, E.; Mourelatos, D.; Kotsis, A.; Yadav, P. N.; Kovala–Demertzi, D. *Anticancer Drugs* **2001**, *12*, 65. (k) Suvarapu, L. N.; Somala, A.R.; Koduru, J. R.; Baek, S. O.; Ammireddy, V. R. *Asian J. Chem*. **2012**, *24*, 1889.

(7) Ragsdale, S. W.; Wood, H. G.; Morton, J. A.; Ljungdahl, L. G.; Dervartanian, D. V.; Lancaster Jr J. R. (Ed.), *The Bioinorganic Chemistry of Nickel*, VCH, New York, **1988** (Chapter 14).

(8) Bertini, I.; Grey, H. B.; Lippard S. J.; Valentine J. S.; Barton, J. K. (Eds.), *Bioinorganic Chemistry*, University Science Book, Mill Valley, **1994**, p. 455.

(9) (a) Kate, A. N.; Kumbhar, A. A.; Khan, A. A.; Joshi P. V.; Puranik, V. G. *Bioconjugate Chem.* **2014**, *25*, 102. (b) Raja, D. S.; Bhuvanesh, N. S. P.; Natarajan, K. *Inorg. Chem.* **2011**, *50*,

12852. (c) Raja, D. S.; Paramaguru, G.; Bhuvanesh, N. S. P.; Reibenspies, J. H.; Renganathan R.; Natarajan, K. *Dalton Trans.* **2011**, *40,* 4548. (d) Jansson, P. J.; Sharpe, P. C.; Bernhardt P. V.; Richardson, D. R. *J. Med. Chem.* **2010**, *53*, 5759. (e) Wang T.; Guo, Z. *Curr. Med. Chem.* **2006**, *13*, 525. (f) Gaál, A.; Orgován, G.; Polgári, Z.; Réti, A.; Mihucz, V. G.; Bősze, S.; Szoboszlai N.; Streli, C. *J. Inorg. Biochem.* **2014**, *130*, 52. (g) Rosu, T.; Pahontu, E.; Pasculescu, S.; Georgescu, R.; Stanica, N.; Curaj, A.; Popescu A.; Leabu, M. *Eur. J. Med. Chem.* **2010**, *45*, 1627. (h) Palanimuthu, D.; Shinde, S. V.; Somasundaram, K.; Samuelson, A. G. *J. Med. Chem.* **2013**, *56*, 722. (i) Raja, D. S.; Bhuvanesh, N. S. P.; Natarajan, K. *Eur. J. Med. Chem.* **2011**, *46*, 4584.

(10) (a) Dutta, S. K.; McConville, D. B.; Youngs, W. J.; Chaudhury, M. *Inorg. Chem.* **1997**, *36*, 2517. (b) Hahn, R.; Kűsthardt, U.; Scherer, W. *Inorg. Chim. Acta* **1993**, *210*, 177. (c) Dinda, R.; Sengupta, P.; Ghosh, S.; Sheldrick, W. S. *Eur. J. Inorg. Chem.* **2003**, 363.

(11) (a) Xie, M. J.; Niu, Y. F.; Yang, X. D.; Liu, W. P.; Li, L.; Gao, L. H.; Yan, S. P.; Meng, Z. H. *Eur. J. Med. Chem.* **2010**, *45*, 6077. (b) Mendes, I. C.; Botion, L. M.; Ferreira, A. V. M. *Inorg. Chim. Acta* **2009**, *362*, 414. (c) Benítez, J.; Guggeri, L.; Tomaz, I.; Pesso, J. C.; Moreno, V.; Lorenzo, J.; Avilés, F. X.; Garat, B.; Gambino, D. *J. Inorg. Biochem.* **2009**, *103*, 1386. (d) Lu, J.; Guo, H.; Zeng, X.; Zhang, Y.; Zhao, P.; Jiang, J.; Zang, L. *J. Inorg. Biochem*. **2012**, *112*, 39.

(12) Sakurai, H.; Watanabe, H.; Tamura, H.; Yasui, H.; Matsushita, R.; Takada, J. *Inorg. Chim. Acta* **1998**, *283*, 175.

(13) Demertzi, D. K.; Alexandratos, A.; Papageorgiou, A.; Yadav, P. N.; Dalezis, P.; Demertzis, M. A. *Polyhedron* **2008**, *27*, 2731.

(14) (a) Prabhakaran, R.; Kalaivoni, P.; Huang, R.; Poornima, P.; Padma, V. V.; Dallemer, F.; Natarajan, K. *J. Biol. Inorg. Chem.* **2013**, *18*, 233. (b) Pahontu, E.; Fala, V.; Gulea, A.; Poier, D.; Tapcov, V.; Rosu, T. *Molecules* **2013**, *18*, 8812. (c) Datta, S.; Seth, D. K.; Gangopadhyay, S.; Karmakar, P.; Bhattacharya, S. *Inorg. Chim. Acta* **2012**, *392*, 118. (d) Ramchandran, E.; Raja, D. S.; Bhuvanesh, N. S. P.; Natarajan, K. *Eur. J. Med. Chem*. **2013**, *64*, 179. (e) Ramchandran, E.; Raja, D. S.; Mike, J. L.; Wagner, T. R.; Zeller, M.; Natarajan, K. *RSC Adv*. **2012**, *2*, 8515. (f) Basu, A.; Thiyagarajan, D.; Kar, C.; Ramesh, A.; Das, G. *RSC Adv*. **2013**, *3*, 14088.

(15) Prabhakaran, R.; Kalaivani, P.; Poorima, P.; Dallemer, F.; Paramaguru, G.; Padma, V. V.; Renganathan, R.; Huang, R.; Natarajan, K. *Dalton Trans*. **2012**, *41*, 9323.

(16) Kalaivani, P.; Saranya, S.; Poornima, P.; Prabhakaran, R.; Dallemer, F.; Padma, V. V.; Natarajan, K. *Eur. J. Med. Chem*. **2014**, *82*, 584.

(17) Lobana, T. S.; Kumari, P.; Castineiras, A.; Butcher, R. J. *Eur. J. Inorg. Chem.* **2013**, 3557.

(18) Panja, A.; Eichhorn D. M. *Inorg. Chim. Acta* **2012**, *391*, 88.

(19) Datta, S.; Seth, D. K.; Butcher, R. J.; Bhattacharya, S. *Inorg. Chim. Acta* **2011**, *377*, 120.

(20) (a) Kraatz, H. B.; Metzler–Nolte, N. *Concepts and Models in Bioinorganic Chemistry*; Wiley–VCH: Weinheim, Germany, **2006**. (b) Lippard, S. J.; Berg, J. M. *Principles of Bioinorganic Chemistry*; University Science Books: Mill Valley, CA, **1994**. (c) Frausto da Silva, J. J. R.; Williams, R. J. P. *The Biological Chemistry of the Elements*; Clarendon: Oxford, U. K., **1991**.

(21) (a) Taylor, M. R.; Gabe, E. J.; Glusker, J. P.; Minkin, J. A.; Patterson, A. L. *J. Am. Chem. Soc*. **1966**, *88*, 1845. (b) Crim, J. A.; Petering, H. G. *Cancer Res.* **1967**, *27*, 1278.

(22) (a) Yu, Y.; Wong, J.; Lovejoy, D. B.; Kalinowski, D. S.; Richardson, D. R. *Clin. Cancer Res*. **2006**, *12*, 6876. (b) Lovejoy, D. B.; Richardson, D. R. *Blood* **2002**, *100*, 666. (c) Ming, L. J. *Med. Res. Rev*. **2003**, *23*, 697. (d) Wolohan, P.; Yoo, J.; Welch, M. J.; Reichert, D. E. *J. Med. Chem.* **2005**, *48*, 5561. (e) Pogni, R.; Baratto, M. C.; Diaz, A.; Basosi, R. *J. Inorg. Biochem.* **2000**, *79*, 333. (f) Zhang, H.; Thomas, R.; Oupicky, D.; Peng, F. *J. Biol. Inorg. Chem.* **2008**, *13*, 47. (g) Kalinowski, D. S.; Quach, P.; Richardson, D. R. *Future Med. Chem*. **2009**, *1*, 1143. (h) Feun, L.; Modiano, M.; Lee, K.; Mao, J.; Marini, A.; Savaraj, N.; Plezia, P.; Almassian, B.; Colacino, E.; Fischer, J.; MacDonald, S. *Cancer Chemother. Pharmacol*. **2002**, *50*, 223. (i) Ainscough, E. W.; Brodie, A. M.; Denny, W. A.; Finlay, G. J.; Ranford, J. D. *J. Inorg. Biochem*. **1998**, *70*, 175. (j) West, D. X.; Liberta, A. E.; Rajendran, K. G.; Hall, I. H. *Anticancer Drugs* **1993**, *4*, 241. (k) Ferrari, M. B.; Bisceglie, F.; Pelosi, G.; Tarasconi, P.; Albertini, R.; Dall'Aglio, P. P.; Pinelli, S.; Bergamo, A.; Sava, G. *J. Inorg. Biochem.* **2004**, *98*, 301. (l) Yu, Y.; Kalinowski, D. S.; Kovacevic, Z.; Siafakas, A. R.; Jansson, P. J.; Stefani, C.; Lovejoy, D. B.; Sharpe, P. C.; Bernhardt, P. V.; Richardson, D. R. *J. Med. Chem*. **2009**, *52*, 5271.

(23) Bacher, F.; Enyedy, É. A.; Nagy, N. V.; Rockenbauer, A.; Bognár, G. M.; Trondl, R.; Novak, M. S.; Klapproth, E.; Kiss, T.; Arion, V. B. *Inorg. Chem*. **2013**, *52*, 8895.

(24) Zeglis, B. M.; Divilov, V.; Lewis, J. S. *J. Med. Chem*. **2011**, *54*, 2391.

(25) Adsule, S.; Barve, V.; Chen, D.; Ahmed, F.; Dou, Q. P.; Padhye, S.; Sarkar, F. H. *J. Med. Chem.* **2006**, *49*, 7242.

(26) Tunney, J. M.; McMaster, J.; Garner, C. D. in *Comprehensive Coordination Chemistry II* (Eds.: J. A. McCleverty, T. J. Meyer), Elsevier Pergamon, Amsterdam, **2004**, vol. 8, pp. 459.

(27) a) Holm, R. H. *Coord. Chem. Rev.* **1990**, *100*, 183. b) Holm, R. H.; Berg, J. M. *Acc. Chem. Res.* **1986**, *19*, 363. c) Holm, R. H.; Berg, J. M. *Pure Appl. Chem.* **1984**, *56*, 1645.

(28) Enemark, J. H.; Young, C. G. *Adv. Inorg. Chem.* **1993**, *40*, 1.

(29) Enemark, J. H.; Cooney, J. J. A.; Wang, J.J.; Holm, R. H. *Chem. Rev.* **2004**, *104*, 1175.

(30) Young, C. G. in *Biomimetic Oxidations Catalyzed by Transition Metals* (Ed.: B. Meunier), Imperial College Press, London, **2004**, pp. 415.

(31) Hille, R. *Chem. Rev.* **1996**, *96*, 2757.

(32) Sheldon, R. A.; Kochi, J. K. *Metal Catalyzed Oxidation of Organic Compounds*, Academic, New York, **1981**.

(33) Mimoun, H. *J. Mol. Catal* **1980**, *7*, 1.

(34) Bottomley, F.; Sutin, L. *Adv. Organomet. Chem.* **1988**, 28, 339.

(35) Arzoumanian, H. *Bull. Soc. Chim. Belg.* **1991**, 100, 717.

(36) Maurya, M. R.; Dhaka, S.; Avecilla, F. *Polyhedron* **2014**, *81*, 154.

(37) Vrdoljak, V.; Đilović, I.; Rubčić, M.; Pavelić, S. K.; Kralj, M.; Čalogović, D. M.; Piantanida, I.; Novak, P.; Rožman, A.; Cindrić, M. Eur. J. Med. Chem. **2010**, *45*, 38.

(38) Eierhoff, D.; Tung, W. C.; Hammerschmidt, A.; Krebs, B.; *Inorg. Chim. Acta* **2009**, *362*, 915.

(39) Sigel H.; Sigel, A.; Dekker, M. ed., *Vanadium and its Role in Life, Metal Ions in Biological Systems*, New York, **1995**, vol. 31.

(40) Crans, D. C.; Smee, J. J.; Gaidamauskas E.; Yang, L. *Chem. Rev.* **2004**, *104*, 849.

(41) Tracey, A. S.; Willsky G. R.; Takeuchi, E. S. *Vanadium Chemistry, Biochemistry, Pharmacology and Practical Applications*, CRC Press, Boca Raton, **2007**.

(42) Rehder, D. *Bioinorganic Vanadium Chemistry*, John Wiley & Sons, Chichester, **2008**.

(43) Butler A.; Walker, J. V. *Chem. Rev.* **1993**, *93*, 1937.

(44) Cornman, C. R.; Zovinka E. P.; Meixner, M. H. *Inorg. Chem.* **1995**, *34*, 5099.

(45) Thompson, K. H.; McNeill J. H.; Orvig, C. *Chem. Rev.* **1999**, *99*, 2561.

(46) Thompson, K. H.; Liboiron, B. D.; Sun, Y.; Bellman, K. D. D.; Karunaratne, V.; Rawji, G.; Wheeler, J.; Sutton, K.; Bhanot, S.; Cassidy, S. B. C.; McNeill, J. H.; Yuen V. G.; Orvig, C. *J. Biol. Inorg. Chem.* **2003**, *8*, 66.

(47) Yasui, H.; Adachi, Y.; Katoh A.; Sakurai, H. *J. Biol. Inorg. Chem*. **2007**, *12*, 843.

(48) Shechter, Y.; Goldwaser, I.; Mironchik, M.; Fridkin M.; Gefel, D. *Coord. Chem. Rev*. **2003**, *237*, 3.

(49) Bastos, A. M. B.; Silva, J. G. da; Maia, P. I. S.; Deflon, V. M.; Batista, A. A.; Ferreira, A. V. M.; Botion, L. M.; Niquet E.; Beraldo, H. *Polyhedron*, **2008**, *27*, 1787.

(50) Eady, R. R. *Coord. Chem. Rev*. **2003**, *237*, 23.

(51) Sasmal, P. K.; Patra A. K.; Chakravarty, A. R. *J. Inorg. Biochem*. **2008**, *102*, 1463.

(52) Lewis, N. A.; Liu, F.; Seymour, L.; Magnusen, A.; Erves, T. R.; Arca, J. F.; Beckford, F. A.; Venkatraman, R.; Sarrías, A. G.; Fronczek, F. R.; VanDerveer, D. G.; Seeram, N. P.; Liu, A.; Jarrett, W. L.; Holder, A. A. *Eur. J. Inorg. Chem.* **2012**, 664.

(53) Rubčić, M.; Milić, D.; Horvat, G.; Đilović, I.; Galić, N.; Tomišić, V.; Cindrić, M. *Dalton Trans.* **2009**, 9914.

(54) Yanardag, R.; Demirci, T. B.; Ülkŭseven, B.; Bolkent, S.; Tunali, S.; Bolkent, S.; *Eur. J. Med. Chem.* **2009**, *44*, 818.

(55) Maia, P.I. da S.; Pavan, F.R.; Leite, C.Q.F.; Lemos, S.S.; Sousa, G.F.de; Batista, A. A.; Nascimento, O. R.; Ellena, J.; Castellano, E. E.; Niquet, E.; Deflon, V. M. *Polyhedron* **2009**, *28*, 398.

(56) Roat–Malone, R. M. *Bioinorganic Chemistry: A Short Course*, John Wiley & Sons, New Jersey, **2002**.

(57) Peariso, K.; Goulding, C. W.; Huang, S.; Matthews, R. G.; Penner–Hahn, J. E. *J. Am. Chem. Soc.* **1998**, *120*, 8410.

(58) Li, M. X.; Zhou, J.; Chen, C. L.; Wang, J. P. *Z. Naturforsch.* **2008**, *63b*, 280.

(59) Palanimuthu, D.; Samuelson, A. G. *Inorg. Chim. Acta* **2013**, *408*, 152.

(60) Stanojkovic, T. P.; Demertzi, D. K.; Primikyri, A.; Santos, I. G.; Castineiras, A.; Juranic, Z.; Demertzis, M. A. *J. Inorg. Biochem*. **2010**, *104*, 467.

(61) Pascu, S. I.; Waghorn, P. A.; Conry, T. D.; Lin, B.; Betts, H. M.; Dilworth, J. R.; Sim, R. B.; Churchill, G. C.; Aigbirhio, F. I.; Warren, J. E. *Dalton Trans.* **2008**, 2107.

(62) Cowley, A. R.; Davis, J.; Dilworth, J. R.; Donnelly, P. S.; Dobson, R.; Nightingale, A.; Peach, J. M.; Shore, B.; Kerrb, D.; Seymour, L. *Chem. Commun*. **2005**, 845.

(63) Baldini, M.; Ferrari, M. B.; Bisceglie, F.; Capacchi, S.; Pelosi, G.; Tarasconi, P. *J. Inorg. Biochem*. **2005**, *99*, 1504.

Chapter 2

Mixed-ligand nickel(II) thiosemicabazone complexes: Synthesis, characterization and biological evaluation

Chapter 2

Mixed-ligand nickel(II) thiosemicabazone complexes: Synthesis, characterization and biological evaluation

ABSTRACT

The syntheses and characterization of some new mixed-ligand nickel(II) complexes {[Ni(L^1)(PPh_3)] (**1**); [Ni(L^1)(Py)] (**2**); [Ni(L^2)(PPh_3)]·DMSO (**3**); [Ni(L^2)(Imz)] (**4**), [Ni(L^3)(4–pic)] (**5**) and [{Ni(L^3)}$_2$(μ–4,4′–byp)]·2DMSO (**6**)} of the selected three thiosemicarbazones {4–(*p*–X–phenyl)thiosemicarbazone of salicylaldehyde} ($H_2L^{1–3}$) (**A, Scheme 2.1**) are described in the present chapter, differing in the inductive effect of the substituent X (X = F, Br and OCH_3), in order to observe their influence, if any, on the redox potentials and biological activity of the complexes. All the synthesized ligands and the metal complexes are successfully characterized by elemental analysis, IR, UV–Vis, NMR spectroscopy and cyclic voltammetry. Molecular structures of four mononuclear (**1**–**3** and **5**) and one dinuclear (**6**) Ni(II) complexes have been determined by X–ray crystallography. The complexes have been screened for their antibacterial activity against *Escherichia coli and Bacillus*. Minimum inhibitory concentration of these complexes indicates compound **4** as the potential lead molecule for drug designing.

2.1. INTRODUCTION

Nickel(II) complexes with nitrogen and sulfur donor ligands are highly interesting[1–5] because several hydrogenases and carbon monoxide dehydrogenases[6] contain such nickel complexes as their active site. Thiosemicarbazones are an important class of N, S donor ligand which has considerable pharmacological interest due to their significant antibacterial, antiviral, antimalarial, antileprotic and anticancer activities.[7–10] Metal complexes of thiosemicarbazone ligands have shown variable bonding properties and structural diversity along with promising biological implications, and ion sensing abilities.[9,11–17] Among transition metals, thiosemicarbazone complexes of nickel(II) also show marked and diverse biological[18–21] as well as catalytic activity,[22,23] but there are limited Ni(II) complexes reported with N1-substituted thiosemicarbazones.[24–29]

Thiosemicarbazones obtained by condensation of ring-substituted 4-phenyl thiosemicarbazides with salicylaldehyde and substituted salicylaldehydes[30–33] form a class of versatile NS/NSO chelating ligands and are known to exhibit diverse biological activities.[32] However, not only the bioinorganic relevance of the complexes the chemistry of transition metal complexes of the thiosemicarbazones are also receiving significant current attention because of the variable binding mode displayed by these ligands in their complexes.[34-43] The variable mode of binding of thiosemicarbazone ligands and the ability of nickel to take up different coordination environments (such as octahedral, square-planar and tetrahedral), has encouraged us to explore its coordination chemistry further, and herein we report the syntheses, X–ray structure and physical properties of some new mixed-ligand nickel(II) complexes of thiosemicarbazone with special reference to their antibacterial activity. Three thiosemicabazones {4–(*p*–X–phenyl)thiosemicarbazone of salicylaldehyde} (H_2L^{1-3}) have been used, differing in the inductive effect of the substituent X (X = F, Br and OCH_3) in order to observe its influence, if any, on the redox potentials and biological activities of the complexes.

2.2. EXPERIMENTAL SECTION

2.2.1. General methods and materials. Reagent grade solvents were dried and distilled prior to use. All other chemicals were reagent grade, available commercially and used as received. HPLC grade DMSO and CH_3CN was used for spectroscopic and electrochemical studies and ethanol, methanol were used for synthesis of ligands and metal complexes. Commercially available TEAP (tetra ethyl ammonium perchlorate) was properly dried and used as a supporting electrolyte for recording cyclic voltammograms of the complexes. Elemental analyses were performed on a Vario ELcube CHNS Elemental analyzer. IR spectra were recorded on a Perkin-Elmer Spectrum RXI spectrometer. ^1H and ^{13}C NMR spectra were recorded with a Bruker Ultrashield 400 MHz spectrometer using $SiMe_4$ as an internal standard. Electronic spectra were recorded on a Lamda25, PerkinElmer spectrophotometer. Electrochemical data were collected using PAR Versastat–II instrument driven by E–chem software (PAR) at 298 K in a dry nitrogen atmosphere. Cyclic voltammetry experiments were carried out with Pt working and auxiliary electrodes and Ag/AgCl as the reference electrode and TEAP as the supporting electrolyte.

2.2.2. Synthesis of ligands ($H_2L^{1–3}$). The thiosemicabazides were prepared from distilled substituted aniline by a known method reported ear1ier.[44] Schiff base ligands, 4–(*p*–fluorophenyl)thiosemicarbazone (H_2L^1), 4–(*p*–bromophenyl)thiosemicarbazone (H_2L^2) and 4–(*p*–methoxyphenyl)thiosemicarbazone (H_2L^3) of salicylaldehyde were prepared in 80–90% yield by stirring equimolar ratio of the substituted thiosemicabazide with salicylaldehyde in methanol medium by standard procedures.[31] The resulting compound was filtered, washed thoroughly with methanol and dried over fused $CaCl_2$.

H_2L^1: Yield: 85%. Anal. calc. for $C_{14}H_{12}N_3SOF$: C, 58.13; H, 4.18; N, 14.52. Found: C, 58.15; H, 4.20; N, 14.51. Main IR peaks (KBr, cm^{-1}): 3357 s ν(O(1)–H), 3247 s ν(N(1)–H), 3028 s ν(N(2)–H), 1605 s ν(C=C), 1543 s, 1438 m ν(C(8)=N(3)), 750 s ν(C(7)=S(1)). ^1H NMR (DMSO-d_6, 400 MHz) δ: 11.81 (s, 1H, –C(14)–O(1)H), 10.06 (s, 1H, –C(7)–N(1)H), 9.99 (s, 1H, –C(7)–N(2)H), 8.48 (s, 1H, –N(3)=C(8)H), 8.11–6.81 (m, 8H, C_6H_4). ^{13}C NMR (DMSO–d_6, 100 MHz) δ: 176.52, 161.25, 158.54, 157.05, 140.52, 135.97, 135.95, 131.81, 128.54, 128.46, 127.48, 120.70, 119.66, 116.48.

H_2L^2: Yield: 88%. Anal. calc. for $C_{14}H_{12}N_3SOBr$: C, 48.01; H, 3.45; N, 12.00. Found: C, 48.04; H, 3.40; N, 12.03. Main IR peaks (KBr, cm^{-1}): 3307 s ν(O(1)–H), 3297 s ν(N(1)–H), 3098 s ν(N(2)–H), 1621 s ν(C=C), 1522 s, 1412 m ν(C(8)=N(3)), 752 s ν(C(7)=S(1)). ^{1}H NMR (DMSO-d_6, 400 MHz) δ: 11.88 (s, 1H, –C(14)–O(1)H), 10.09 (s, 1H, –C(7)–N(1)H), 9.96 (s, 1H, –C(7)–N(2)H), 8.49 (s, 1H, –N(3)=C(8)H), 8.09–6.82 (m, 8H, C_6H_4). ^{13}C NMR (DMSO-d_6, 100 MHz) δ: 176.07, 157.17, 140.79, 139.09, 132.04, 131.85, 131.28, 129.12, 128.09, 127.53, 120.62, 119.63, 117.82, 116.51.

H_2L^3: Yield: 87%. Anal. calc. for $C_{15}H_{15}N_3SO_2$: C, 59.78; H, 5.02; N, 13.94. Found: C, 59.75; H, 5.04; N, 13.91. Main IR peaks (KBr, cm^{-1}): 3325 s ν(O(1)–H), 3278 s ν(N(1)–H), 3019 s ν(N(2)–H), 1623 s ν(C=C), 1563 s, 1457 m ν(–C(8)=N(3)), 749 s ν(C(7)=S(1)). ^{1}H NMR (DMSO-d_6, 400 MHz) δ: 11.70 (s, 1H, –C(14)–O(1)H), 10.07 (s, 1H, –C(7)–N(1)H), 9.95 (s, 1H, –C(7)–N(2)H), 8.47 (s, 1H, –N(3)=C(8)H), 8.10–6.81 (m, 8H, C_6H_4), 3.76 (s, 3H, –C(4)–OCH_3). ^{13}C NMR (DMSO-d_6, 100 MHz) δ: 176.58, 157.32, 156.99, 140.29, 139.13, 132.51, 131.69, 131.06, 127.91, 127.53, 120.78, 119.67, 116.48, 113.69, 55.6.

2.2.3. Synthesis of Ni (II) complexes (1–6)

2.2.3.1. Synthesis of [Ni(L^1)(PPh_3)] (1). To a solution of H_2L^1 (0.289 g, 0.100 mmol) in hot methanol, triethylamine (0.202 g, 0.2 mmol) was added followed by solid $Ni(OAc)_2$ salt (0.248 g, 0.100 mmol) and triphenylphosphine (0.262 g, 0.100 mmol). The mixture was refluxed for 3 h and a clear reddish brown solution was obtained, which was filtered and allowed to evaporate at room temperature. Reddish brown colored crystals were obtained from the filtrate after 3–4 days.

[Ni(L^1)(PPh_3)] (1): Yield: 67%. Anal. calc. for $C_{32}H_{25}FN_3NiOPS$: C, 63.18; H, 4.14; N, 6.91. Found: C, 63.13; H, 4.17; N, 6.87. Main IR peaks (KBr, cm^{-1}): 3215 s ν(N(1)–H), 1627 s ν(C=C), 1542 s, 1408 m ν(–C(8)=N(3)), 1094 s ν(P–C), 739 s ν(C(7)–S(1)). ^{1}H NMR (DMSO-d_6, 400 MHz) δ: 9.45 (s, 1H, –C(7)–N(1)H), 8.66 (s,1H, –N(3)=C(8)H), 7.78–6.34 (m, 23H, C_6H_4).

2.2.3.2. Synthesis of [Ni(L^1)(Py)] (2); [Ni(L^2)(PPh_3)]·DMSO (3); [Ni(L^2)(Imz)] (4) and [Ni(L^3)(4–pic)] (5). Complexes 2–5 were prepared following the same procedure as complex 1. Reddish brown crystals of complex **3**, suitable for X–ray crystallography were obtained by slow evaporation from DMSO.

[Ni(L^1)(Py)] (2): Yield: 70%. Anal. calc. for $C_{19}H_{15}FN_4NiOS$: C, 53.68; H, 3.56; N, 13.18. Found: C, 53.65; H, 3.59; N, 13.16. Main IR peaks (KBr, cm^{-1}): 3229 s ν(N(1)–H), 1613 s ν(C=C), 1521 s, 1417 m ν(–C(8)=N(3)), 736 s ν(C(7)–S(1)). ^{1}H NMR (DMSO–d_6, 400 MHz) δ: 9.47 (s, 1H, –C(7)–N(1)H), 8.35 (s, 1H, –N(3)=C(8)H), 8.84–6.59 (m, 13H, C_6H_4).

[Ni(L^2)(PPh_3)]·DMSO (3): Yield: 65%. Anal. calc. for $C_{34}H_{31}BrN_3NiO_2PS_2$: C, 54.64; H, 4.18; N, 5.62. Found: C, 54.69; H, 4.19; N, 5.78. Main IR peaks (KBr, cm^{-1}): 3257 s ν(N(1)–H), 1624 s ν(C=C), 1545 s, 1425 m ν(–C(8)=N(3)), 1098 s ν(P–C), 747 s ν(C(7)–S(1)). ^{1}H NMR (DMSO–d_6, 400 MHz) δ: 9.58 (s, 1H, –C(7)–N(1)H), 8.69 (s, 1H, –N(3)=C(8)H), 7.77–6.35 (m, 23H, C_6H_4), 2.54(s, 6H, DMSO).

[Ni(L^2)(Imz)] (4): Yield: 68%. Anal. calc. for $C_{17}H_{14}BrN_5NiOS$: C, 42.99; H, 2.97; N, 14.74. Found: C, 42.95; H, 2.99; N, 14.72. Main IR peaks (KBr, cm^{-1}): 3251 s ν(N(1)–H), 1619 s ν(C=C), 1556 s, 1428 m ν(–C(8)=N(3)), 741 s ν(C(7)–S(1)). ^{1}H NMR (DMSO–d_6, 400 MHz) δ: 9.60 (s, 1H, –C(7)–N(1)H), 8.71 (s,1H, –N(3)=C(8)H), 7.03–6.79 (m, 12H, C_6H_4).

[Ni(L^3)(4–pic)] (5): Yield: 67%. Anal. calc. for $C_{21}H_{20}N_4NiO_2S$: C, 55.90; H, 4.47; N, 12.42. Found: C, 55.87; H, 4.43; N, 12.46. Main IR peaks (KBr, cm^{-1}): 3263 s ν(N(1)–H), 1622 s ν(C=C), 1542 s, 1430 m ν(–C(8)=N(3)), 739 s ν(C(7)–S(1)). ^{1}H NMR (DMSO–d_6, 400 MHz) δ: 9.23 (s, 1H, –C(7)–N(1)H), 8.19 (s, 1H, –N(3)=C(8)H), 8.68–6.57 (m, 12H, C_6H_4), 3.69 (s, 3H, –C(4)–OCH_3), 2.37 (s, 3H, 4–pic–CH_3).

2.2.3.3. Synthesis of [{Ni(L^3)}$_2$(μ–4,4′–byp)]·2DMSO (6). To a solution of H_2L^3 (0.301 g, 0.100 mmol) in hot methanol, triethylamine (0.202 g, 0.2 mmol) was added followed by solid $Ni(OAc)_2$ salt (0.248 g, 0.100 mmol) and 4,4′–bypiridine (0.078 g, 0.050 mmol). The mixture was refluxed for 3 h, clear reddish brown solution was obtained which was filtered and allowed to evaporate at room temperature. Reddish brown crystals suitable for X–ray crystallography were obtained from DMSO by slow evaporation. Yield: 65%. Anal. calc. for $C_{44}H_{46}N_8Ni_2O_6S_4$:

C, 51.38; H, 4.51; N, 10.89. Found: C, 51.43; H, 4.50; N, 10.84. Main IR peaks (KBr, cm^{-1}): 3268 s ν(N(1)–H), 1624 s ν(C=C), 1524 s, 1416 m ν(–C(8)=N(3)), 741 s ν(C(7)–S(1)). ^{1}H NMR (DMSO–d_6, 400 MHz) δ: 9.25 (s, 1H, –C(7)–N(1)H), 8.27 (s, 1H, –N(3)=C(8)–H), 9.00–6.59 (m, 12H, C_6H_4), 3.70 (s, 3H, –C(4)–OCH_3).

2.2.4. X–ray crystallography. Single crystals of complexes were mounted on a Bruker Smart Apex CCD diffractometer (**1** and **2**), Bruker Smart Apex II diffractometer (**3** and **6**) and Stoe Mark II–Image Plate diffracttometer (**5**) equipped with a graphite monochromator and a Mo Kα radiator (λ) 0.71073 Å. Crystallographic data and details of refinement are given in **Table 2.1**. Details of the classical hydrogen bonding are given in **Table 2.2**. The unit cell dimensions and intensity data were measured at 293 (2) K for **1** and **2**, 100 (2) K for **3** and **6** and 173 K for **5**. The intensity data were corrected for Lorentz, polarization and absorption effects. Absorption corrections were applied using SADABS[45] and the structures were solved by direct methods using the program SHELXS–97[46] and refined using least squares with the SHELXL–97[46] software program. Hydrogens were either found or placed in calculated positions and isotropically refined using a riding model. The non–hydrogen atoms were refined anisotropically.

Table 2.1. Crystal and refinement data of complexes 1–3, 5 and 6

Compound	**1**	**2**	**3**	**5**	**6**
Formula	$C_{32}H_{25}FN_3NiOPS$	$C_{19}H_{15}FN_4NiOS$	$C_{34}H_{31}BrN_3NiO_2PS_2$	$C_{21}H_{20}N_4NiO_2S$	$C_{44}H_{46}N_8Ni_2O_6S_4$
M	608.29	425.12	747.33	451.18	1028.55
Crystal system	Triclinic	Monoclinic	Triclinic	Triclinic	monoclinic
Space group	*P* 1	*P* $2_1/c$	*P* ī	*P* ī	*P* $2_1/n$
a(Å)	7.772(11)	13.081(8)	14.536(6)	9.858(7)	9.106(4)
b(Å)	9.098(13)	5.800(3)	14.901(7)	10.134(8)	22.964(10)
c(Å)	11.332(16)	23.584(15)	16.450(7)	11.915(8)	11.561(5)
α (°)	68.759(2)	90	91.83(4)	112.224(5)	90
β (°)	82.879(2)	102.298(4)	98.69(3)	98.817(5)	111.370(10)
γ (°)	69.544(2)	90	110.60(4)	103.001(6)	90
V($Å^3$)	699.91(17)	1748.53(18)	3283.00(2)	1035.57(15)	2251.61(17)
Z	1	4	4	2	2
D_{calc}($g.cm^{-3}$)	1.443	1.615	1.512	1.447	1.517
F(000)	314	872	1528	468	1068
μ(Mo-Kα)(mm^{-1})	0.863	1.256	2.020	1.062	1.080
max./min.trans.	0.991 and 0.874	0.987 and 0.895	0.927 and 0.435	1.000 and 0.919	0.963 and 0.856
2θ(max)(^{o})	26.00	30.5	27.71	25.63	29.51
Reflections collected / unique	7228/5331 [R(int) = 0.0176]	26906/5357 [R(int) = 0.0808]	53431/15052 [R(int) = 0.0713]	12009/3894 R(int) = 0.024]	40605/5975 [R(int) = 0.0868]
R_1[I>2σ(I)]	R1 = 0.0405, wR2 = 0.0689	R1 = 0.0457, wR2 = 0.0722	R1 = 0.0454, wR2 = 0.1110	R1 =0.0239, wR2 = 0.0564	R1 = 0.0413, wR2 = 0.1106
wR_2[all data]	R1 = 0.0474, wR2 = 0.0733	R1 = 0.1269, wR2 = 0.0916	R1 = 0.1019, wR2 = 0.1459	R1 =0.0239, wR2 = 0.0581	R1 = 0.0753, wR2 = 0.1354
S[goodness of fit]	1.053	0.969	0.811	1.01	0.844
min./max. res. ($e.Å^{-3}$)	0.468/-0.205	0.298/-0.398	0.546/-0.717	-0.23/0.23	0.377/-0.544

Table 2.2. Hydrogen bond distances (Å) and angles (°) for 1–3, 5 and 6

D–H...A	D–H(Å)	D···A(Å)	H····A(Å)	<D–H····A(°)
*[Ni(L^1)(PPh_3)] (**1**)*				
C22–H22····S1[a]	0.91(4)	3.707(6)	2.92(5)	144.8(31)
C30–H30····F1[b]	0.93(1)	3.211(7)	2.50(1)	133.4(43)
C24–H24····O1[c]	0.99(5)	3.428(7)	2.57(4)	145.9(35)
Symmetry transformations used to generate equivalent atoms: (a) x,y,z ; (b) x+2,+y–1,+z+1; (c) x,+y+1,+z				
*[Ni(L^1)(Py)] (**2**)*				
N1–H1····S1[b]	0.77(3)	3.584(3)	2.84(3)	162.6(24)
C12–H12····F1[a]	0.88(3)	3.436(4)	2.60(3)	159.2(25)
Symmetry transformations used to generate equivalent atoms: (a) –x,+y+1/2+1,–z+1/2; (b) -x,-y-1,–z+1				
*Ni(L^2)(PPh_3)]·DMSO (**3**)*				
N1A–H1A····S2[a]	0.88	3.769(4)	2.90	169.0
N1A–H1A····O2[a]	0.88	2.854(4)	2.01	161.5
N1–H1····S2A[b]	0.88	3.829(4)	3.01	155.0
N1–H1····O2A[b]	0.88	2.917(4)	2.04	171.7
Symmetry transformations used to generate equivalent atoms: (a) –x, –y+1, –z+1; (b)–x+1, –y+1, –z+1				
*Ni(L^3)(4-Pic)] (**5**)*				
N1–H1N .. N2[a]	0.83(2)	2.14(2)	2.962(2)	173(2)
C20–H20B .. S1[b]	0.98	2.86	3.764(2)	154
Symmetry transformations used to generate equivalent atoms: (a) −*x*+1, −*y*+1, −*z*+1; (b) −*x*, −*y*+1, −*z*				
[{Ni(L^3)}$_2$(μ–4,4′-byp)]·2DMSO (**6**)				
N1–H1····O3[b]	0.93(4)	2.839(3)	1.91(4)	178.2(33)
N1–H1····S2[b]	0.93(4)	3.807(2)	2.95(3)	153.0(29)
C15–H15····O3[a]	0.93(4)	3.308(4)	2.55(4)	138.7(34)
C6–H6····O3[b]	0.94(3)	3.359(3)	2.61(3)	136.7(26)
C8–H8····O1[c]	0.97(3)	3.563(3)	2.61(3)	165.8(24)
C21–H21a····O2[d]	0.99(3)	3.332(4)	2.39(3)	159.2(27)
C21–H21c····S1[e]	0.92(3)	3.814(3)	2.97(4)	153.9(30)
Symmetry transformations used to generate equivalent atoms: (a) x, y, z ; (b) –x+1,-y,–z+1; (c) x+1/2,–y+1/2,+z+1/2; (d) x,+y,+z–1; (e) x+1,+y,+z				

2.2.5. Antibacterial activity. The antibacterial activity of the compounds (ligands and complexes) was studied against *Escherichia coli (E. coli) and Bacillus* by agar well diffusion technique. Mueller Hinton-agar (containing 1% peptone, 0.6% yeast extract, 0.5% beef extract and 0.5% NaCl, at pH 6.9–7.1) plates were prepared and 0.5 – McFarland culture (1.5×10^8 cells/mL) of the test organisms were swabbed onto the agar plate (as per CLSI guidelines, 2006). The compounds were dissolved in DMSO varying their concentration from 1000 µg/mL–1.95 µg/mL. Nine millimetre wide wells were dug on the agar plate using a sterile cork borer. 100 µg/mL of each compound from all dilutions were added into the wells using a micropipette. These plates were incubated for 24 h at 35 ± 2 °C. The growth of the test organisms was inhibited by diffusion of the compounds and then the inhibition zones developed on the plates were measured.[47,48] The effectiveness of an antibacterial agent in sensitivity is based on the diameter of the zones of inhibition, which was measured to the nearest millimeter (mm). The standard drug Vancomycin was also tested for its antibacterial activity at the same concentration and under similar conditions to that of the compounds as a positive control. DMSO was used as a negative control under the same conditions for each organism.

2.3. RESULTS AND DISCUSSION

2.3.1. Synthesis. In order to explore the possibility of forming monomeric complexes by splitting the sulfur bridge in the {M(L)}n type complexes, the reaction of the thiosemicarbazones with $Ni(OAc)_2$ has been carried out with different monodentate ligands (Q), viz. triphenylphosphine (PPh_3), pyridine (Py), imidazole (Imz) and 4–picoline (4–Pic) in refluxing methanol. From each of these reactions a mixed-ligand monomeric complex of type [Ni(L)(Q)] (Q = PPh_3, Py, Imz, 4–Pic) (**1**–**5**) has been obtained. The mixed-ligand dinuclear dinickel(II) complex $[\{Ni(L^3)\}_2(\mu\text{–}4,4'\text{–byp})]\cdot 2DMSO$ (**6**) was achieved by the reaction of thiosemicarbazone (H_2L^3) with $Ni(OAc)_2$ using 4,4'–bipyridine as exo–bidentate ligand under reflux condition. The synthetic methods of all the complexes are illustrated in **Scheme 2.1**.

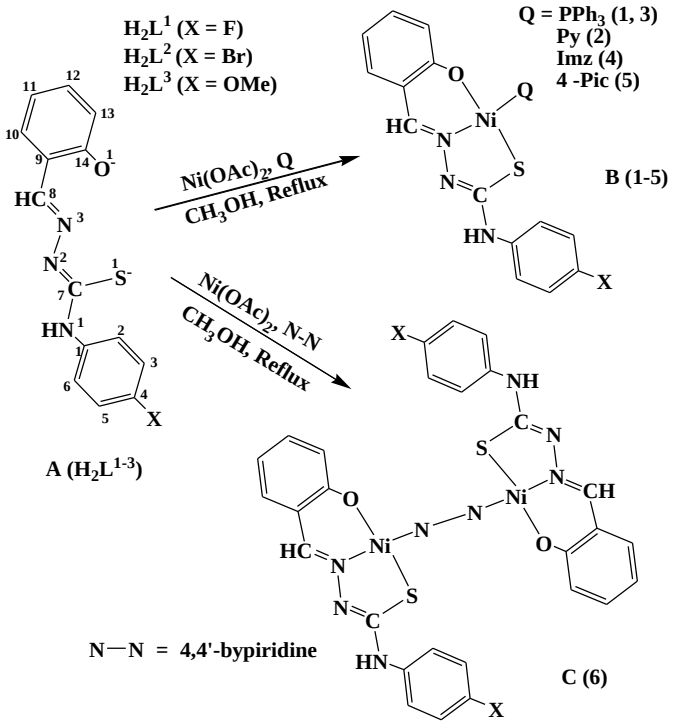

Scheme 2.1. Schematic representation of ligands (**A**) and synthesis of mixed–ligand Ni(II) complexes (**B** and **C**).

2.3.2. Structure. The observed elemental (C, H, N) analytical data of all the complexes are consistent with their compositions. It appears from the formulation of the complexes that the thiosemicarbazones are serving as tridentate ligands in them. In order to authenticate the coordination mode of the thiosemicarbazones in these complexes, the structure of few complexes have been determined by X–ray crystallography.

2.3.2.1. Description of X-ray structures of complexes 1–3 and 5. The atom numbering schemes for these complexes are given in **Figures 2.1–2.4** respectively with the relevant bond distances and angles collected in **Table 2.3**. The structures show that the thiosemicarbazone ligand (L^{2-}) is coordinated to nickel in the expected tridentate fashion (B, **Scheme 2.1**), forming a six- and a five-membered chelate ring with O(1)–Ni(1)–N(3) and N(3)–Ni(1)–S(1) bite angles of 94.4 (2)° and 87.0(1)° (**1**), 95.3(8)° and 87.3(6)° (**2**), 95.2(1)° and 87.1(1)° (**3**) and 96.16(6)° and 87.49(4)° (**5**) respectively. The co-ligand {Q = triphenylphosphine (**1** and **3**), pyridine (**2**) and 4-pic (**5**)} is coordinated to the metal center, and is trans to the nitrogen atom. The rather large Ni(1)–P(1)/N(4) distance are [2.224(1) Å (**1**), 1.912(2) Å (**2**), 2.205(2) Å (**3**) and 1.921(16) Å(**5**)] revealed that the triphenylphosphine, pyridine or picoline moiety are also rather weakly coordinated to the Ni-centre.[49] The nickel center in all compounds is thus nested in a NOSN or NOSP core, which is slightly distorted from an ideal square-planar geometry, as reflected in the bond parameters around the metal center. The Ni–N, Ni–O, Ni–P/N (co-ligand) and Ni–S distances are normal, as observed in other structurally characterized complexes of nickel containing these bonds.[22,27,28] Structural characterization of complex **4** by X–ray crystallography has not been possible, as its single crystals could not be grown. As all five complexes have been synthesized similarly and display similar properties, the [Ni(L^2)(Q)] (Q = Imz) complex is assumed to have the similar structure as **1**–**3** and **5**.

All the molecules are found to show either inter (**1, 2** and **5**) or intra (**1** and **3**) molecular hydrogen bonding. Complex **1** is found to show both inter and intra molecular hydrogen bonding. [Ni(L^1)(PPh_3)] (**1**) molecules form a polymeric unit via a pair of hydrogen bonds between the phenolic oxygen O(1) of one molecule with the phenyl (PPh_3) proton C(24)–H of other moiety (**Figure 2.5**) and between the fluorine F(1) of one molecule with the phenyl (PPh_3) proton C(30)–H of other moiety (**Figure 2.6**) forming intermolecular hydrogen bonding. Another hydrogen bonding between thione sulfur S(1) and phenyl (PPh_3) hydrogen, C(22)–H, is also observed constituting intramolecular hydrogen bond for **1**. The complex **2** is found to show only

inter molecular hydrogen bonding. Two [Ni(L^1)(Py)] (**2**) molecules form a dimeric unit via a pair of reciprocal hydrogen bonds between the N(1)–H proton of one molecule with the thione sulfur S(1) of other moiety. The complex **2** is also found to show a polymeric one-dimensional zig–zag chain (**Figure 2.7**) through inter molecular hydrogen bonding between the fluorine F(1) of one molecule with the phenyl proton C(12)–H of other moiety. For complex **3** there is only one possible hydrogen bonding found between the N(1)–H proton of the ligand and the O(2) and S(2) atom of solvent (DMSO) molecule. The complex **5** is found to show only inter molecular hydrogen bonding (**Figure 2.8**). In the crystal, [Ni(L^3)(4–Pic)] (**5**) molecules are linked to form inversion dimmers via a pair of N–H...N hydrogen bonds between the N(1)–H proton of one molecule with the imine nitrogen N(2) of other molecule. The consequence of this is that to minimize steric hindrance the ligand is no longer relatively planar, with the methoxybenzene ring [(C(1)–C(6)] being inclined to the mean plane of the remaining hetero atoms [N(1)–N(3)/S(1)/O(1)/C(7)–C(14); maximum deviation 0.056(2) Å for atom C(7)] of the ligand by 76.84(8)°. The same dihedral angle in compounds **1**–**3** varies between 15.74(10) to 25.70(17)°. Complex **5** is also found to show inter molecular C–H...S hydrogen bonding between the thione sulphur S(1) of one molecule with a methoxy proton C(20)–H of a neighboring molecule.

2.3.2.2. Description of the X-ray structure of complex 6. The molecular structure and atom-labeling scheme for complex **6** are shown in **Figure 2.9**. Selected bond distances and angles are collected in **Table 2.3**. Complex, **6** crystallizes in the monoclinic space group $P\ 2_1/n$ with the molecule sitting across a crystallographic center of inversion. Each half of the complex *[{Ni(L^3)}$_2$(μ–4,4'–byp)]·2DMSO* closely resembles the structure of **2**, which essentially consists of the same donor atoms attached to its Ni(II) center in the same geometric pattern with closely matching dimensions. The only significant difference observed in the case of **6** is that the Ni(1)–N(4) bond involving the nickel acceptor center and the N(4) aromatic nitrogen atom of 4,4'-byp is longer (1.920(2) Å) than the corresponding Ni(1)–N(4) (pyridine) bonds in **2**, which is 1.912(2) Å. This lengthening indicates comparatively weaker binding of 4,4'–byp nitrogen N(4) to the Ni(II) center. This is quite usual for this type of bridging systems.[50,51] The two pyridine rings of 4,4'–byp lie in the same plane and are perpendicular to the equatorial planes of the two halves of the two [Ni(L)] units. The chelate bite angles for the five- and six-membered

rings have values within the expected ranges [S(1)–Ni(1)–N(3), 87.1(7)°; O(1)–Ni(1)–N(3), 96.1(9)°].[52] Complex **6** is found to show both inter and intra molecular hydrogen bonding.

Table 2.3. Selected geometric parameters (Å, º) for [Ni(L^1)(PPh_3)] (1), [Ni(L^1)(Py)] (2), [Ni(L^2)(PPh_3)]·DMSO (3), Ni(L^3)(4-Pic)] (5) and [{Ni(L^3)}$_2$(μ–4,4′–byp)]·2DMSO (6)

	Complex (**1**)	Complex (**2**)	Complex (**3**)	Complex (**5**)	Complex (**6**)
			Bond Distances		
Ni(1)–O(1)	1.848(4)	1.854(2)	1.838(3)	1.846(11)	1.851(2)
Ni(1)–N(3)	1.882(3)	1.849(2)	1.877(3)	1.858(15)	1.856(2)
Ni(1)–S(1)	2.137(1)	2.154(8)	2.146(1)	2.148(5)	2.139(8)
Ni(1)–P(1)	2.224(1)	—	2.205(2)	—	—
Ni(1)– N(4)	—	1.912(2)	—	1.921(16)	1.920(2)
			Bond Angles		
O(1)–Ni(1)–N(3)	94.4(2)	95.3(8)	95.2(1)	96.16(6)	96.1(9)
O(1)–Ni(1)–S(1)	178.1(1)	176.1(6)	177.3(9)	176.00(5)	175.6(6)
N(3)–Ni(1)–S(1)	87.0(1)	87.3(6)	87.1(1)	87.49(4)	87.1(7)
O(1)–Ni(1)–P(1)	88.0(1)	—	86.5(9)	—	—
O(1)–Ni(1)–N(4)	—	85.8(8)	—	87.18(6)	87.5(9)
N(3)–Ni(1)–P(1)	177.5(1)	—	173.1(1)	—	—
N(3)–Ni(1)–N(4)	—	177.9(9)	—	176.60(6)	176.3(1)
S(1)–Ni(1)–P(1)	90.5(5)	—	91.5(5)	—	—
N(4)–Ni(1)–S(1)	—	91.7(6)	—	89.20(4)	89.4(7)

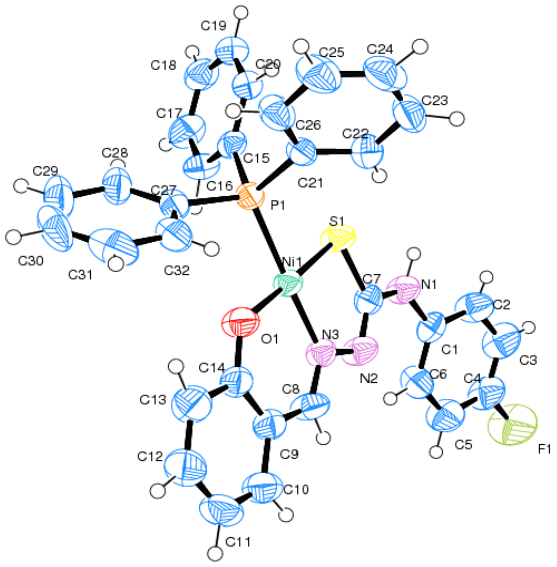

Figure 2.1. ORTEP diagram of [Ni(L^1)(PPh_3)] (**1**) with atom labeling scheme.

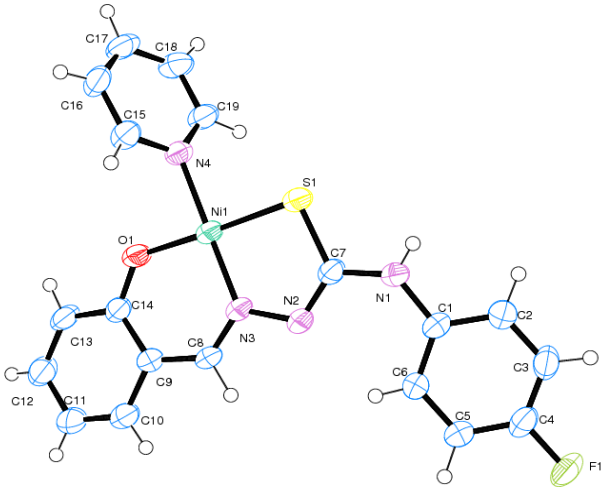

Figure 2.2. ORTEP diagram of [Ni(L^1)(Py)] (**2**) with atom labeling scheme.

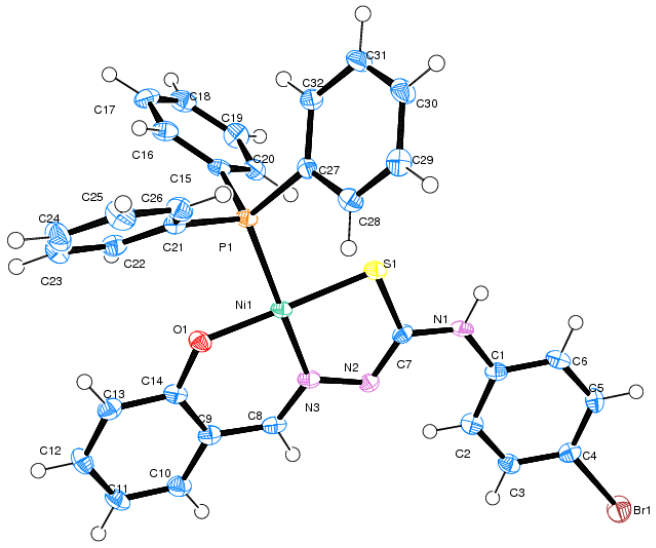

Figure 2.3. ORTEP diagram of [Ni(L^2)(PPh_3)]·DMSO (**3**) with atom labeling scheme.

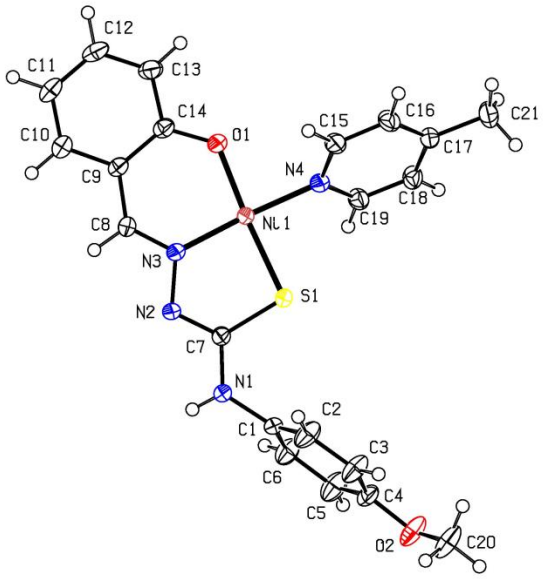

Figure 2.4. ORTEP diagram of [Ni(L^3)(4–Pic)] (**5**) with atom labeling scheme

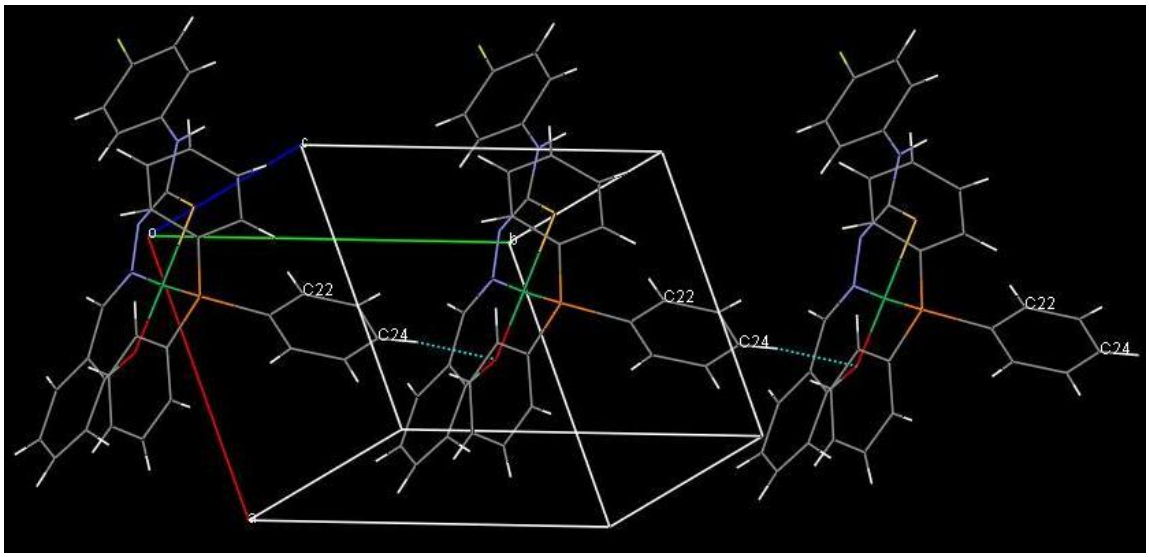

Figure 2.5. Inter molecular hydrogen bonding diagram of complex **1**.

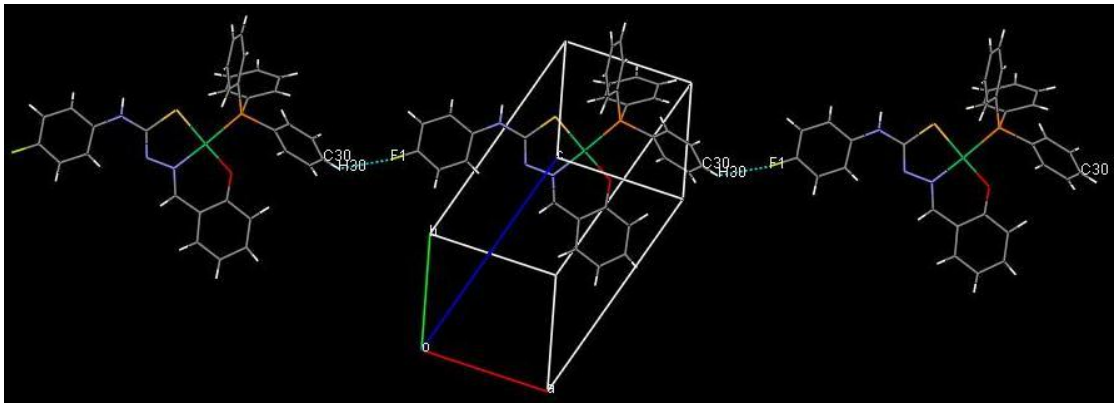

Figure 2.6. One-dimensional zig–zag chain through inter molecular hydrogen bonding in **1**.

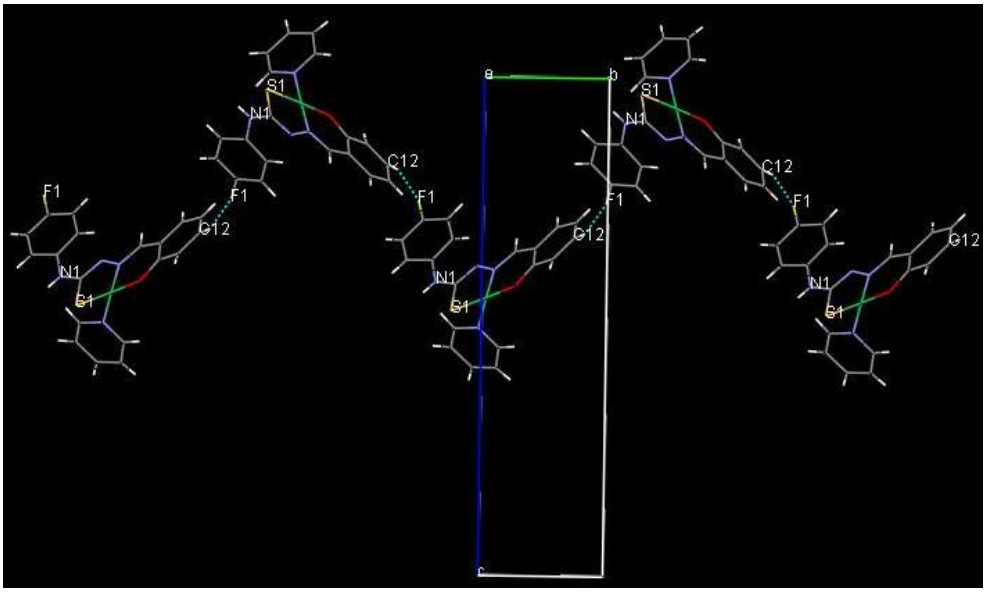

Figure 2.7. One-dimensional zig-zag chain through inter molecular hydrogen bonding in **2**.

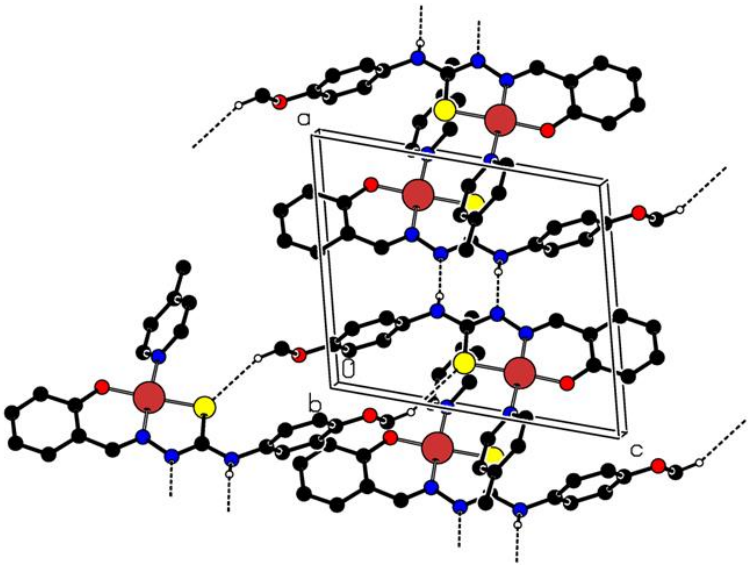

Figure 2.8. Hydrogen bonding diagram of complex **5**.

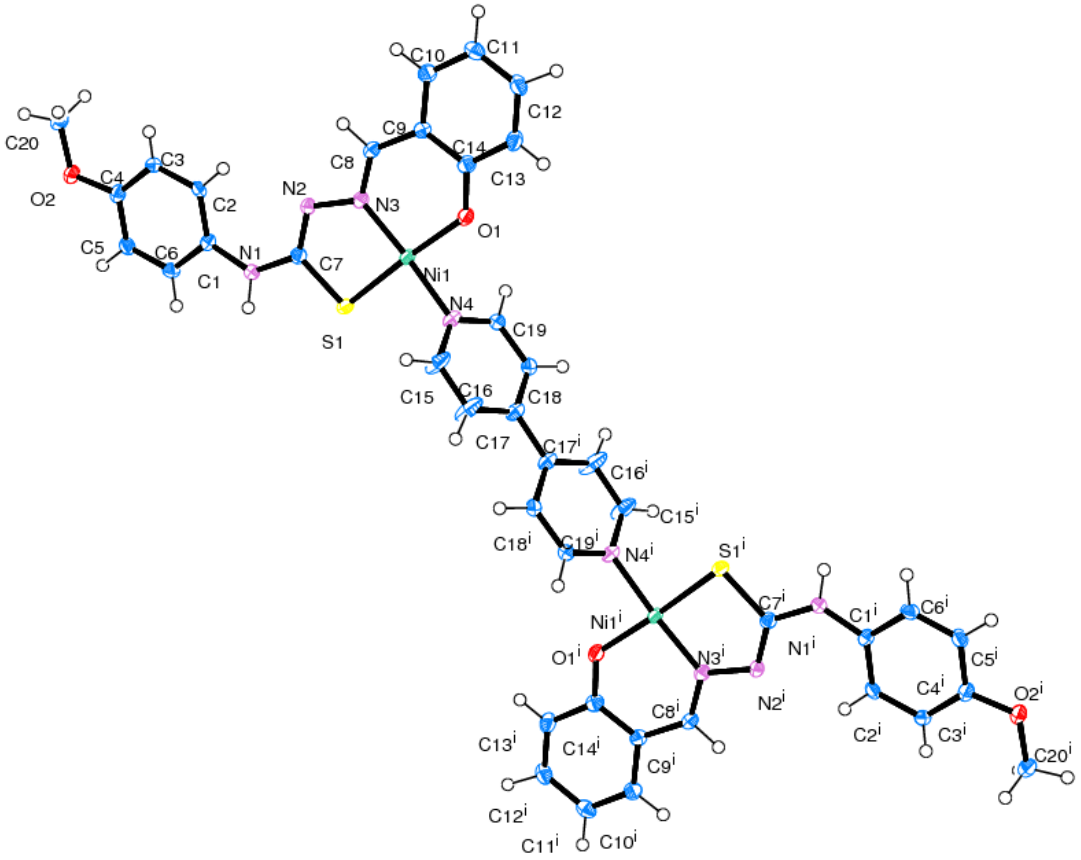

Figure 2.9. ORTEP diagram of [{Ni(L^3)}$_2$(μ–4,4′–byp)]·2DMSO (**6**) with atom labeling scheme.

2.3.3. Spectral characteristics

2.3.3.1. IR spectroscopy. The infrared spectra of all the complexes are mostly similar. The ligands exhibit, bands due to ν(–C(7)N(1)–H), ν(–C(7)N(2)–H) and ν(–C(14)O(1)–H) moieties in 3357–2994 cm^{-1} region, however the complexes do not exhibit, ν(–C(7)N(2)–H) as well as the ν(–C(14)O(1)–H) bands. Thus it reveals that the ligands coordinate to the metal centre in the anionic forms. The sharp band in the range, 752–749 cm^{-1} due to ν(C(7)–S(1)) stretching in the ligand is lowered by 10–15 cm^{-1}, indicating participation of the thione sulfur in coordination.[53,54] The characteristic ν(P–C) bands at 1094 and 1098 cm^{-1} in complexes **1** and **3** respectively attribute to the presence of PPh_3.[27] The representative IR Spectra of complex [Ni(L^1)(PPh_3)] (**1**) is shown in **Figure 2.10**.

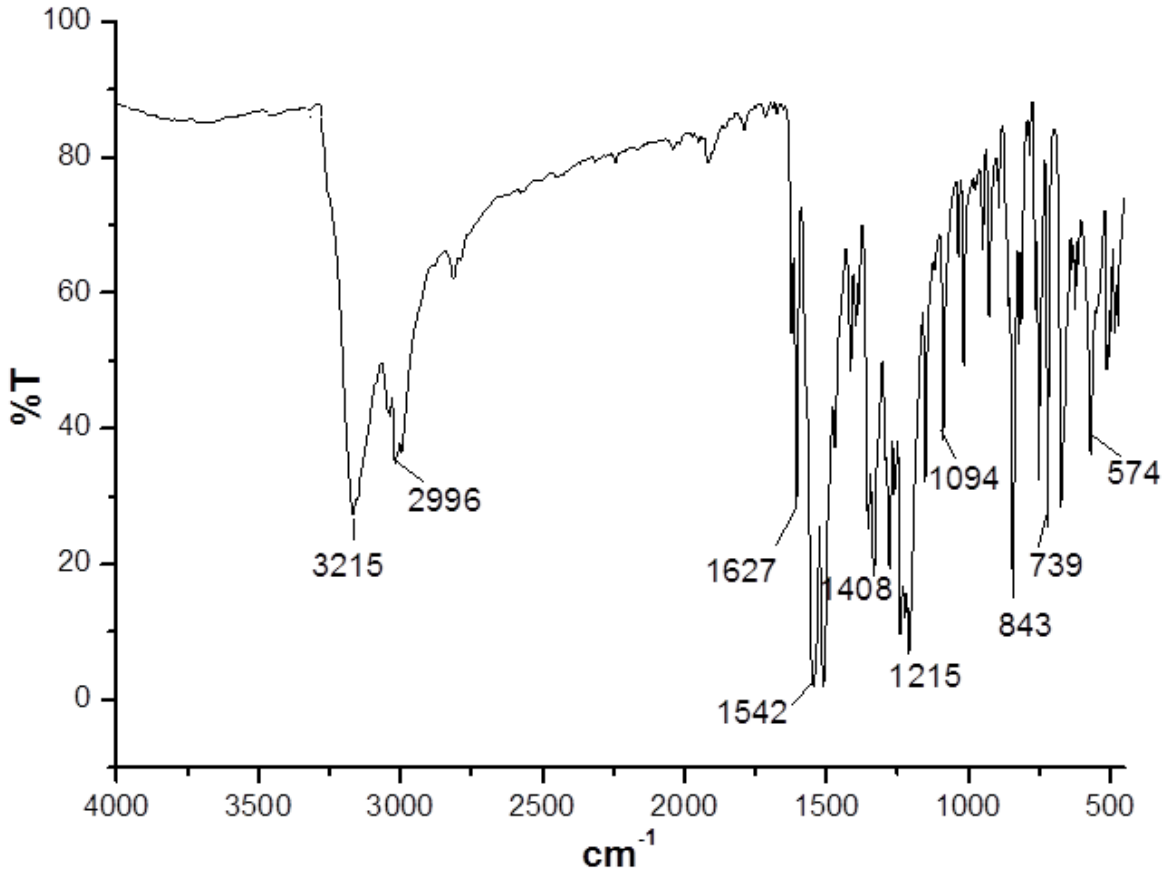

Figure 2.10. FTIR spectra of [Ni(L^1)(PPh_3)] (**1**).

2.3.3.2. UV spectroscopy. The electronic spectra of the complexes (**Table 2.4**) were recorded using DMSO solutions. The main features of all the spectra are quite similar. Three strong absorptions are observed in the wavelength range 430–220 nm. The lower energy absorptions at around 404–428 nm are ascribable to the ligand–to–metal charge transfer transitions whereas the higher energy absorptions are likely to be due to ligand centered transitions.[55] The representative electronic absorption spectra of [Ni(L^1)(Py)] (**2**) is shown in **Figure 2.11**.

Table 2.4. Electronic spectral[a] data for the studied complexes

Complex	λ_{max}/nm (ε/dm^3 mol^{-1} cm^{-1})
[Ni(L^1)(PPh_3)] (**1**)	416 (7300), 372 (14100), 269 (22700)
[Ni(L^1)(Py)] (**2**)	420 (8400), 371 (13400), 262 (23300)
[Ni(L^2)(PPh_3)]·DMSO (**3**)	412 (5500), 368 (13510), 264 (19654)
[Ni(L^2)(Imz)] (**4**)	422 (7600), 354 (13650), 256 (18968)
[Ni(L^3)(4–Pic)] (**5**)	428 (8500), 335 (13480), 292 (20843)
[{Ni(L^3)}$_2$(μ–4,4′–byp)]·2DMSO (**6**)	404 (6700), 357 (13780), 280 (22156)

[a] In DMSO

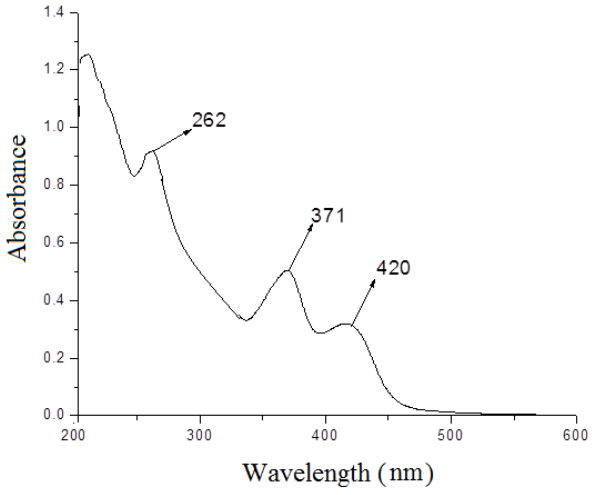

Figure 2.11. Electronic absorption spectra of [Ni(L^1)(Py)] (**2**).

2.3.3.3. NMR spectroscopy. The ^{1}H NMR spectral data of the free ligands and its corresponding nickel(II) complexes (**1**–**6**) were recorded using DMSO-d_6. The spectrum of the free ligands exhibit two close but separate singlets in the range 11.88–9.95 ppm due to OH(–C(14)–O(1)H) and NH (–C(7)–N(2)H) groups respectively which are absent in the spectra of complexes indicating coordination of these groups to the metal center. Signals for aromatic protons are found as multiplets in the 9.00–6.34 ppm range.[56] Detailed NMR data has been included in the experimental section. The representative ^{1}H NMR spectra of [Ni(L^1)(PPh_3)] (**1**) in DMSO–d_6 is shown in **Figure 2.12**.

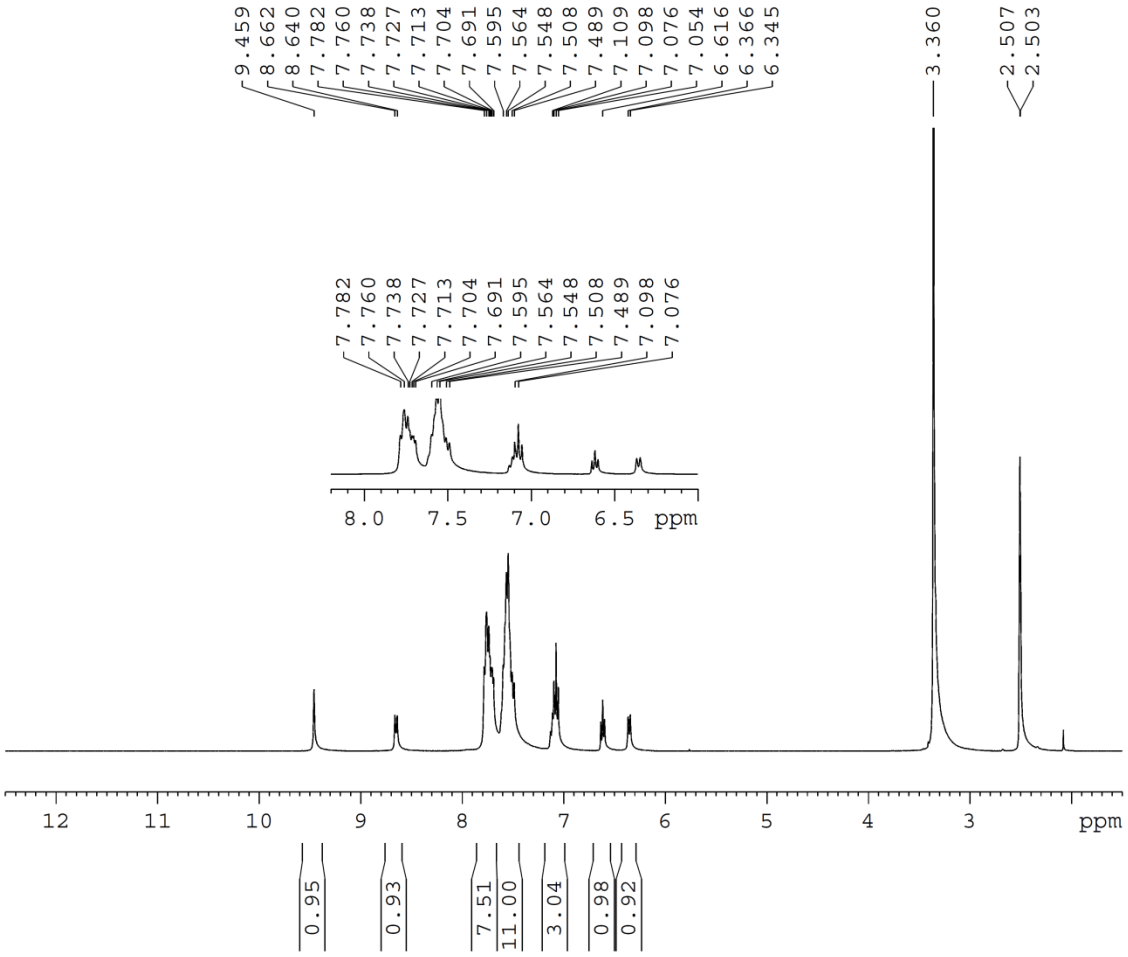

Figure 2.12. ^{1}H NMR spectra of [Ni(L^1)(PPh_3)] (**1**) in DMSO–d_6.

2.3.4. Electrochemical properties. Electrochemical properties of the complexes (**1**–**6**) have been studied by cyclic voltammetry in acetonitrile solution (0.1 M TEAP). Voltammetric data are given in **Table 2.5**, and a selected representative voltammogram of $[Ni(L^2)(PPh_3)]\cdot DMSO$ (**3**) is shown in **Figure 2.13**. All the mononuclear complexes (**1**–**5**) show one irreversible oxidative response[57] on the positive side of Ag/AgCl and two irreversible reductive responses[57] on the negative side. The two waves on the negative side of Ag/AgCl at E_{pa} values within the potential window –0.886 to –1.093 V and –1.681 to –1.793 V, are assigned to the reduction of the central metal Ni(II)/Ni(I) and ligand respectively. The wave on the positive side of Ag/AgCl at E_{pa} values within the potential window 0.894 to 1.029V is assigned to the oxidation of the metal Ni(II)/Ni(III). The dinuclear complex **6** exhibits three successive irreversible one-electron reductions within the potential window -1.096 to -1.251 V versus Ag/AgCl in acetonitrile which are assigned to Ni^{II}–Ni^{II}/Ni^{I}–Ni^{II} and Ni^{I}–Ni^{II}/Ni^{I}–Ni^{I} processes and the ligand-centered reduction, respectively.[51] The dinickel(II) also shows two irreversible oxidative response[58] on the positive side of Ag/AgCl within the potential window 0.674 to 0.980 V, are assigned to the oxidation of the metal Ni(II)/Ni(III).

The potentials of both Ni(II)–Ni(III) oxidation and Ni(II)–Ni(I) reduction in the complexes has been found to be dependent to the nature of the substituent X in the phenyl fragment of 4–X–phenylthiosemicarbazone, this reflects the effect of the electronic nature of the substituents. The potential increases with increasing electron-withdrawing character of the substituent X. Both the reduction and oxidation of the metal centre occurs at the highest potential for the most electron withdrawing substituent (X = F, complexes **1** & **2**) while for the most electron releasing substituent (X = OMe, complexes **5** & **6**) it occurs at the lowest potential.[59–61]

Table 2.5. Cyclic voltammetric[a] results for nickel(II) complexes at 298 K

Complex	Potentials (V) versus Ag/AgCl		
	M(II)/M(III)	M(II)/M(I)	Ligand–centered reduction
$[Ni(L^1)(PPh_3)]$ (**1**)	1.023	–0.984	–1.684
$[Ni(L^1)(Py)]$ (**2**)	1.029	–0.886	–1.681
$[Ni(L^2)(PPh_3)]\cdot DMSO$ (**3**)	0.998	–1.012	–1.774
$[Ni(L^2)(Imz)]$ (**4**)	0.921	–1.008	–1.781
$[Ni(L^3)(4\text{–}Pic)]$ (**5**)	0.894	–1.093	–1.793
$[\{Ni(L^3)\}_2(\mu\text{–}4,4'\text{–}byp)]\cdot 2DMSO$ (**6**)	0.674, 0.980	–1.096, –1.251	–1.803

[a] Solvent: CH_3CN; working electrode: platinum; auxiliary electrode: platinum; reference electrode: Ag/AgCl; supporting electrolyte: 0.1 M TEAP; scan rate: 100 mV/s.

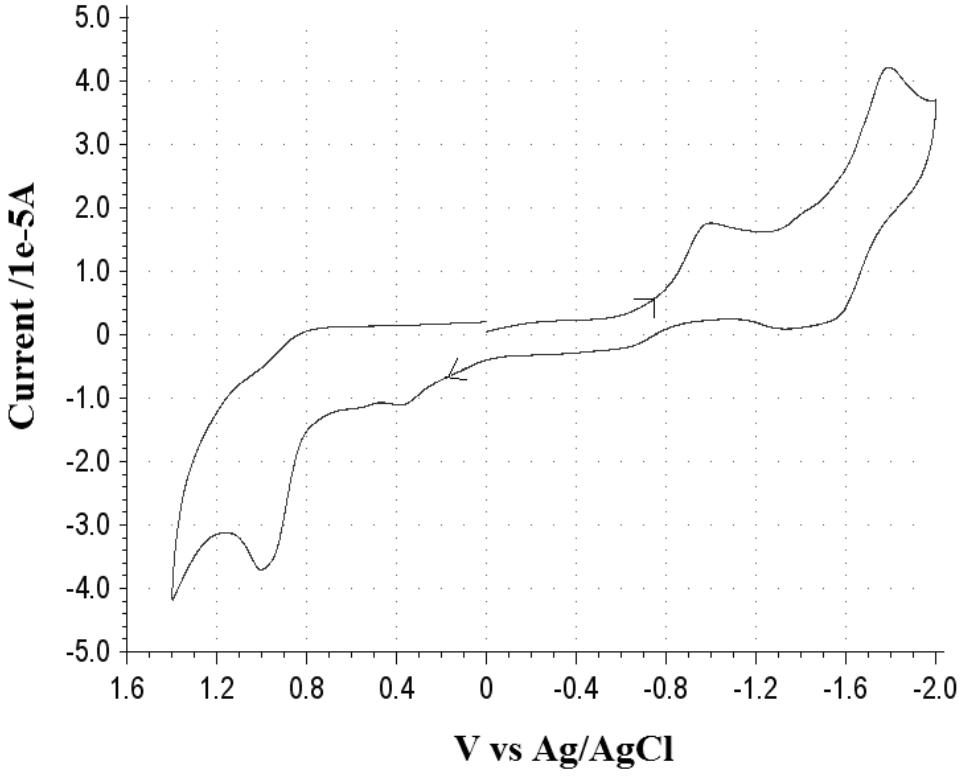

Figure 2.13. Cyclic voltammogram of $[Ni(L^2)(PPh_3)]\cdot DMSO$ (**3**).

2.3.5. Antimicrobial activity. In the present study, the synthesized compounds (**1–6**) showed potential antibacterial activity against the pathogens tested (*E. coli and Bacillus)* by agar well-diffusion method and in some cases they showed promising results by giving the MIC value lesser than the standard drug examined. The results (**Table 2.6**, **Figure 2.14**) also indicate that the corresponding nickel(II) complexes showed much better antibacterial activity with respect to the individual ligand against the same microorganism under identical experimental conditions which is in agreement with reported results.[47,48,62–65] A possible explanation is that, by coordination, the polarity of the ligand and the central metal ion are reduced through the charge equilibration, which favors permeation of the complexes through the lipid layer of the bacterial cell membrane. [47,48,62–65]

From the zone of inhibition, it is observed that the complex **4** showed most promising results as compared to the other compounds of this study and the difference in value may be attributed to the nature of compounds synthesized with imidazole as co–ligands.[66,67]. The antibacterial activity of a similar type of oxo–metal complexes has also been reported [68, 69] recently using the agar well diffusion technique against *E. coli, Shigella, Pseudomonas, Salmonella, Staphylococcus* and *Bacillus*, and the present results are in accordance with the reported values. However, the difference in value may be attributed to the nature of compounds synthesized with different ligands.

Table 2.6. Minimum inhibitory concentration (MIC) value in µg/mL of the Schiff base ligand ($H_2L^{1–3}$), nickel(II) complexes and standard drugs against pathogenic strains

	E.coli	*Bacillus*
H_2L^1	500	250
$[Ni(L^1)(PPh_3)]$ (**1**)	125	125
$[Ni(L^1)(Py)]$ (**2**)	62.5	125
H_2L^2	125	250
$[Ni(L^2)(PPh_3)]\cdot DMSO$ (**3**)	31.2	125
$[Ni(L^2)(Imz)]$ (**4**)	15.6	15.6
H_2L^3	125	250
$[Ni(L^3)(4\text{-Pic})]$ (**5**)	31.2	31.2
$[\{Ni(L^3)\}_2(\mu\text{-}4,4'\text{-byp})]\cdot 2DMSO$ (**6**)	62.5	125
Vancomycin	30	30

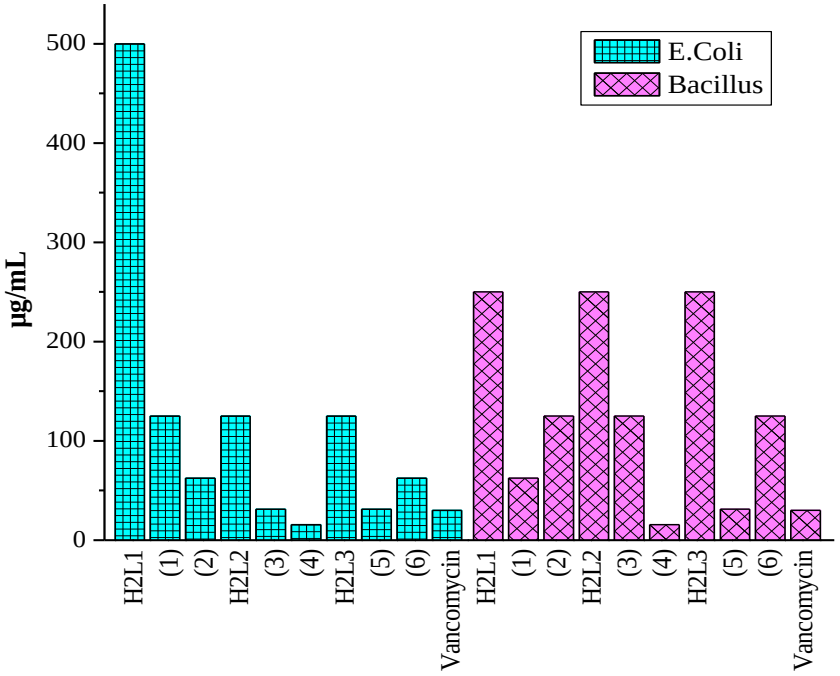

Figure 2.14. Minimum inhibitory concentration (MIC) of the Schiff base ligand ($H_2L^{1–3}$), their corresponding nickel(II) complexes (**1**–**6**) and standard drugs against pathogenic strains.

2.4. CONCLUSION

The study of 6 new Ni(II) complexes of 4–(*p*–X–phenyl)thiosemicarbazone of salicylaldehyde reported in this chapter reveals that the structural parameters (e.g., Ni–N and Ni–P bond distances) and the redox potentials of these complexes can be fine-tuned by changing the substitution in the 4–aryl (X) part. The complexes have been screened for their antibacterial activity against *E. coli and Bacillus*. The minimum inhibitory concentration of these complexes and antibacterial activity indicates compound **4** is the potential lead molecule for drug designing.

2.5. REFERENCES

(1) Kruger, H. J.; Holm, R. H. *J. Am. Chem. Soc.* **1990**, *112*, 2955.

(2) Lu, Z.; White, C.; Rheingold, A. L.; Crabtree, R. H. *Inorg. Chem*. **1993**, *32*, 3991.

(3) Mandal, S.; Bharadwaj, P. K.; Zhou, Z. Y.; Mak, T. C. W. *Polyhedron* **1995**, *14*, 919.

(4) Colpas, G. J.; Kumar, M.; Day, R. O.; Maroney, M. J. *Inorg. Chem.* **1990**, *29*, 4779.

(5) Choudhury, S. B.; Ray, D.; Chakravorty, A. *Inorg. Chem.* **1990**, *29*, 4603.

(6) Ragsdale, S. W.; Wood, H. G.; Morton, J. A.; Ljungdahl, L. G.; Dervartanian, D. V. in: J.*R. Lancaster Jr. (Ed.), The Bioinorganic Chemistry of Nickel, VCH*, New York, **1988** (Chapter 14).

(7) Campbell, M. J. M. *Coord. Chem. Rev.* **1975**, *15*, 279.

(8) Padhye, S. B.; Kauffman, G. B. *Coord. Chem. Rev.* **1985**, *63*, 127.

(9) West, D. X.; Liberta, A. E.; Padhye, S. B.; Chikate, R. C.; Sonawane, P. B.; Kumbhar, A. S.; Yerande, R. G. *Coord. Chem. Rev.* **1993**, *123*, 49.

(10) Klayman, D. L.; Scovill, J. P.; Bartosevich, J. F.; Bruce, J. *J. Med. Chem.* **1983**, *26*, 39.

(11) Casas, J. S.; García-Tasende, M. S.; Sordo, J. *Coord. Chem. Rev.* **2000**, *209*, 197.

(12) Smith, D. R. *Coord. Chem. Rev.* **1997**, *164*, 575.

(13) Ainscough, E. W.; Brodie, A. M.; Ransford, J. D.; Waters, J. M. *Dalton Trans.* **1997**, 1251.

(14) Ali. M. A.; Mirza. A. H.; Hossain. A. M. S.; Nazimuddin. M. *Polyhedron* **2001**, *20*, 1045.

(15) Baldini, M.; Ferrari, M. B.; Bisceglie, F.; Pelosi, G.; Pinelli, S.; Tarasconi, P. *Inorg. Chem.* **2003**, *42*, 2049.

(16) Ferrari, M. B.; Bisceglie, F.; Pelosi, G.; Tarasconi, P.; Albertini, R.; Fava, G. G.; Pinelli, S. *J. Inorg. Biochem.* **2002**, *89*, 36.

(17) Ferrari, M. B.; Bisceglie, F.; Pelosi, G.; Albertini, P.; Dall'Aglio, P. P.; Bergamo, A.; Sava, G.; Pinelli, S. *J. Inorg. Biochem.* **2004**, *98*, 301.

(18) Garcia-Tojal, J.; Pizarro, J. L.; Garcia-Orad, A.; Perez-Sanz, A. R.; Ugalde, M.; Diaz, A. A.; Serra, J. L.; Arriortua, M. I.; Rojo, T. *J. Inorg. Biochem*. **2001**, *86*, 627.

(19) Ferrari, M. B.; Bisceglie, F.; Pelosi, G.; Tarasconi, P.; Albertini, R.; Bonati, A.; Lunghi, P.; Pinelli, S. *J. Inorg. Biochem.* **2001**, *83*, 169.

(20) Afrasiabi, Z.; Sinn, E.; Padhye, S.; Duttab, S.; Padhye, S.; Newton, C.; Anson, C. E.; Powell, A. K. *J. Inorg. Biochem*. **2003**, *95*, 306.

(21) Bermejo, E.; Carballo, R.; Castiñeiras, A.; Domínguez, R.; Liberta, A. E.; Maichle-Mössmer, C.; Salberg, M. M.; West, D. X. *Eur. J. Inorg. Chem*. **1999**, 965.

(22) Datta, S.; Seth, D. K.; Butcher, R. J.; Bhattacharya, S. *Inorg. Chim. Acta* **2011**, *377*, 120.

(23) Priyarega, S.; Kalaivani, P.; Prabhakaran, R.; Hashimoto, T.; Endo, A.; Natarajan, K. *J. Mol. Struct.* **2011**, *1002*, 58.

(24) West, D. X.; Bain, G. A.; Butcher, R. J.; Jasinski, J. P.; Li, Y.; Pozdniakiv, R. Y.; Valdes-Martinez, J.; Toscano, R. A.; Hernandez-Ortega, S. *Polyhedron* **1996**, *15*, 665.

(25) Valdes-Martinez, J.; Hernandez-Ortega, S.; Jimenez, V. B. *Acta Crystallogr., Sect. E: Struct. Rep. Online* **2002**, *58*, m710.

(26) Valdes-Martinez, J.; Hernandez-Ortega, S.; Jimenez, V. B. *Acta Crystallogr., Sect E: Struct. Rep. Online* **2004**, *60*, 42.

(27) Lobana, T. S.; Kumari, P.; Hundal, G.; Butcher, R. J. *Polyhedron* **2010**, *29*, 1130.

(28) Lobana, T. S.; Kumari, P.; Zeller, M.; Butcher, R. J. *Inorg. Chem. Commun*. **2008**, *11*, 972.

(29) Prabhakaran, R.; Karvembu, R.; Hashimoto, T.; Shimizu, K.; Natarajan, K. *Inorg. Chim. Acta* **2005**, *358*, 2093.

(30) Leovac, V. M.; Petrovic, A. F.; Ivegeš, E. Z.; Lukic, S. R. *J. Therm. Anal. Calorim*. **1990**, *36*, 2427.

(31) Purohit, S.; Koley, A. P.; Prasad, L. S.; Manoharan, P. T.; Ghosh, S. *Inorg. Chem*. **1989**, *28*, 3735.

(32) Sengupta, P.; Dinda, R.; Ghosh, S. *Transition Met. Chem*. **2002**, *27*, 665.

(33) Bon, V. V.; Orysyk, S. I.; Pekhnyo, V. I.; Volkov, S. V. *J. Mol. Struct.* **2010**, *984*, 15.

(34) Lhuachan, S.; Siripaisarnpipat, S.; Chaichat, N. *Eur. J. Inorg. Chem.* **2003**, 263.

(35) Yang, J. M.; Ma, W. B.; Chen, B. H.; Huang, G. S.; Ma, Y. X. *Acta Crystallogr. Sect.* **2004**, *E60*, m852.

(36) Kovala-Demertzi, D.; Demertzis, M. A.; Mille,r J. R.; Prampton, C. S.; Jasinski, J. P.; West, D. X. *J. Inorg. Biochem*. **2002**, *92*, 137.

(37) Yadav, P. N.; Demertzis, M. A.; Kovala-Demertzi, D.; Skoulika, S.; West, D. X. *Inorg. Chim. Acta* **2003**, *349*, 30.

(38) Carballo, R.; Casas, J. S.; Garcia-Martinez, E.; Gabian, G. P.; Sanchez, A.; Sordo, J.; Vazquez-Lopez, E. M.; Garcia-Monteagudo, J. C.; Abram, U. J. *J. Organomet. Chem.* **2002**, *656*, 1.

(39) Ashfield, L. A.; Cowley, A. R.; Dilworth, J. R.; Donnely, P. S. *Inorg. Chem.* **2004**, *43*, 4121.

(40) Paul, I.; Basuli, F.; Mak, T. C. W.; Bhattacharya, S. *Angew. Chem., Int. Ed*. **2001**, *40*, 2923.

(41) Orysyk, S. I.; Bon, V. V.; Obolentseva, O. O.; Zborovskii, Y. L.; Orysyk, V. V.; Pekhnyo, V. I.; Staninets, V. I.; Vovk, V. M. *Inorg. Chim. Acta* **2012**, *382*, 127.

(42) Santos, I. G.; Abram, U.; Alberto, R.; Lopez, E. V.; Sanchez, A. *Inorg. Chem*. **2004**, *43*, 1834.

(43) Lobana, T. S.; Bhargava, G.; Sharma, V.; Kumar, M. *Indian J. Chem., Sect. A: Inorg., Bio-inorg., Phys., Theor., Anal. Chem.* **2003**, *42A*, 309.

(44) Part 1: Ghosh S.; Purohit S.; *Indian J. Chem., Sect. A: Inorg., Bio-inorg., Phys., Theor., Anal. Chem.* **1987**, *26A*, 131.

(45) Bruker, SADABS, SAINT, SHELXTL and SMART, Bruker AXS Inc., Madison, Wisconsin, SA, **2003**.

(46) Sheldrick, G. M. *Acta Crystallogr., Sect.* **2008**, *A64*, 112.

(47) Yaul, A. R.; Dhande, V. V.; Bhadange, S. G.; Aswar, A. S. *Russ. J. Inorg. Chem*. **2011**, *56*, 549.

(48) Aziz, A. A. A. *J. Mol. Struct*. **2010**, *979*, 77.

(49) Halder, S.; Butcher, R. J.; Bhattacharya, S. *Polyhedron* **2007**, *26*, 2741.

(50) Dinda, R.; Ghosh, S.; Falvello, L. R.; Tomás, M.; Mak, T. C. W. *Polyhedron* **2006**, *25*, 2375.

(51) Pasayat, S.; Dash, S. P.; Saswati; Majhi, P. K.; Patil, Y. P.; Nethaji, M.; Dash, H. R.; Das, S.; Dinda, R. *Polyhedron* **2012**, *38*, 198.

(52) Sutradhar, M.; Mukherjee, G.; Drew, M. G. B.; Ghosh, S. *Inorg. Chem.* **2006**, *45*, 5150.

(53) Chattopadhyay, S. K.; Chattopadhyay, D.; Banerjee, T.; Kuroda, R.; Ghosh, S. *Polyhedron* **1997**, *16*, 1925.

(54) Pérez-Rebolledo, A.; Mendes, I. C.; Speziali, N. L.; Bertani, P.; Resende, J. M.; Alcôntara, A. F. de C.; Beraldo, H. *Polyhedron* **2007**, *26*, 1449.

(55) Dinda, R.; Sengupta, P.; Ghosh, S.; Mak, T. C. W. *Inorg. Chem*. **2002**, *41*, 1684.

(56) Naskar, S.; Mishra, D.; Butcher, R. J.; Chattopadhyay, S. K. *Polyhedron* **2007**, *26*, 3703.

(57) Choi, Ki-Y.; Yang, S. M.; Lee, K. C.; Ryu, H.; Lee, C. H.; Seo, J.; Suh, M. *Transition Met. Chem.* **2008**, *33*, 99.

(58) Al-Kubaisi, A. H. *Bull. Korean Chem. Soc*. **2004**, *25*, 37.

(59) Halder, S.; Acharyya, R.; Peng, S. M.; Lee, G. H.; Drew, M. G. B.; Bhattacharya, S. *Inorg. Chem.* **2006**, *45*, 9654.

(60) Sarkar, A.; Pal, S. *Inorg. Chim. Acta* **2008**, *361*, 2296.

(61) Dash, S. P.; Pasayat, S.; Saswati; Dash, H. R.; Das, S.; Butcher, R. J.; Dinda, R. *Polyhedron* **2012**, *31*, 524.

(62) Tarushi, A.; Efthimiadou, E. K.; Christofis, P.; Psomas, G. *Inorg. Chim. Acta* **2007**, *360*, 3978.

(63) Efthimiadou, E. K.; Sanakis, Y.; Katsaros, N.; Karaliota, A.; Psomas, G. *Polyhedron* **2007**, *26*, 1148.

(64) Ramadan, A. M. *J. Inorg. Biochem.* **1997**, *65*, 183.

(65) Avaji, P. G.; Kumar, C. H. V.; Patil, S. A.; Shivananda, K. N.; Nagaraju, C. *Eur. J. Med. Chem.* **2009**, *44*, 3552.

(66) Anderson, E. B.; Long, T. E. *Polymer* **2010**, *51*, 2447.

(67) Dahiya, R.; Gautam, H. *Afr. J. Pharm. Pharacol*. **2011**, *5*, 447.

(68) Sharma, N.; Kumari, M.; Kumar, V. *J. Coord. Chem.* **2010**, *63*, 1940.

(69) Chohan, Z. H.; Sumrra, S. H.; Youssoufi, M. H. *Eur. J. Med. Chem.* **2010**, *45*, 2739.

Chapter 3

Synthesis, X-ray structure and in vitro cytotoxicity studies of Cu(I/II) complexes of thiosemicarbazone: Special emphasis on their interactions with DNA

Chapter 3

Synthesis, X-ray structure and *in vitro* cytotoxicity studies of Cu(I/II) complexes of thiosemicarbazone: Special emphasis on their interactions with DNA

ABSTRACT

4–(*p*–X–phenyl)thiosemicarbazone of napthaldehyde {where, X = Cl (HL^1) and X = Br (HL^2)}, thiosemicarbazone of quinoline–2–carbaldehyde (HL^3) and 4–(*p*–fluorophenyl)thiosemicarbazone of salicylaldehyde (H_2L^4) and their copper(I), {$[Cu(HL^1)(PPh_3)_2Br]\cdot CH_3CN$ (**1**) and $[Cu(HL^2)(PPh_3)_2Cl]\cdot DMSO$ (**2**)} and copper(II), {$[(Cu_2L^3{}_2Cl)_2(\mu\text{–}Cl)_2]\cdot 2H_2O$ (**3**) and $[Cu(L^4)(Py)]$ (**4**)} complexes are reported herein. The synthesized ligands and their copper complexes were successfully characterized by elemental analysis, cyclic voltammetry, NMR, ESI–MS, IR and UV–Vis spectroscopy. Molecular structures of all the Cu(I) and Cu(II) complexes have been determined by X–ray crystallography. All the complexes (**1**–**4**) were tested for their ability to exhibit DNA-binding and -cleavage activity. The complexes effectively interact with CT–DNA possibly by groove binding mode, with binding constants ranging from $10^4 - 10^5$ M^{-1}. Among the complexes, **3** show highest chemical (60%) as well as photo-induced (80%) DNA cleavage activity against pUC19 DNA. Finally, the *in vitro* antiproliferative activity of all the complexes was assayed against the HeLa cell line. Some of the complexes have proved to be as active as the clinical referred drugs, and the greater potency of **3** may be correlated with its aqueous solubility and the presence of quinonoidal group in the thiosemicarbazone ligand coordinated to the metal.

3.1. INTRODUCTION

Cisplatin (*cis*−diamminedichloroplatinum(II)) is a well-known metal based drug for cancer; despite its wide application as a chemotherapeutic agent, cisplatin exhibits severe side effects, such as nausea, kidney and liver failure, typical of heavy metal toxicity.[1–5] Therefore endeavors are constantly made to replace it with suitable alternatives; hence various transition metal complexes have been synthesized and tried for their anticancer properties.

Metal complexes which efficiently bind and cleave DNA under physiological conditions are considered as potential to be used as therapeutic agents for medicinal applications and for genomic research.[6–9] Depending on the exact nature of the metal and ligand, the complexes can bind with nucleic acid covalently or non-covalently.[10,11] Non-covalent interactions between transition-metal complexes and DNA can occur by intercalation, groove binding, or external electrostatic binding. Therefore, the study on the interaction of the transition metal complexes with DNA is of great significance for the design of new drugs and their application.

Among the transition metals, the coordination chemistry of the copper attracts increasing interest because of the use of many copper complexes as models for biological functions, such as amine oxidases,[12] catechol oxidase,[13] nitrite reductase,[14] superoxide dismutase[15] and tyrosinase.[16] Copper complexes have been extensively utilized in metal ion mediated DNA cleavage through the hydrogen ion abstraction by activated oxygen species.[17] In the recent years, a large number of biocompatible Cu(II) complexes, have been investigated for their anticancer properties.[18]

Additionally, thiosemicarbazones (TSCs) are a class of Schiff bases which are considered as one of the most important scaffolds and are embedded in many biologically active compounds.[19] Brockman et al. first reported that 2-formylpyridine TSC possesses antileukemic activity in mice.[20] Following this report, various aliphatic, aromatic, and heteroaromatic carbaldehyde TSCs were synthesized and evaluated for their antitumor activity against a wide spectrum of transplanted murine neoplasms.[21–25] The lists of TSC derivatives have been found to exhibit intense anticancer activities are shown in **Chart 3.1**.[18b,26] Again, the transition metal complexes with TSCs as ligands have raised interest amongst many researchers, and they continue to be the subject of many studies, especially as anticancer chemotherapeutic[27–29] and as DNA–binding and cleaving agents.[18b,30] TSC complexes have also demonstrated significant activity as antitumor,

antiviral, antimicrobial, anti–amoebic and anti–inflammatory agents.[31–33]Many Cu complexes of TSCs have demonstrated efficient antitumor potential.[18b,18c,26a,26b,34–38] Although the chemistry of Cu(II) TSC complexes is well developed,[30g,39–41] relatively less information is available for Cu(I) complexes,[42–46] particularly related to their pharmacological properties.

Again, while many TSC complexes exhibit good biological activities, their water solubility is still unsatisfactory, which may restrict their application. Hence, it seemed of interest to synthesize some new water–soluble transition metal complexes of TSCs which may have significant pharmacological effects.

Considering these facts and as a continuation of ongoing research our group on the study of pharmacological properties[47] of transition metal complexes, in this chapter, two new Cu(I) complexes {$[Cu(HL^1)(PPh_3)_2Br]\cdot CH_3CN$ (**1**) and $[Cu(HL^2)(PPh_3)_2Cl]\cdot DMSO$ (**2**)}, a novel tetranuclear copper(II) complex $[(Cu_2L^3{}_2Cl)_2(\mu\text{–}Cl)_2]\cdot 2H_2O$ (**3**) and a new Cu(II) monomeric complex $[Cu(L^4)(Py)]$ (**4**) were synthesized and fully characterized. The interaction of these complexes with calf−thymus DNA (CT–DNA) utilizing UV–Vis absorption titration, competitive DNA binding fluorescence experiments, circular dichroism and thermal denaturation studies were studied. Their chemical as well as photo-induced cleavage activity with pUC19 supercoiled plasmid DNA were investigated. Furthermore, the cytotoxicity of the complexes against the HeLa cell line was surveyed by the MTT assay.

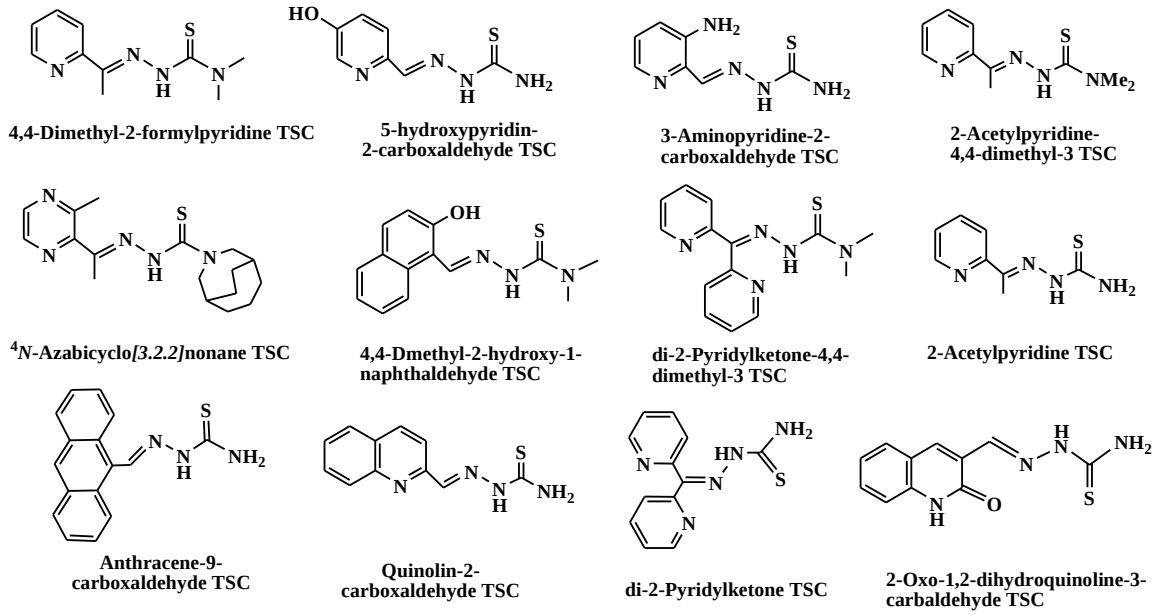

Chart 3.1. Lists of TSC derivatives exhibiting intense anticancer activities.

3.2. EXPERIMENTAL SECTION

3.2.1. General methods and materials. All chemicals were purchased from commercial sources and used without further purification. Reagent grade solvents were dried and distilled prior to use. The thiosemicabazides were prepared from distilled substituted aniline by a known method reported ear1ier.[48] The ligands 4–(*p*–X–phenyl)thiosemicarbazone of napthaldehyde {where X = Cl (HL^1) and X = Br (HL^2)}, thiosemicarbazone of quinoline–2–carbaldehyde, (HL^3) and 4–(*p*–fluorophenyl)thiosemicarbazone of salicylaldehyde (H_2L^4) were prepared by reported methods.[47c,49] MTT (3–[4,5–dimethylthiazol–2–yl]–2,5–diphenyl tetrazolium) and DAPI (4′,6–diamidino–2–phenylindole dihydrochloride) were purchased from Sigma Aldrich (USA). Minimal essential medium (MEM) was purchased from Gibco, India. The supercoiled (SC) pUC19 DNA was purified from *E. coli* cells with the aid of GeneJET Plasmid Isolation Kit (Thermo Scientific, USA). Calf thymus (CT) DNA was purchased from SRL (India) (biochemistry grade). Elemental analyses were performed on a Vario ELcube CHNS Elemental analyzer. IR spectra were recorded on a Perkin–Elmer Spectrum RXI spectrometer. ^1H, ^{13}C and ^{31}P NMR spectra were recorded with a Bruker Ultrashield 400 MHz spectrometer using $SiMe_4$ as an internal standard. Electronic spectra were recorded on a Lamda25, Perkin-Elmer spectrophotometer. Mass spectra were obtained on a SQ–300 MS instrument operating in ESI mode. Electrochemical data were collected using PAR electrochemical analyzer and a PC-controlled potentiostat/galvanostat (PAR 273A) at 298 K in a dry nitrogen atmosphere. Cyclic voltammetry experiments were carried out with Pt working and auxiliary electrodes and Ag/AgCl as reference electrode and TEAP as supporting electrolyte. Commercially available TEAP (tetra ethyl ammonium perchlorate) was properly dried and used as a supporting electrolyte for recording cyclic voltammograms of the complexes.

3.2.2. Synthesis of complexes {$[Cu(HL^1)(PPh_3)_2Br]\cdot CH_3CN$ (1) and $[Cu(HL^2)(PPh_3)_2Cl]\cdot DMSO$ (2)}. Cu(I)X (X = Br/Cl) (1.0 mmol) was added to a solution of the ligand $HL^{1–2}$ (1.0 mmol) in 20 mL of CH_3CN, the contents were refluxed for 1 h, followed by the addition of PPh_3 (1.0 mmol) and continued refluxing for another 1 h. The resulting yellow solution was filtered and slow evaporation of the filtrate over 4–5 days produced yellow crystalline product. Crystals suitable for X–ray analysis were isolated for complex **1**. X–ray quality crystals of complex **2** were obtained by recrystallizing in DMSO.

[Cu(HL^1)(PPh$_3$)$_2$Br]·CH$_3$CN (1): Yield: 67%. Anal. calc. for $C_{56}H_{47}BrClCuN_4P_2S$: C, 64.12; H, 4.52; N, 5.34. Found: C, 64.13; H, 4.54; N, 5.38. Main IR peaks (KBr, cm^{-1}): 3285 m *ν*(N(1)–H), 3049 m *ν*(N(2)–H), 2901 m *ν*(C(8)–H), 1632 s *ν*(C=C), 1547 s *ν*(–C(8)=N(3)), 1096 s ν(P–C_{Ph}), 770 s ν(C(7)=S). ^{1}H NMR (DMSO–d_6, 400 MHz) δ: 12.03 (s, 1H, –C(7)–N(1)H), 10.25 (s, 1H, –C(7)–N(2)H), 9.094 (s, 1H, –N(3)=C(8)H), 8.42–7.27 (m, 26H, Ph + PPh$_3$). ^{13}C NMR (DMSO–d_6, 100 MHz) δ: 175.39 (C(7), C–S), 138.6 (C(8), N=CH), 136.72, 136.32, 135.87, 135.23, 134.85, 134.43, 133.81, 133.12, 132.83, 132.25, 131.91, 131.33, 130.78, 130.26, 130.02, 129.83 (16C, C_6H_6), 128.96, 128.47, 127.80 (PPh$_3$). ^{31}P NMR (DMSO–d_6, 162 MHz) δ: 46.26 and 44.79 (2s, 2PPh$_3$). ESI MS (CH$_3$OH): *m/z* 1047.74 (100%, [M – H]$^+$); *m/z* 1071.95 (30%, [M + Na]$^+$); *m/z* 1087.69 (65%, [M + K]$^+$).

[Cu(HL^2)(PPh$_3$)$_2$Cl]·DMSO (2): Yield: 67%. Anal. calc. for $C_{56}H_{50}BrClCuN_3OP_2S_2$: C, 61.93; H, 4.64; N, 3.87. Found: C, 61.90; H, 4.67; N, 3.88. Main IR peaks (KBr, cm^{-1}): 3284 m ν(N(1)–H), 3047 m ν(N(2)–H), 2908 m *ν*(C(8)–H), 1627 s *ν*(C=C), 1551 s *ν*(–C(8)=N(3)), 1090 s ν(P–C_{Ph}), 768 s ν(C(7)=S). ^{1}H NMR (DMSO–d_6, 400 MHz) δ: 12.47 (s, 1H, –C(7)–N(1)H), 10.29 (s, 1H, –C(7)–N(2)H), 9.09 (s, 1H, –N(3)=C(8)H), 8.07–7.25 (m, 26H, Ph + PPh$_3$), 2.53 (s, 6H, DMSO). ^{13}C NMR (DMSO–d_6,100 MHz) δ:178.18 (C(7), C–S), 140.51 (C(8), N=CH), 137.82, 137.12, 136.87, 135.73, 134.95, 134.41, 133.85, 133.19, 132.79, 132.41, 131.86, 131.23, 130.96, 130.26, 130.12, 129.92 (16C, C_6H_6), 129.12, 128.87, 128.17 (PPh$_3$). ^{31}P NMR (DMSO–d_6, 162 MHz) δ: 46.85 and 44.72 (2s, 2PPh$_3$). ESI MS (CH$_3$OH): *m/z* 1086.70 (12%, [M + H]$^+$); *m/z* 1051.92 (20%, [M – Cl]).

3.2.3. Synthesis of complex [(Cu$_2$L$^3{}_2$Cl)$_2$(μ–Cl)$_2$]·2H$_2$O (3). $CuCl_2·2H_2O$ (1.0 mmol) was added to a solution of ligand, HL^3 (1.0 mmol) in 20 mL of hot methanol and the mixture was refluxed for 2 h. The resulting dark green solution was filtered and slow evaporation of the filtrate over 4–5 days produced deep green crystals suitable for X–ray analysis.

[(Cu$_2$L$^3{}_2$Cl)$_2$(μ–Cl)$_2$]·2H$_2$O: Yield: 58%. Anal. calc. for $C_{44}H_{40}Cl_4Cu_4N_{16}S_4O_2$: C, 39.17; H, 2.99; N, 16.61. Found: C, 39.19; H, 2.97; N, 16.63. Main IR peaks (KBr, cm^{-1}): 3228 m ν(–N(1)–H$_2$), 3047 m *ν*(C(2)–H), 1635 s *ν*(C=C), 1557 s, *ν*(–C(2)=N(3)) 752 s ν(C(1)–S). ESI MS (CH$_3$OH): *m/z* 1318.80 (68%, [(M – 2H$_2$O) + 5H]$^+$); *m/z* 1352.55 (100% [(M + 3H]$^+$).

3.2.4. Synthesis of complex [Cu(L^4)(Py)] (4). $CuCl_2 \cdot 2H_2O$ (1.0 mmol) was added to a solution of H_2L^4 (1.0 mmol) in 20 ml of hot methanol followed by the addition of pyridine (1.0 mmol). The mixture was refluxed for 3 h and a clear bluish green solution was obtained, which was filtered and slow evaporation of the filtrate over 3–4 days produced bluish green crystals suitable for X–ray analysis.

[Cu(L^4)(Py)]: Yield: 67%. Anal. calc. for $C_{19}H_{15}CuFN_4OS$: C, 53.08; H, 3.52; N, 13.03. Found: C, 53.11; H, 3.56; N, 13.07. Main IR peaks (KBr, cm^{-1}): 3224 s ν(N(1)–H), 2356 m *ν*(C(8)–H), 1602 s ν(C=C), 1531 s ν(–C(8)=N(3)), 748 s ν(C(7)–S(1)). ESI MS (CH_3OH): *m/z* 430.07 (100%, $[M]^+$); *m/z* 431.72 (50%, $[M + H]^+$); *m/z* 351.14 (46%, $[M – Py]^+$).

3.2.5. X–ray crystallography. Single crystals of complexes were mounted on Stoe IPDS 2 diffractometer equipped with an Oxford Cryosystem open flow cryostat. (**1** & **2**) & on a Bruker Smart Apex CCD diffractometer (**3** & **4**), equipped with a graphite monochromator and a Mo Kα radiator (λ) 0.71073 Å. Crystallographic data and details of refinement of **1**–**4** are given in **Table 3.1**. The unit cell dimensions and intensity data were measured at 200(2) K for **1** & **2**, 273(2) K for **3** & 296(2) for **4**. Absorption correction was partially integrated in the data reduction procedure for crystals of **1** & **2**.[50] The intensity data were corrected for Lorentz, polarization and absorption effects. Absorption corrections were applied using SADABS[51] and the structures were solved by direct methods using the program SHELXS−97[52] and refined using least squares with the SHELXL−97[52] software program. Hydrogens were either found or placed in calculated positions and isotropically refined using a riding model. The non-hydrogen atoms were refined anisotropically.

Table 3.1. Crystal and refinement data of complexes 1–4

Compound	**1**	**2**	**3**	**4**
Formula	$C_{56}H_{47}BrClCuN_4P_2S$	$C_{56}H_{50}BrClCuN_3OP_2S_2$	$C_{44}H_{40}Cl_4Cu_4N_{16}S_4O_2$	$C_{19}H_{15}CuFN_4OS$
M	1048.88	1085.95	1349.12	429.95
Crystal system	Triclinic	Triclinic	Triclinic	Monoclinic
Space group	$P\bar{1}$	$P\bar{1}$	$P\bar{1}$	$P\,2_1/c$
a(Å)	9.498(4)	9.660(5)	8.947(15)	13.304(5)
b(Å)	13.122(5)	13.154(6)	9.813(16)	5.839(2)
c(Å)	20.658(9)	20.341(10)	14.928(2)	23.187(9)
α (°)	100.185(3)	99.305(4)	85.086(3)	90
β (°)	95.359(3)	94.696(4)	72.973(3)	102.115(2)
γ (°)	96.502(3)	93.570(4)	80.782(3)	90
V(Å^3)	2500.96(18)	2534.7(2)	1236.0(4)	1761.22(11)
Z	2	2	1	4
D_{calc}(Mg.cm^{-3})	1.393	1.423	1.813	1.621
F(000)	1076	1116	680	876
μ(Mo-Kα)(mm^{-1})	1.436	1.460	2.142	1.386
max./min.trans.	0.9460 and 0.8576	0.8921 and 0.7026	0.9873 and 0.8343	0.9728 and 0.7787
2θ(max)(°)	25.00	25.00	21.99	30.5
Reflections collected / unique	48158/8790 [R(int) = 0.0383]	48925/8938 [R(int) = 0.0576]	8969/4328 [R(int) = 0.0406]	33365/5407 [R(int) = 0.0410]
R_1[I>2σ(I)]	R1 = 0.0301, wR2 = 0.0788	R1 = 0.0477, wR2 = 0.1269	R1 = 0.0743, wR2 = 0.1738	R1 = 0.0345, wR2 = 0.0796
wR_2[all data]	R1 = 0.0353, wR2 = 0.0814	R1 = 0.0754, wR2 = 0.1400	R1 = 0.1261, wR2 = 0.1963	R1 = 0.0581, wR2 = 0.0885
S[goodness of fit]	1.040	1.034	1.018	1.015
min./max. res. (e.Å^{-3})	0.788 / –0.755	0.824 / –0.867	2.059 / –0.897	0.315 /–0.295

3.2.6. DNA binding experiments

3.2.6.1. Absorption spectral studies. The DNA binding experiments were performed with Perkin−Elmer Lamda35 spectrophotometer as described previously.[47e] Briefly, the absorption titration experiments were performed by varying the concentration of CT−DNA from 0 to 70 μM and keeping the metal complex concentration constant at 25 μM in 10 mM Tris–HCl buffer (pH 8.0) containing 1% DMF. The binding constant K_b was computed from the data obtained using the following equation[47e]

$$\frac{[DNA]}{\varepsilon_a - \varepsilon_f} = \frac{[DNA]}{\varepsilon_b - \varepsilon_f} + \frac{1}{K_b(\varepsilon_b - \varepsilon_f)}; \qquad (1)$$

where [DNA] is the concentration of DNA base pairs, and ε_a, ε_f and ε_b correspond to apparent extinction co−efficient for the complex *i.e.* Abs/[complex] in presence of DNA, in the absence of DNA and to fully bound DNA respectively. A plot of [DNA]/($\varepsilon_a - \varepsilon_f$) *vs* [DNA] gave a slope and the intercept equal to 1/($\varepsilon_b - \varepsilon_f$) and 1/$K_b$($\varepsilon_b - \varepsilon_f$), respectively. The binding constant K_b was calculated from the ratio of the slope to the intercept. Ligand interaction with CT−DNA were also studied by titrating a fixed concentration of ligand (25 μM) with variable CT−DNA concentration ranging from 0−350 μM in 10 mM Tris–HCl buffer (pH 8.0) containing 1% DMF.

3.2.6.2. Competitive DNA binding fluorescence measurements. The apparent binding constant (K_{app}) for the complexes were determined by fluorescence measurements using ethidium bromide (2 μM) (EB) bound CT−DNA (50 μM) solution in 10 mM Tris–HCl buffer (pH 8.0) containing 1% DMF with the aid of Fluoromax 4P spectrofluorimeter (Horiba Jobin Mayer, USA). The fluorescence intensities of EB at 597 nm (excitation 510 nm) with an increase of the complex concentration (0−60 μM) were measured. In the presence of DNA, EB showed enhanced emission intensity due to intercalative binding with DNA. A competitive binding of metal complexes with CT−DNA leads to the decrease in the emission intensity due to emission quenching or the displacement of bound EB to CT−DNA by the complexes. The quenching constant was calculated by using the following Stern−Volmer equation[53]

$$\frac{F_0}{F} = 1 + K_{SV}[Q] \qquad (2)$$

where F_0 and F are the emission intensity of EB bound CT–DNA in absence and in presence of the quencher (complexes) concentration [Q] respectively, which gave the Stern−Volmer

quenching constant (K_{SV}). The apparent binding constant (K_{app}) was calculated from the following equation.

$$K_{EB} \times [EB] = K_{app} \times [complex]_{50} \quad (3)$$

where K_{app} is the apparent binding constant of the complex, $[complex]_{50}$ is the concentration of the complex at 50% quenching of the emission intensity of EB bound CT–DNA, K_{EB} is the binding constant of EB ($K_{EB} = 1.0 \times 10^7\ M^{-1}$) and [EB] is the concentration of ethidium bromide (2 μM).[53]

3.2.6.3. Thermal melting studies. Thermal melting studies of CT−DNA (100 μM) in the absence and presence of complexes (50 μM) were carried out by monitoring the absorbance at 260 nm in the temperature range of 30−90^{o}C with a ramp rate of 0.5^{o}C/min in 10 mM Tris−HCl buffer (pH 8.0) containing 1% DMF. The experiments were carried out using a Chirascan CD spectropolarimeter (Applied Photophysics, UK) in absorbance mode equipped with temperature controller. The melting temperature (T_m) was determined from the derivative plot (dA_{260}/dT *vs* T) of the melting profile.[47e]

3.2.6.4. Circular dichroism studies. The Circular Dichroism (CD) spectroscopic studies were performed using Chirascan CD spectropolarimeter (Applied Photophysics, UK) at 25^{o}C. CD spectra of CT–DNA (50 μM) in absence and presence of complexes (10 μM) were obtained in the wavelength range of 240–400 nm in 10 mM Tris–HCl buffer (pH 8.0) containing 1% DMF, using quartz cell with 10 mm path length.[47e]

3.2.7. DNA cleavage experiments. DNA cleavage was carried out as previously reported.[47e] The chemical−induced and photo−induced DNA cleavage experiments were done with 300 ng supercoiled (SC) pUC19 DNA in 50 mM Tris–HCl buffer (pH 8.0) containing 1% DMF.

3.2.7.1. Chemical−induced DNA cleavage. In order to study the chemical nuclease activity of the complexes, reactions were performed in the dark using hydrogen peroxide (0.5 mM) as the oxidising agent in absence and presence of complexes (1–300 μM). The solutions were incubated at 37^{o}C for 1 h and analysed for DNA cleaved products by agarose gel electrophoresis.

3.2.7.2. Photo-induced DNA cleavage. The photo−induced DNA cleavage activity was performed as described previously.[47e] Briefly, the photo−induced DNA cleavage experiments were carried out using UVA source at 350 nm (Luzchem Photoreactor Model LZC–1, Ontario, Canada) fitted with 14 UVA tubes (84 W) for 1 h, on supercoiled (SC) pUC19 DNA (300 ng) with complexes (1–300 μM) in 50 mM Tris−HCl buffer (pH 8.0) containing 1% DMF. DNA cleavage was indicated by the decrease in the supercoiled pUC19 DNA (Form I) and subsequent formation of nicked circular DNA (Form II) and linear DNA (Form III). The percentage of net DNA cleavage was calculated by the following equation:

$$\text{Net DNA cleavage } \% = \frac{\text{Form IIs}+2\times\text{Form IIIs}}{\text{Form Is}+\text{Form IIs}+2\times\text{Form IIIs}} - \frac{\text{Form IIc}+2\times\text{Form IIIc}}{\text{Form Ic}+\text{Form IIc}+2\times\text{Form IIIc}} \quad (4)$$

The subscripts "s" and "c" refers to the sample and control respectively.[54] Appropriate DNA controls were taken to calculate the net DNA cleavage percent. The observed error in measuring the band intensities ranged between 3% – 6%.

For mechanistic investigations of both hydrolytic and photolytic DNA cleavage, experiments were carried out with singlet oxygen quenchers such as sodium azide (NaN_3) and L−histidine, while for hydroxyl radical scavengers potassium iodide (KI) and D−mannitol were used. Each of the additives was used at a concentration of 0.5 mM.

3.2.8. Anticancer activity

3.2.8.1. Cell culture. Human cervical cells HeLa were obtained from National Centre of Cell Science (NCCS), Pune, India and were maintained in minimal essential medium supplemented with 10% fetal bovine serum, penicillin-streptomycin solution and incubated at 37°C in 5% CO_2 and 95% humidified incubator. The complexes were dissolved in DMSO at a concentration of 100 mM as stock solution, and diluted in culture medium at concentrations of 12.5, 25.0, 50.0 and 100.0 μM as working solution. To avoid DMSO toxicity, the concentration of DMSO was less than 0.1% (v/v) in all experiments.

3.2.8.2. Cytotoxic assay. HeLa cells were harvested from maintenance cultures in logarithmic phase, after counting in a hemocytometer using trypan blue solution. The cell concentration was adjusted to $5x10^4$ cells/ml and the cells were plated in 96 well flat bottom culture plates and incubated for 72 h with various concentrations of the test compounds. The effect of the drugs on

the cancer cell viability was studied using MTT dye reduction assay by measuring the optical density at 595 nm using micro−plate reader spectrophotometer (Perkin−Elmer 2030).[55]

3.2.8.3. Nuclear staining. Nuclear staining using DAPI stain was performed according to the method previously described.[56] Briefly, HeLa cells either treated or untreated with test compounds were smeared on a clean glass slide, cells were fixed with 3.7% formaldehyde for 15 minutes, permeabilized with 0.1% Triton X−100 and stained with 1 μg/ml DAPI for 5 min at 37°C. The cells were then washed with PBS and examined by fluorescence microscopy (Olympus IX 71) to ascertain any condensation or fragmentation of the nuclei indicating cells undergoing apoptosis.

3.3. RESULTS AND DISCUSSION

3.3.1. Synthesis. Reaction of Cu(I)X (X = Cl, Br) with 4–(*p*–X–phenyl)thiosemicarbazone of napthaldehyde {X = Cl (HL^1); X = Br (HL^2)} in the molar ratio of 1:1 in CH_3CN formed an insoluble product of stoichiometry [$CuX(HL^{1-2})$] which after addition of two moles of PPh_3 yielded light yellow colored monomeric complexes [$CuX(HL^{1-2})(PPh_3)_2$]·Solvent (X = Br, **1**; Cl, **2**). Reaction of copper(II) chloride with quinoline–2–carbaldehyde thiosemicarbazone (HL^3) in the molar ratio of 1:1 in CH_3OH yielded dark green colored tertrameric complex [$(Cu_2L^3{}_2Cl)_2(\mu$–$Cl)_2$]·$2H_2O$ (**3**) whereas with 4–(*p*–F–phenyl)thiosemicarbazone of salicylaldehyde (H_2L^4) in presence of pyridine as coligand yielded dark green monomeric complex [$Cu(L^4)(Py)$] (**4**). The electrospray mass spectra (ESI MS) and NMR spectra were consistent with the X–ray structures. The purity of these compounds was further confirmed by elemental analyses. The synthetic methods of all the complexes are illustrated in **Scheme 3.1**. All complexes were soluble in MeOH, MeCN, DMF and DMSO. Complex **3** was completely and other three complexes (**1**, 38%; **2**, 35% and **4**, 45%, H_2O–DMSO solution) were partially soluble in H_2O. All the complexes were stable in both solid and solution phases. The solution phase stability of the complexes was confirmed by electronic absorption, NMR and ESI–MS spectral studies.

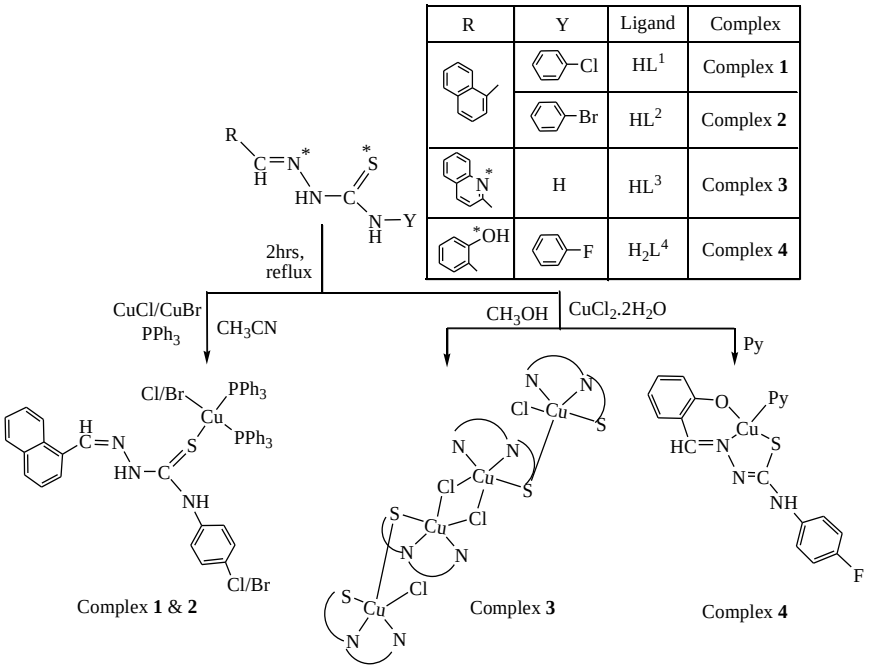

Scheme 3.1. Schematic representation of ligands and syntheses of copper complexes.

3.3.2. Structure. The observed elemental (C, H, N) analytical data of all the complexes **(1**–**4**) are in consistent with their composition. It appears from the formulation of **1** & **2** that the TSC is serving as a monodentate ligand where as in **3** & **4** it is serving as a tridentate ligand. In order to authenticate the coordination mode of the TSC in the complexes, the structures have been determined by X–ray crystallography.

3.3.2.1. Description of X-ray structures of $[Cu(HL^1)(PPh_3)_2Br]\cdot CH_3CN$ (1) and $[Cu(HL^2)(PPh_3)_2Cl]\cdot DMSO$ (2). The molecular structure and the atom numbering scheme for the complexes $[Cu(HL^1)(PPh_3)_2Br]\cdot CH_3CN$ (**1**) and $[Cu(HL^2)(PPh_3)_2Cl]\cdot DMSO$ (**2**) are shown in **Figure 3.1** and **Figure 3.2** respectively; the relevant bond distances and angles are collected in **Table 3.2**. Compounds **1** and **2** contain CH_3CN and DMSO as a solvent of crystallization respectively. The coordination geometry around the Cu(I) atom in **1** and **2** reveals a distorted tetrahedral environment with an SXP_2 [X = Br (**1**) and Cl (**2**)] coordination sphere as the bond angles around the copper atom vary from ca. 100–124° in **1** and **2** with P−Cu−P being the largest angle.[49,57] The ligand $HL^{1\text{-}2}$ acts as a monodentate ligand coordinating through the S atom. The other positions of the tetrahedron are occupied by one halogen atom and two triphenylphosphine ligands. In the compound, the Cu−S bond lengths are 2.401(7) Å for **1** and 2.387(1) Å for **2**, while the Cu-halogen bond distances lie in ranges 2.374(1)–2.517(4) Å as is usually found for tetrahedrally coordinated copper(I) and S atom donors.[44,49] The Cu−P distances [2.276(6), 2.290(7) Å for **1**, 2.274(1), 2.295(1) Å for **2**] are comparable to those found in similar complexes. [44,49]

Table 3.2. Selected geometric parameters (Å, º) for $[Cu(HL^1)(PPh_3)_2Br]\cdot CH_3CN$ (1) and $[Cu(HL^2)(PPh_3)_2Cl]\cdot DMSO$ (2)

	Complex (**1**)	Complex (**2**)
	Bond Distances	
Cu(1)–S(1)	2.401(7)	2.387(1)
Cu(1)–P(1)	2.277(6)	2.274(1)
Cu(1)–P(2)	2.290(7)	2.295(1)
Br(1)–Cu(1)	2.517(4)	–
Cl(1)–Cu(1)	–	2.374(1)
	Bond Angles	
P(2)–Cu(1)–P(1)	124.51(2)	122.72(4)
P(2)–Cu(1)–S(1)	109.26(2)	107.07(4)
P(1)–Cu(1)–S(1)	104.48(2)	105.19(4)
P(2)–Cu(1)–Br(1)	108.41 (2)	–
P(2)–Cu(1)–Cl(1)	–	108.07(4)
P(1)–Cu(1)–Br(1)	100.29(2)	–
P(1)–Cu(1)–Cl(1)	–	104.81(4)
S(1)–Cu(1)–Br(1)	108.97(2)	–
Cl(1)–Cu(1)–S(1)	–	108.35(4)

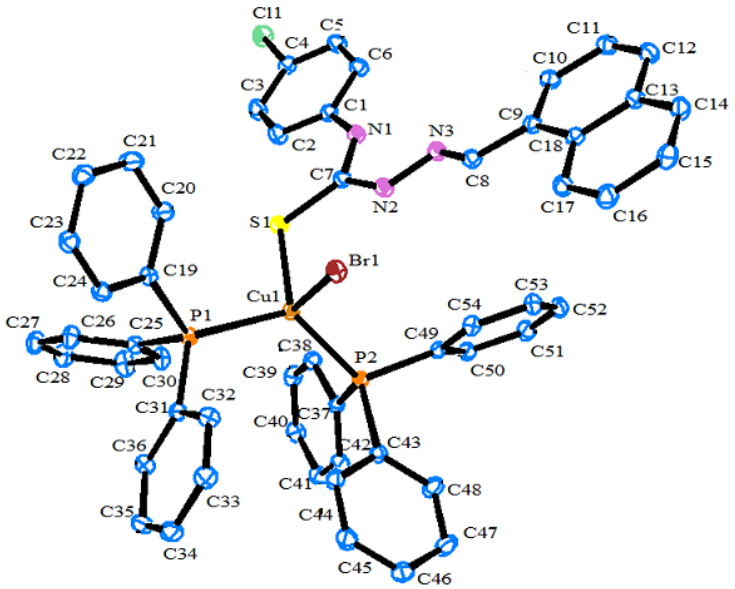

Figure 3.1. ORTEP diagram of $[Cu(HL^1)(PPh_3)_2Br]\cdot CH_3CN$ (**1**) with atom labeling scheme.

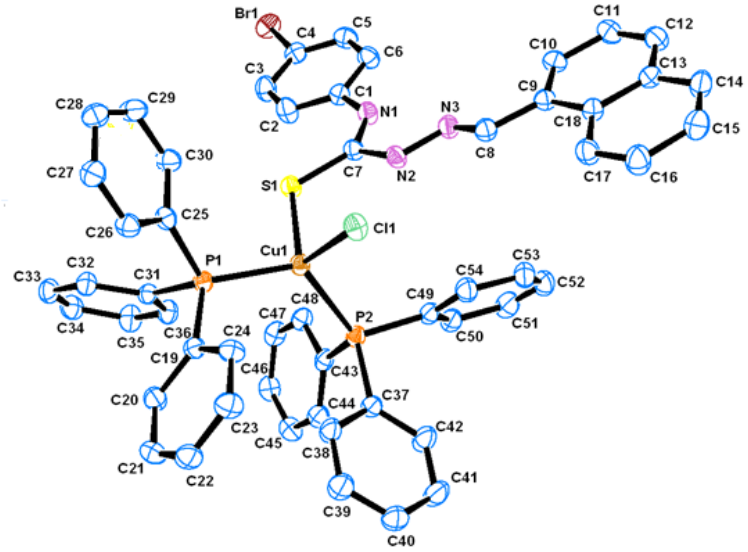

Figure 3.2. ORTEP diagram of $[Cu(HL^2)(PPh_3)_2Cl]\cdot DMSO$ (**2**) with atom labeling scheme.

3.3.2.2. Description of X-ray structure of $[(Cu_2L^3{}_2Cl)_2(\mu\text{–}Cl)_2]\cdot 2H_2O$ (3). The structure of the tetranuclear Cu(II) complex $[(Cu_2L^3{}_2Cl)_2(\mu\text{–}Cl)_2].2H_2O$ is illustrated in **Figure 3.3** and selected bond parameters are collected in **Table 3.3**. Compound **3** contains two H_2O molecules as solvent of crystallization. The structure contains four units comprising of two identical Cu(1)LCl outer units and two identical Cu(2)LCl inner units. In other words, the tetranuclear Cu(II) species is formed by the dimerisation of two binuclear $Cu_2L_2Cl_2$ units bridged by two reciprocal coordinated chlorine atoms of the individual $Cu_2L_2Cl_2$ unit. Each copper atom in the outer unit is coordinated by a quinoline nitrogen, azomethine nitrogen and thiolate sulfur of the thiosemicarbazone moiety and a chlorine group. The $Cu–N_{quinoline}$ bonds are ~ 0.131 Å farther away than $Cu–N_{imine}$ bonds, indicating the strength of the azomethine nitrogen coordination. The length of the other metal coordinated bonds (Cu−S and Cu−Cl) is usual like similar systems reported earlier.[58,59] The bond angles also are in conformity with a distorted square pyramidal structure around the copper centers. Each copper atom in the inner subunit is pentacoordinate with the bonds Cu(2)–S(2), Cu(2)–Cl(2), Cu(2)–N(8), Cu(2)–N(7) and Cu(2)–Cl(2)# adapting a distorted square pyramidal geometry with bridging Cl(2)# of the other inner moiety at the apical site. The quinoline nitrogen N(8), the imine nitrogen N(7), and the thiolate sulfur S(2) atom, together with Cl(2), constitute the basal plane. The bond lengths in the basal plane agree with those found in copper(II) complexes containing thiosemicarbazones which act as uninegative tridentate ligands.[58,59] The bond lengths and bond angles reveal a distorted square pyramidal geometry around Cu(2).

3.3.2.3. Description of X-ray structure of $[Cu(L^4)(Py)]$ (4). The atom numbering scheme for the complex **4** is given in **Figure 3.4** with the relevant bond distances and angles collected in **Table 3.3**. The structure shows that the thiosemicarbazone ligand (L^{2-}) is coordinated to copper in the expected tridentate fashion (**Scheme 3.1**), forming a six− and a five−membered chelate ring with O(1)–Cu(1)–N(3) and S(1)–Cu(1)–N(3) bite angles of 94.04(7)º and 85.92(5)° respectively. The coligand pyridine is coordinated to the metal center, and is trans to the nitrogen atom N(3). The rather large Cu(1)−N(4) distance is 2.013(1) Å revealed that the pyridine moiety is weakly coordinated to the Cu−center.[60] Copper is thus nested in a NOSN core, which is slightly distorted from an ideal square-planar geometry, as reflected in the bond parameters around the metal center. The Cu–N(3), Cu–O(1), Cu–N(4) (coligand) and Cu–S(1) distances are

normal, as observed in other structurally characterized complexes of Cu containing these bonds.[60,61]

Table 3.3. Selected geometric parameters (Å, º) for $[(Cu_2L^3{}_2Cl)_2(\mu\text{–}Cl)_2]\cdot 2H_2O$ (3) & $[Cu(L^4)(Py)]$ (4)

	Complex (**3**)	Complex (**4**)
	Bond Distances	
Cu(1)–Cl(1)	2.253(3)	–
Cu(1)–O(1)	–	1.906 (2)
Cu(1)–S(1)	2.304(3)	2.247(6)
Cu(1)–S(2)	2.715(2)	–
Cu(1)–N(3)	1.975(7)	1.932(1)
Cu(1)–N(4)	2.107(7)	2.013(1)
Cu(2)–Cl(2)	2.290(2)	–
Cu(2)–S(2)	2.303(2)	–
Cu(2)–N(7)	1.973(6)	–
Cu(2)–N(8)	2.146(6)	–
Cu(2)–Cl(2)1	2.691(2)	–
	Bond Angles	
Cl(1)–Cu(1)–S(1)	92.60(1)	–
O(1)–Cu(1)–N(3)	–	94.04(7)
Cl(1)–Cu(1)–S(2)	101.30(1)	–
O(1)–Cu(1)–N(4)	–	86.40(7)
Cl(1)–Cu(1)–N(3)	150.60(2)	–
O(1)–Cu(1)–S(1)	–	177.41(5)
Cl(1)–Cu(1)–N(4)	104.10(2)	–
S(1)–Cu(1)–S(2)	94.15(8)	–
S(1)–Cu(1)–N(3)	82.30(2)	85.92(5)
S(1)–Cu(1)–N(4)	161.90(2)	93.72(5)
S(2)–Cu(1)–N(3)	107.90(2)	–

S(2)–Cu(1)–N(4)	89.40(2)	–
N(3)–Cu(1)–N(4)	79.70(3)	178.10(7)
Cl(2)–Cu(2)–S(2)	89.88(8)	–
Cl(2)–Cu(2)–N(7)	171.20(2)	–
Cl(2)–Cu(2)–N(8)	108.60(2)	–
Cl(2)–Cu(2)–Cl(2)1	87.25(7)	–
S(2)–Cu(2)–N(7)	81.60(2)	–
S(2)–Cu(2)–N(8)	155.20(2)	–
Cl(2)1–Cu(2)–S(2)	102.01(9)	–
N(7)–Cu(2)–N(8)	79.20(3)	–
Cl(2)1–Cu(2)–N(7)	96.30(2)	–
Cl(2)1–Cu(2)–N(8)	95.50(2)	–
Cu(2)–Cl(2)–Cu(2)1	92.80(9)	–

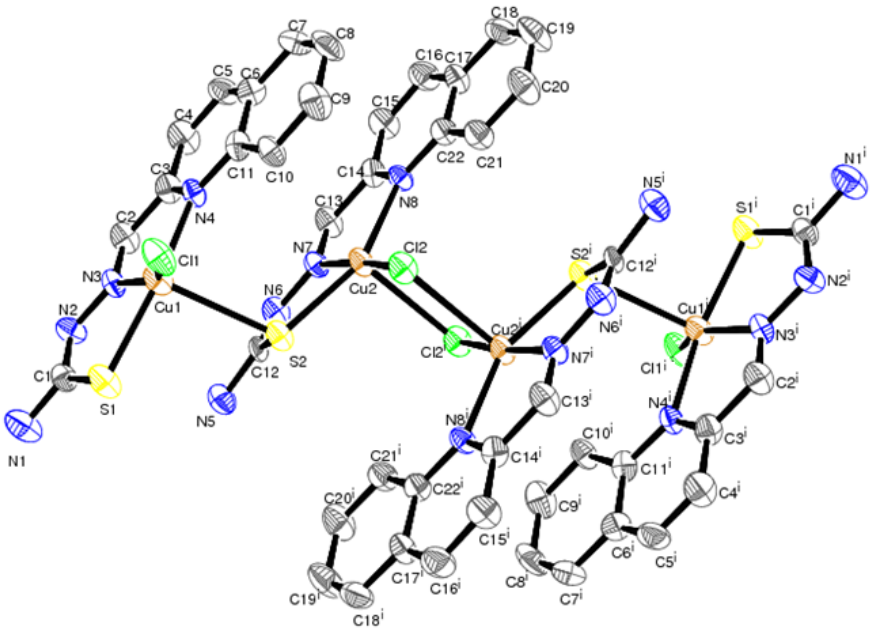

Figure 3.3. ORTEP diagram of $[(Cu_2L^3{}_2Cl)_2(\mu\text{–}Cl)_2]\cdot 2H_2O$ (**3**) with atom labeling scheme.

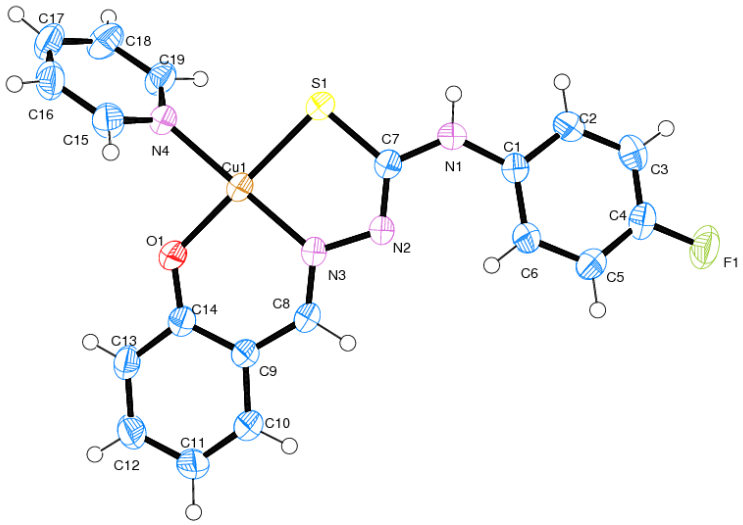

Figure 3.4. ORTEP diagram of $[Cu(L^4)(Py)]$ (**4**) with atom labeling scheme.

3.3.3. Spectral characteristics

3.3.3.1. IR spectroscopy. The IR spectra of **1** & **2** showed the presence of *ν*(N–H) bands in the ranges 3284–3285 cm^{-1} for –N(1)–H and 3047–3049 cm^{-1} for –N(2)–H stretching, which suggests that the thiosemicarbazone ligand is coordinated to the Cu(I) centre in the neutral form. In all the complexes (**1**–**4**) ν(C=N) and ν(C=C) vibrational modes appeared in the range 1635–1531 cm^{-1}, while the thioamide bands ν(C–S (**1** & **2**) & C=S (**3** & **4**)) appeared in the range 770–748 cm^{-1} (compared to free ligands, 854–785 cm^{-1}).[47c] The characteristic ν(P–C_{Ph}) bands at 1096–1090 cm^{-1} indicate the presence of Ph_3P in **1** & **2**.

3.3.3.2. UV spectroscopy. The electronic spectra of all the complexes (**Table 3.4**) were recorded in methanol solutions. In the spectra of **1**–**4** three strong absorptions are observed in the wavelength range 448–220 nm. The lower energy absorptions at around 448–349 nm are ascribable to metal to ligand (**1** & **2**) the ligand to metal (**3** & **4**) charge transfer transitions whereas the higher energy absorptions are likely to be due to ligand centered transitions.[46,47c] Weak absorptions in the range 676−668 nm are also observed for **3** & **4** (Cu(II) complexes), which are assigned to d−d transitions.[62] A representative spectrum of complex **1** is shown in **Figure 3.5**.

Table 3.4. Electronic spectra for complexes 1–4 in CH_3OH

Complex	λ_{max}/nm (ε/dm^3mol^{-1} cm^{-1})
$[Cu(HL^1)(PPh_3)_2Br]\cdot CH_3CN$ (**1**)	239(51814), 349(26982)
$[Cu(HL^2)(PPh_3)_2Cl]\cdot$DMSO (**2**)	227(45121), 385(27637)
$[(Cu_2L^3{}_2Cl)_2(\mu\text{–}Cl)_2]\cdot 2H_2O$ (**3**)	230(29790), 306(23258), 364(12917), 448(11768), 676(17788)
$[Cu(L^4)(Py)]$ (**4**)	220(5132), 256(8526), 332(3310), 395(2574), 668(4353)

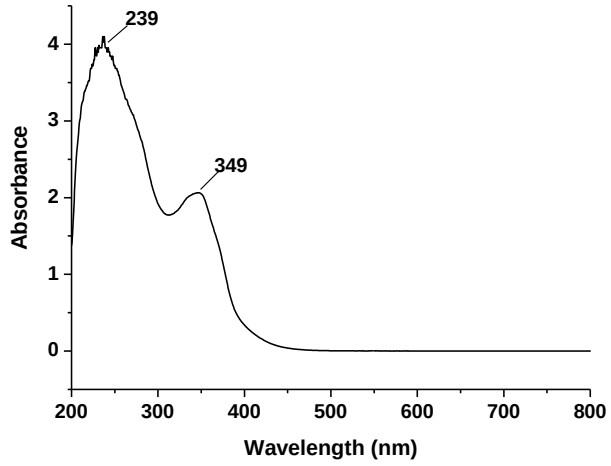

Figure 3.5. Electronic absorption spectra of $[Cu(HL^1)(PPh_3)_2Br]\cdot CH_3CN$ (**1**).

3.3.3.3. NMR spectroscopy. The NMR spectra (^1H, ^{13}C and ^{31}P) of **1** & **2** were recorded using DMSO–d_6. The ^1H NMR spectrum exhibits three singlets in the range 12.47–9.09 ppm due to NH (–C(7)–N(1)H), NH (–C(7)–N(2)H) and CH (–N(3)=C(8)H) groups respectively. Signals for aromatic protons found as multiplets in 8.42–7.25 ppm range.[47c] The ^{13}C NMR spectra of the complexes (**1** & **2**) showed a sharp singlet appearing at 178.18–175.39 ppm due to C–S carbon. The peak for the azomethine (–CH=N) carbon exhibited a peak in the region 140.51–138.6 ppm. The peaks observed in the 137.82–129.83 ppm region have been assigned to aromatic carbons. The PPh_3 peaks are assigned in the range 129.12–127.80 ppm.[63] ^{31}P NMR spectra were recorded in order to confirm the presence of triphenyl phosphine group. The two signals appeared at 46.85–44.72 ppm and indicated that the two triphenyl phosphine ligands were *cis* to each other in these complexes.[63] The detailed NMR data has been included in the experimental section. The representative ^1H NMR spectrum of complex **2** is shown in **Figure 3.6**.

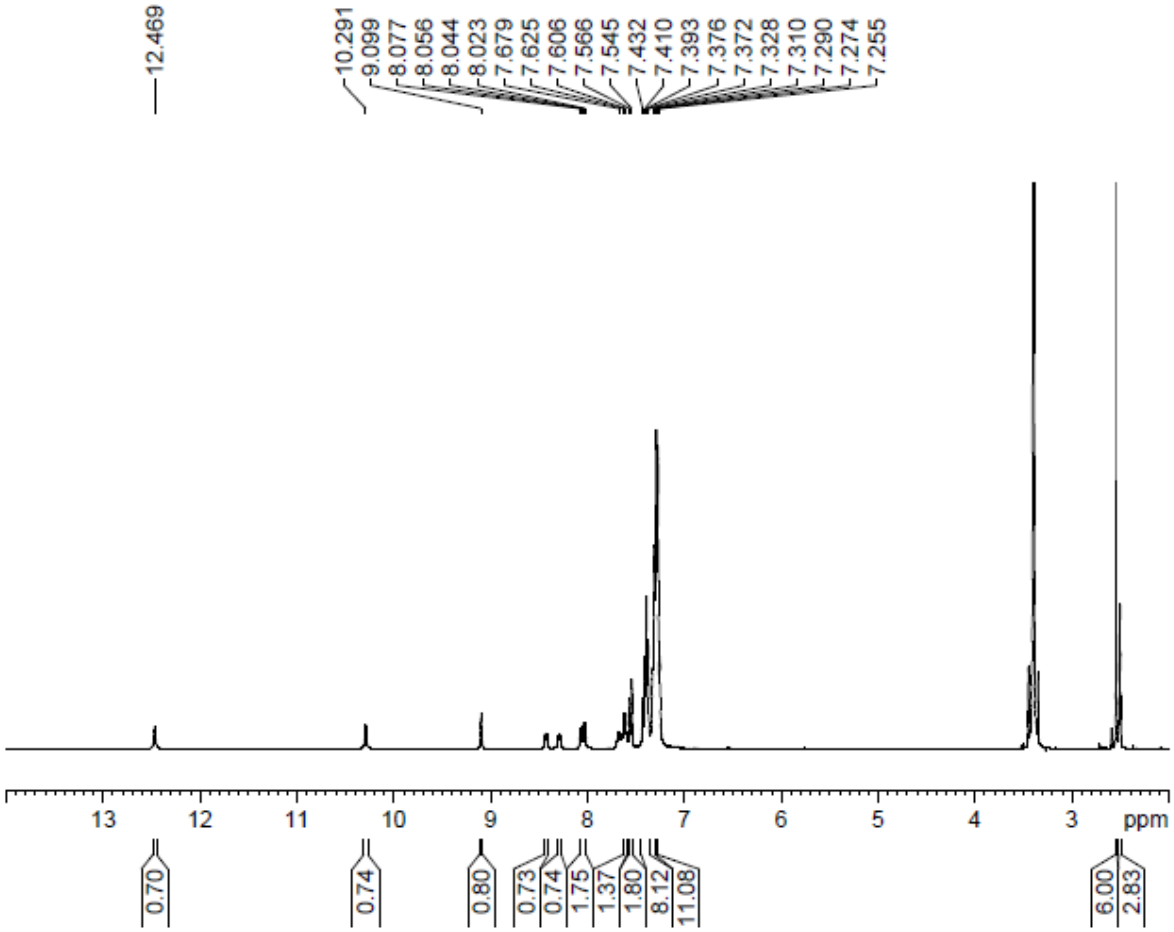

Figure. 3.6. ^{1}H NMR spectra of complex [Cu(HL^{2})(PPh$_3$)$_2$Cl]·DMSO (**2**).

3.3.3.4. ESI-MS spectroscopy. ESI mass spectra of **1**−**4** have been recorded in methanol solution. Mass spectral analysis for **1** and **2** shows peaks at m/z 1047.34 [(M + H)$^+$] and 1086.70 [(M + H)$^+$] respectively, whereas **3** shows the molecular ion peak [(M + 3H)$^+$] at m/z 1352.55. ESI–MS peak for **4** shows the characteristic molecular ion peak (M$^+$) at m/z 430.07. **Figure 3.7** depicts a representative ESI mass spectrum of **4**.

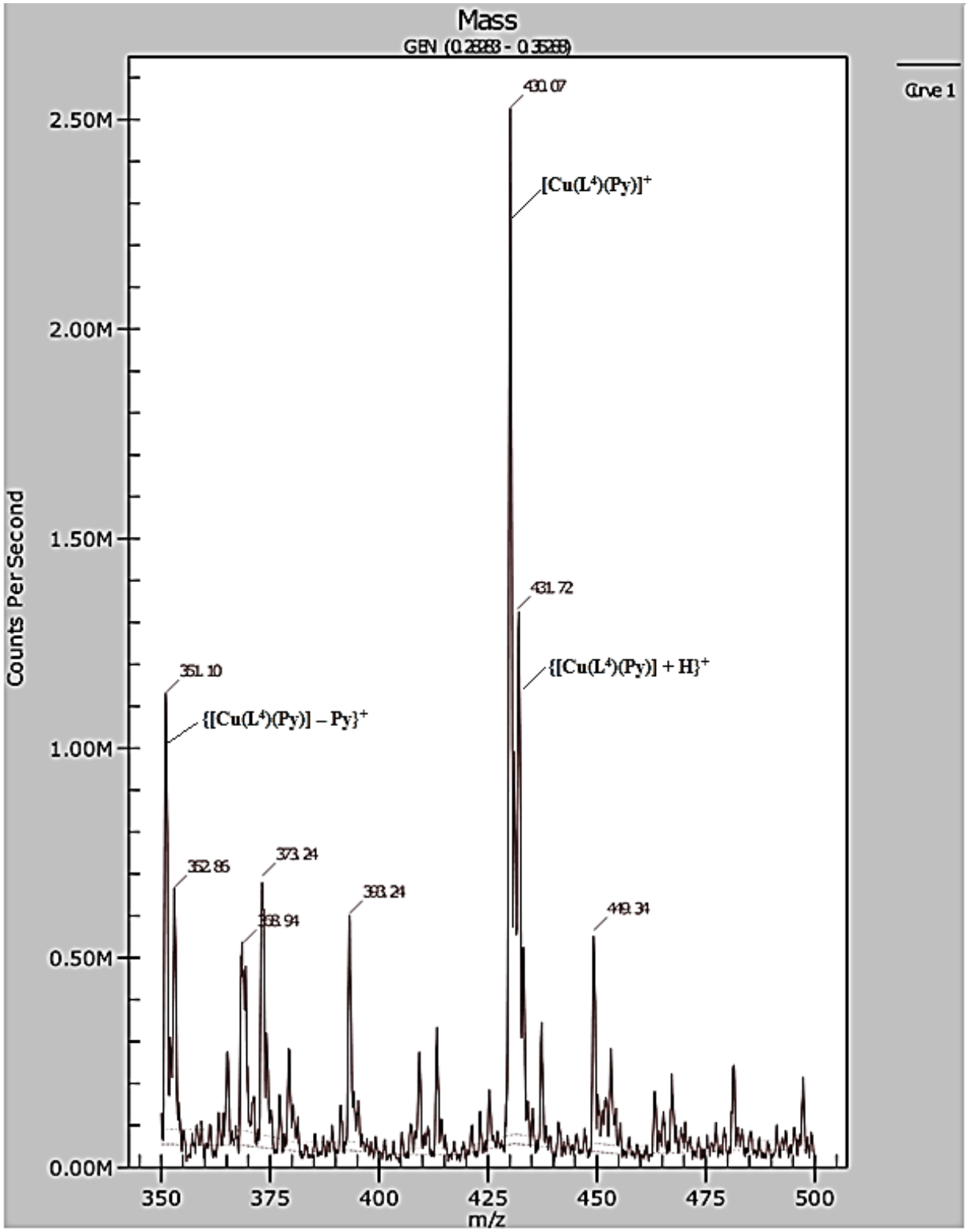

Figure 3.7. ESI-MS of complex **4** in CH_3OH.

3.3.4. Electrochemical properties. The electrochemical properties of **1**–**4** were examined in CH_3CN solution (0.1 M TEAP) by cyclic voltammetry using a platinum working electrode, platinum auxiliary electrode and an Ag/AgCl reference electrode. The potential data are listed in **Table 3.5**. **Figure 3.8, 3.9** and **3.10** depicts the representative voltammogram of **1** {Cu(I)}, **3** {Cu(II)} and **4** {Cu(II)} respectively. The voltammograms of all four complexes include both oxidation and reduction processes. The voltammogram pattern is similar for **1** & **2**, which includes a quasireversible (**Figure 3.8**) process at $E_{1/2}$ value 0.37 to 0.40 V corresponding to Cu(I)/Cu(II) redox couple,[46] whereas in the cathodic region Cu(I) is reduced to Cu(0) showing an irreversible single electron wave at E_{pc} values within the potential window –0.70 to –0.72 V.[64]

In the voltammogram of tetrameric Cu(II) complex (**3**), there are three quasireversible/reversible (**Figure 3.9**) processes at $E^{c/a}{}_{1/2}$ values –0.62, 0.10 and 0.36 V corresponding to Cu(II)/Cu(I) redox couples[65] of four different Cu(II) centers, whereas for the monomeric Cu(II) complex (**4**) a quasireversible (**Figure 3.10**) process for the above couple appears at $E^{c}{}_{1/2}$ value –0.52 V.

For all four complexes (**1**−**4**) an oxidation peak in the range 0.87 to 0.91 V[66] and two reduction peaks in the range –1.37 to –1.45 and –1.61 to –1.65 V[31,47c] belong to ligand centered processes respectively.

Table 3.5. Cyclic voltammetric[a] results for complexes 1–4 at 298 K

Complex	Potentials (V) versus Ag/AgCl				
	Cu^{I}/Cu^{II} $E^{a}_{1/2}(\Delta E^{a}_{P})$	Cu^{I}/Cu^{0} E_{pc}	Ligand – centered oxidation $E^{a}_{1/2}(\Delta E^{a}_{P})$	Ligand – centered reduction E_{pc}	Cu^{II}/Cu^{I} $E^{c/a}_{1/2}$ $(\Delta E^{c/a}_{P})$
$[Cu(HL^{1})(PPh_3)_2Br]\cdot CH_3CN$ (**1**)	0.40(320)	–0.72	0.89(240)	–1.41, –1.63	–
$[Cu(HL^{2})(PPh_3)_2Cl]\cdot DMSO$ (**2**)	0.37(326)	–0.70	0.87(156)	–1.45, –1.65	–
$[(Cu_2L^{3}{}_2Cl)_2(\mu\text{–}Cl)_2]\cdot 2H_2O$ (**3**)	–	–	0.88(190)	–1.39, –1.63	–0.62(50) 0.10(77), 0.36(113),
$[Cu(L^{4})(Py)]$ (**4**)	–	–	0.91(264)	–1.37, –1.61	– 0.52(100)

[a]In CH_3CN at a scan rate 100 mV/s. $E_{1/2} = (E_{pa} + E_{pc})/2$, where E_{pa} and E_{pc} are anodic and cathodic peak potentials vs. Ag/AgCl, respectively. $\Delta E_P = E_{pa} - E_{pc}$.

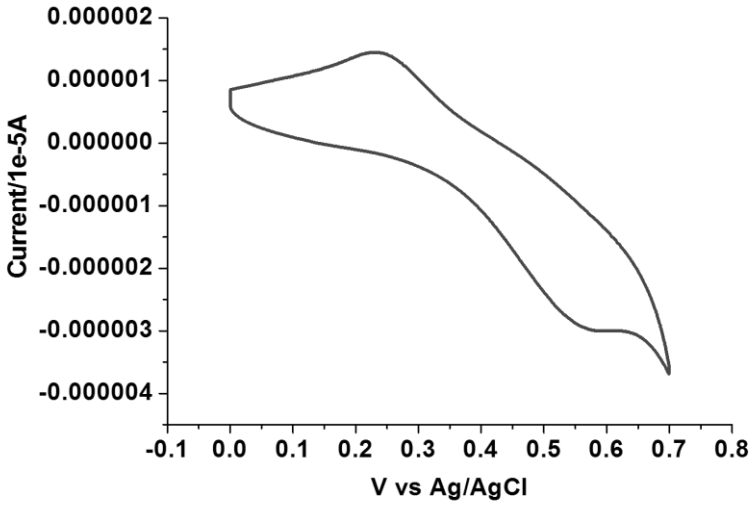

Figure 3.8. Cyclic voltammogram of complex **1**.

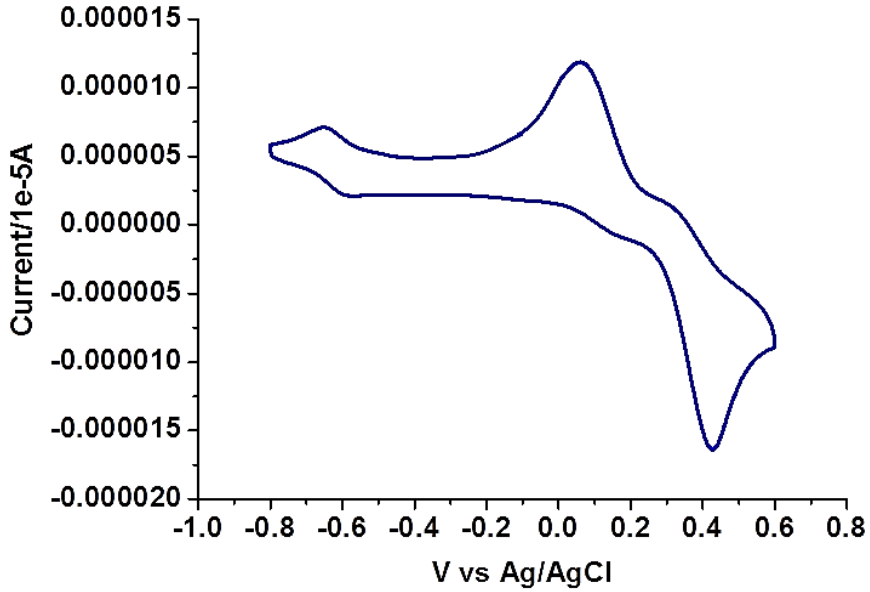

Figure 3.9. Cyclic voltammogram of complex **3**.

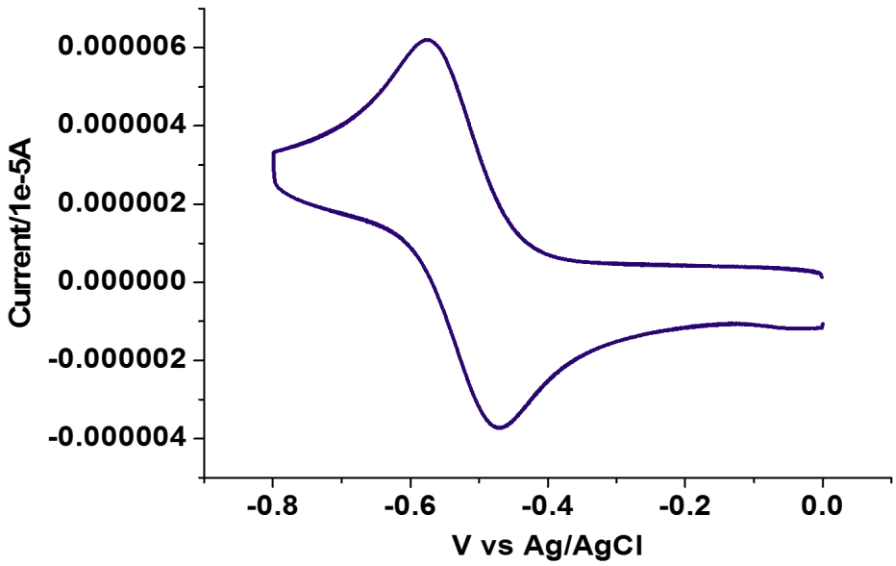

Figure 3.10. Cyclic voltammogram of complex **4**.

3.3.5. DNA binding studies

3.3.5.1. Absorption spectroscopic studies. DNA is often a vital target to mediate apoptosis or necrosis to a cell. Therefore the binding affinity of the complexes to CT–DNA was studied using different spectral methods. UV–Vis titration experiments were carried out to determine the binding constant (K_b) of the complexes to CT–DNA (**Figure 3.11** and **Table 3.6**). The complexes **1**–**4** shows absorption bands in the region 448–349 nm which are attributed to metal to ligand (**1** & **2**) and ligand to metal (**3** & **4**) charge transfer transitions whereas the absorption bands at higher energy is due to intra-ligand transitions. The binding of complexes to DNA either leads to hypochromism or hyperchromism which provides a measure of the strength of the intercalative or groove binding respectively.[67]

In order to quantify the binding affinity of the interaction between CT–DNA and each of **1**–**4**, the binding constant (K_b) was calculated using Eq. 1 (*Experimental Section*). The binding constant (K_b) of the complexes were in the range of 1.30×10^4 to 9.60×10^5 M^{-1}. Complexes **3** exhibited higher binding affinity than the other complexes (**1**, **2** and **4)**. The binding propensities of ligands to CT–DNA were also estimated. All the ligands showed lower DNA binding affinity than their respective complexes, yielding K_b values in the order of 10^3 M^{-1}.

3.3.5.2. Competitive DNA binding fluorescence studies. Ethidium dibromide (EB) is a standard intercalating agent and exhibits fluorescence upon binding to DNA. The relative binding of the complexes **1**–**4** to CT–DNA was also investigated by monitoring the quenching of the fluorescence emission from EB bound CT–DNA, on successive addition of the complexes. EB is nonemissive in 10 mM Tris–HCl buffer (pH 8.0) containing 1% DMF due to fluorescence quenching of free EB by solvent molecules, while in the presence of DNA, EB shows enhanced emission intensity due to intercalative binding.[68] On addition of the copper complexes to EB bound CT–DNA, the emission intensity at 597 nm was quenched by ~ 14% and ~ 13% for copper(I) complexes **1** and **2** respectively, whereas copper(II) complexes **3** and **4** exhibited a decrease of ~ 82% and ~ 10% respectively (**Figure 3.12**). The quenching of emission intensity of ethidium bromide upon addition of **1**–**4** showed that the complexes probably compete with EB for the binding with DNA. Copper(I) complexes **1** and **2** exhibited a K_{sv} value of 3.06×10^3 and 2.22×10^3 M^{-1} as calculated from Eq. 2 and the K_{app} value of 6.87×10^5 and 6.70×10^5 M^{-1} as calculated from Eq. 3 respectively (**Table 3.6**). Similarly for copper(II) complexes, **3** exhibited

the highest decrease in the emission intensity of EB which is well reflected in its K_{sv} and K_{app} values of 5.36×10^4 and 7.34×10^5 M^{-1} respectively. Complex **4** showed the least decrease in the emission intensity of EB which is consistent with its lower K_{sv} and K_{app} values of 1.32×10^3 and 5.79×10^5 M^{-1} respectively (**Table 3.6**). The higher K_{sv} and K_{app} value of **3** than the other complexes may be attributed to its higher solubility in aqueous medium and the presence of quinonoidal group in the thiosemicarbazone ligand coordinated to the metal.

The Kapp of the complexes were of the order of $\sim 10^2$ lower than the classical intercalator EB (i.e. 1.00×107 M^{-1}), which suggests that the interactions between the complexes and CT–DNA were possibly groove binding in nature. The trend in K_{app} values are in line with the trend in the K_b values which were obtained from the UV–Vis absorption spectral studies (**Table 3.6**).Control competitive DNA binding experiments with ligands (**Table 3.7**) showed that ligands have lesser K_{sv} and K_{app} values than their corresponding complexes.

3.3.5.3. Thermal melting studies. In order to have an insight into the nature of interaction and the conformational changes brought about by the complexes on interaction with CT–DNA, thermal denaturation experiments were performed.[69] The melting temperature of CT–DNA (T_m) in absence of any complexes was ~65.7^{o}C (**Figure 3.13**). In the presence of the copper complexes the DNA melting temperature (T_m) showed a slight increase from ~1.05^{o}C to 1.83^{o}C (**Table 3.6**). Among all the complexes, **3** showed the highest shift of the DNA melting temperature (ΔT_m) of + 1.83^{o}C which may be attributed to its better interaction with CT–DNA as evidenced from UV–Vis absorption and competitive DNA binding studies. The lower ΔT_m values suggest that the complexes interact with CT–DNA primarily through groove binding mode rather than an intercalative mode of binding to DNA which generally results in higher positive shift in the T_m of CT–DNA.[69,70]

3.3.5.4. Circular dichroism studies. Circular dichroism was used to investigate the conformational changes in CT–DNA due to the interaction with the complexes. CT–DNA shows two conserved bands in the UV region, a positive band at 275 nm due to base stacking interaction and a negative band at 245 nm due to right handed helicity.[71] The interaction of **1**, **2** and **4** showed marginal changes in the CD spectra of CT–DNA, whereas the interaction of **3** with CT–DNA induced a decrease in the intensity for the negative ellipticity at 245 nm and an increase in the positive ellipticity band at 275 nm (**Figure 3.14**). These results suggest that

interaction of **1**, **2** and **4** did not bring about any conformational changes in CT–DNA while **3** perturbed the stacking interaction as well as the right handed helicity of CT–DNA.

3.3.6. DNA cleavage studies

3.3.6.1. Chemical–induced DNA cleavage. To assess whether the DNA binding properties of the complexes are associated with the chemical nuclease activity, 300 ng of pUC19 DNA was incubated in presence of hydrogen peroxide as an oxidising agent, with different concentration of the complexes (1–300 μM) in 50 mM Tris–HCl buffer (pH 8.0) containing 1% DMF in dark for 1h. Upon gel electrophoresis, complexes **1**, **2** and **4** showed slight DNA cleavage activity ranging from ~ 2–10%, whereas complex **3**, exhibited a maximum chemical nuclease activity of ~ 60% at complex concentration of 100 μM (**Figure 3.15** and **3.16**). This enhanced chemical nuclease activity of **3** can be possibly rationalized on the basis of its higher binding affinity towards CT–DNA as observed from the DNA binding studies. Control experiments using the oxidizing agent hydrogen peroxide and the ligands showed that, neither hydrogen peroxide nor the ligands were cleavage active under similar experimental condition. All the complexes, in the absence of the oxidising agent, were cleavage inactive under dark conditions.

In order to elucidate the probable mechanistic aspects of the chemical–induced DNA cleavage activity by these complexes various inhibitors were used. The chemical−induced DNA cleavage reactions may involve reactive oxygen species (ROS) such as singlet oxygen ($^1O_2$) and hydroxyl radicals (*OH). Therefore, NaN_3 and L–histidine were used as singlet oxygen quenchers, while KI and D−mannitol were employed as hydroxyl radical quenchers. Complexes **1**, **2** and **4** did not show any appreciable inhibition in the chemical–induced DNA cleavage activity in the presence of the various additives which may be due to the diminished chemical nuclease activity of these complexes. On the other hand, addition of singlet oxygen quenchers like NaN_3 and L–histidine inhibited the DNA cleavage activity of complex **3** by ~ 6 % and ~ 22 % respectively. Similarly in the presence of the hydroxyl radical scavengers KI and D–mannitol, the chemical nuclease activity of complex **3** was reduced by ~ 14 % and ~ 11 % respectively (**Figure 3.17**). These results suggest that among all the copper complexes, **3** exhibits chemical−induced DNA cleavage activity probably *via* both singlet oxygen and hydroxyl radical pathways.

3.3.6.2. Photo-induced DNA cleavage. To investigate if the chemical nuclease activity of the complexes was also associated with photo nuclease activity, photo–induced DNA cleavage was carried out with 300 ng pUC19 DNA in the presence and absence of the complexes **1**–**4** (**Figure 3.18**). The extent of DNA cleavage by the complexes was monitored in a concentration dependent manner as shown in **Figure 3.19**. All the complexes (except **4**) showed ~ 10% or more photo−induced DNA cleavage activity at a complex concentration of 10 μM, which ultimately was saturated at a complex concentration of 100 μM. Among the copper(I) complexes, **2** exhibited greater (~ 55 %) photo-induced DNA cleavage activity than **1** (~ 40 %). On the other hand, in copper(II) complexes, **3** showed an abruptly higher photo-induced DNA cleavage activity of ~ 80 %, whereas **4** exhibited a minimal DNA cleavage activity of ~ 18 % (**Figure 3.19**). The higher DNA cleavage activity of **3** may be attributed due to its higher binding affinity to DNA as shown in binding studies and may also is because of its solubility in aqueous medium and the presence of quinonoidal group in the thiosemicarbazone ligand coordinated to the metal. Control experiments suggest that neither DMF (1%) nor the ligands showed any photo-induced DNA cleavage activity, which implies that, the ligands or DMF alone are cleavage inactive under similar conditions.

To understand the mechanistic aspect of the photo nuclease activity of these complexes, we used the same additives as used in exploring the mechanism of chemical nuclease activity. The DNA cleavage reaction involving molecular oxygen can proceed in two mechanistic pathways, namely, by a type–II process involving singlet oxygen species ($^1O_2$) or by a photo-redox pathway involving reactive hydroxyl radicals (*OH).[72] In case of copper(I) complexes, the singlet oxygen quenchers, like NaN_3 and L–histidine showed a reduced photo nuclease activity of complex **1** by ~ 9 % and ~ 8 % and of complex **2** by ~ 4 % and ~ 12 % respectively. Similarly the hydroxyl radical scavengers, KI and D–mannitol, exhibited a significant inhibition of photo–induced DNA cleavage activity of complex **1** by ~ 26 % and ~ 13 % and of complex **2** by ~ 19 % and ~ 7 % respectively (**Figure 3.20**). While in case of copper(II) complexes, the presence of singlet oxygen quenchers, NaN_3 and L−histidine, decreased the photo nuclease activity of complex **3** by ~ 4 % and ~ 5 % and complex **4** by ~ 3 % and ~ 10 % respectively. Similarly KI and D–mannitol (hydroxyl radical quenchers) showed an inhibition of DNA cleavage activity by ~ 12 % and ~ 28 % for complex **3** and ~ 5 % and ~ 3 % for complex **4** (**Figure 3.20**). These results suggest that, **1** & **2** exhibit photo-induced DNA cleavage activity possibly *via* both singlet oxygen and hydroxyl

radical pathways while the mechanistic pathway for **3** & **4** cannot be stated with a degree of certainty. Among the two pathways, hydroxyl radical dominates over the singlet oxygen pathway as the hydroxyl radical scavengers showed higher inhibitory effect than the singlet oxygen quenchers.

Table 3.6. DNA binding parameters for the complexes 1–4

Complex	Binding Constant (K_b)[a] (M^{-1})	ΔT_m [b] (^oC)	Stern–Volmer quenching Constant (K_{SV}) (M^{-1})[c]	K_{app} [d] (M^{-1})
1	3.40×10^5	+1.05	3.06×10^3	6.87×10^5
2	1.20×10^5	+1.65	2.22×10^3	6.70×10^5
3	9.60×10^5	+1.83	5.36×10^4	7.34×10^5
4	1.30×10^4	+1.11	1.32×10^3	5.79×10^5

[a]DNA binding constant by UV–vis spectral method. [b]Change in the melting temperature of CT–DNA. [c]Stern–Volmer quenching constant for the CT–DNA–EB complex. [d]The apparent DNA binding constant.

Table 3.7. DNA binding parameters for the ligands

Ligands	Binding Constant (K_b) [a] (M^{-1})	Stern–Volmer Quenching Constant (K_{SV}) (M^{-1}) [b]	K_{app} [c] (M^{-1})
HL^1	5.50×10^3	5.01×10^2	3.02×10^5
HL^2	5.20×10^3	5.80×10^2	3.60×10^5
HL^3	1.80×10^3	9.28×10^2	6.70×10^5
H_2L^4	7.00×10^3	4.50×10^2	2.69×10^5

[a]DNA binding constant by UV–vis spectral method. [b]Stern–Volmer Quenching constant for CT–DNA–EB complex. [c]The apparent DNA binding constant.

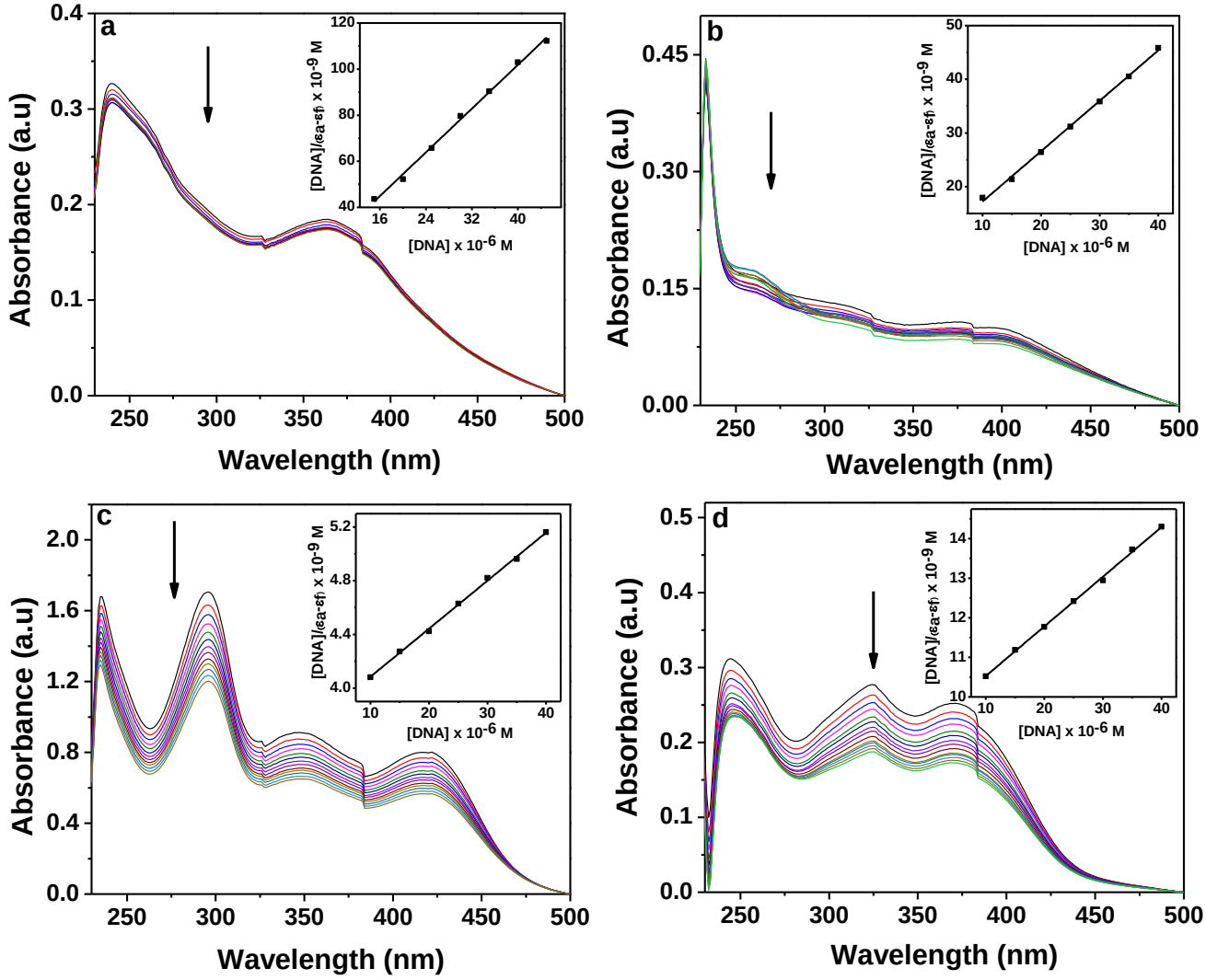

Figure 3.11. Electronic absorption spectra of **1** (a), **2** (b), **3** (c) and **4** (d) (25 μM each) upon the titration of CT–DNA (0–70 μM) in 10 mM Tris–HCl buffer (pH 8.0) containing 1% DMF. The arrow shows the changes in absorbance with respect to an increase in the CT–DNA concentration. The inset shows the linear fit of $[DNA]/(\varepsilon_a - \varepsilon_f)$ vs [DNA] and the binding constant (K_b) was calculated using Eq. 1.

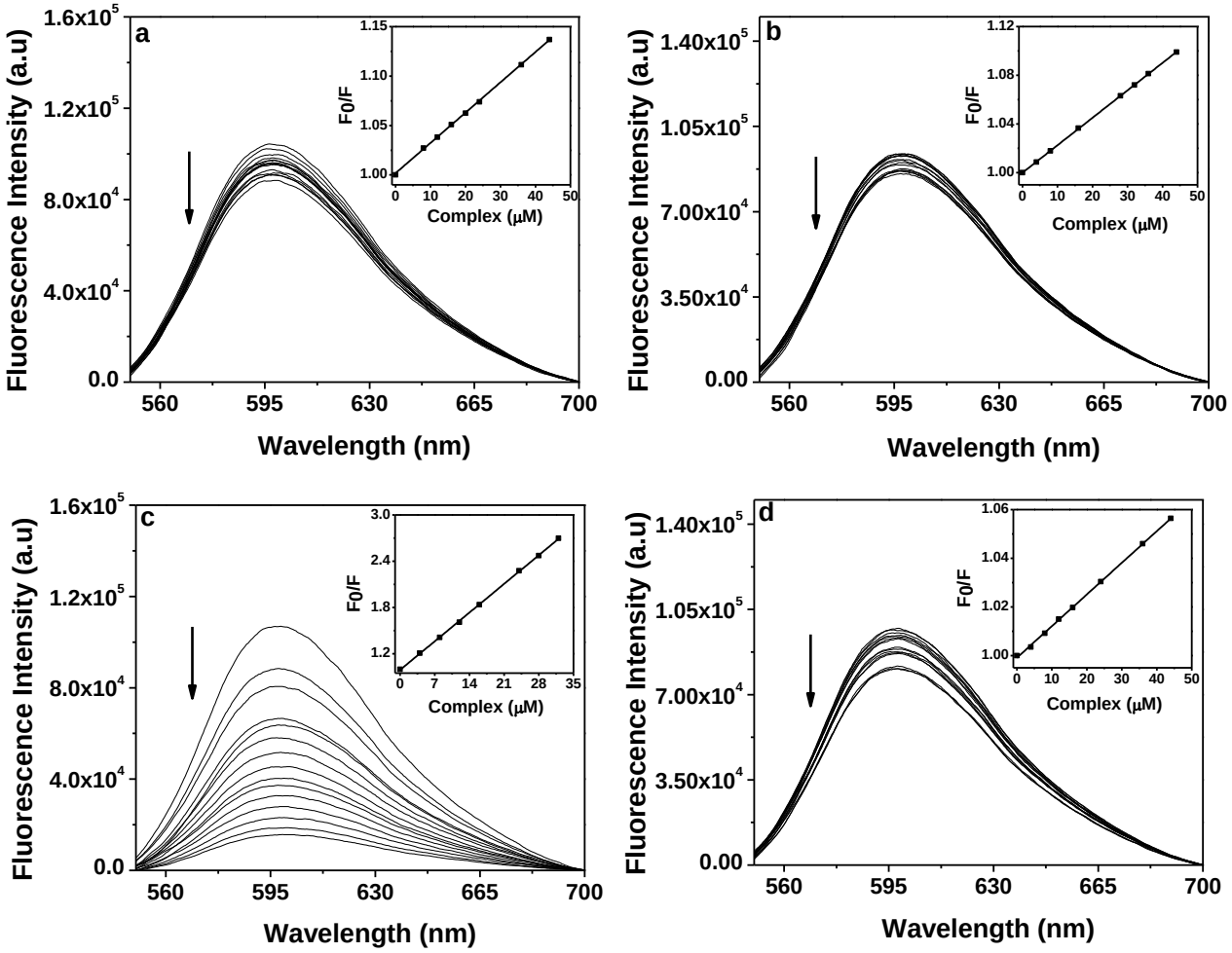

Figure 3.12. Fluorescence emission spectra of ethidium bromide (2 μM) bound to CT-DNA (50 μM) in the presence of complex **1** (a), **2** (b), **3** (c) and **4** (d) (0–60 μM) in 10 mM Tris–HCl buffer (pH 8.0) containing 1% DMF. The arrow indicates the effect of increasing concentration of complex on the fluorescence emission of ethidium bromide bound CT–DNA. The inset shows the linear fit of F_0/F *vs* [complex] and Stern–Volmer quenching constant (K_{SV}) was calculated using Eq. 2.

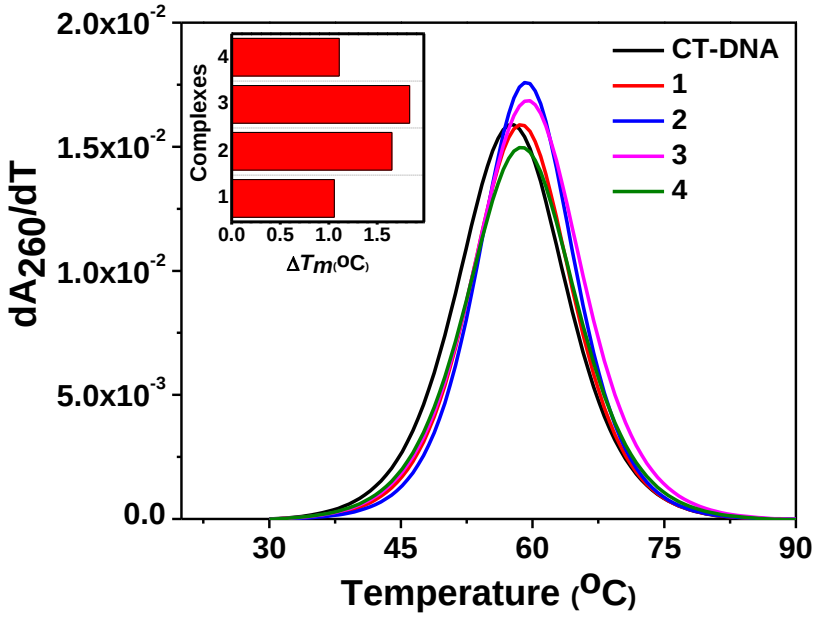

Figure 3.13. Derivative plot of thermal denaturation of CT–DNA (100 μM) in absence and presence of **1**–**4** (50 μM). The experiment was done in 10 mM Tris–HCl buffer (pH 8.0) containing 1% DMF. Inset shows the ΔT_m (^oC) of the complexes as compared to CT–DNA.

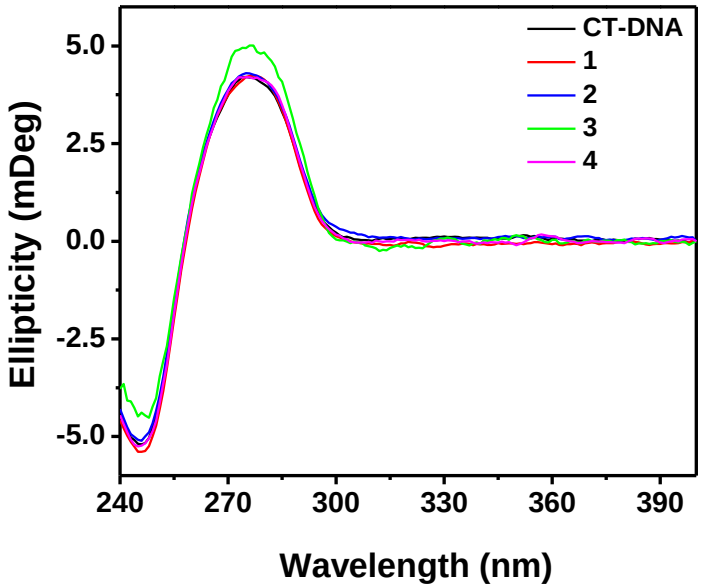

Figure 3.14. Circular dichroism spectra of CT–DNA (50 μM) in the presence and absence of **1**–**4** (20 μM) in 10 mM Tris–HCl buffer (pH 8.0) containing 1% DMF. The path length of the cuvette was 10 mm.

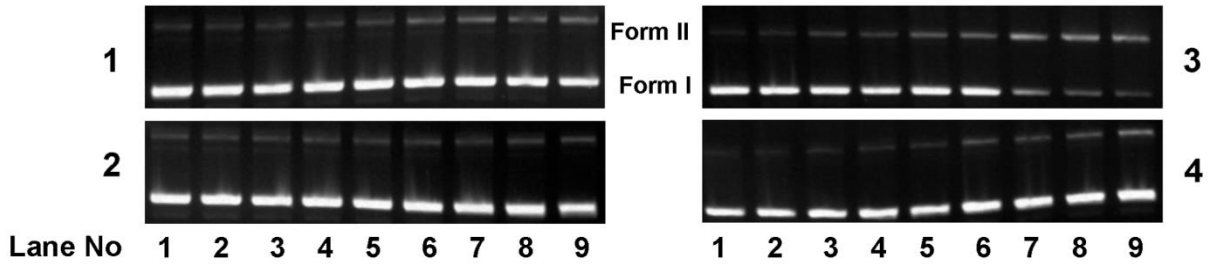

Figure 3.15. Gel diagram showing concentration dependent chemical nuclease activity by **1**–**4**; 300ng of SC pUC19 DNA at different concentrations of the complexes [1–300 µM in 50 mM Tris–HCl buffer (pH 8.0) containing 1% DMF] was treated with hydrogen peroxide (0.5mM) in dark for 1 h at 37°C. Lanes 1–9: 1, 2.5, 5.0, 7.5, 10, 50, 75, 100 and 300 µM of **1**–**4**.

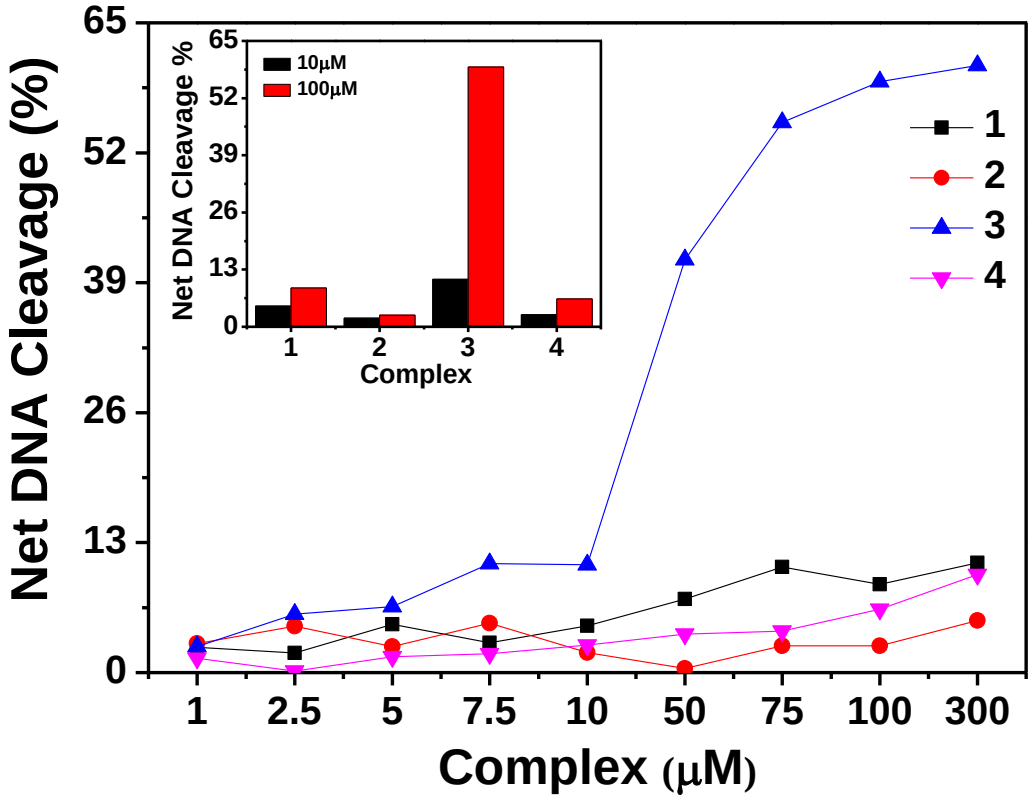

Figure 3.16. Concentration dependent chemical nuclease activity by **1**–**4**; 300 ng of SC pUC19 DNA at different concentration of the complexes [1–300 µM in 50 mM Tris–HCl buffer (pH 8.0) containing 1% DMF] was treated with hydrogen peroxide (0.5 mM) in dark for 1 h at 37°C. The net DNA cleavage percent was calculated using Eq. 4. Inset shows a bar diagram representation of the net DNA cleavage of different complexes at 10 and 100 µM.

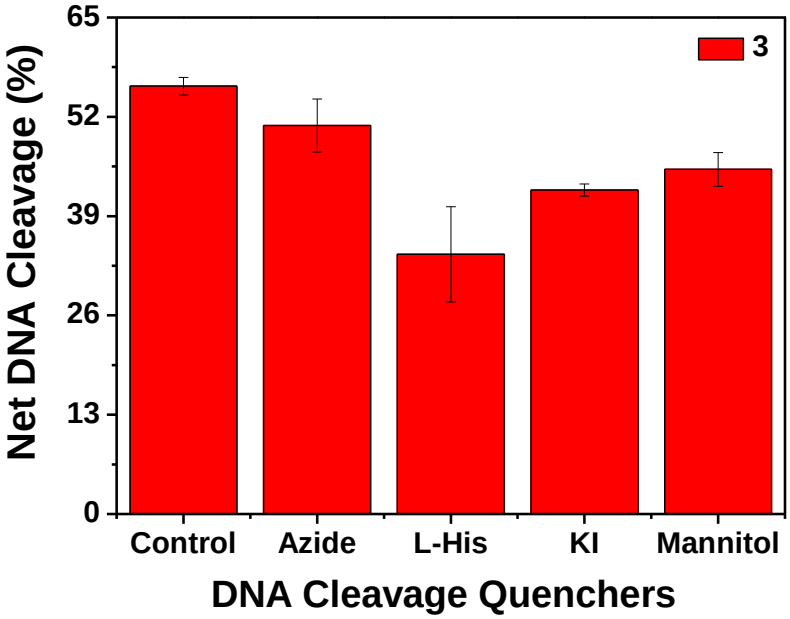

Figure 3.17. Chemical nuclease activity of SC pUC19 DNA by **3** in the presence of various additives in 50 mM Tris–HCl buffer (pH 8.0) containing 1% DMF. SC pUC19 DNA (300 ng) in the presence of various additives was treated with hydrogen peroxide (0.5 mM) in the dark for 1 h at 37^{o}C with **3** (100 µM). The additive concentrations were: sodium azide (0.5 mM), L–histidine (0.5 mM), KI (0.5 mM) and D–mannitol (0.5 mM).

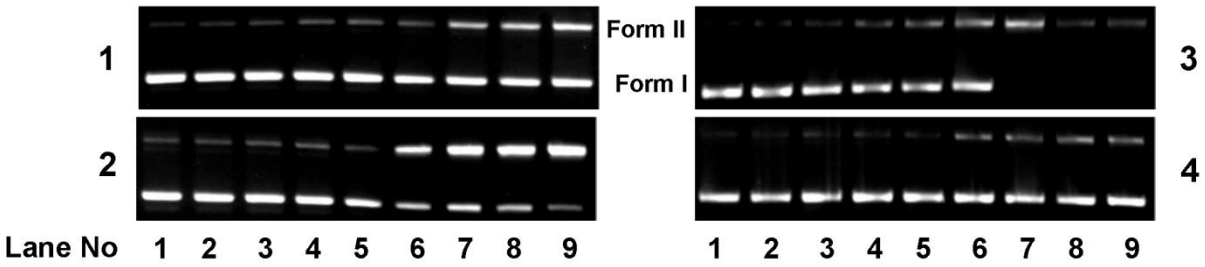

Figure 3.18. Gel diagram showing concentration dependent DNA cleavage by **1**–**4**; 300ng of SC pUC19 DNA at different concentrations of the complexes [1–300 µM in 50 mM Tris–HCl buffer (pH 8.0) containing 1% DMF] was photo–irradiated with UVA at 350 nm for 1 h. Lanes 1–9: 1, 2.5, 5.0, 7.5, 10, 50, 75, 100 and 300 µM of **1**–**4**.

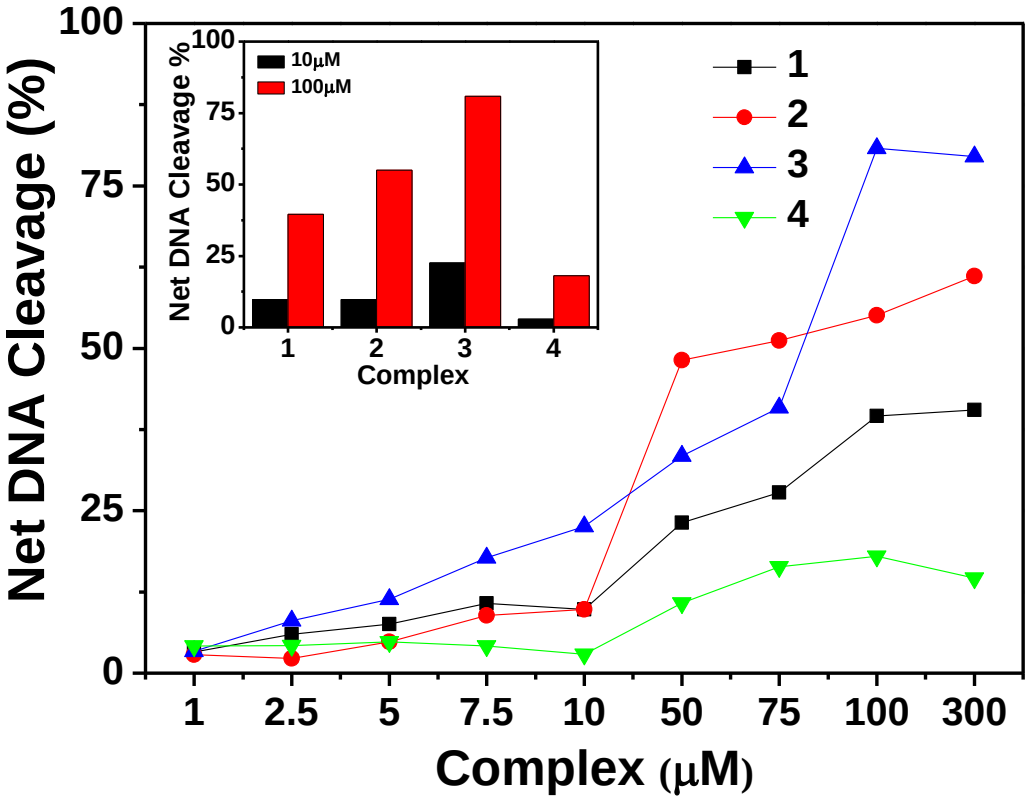

Figure 3.19. Concentration dependent DNA cleavage by **1**–**4**; 300 ng of SC pUC19 DNA at different concentration of the complexes [1–300 μM in 50 mM Tris–HCl buffer (pH 8.0) containing 1% DMF] was photo–irradiated with UVA at 350 nm for 1 h. The net DNA cleavage percent was calculated using Eq. 4. Inset shows a bar diagram representation of the net DNA cleavage of different complexes at 10 and 100 μM.

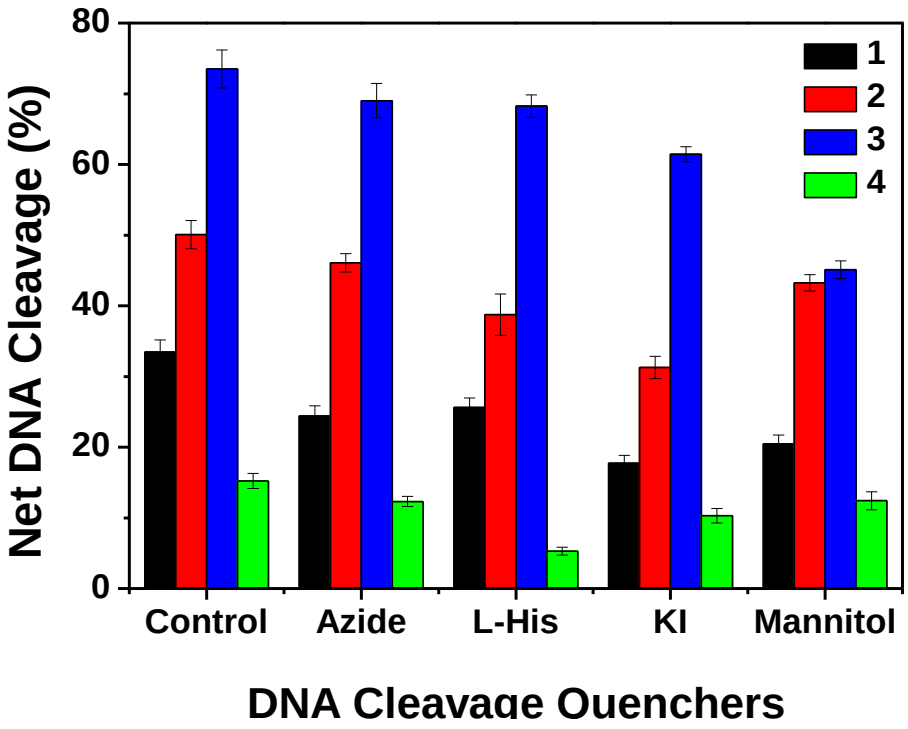

Figure 3.20. DNA cleavage of SC pUC19 DNA by **1**–**4** in the presence of various additives in 50 mM Tris–HCl buffer (pH 8.0) containing 1% DMF. SC pUC19 DNA (300 ng) in the presence of various additives was photo–irradiated at 350 nm for 1 h with **1**–**4** (100 µM). The additive concentrations were: sodium azide (0.5 mM), L–histidine (0.5 mM), KI (0.5 mM) and D–mannitol (0.5 mM).

3.3.7. Anticancer activity

3.3.7.1. Inhibition of cancer cell viability. In the present study, the antiproliferative efficacy of **1**–**4** was assayed by determining the viability of HeLa cells using the MTT assay. The ligands (HL^1, HL^2 and H_2L^4) and metal precursors (CuBr, CuCl & $CuCl_2$) gave IC_{50} values of >200 μM but the other ligand (HL^3) gave IC_{50} values of 98 μM, whereas corresponding complexes **1**–**4** gave values in the range 20–36 μM. The significant decrease in the inhibitory activity for the ligand compared to the metal complex clearly indicates that incorporation of copper into the ligand environment has a marked effect on cytotoxicity. A possible explanation is that by coordination the polarity of the ligand and the central metal ion are reduced through the charge equilibration, which favors permeation of the complexes through the lipid layer of the cell membrane.[73] The present results are consistent with the observation that metal complexes can exhibit greater biological activities than the free ligand.[36]

Comparing the activity of four complexes, the cytotoxic activity follows the order **3** > **2** > **1** > **4**, which is reflected from the IC_{50} values with dose dependency illustrated in **Table 3.8** & **Figure 3.21**. It is remarkable that **3**, having quinonoidal group in the thiosemicarbazone ligand coordinated to the metal is most active. This is in correlation with the fact that the derivatives of quinoline are found to show good biological activities such as antioxidation, antiproliferation, and anti–inflammation.[74,75]

A possible single shot drug for cancer cure has been elusive till date, due to their multiple occurrences in more than a hundred forms and several cases of recurrence of cancer post chemotherapy and surgery are well known. Interestingly, equating the efficacy of our synthesized novel copper compounds against the presently available common chemo drugs sold to the patients, we found out that Cisplatin, Gefitinib, Gemcitabine, 5–Florouracil, Vinorelbine had an IC_{50} of 13μM, 20μM, 35μM, 40 μM and 48μM respectively on HeLa cells, under conditions similar to our experiment.[76] These findings give a positive revelation about the potential of our copper compounds as future neoplastic precursor drug candidates.

3.3.7.2. Nuclear staining assay. To investigate the apoptotic potential of test compounds in HeLa cells, DAPI staining was performed. Chromatin condensation during the process of apoptosis (type I programmed cell death) is a characterizing marker of nuclear alteration. HeLa cells were treated with 30 μM, 25 μM, 15 μM and 30 μM of **1**, **2**, **3** and **4** respectively. All the doses were given below the calculated IC_{50} and the cells were incubated for 24h before DAPI nuclear staining assay. Control cells hardly showed any sort of condensation in comparison to the test compound's activity (as shown in **Figure 3.22**), when the cells were examined under fluorescent microscope, DAPI filter. All images clearly demonstrate the brightly condensed chromatin bodies and the nuclear blebbings as marked by arrows in the figure. The drug treated groups besides showing nuclear changes also revealed a shrinking morphology, which is another important hallmark of apoptosis.

Table 3.8. Cytotoxic scores in HeLa cancer cells for 1–4

Compounds	IC_{50} (μM)
1	33.5 ± 4.67
2	31.5 ± 5.72
3	19.8 ± 3.54
4	36 ± 6.74

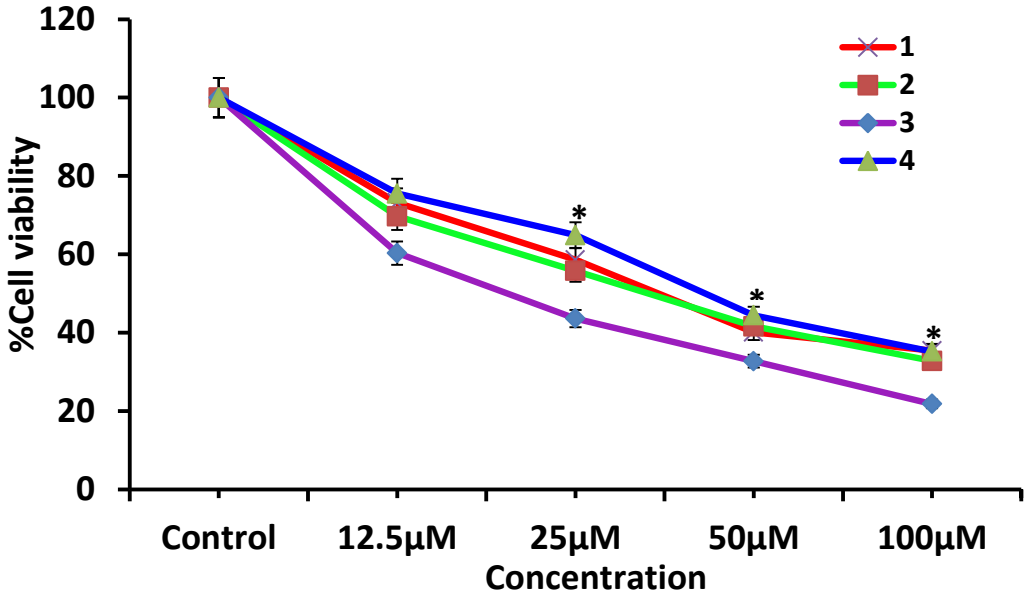

Figure 3.21. Effect of **1**, **2**, **3** and **4** on cancer cell viability and growth: HeLa cells were treated with different concentrations of the test compounds for 72h and then cell viability was measured by MTT assay. Data reported as the mean ± S.D. for *n* = 6 and compared against control by using a Student's *t*–test. (*denotes significance compared to control).

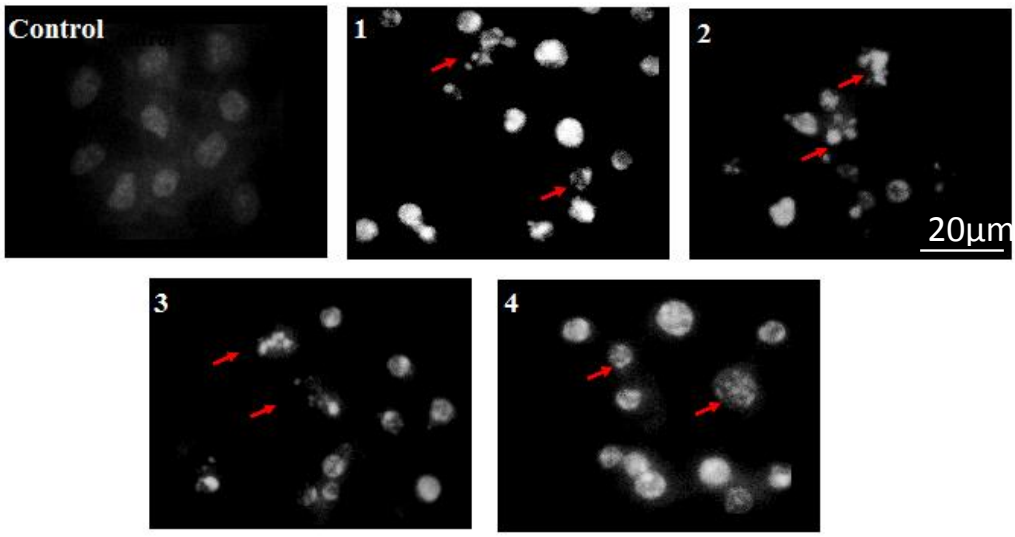

Figure 3.22. Study of apoptosis by morphological changes in nuclei of HeLa cells: After treatment, HeLa cells from the control and the treated group were fixed with 3.7% formaldehyde for 15 min, permeabilized with 0.1% Triton X–100 and stained with 1µg/ml DAPI for 5 min at 37°C. The cells were then washed with PBS and examined by fluorescence microscopy (Olympus IX 71) (200×).

3.4. CONCLUSION

The following are the salient observations and findings of the work in this chapter:

a) Two Cu(I) complexes **1** $[Cu(HL^1)(PPh_3)_2Br]\cdot CH_3CN$ & **2** $[Cu(HL^2)(PPh_3)_2Cl]\cdot DMSO$ and two Cu(II) complexes **3** $[(Cu_2L^3{}_2Cl)_2(\mu\text{–}Cl)_2]\cdot 2H_2O$ & **4** $[Cu(L^4)(Py)]$ of thiosemicarbazone ligands were synthesized and characterized by structural, analytical, and spectral methods.

b) The copper complexes **1**–**4** showed good DNA binding propensity. Their DNA binding activities were determined using UV–Vis absorption titration, competitive DNA binding fluorescence experiments, thermal denaturation studies and circular dichroism spectroscopy. The experimental results show that the complexes interact with CT–DNA probably by groove binding mode, with binding constants ranging from 10^4−10^5 M^{-1}. The competitive DNA binding fluorescence experiments suggest that among all the complexes, **3** showed highest quenching constant (K_{sv}) and K_{app} values.

c) Among all the complexes, **3** displayed significant chemical nuclease activity in presence of hydrogen peroxide of ~ 60 %. All the complexes showed good photo–induced cleavage of pUC19 supercoiled plasmid DNA with complex **3** showing the highest photo induced DNA cleavage activity of ~ 80%.

d) The results from the mechanistic study suggested that, the chemical nuclease activity of complex **3** and the photo nuclease activity of complex **1**–**2** proceeds probably by both singlet oxygen and hydroxyl radical pathways.

e) In addition, the *in vitro* antiproliferative activity of complexes **1**–**4** against HeLa cell line was assayed. The cytotoxicity of the complexes is affected by the various functional groups attached to the thiosemicarbazone derivative whereby **3** was particularly potent against the cells tested.

f) The results of pharmacological activity of the copper complexes reported in this chapter reveals that the compound **3** shows the highest activity, which may be due to its solubility in aqueous medium and the presence of quinonoidal group in the thiosemicarbazone ligand coordinated to the metal.

g) The results obtained from the present copper complexes are of importance for the development of metal–based agents for anti–cancer applications. Further work is in progress to better identify the mechanism of action and to prepare more potent related compounds for the treatment of cancer.

3.5. REFERENCES

(1) Boulikas, T.; Vougiouka, M. *Oncol. Rep.* **2003**, *10*, 1663.

(2) Wong, E.; Giandomenico, C. M. *Chem. Rev.* **1999**, *99*, 2451.

(3) Galanski, M.; Arion, V. B.; Jakupec, M. A.; Keppler, B. K. *Curr. Pharm. Des.* **2003**, *9*, 2078.

(4) Wang, D.; Lippard, S. J. *Nat. Rev. Drug Discovery* **2005**, *4*, 307.

(5) Angeles-Boza, A. M.; Bradley, P. M.; Fu, P. K. L.; Wicke, S. E.; Bacsa, J.; Dunbar, K. M.; Turro, C. *Inorg. Chem.* **2004**, *43*, 8510.

(6) Rosenberg, B.; Vam, C. L.; Trosko J. E.; Mansour V. H. *Nature* **1969**, *222*, 385.

(7) Wu, Z.; Liu, Q.; Liang, X.; Yang, X.; Wang, N.; Wang, X.; Sun, H.; Lu, Y.; Guo, Z. *J. Biol. Inorg. Chem.* **2009**, *14*, 1313.

(8) Raja, D. S.; Bhuvanesh, N. S. P.; Natarajan, K. *Dalton Trans*. **2012**, *41*, 4365.

(9) Bednarski, P. J.; Mackay, F. S.; Sadler, P. J. *Anti-Cancer Agents Med. Chem.* **2007**, *7*, 75.

(10) Sharma, S.; Singh, S. K.; Chandra, M.; Pandey, D. S. *J. Inorg. Biochem.* **2005**, *99*, 458.

(11) Metcalfe, C.; Thomas, J. A. *Chem. Soc. Rev.* **2003**, *32*, 215.

(12) Chang, C. M.; Klema, V. J.; Johnson, B. J.; Mure, M.; Klinman, J. P.; Wilmot, C. M. *Biochemistry* **2010**, *49*, 2540.

(13) Solomon, E. I.; Chen, P.; Metz, M.; Sang-Kyu, L.; Palmer, A. E. *Angew. Chem., Int. Ed.* **2001**, *40*, 4570.

(14) Wojciech, P.; Nicholas, M. D. J. D. *BBA-Protein Struct. M.* **1985**, *828*, 130.

(15) Tainer, J. A.; Getzoff, E. D.; Richardson, J. S.; Richardson, D. C. *Nature* **1983**, *306*, 284.

(16) Matoba, Y.; Kumagai, T.; Yamamoto, A.; Yoshitsu, H.; Sugiyama, M. *J. Biol. Chem.* **2006**, *281*, 8981.

(17) Barton, J. K. *Bioinorganic Chemistry*, in: Bertini, I.; Grey, H. B.; Lippard, S. J.; Valentine, J. S.; (Eds.), University Science Book, Mill Valley, **1994**, p. 455.

(18) (a) Santini, C.; Pellei, M.; Gandin, V.; Porchia, M.; Tisato, F.; Marzano, C. *Chem. Rev.* **2014**, *114*, 815. (b) Kate, A. N.; Kumbhar, A. A.; Khan, A. A.; Joshi, P. V.; Puranik, V. G. *Bioconjugate Chem.* **2014**, *25*, 102. (c) Raja, D. S.; Bhuvanesh, N. S. P.; Natarajan K. *Inorg. Chem.* **2011**, *50*, 12852. (d) Cater, M. A.; Pearson, H. B.; Wolyniec, K.; Klaver, P.; Bilandzic, M.; Paterson, B. M.; Bush, A. I.; Humbert, P. O.; Fontaine, S. L.; Donnelly, P. S.; Haupt, Y. *ACS Chem. Biol.* **2013**, *8*, 1621.

(19) (a) Easmon, J.; Purstinger, G.; Heinisch, G.; Roth, T.; Fiebig, H. H.; Holzer, W.; Jager, W.; Jenny, M.; Hofmann, J. *J. Med. Chem.* **2001**, *44*, 2164. (b) Jutten, P.; Schumann, W.; Hartl, A.; Dahse, H. M.; Grafe, U. *J. Med. Chem.* **2007**, *50*, 3661. (c) Greenbaum, D. C.; Mackey, Z.; Hansell, E.; Doyle, P.; Gut, J.; Caffrey, C. R.; Lehrman, J.; Rosenthal, P. J.; McKerrow, J. H.; Chibale, K. *J. Med. Chem.* **2004**, *47*, 3212.

(20) Brockman, R. W; Thomson, J. R.; Bell, M. J.; Skipper, H. E. *Cancer Res.* **1956**, *16*, 167.

(21) Ferrari, M. B.; Bisceglie, F.; Casoli, C.; Durot, S.; Badarau, I. M.; Pelosi, G.; Pilotti, E.; Pinelli, S.; Tarasconi, P. *J. Med. Chem.* **2005**, *48*, 1671.

(22) Richardson, D. R.; Sharpe, P. C.; Lovejoy, D. B.; Senaratne, D.; Kalinowski, D. S.; Islam, M.; Bernhardt, P. V. *J. Med. Chem.* **2006**, *49*, 6510.

(23) Ludwig, J. A.; Szakacs, G.; Martin, S. E.; Chu, B. F.; Cardarelli, C.; Sauna, Z. E.; Caplen, N. J.; Fales, H. M.; Ambudkar, S. V.; Weinstein, J. N.; Gottesman, M. M. *Cancer Res.* **2006**, *66*, 4808.

(24) Kalinowski, D. S.; Yu, Y.; Sharpe, P. C.; Islam, M.; Liao, Y. T.; Lovejoy, D. B.; Kumar, N.; Bernhardt, P. V.; Richardson, D. R. *J. Med. Chem.* **2007**, *50*, 3716.

(25) Chen, J.; Huang, Y. W.; Liu, G.; Afrasiabi, Z.; Sinn, E.; Padhye, S.; Ma, Y. *Toxicol. Appl. Pharmacol.* **2004**, *197*, 40.

(26) (a) Raja, D. S.; Paramaguru, G.; Bhuvanesh, N. S. P.; Reibenspies, J. H.; Renganathan, R.; Natarajan, K. *Dalton Trans.* **2011**, *40*, 4548. (b) Jansson, P. J.; Sharpe, P. C.; Bernhardt, P. V.; Richardson, D. R. *J. Med. Chem.* **2010**, *53*, 5759. (c) Adsule, S.; Barve, V.; Chen, D.; Ahmed, F.; Dou, Q. P.; Padhye, S.; Sarkar, F. H. *J. Med. Chem.* **2006**, *49*, 7242. (d) Huang, H.; Chen, Q.; Ku, X.; Meng, L.; Lin, L.; Wang, X.; Zhu, C.; Wang, Y.; Chen, Z.; Li, M.; Jiang, H.; Chen, K.; Ding, J.; Liu, H. *J. Med. Chem.* **2010**, *53*, 3048.

(27) West, D. X.; Hall, I. H.; Rajendran, K. G.; Liberta, A. E. *Anti-cancer Drugs* **1993**, *4*, 231.

(28) Matesanz, A. I.; Joie, C.; Souza, P. *Dalton Trans.* **2010**, *39*, 7059.

(29) (a) Padhye, S.; Afrasiabi, Z.; Sinn, E.; Fok, J.; Mehta, K.; Rath, N. *Inorg. Chem.* **2005**, *44*, 1154. (b) Afrasiabi, Z.; Sinn, E.; Lin, W.; Ma, Y.; Campana, C.; Padhye, S. *J. Inorg. Biochem.* **2005**, *99*, 1526.

(30) (a) Kalaivani, P.; Prabhakaran, R.; Poornima, P.; Dallemer, F.; Vijayalakshmi, K.; Padma, V. V.; Natarajan, K. *Organometallics* **2012**, *31*, 8323. (b) Otero, L.; Vieites, M.; Boiani, L.; Denicola, A.; Rigol, C.; Opazo, L.; Olea-Azar, C.; Maya, J. D.; Morello, A.; Siegel, R. L. K.;

Piro, O. E.; Castellano, E.; González, M.; Gambino, D.; Cerecetto, H. *J. Med. Chem.* **2006**, *49*, 3322. (c) Baldini, M.; Ferrari, M. B.; Bisceglie, F.; Dall'Aglio, P.P.; Pelosi, G.; Pinelli, S.; Tarasconi, P. *Inorg. Chem.* **2004**, *43*, 7170. (d) Baldini, M.; Ferrari, M. B.; Bisceglie, F.; Pelosi, G.; Pinelli, S.; Tarasconi, P. *Inorg. Chem.* **2003**, *42*, 2049. (e) Kalaivani, P.; Prabhakaran, R.; Ramachandran, E.; Dallemer, F.; Paramaguru, G.; Renganathan, R.; Poornima, P.; Padma, V. V.; Natarajan, K. *Dalton Trans.* **2012**, *41*, 2486. (f) Sampath, K.; Sathiyaraj, S.; Jayabalakrishnan, C.; *Med. Chem. Res.* **2014**, *23*, 958. (g) Silva, J. G. D.; Despaigne, A. A. R.; Louro, S. R. W.; Bandeira, C. C.; Souza-Fagundes, E. M.; Beraldo, H. *Eur. J. Med. Chem.* **2013**, *65*, 415. (h) Ramachandran, E.; Thomas, S. P.; Poornima, P.; Kalaivani, P.; Prabhakaran, R.; Padma, V. V.; Natarajan, K. *Eur. J. Med. Chem.* **2012**, *50*, 405. (i) Lu, J.; Guo, H.; Zeng, X.; Zhang, Y.; Zhao, P.; Jiang, J.; Zang, L. *J. Inorg. Biochem.* **2012**, *112*, 39.

(31) Afrasiabi, Z.; Sinn, E.; Padhye, S.; Dutta, S.; Padhye, S.; Newton, C.; Anson, C. E.; Powell, A. K. *J. Inorg. Biochem.* **2003**, *95*, 306.

(32) Jouad, E. M.; Larcher, G.; Allain, M.; Riou, A.; Bouet, G. M.; Khan, M. A.; Thanh, X. D. *J. Inorg. Biochem.* **2001**, *86*, 565.

(33) Sharma, S.; Athar, F.; Maurya, M. R.; Naqvi, F.; Azam, A. *Eur. J. Med. Chem.* **2005**, *40*, 557.

(34) Wang, T.; Guo, Z. *Curr. Med. Chem.* **2006**, *13*, 525.

(35) Gaál, A.; Orgován, G.; Polgári, Z.; Réti, A.; Mihucz, V. G.; Bősze, S.; Szoboszlai, N.; Streli, C. *J. Inorg. Biochem.* **2014**, *130*, 52.

(36) Rosu, T.; Pahontu, E.; Pasculescu, S.; Georgescu, R.; Stanica, N.; Curaj, A.; Popescu, A.; Leabu, M. *Eur. J. Med. Chem.* **2010**, *45*, 1627.

(37) Palanimuthu, D.; Shinde, S. V.; Somasundaram, K.; Samuelson, A. G. *J. Med. Chem.* **2013**, *56*, 722.

(38) Raja, D. S.; Bhuvanesh, N. S. P.; Natarajan, K. *Eur. J. Med. Chem.* **2011**, *46*, 4584.

(39) Bisceglie, F.; Baldini, M.; Ferrari, M. B.; Buluggiu, E.; Careri, M.; Pelosi, G.; Pinelli, S; Tarasconi, P. *Eur. J. Med. Chem.* **2007**, *42*, 627.

(40) Liu, Z. C.; Wang, B. D.; Yang, Z. Y.; Li, Y.; Qin, D. D.; Li, T. R. *Eur. J. Med. Chem.* **2009**, *44*, 4477.

(41) Afrasiabi, Z.; Sinn, E.; Kulkarni, P. P.; Ambike, V.; Padhye, S.; Deobagakar, D.; Heron, M.; Gabbutt, C.; Anson, C. E.; Powell, A. K. *Inorg. Chim. Acta* **2005**, *358*, 2023.

(42) Cowley, A. R.; Dilworth, J. R.; Donnelly, P. S.; White, J. M.; *Inorg. Chem.* **2006**, *45*, 496.

(43) Rodriguez-Arguelles, M. C.; Lopez-Silva, E.; Sanmartin, J.; Pelagatti, P.; Zami, F. *J. Inorg. Biochem.* **2005**, *99*, 2231.

(44) Ashfield, L. J.; Cowley, A. R.; Dilworth, J. R.; Donnelly, P. S. *Inorg. Chem.* **2004**, *43*, 4121.

(45) Lobana, T. S.; Khanna, S.; Butcher, R. J.; Hunter, A. D.; Zeller, M. *Polyhedron* **2006**, *25*, 2755.

(46) Krishna, P. M.; Reddy, K. H. *Inorg. Chim. Acta* **2009**, *362*, 4185.

(47) (a) Dash, S. P.; Pasayat, S.; Saswati; Dash, H. R.; Das, S.; Butcher, R. J.; Dinda, R. *Polyhedron* **2012**, *31*, 524. (b) Pasayat, S.; Dash, S. P.; Saswati; Majhi, P. K.; Patil, Y. P.; Nethaji, M.; Dash, H. R.; Das, S.; Dinda, R. *Polyhedron* **2012**, *38*, 198. (c) Saswati; Dinda, R.; Schmiesing, C. S.; Sinn, E.; Patil, Y. P.; Nethaji, M.; Stoeckli-Evans, H.; Acharyya, R. *Polyhedron* **2013**, *50*, 354. (d) Dash, S. P.; Pasayat, S.; Bhakat, S.; Roy, S.; Dinda, R.; Tiekink, E. R. T.; Mukhopadhyay, S.; Bhutia, S. K.; Hardikar, M. R.; Joshi, B. N.; Patil, Y. P; Nethaji, M. *Inorg. Chem.* **2013**, *52*, 14096. (e) Dash, S. P.; Panda, A. K.; Pasayat, S.; Dinda, R.; Biswas, A.; Tiekink, E. R. T.; Patil, Y. P.; Nethaji, M.; Kaminsky, W.; Mukhopadhyay, S.; Bhutia, S. K. *Dalton Trans.* **2014**, *43*, 10139.

(48) Part 1: Ghosh, S; Purohit, S. *Indian J. Chem., Sect. A: Inorg., Bio-inorg., Phys., Theor. Anal. Chem.* **1987**, *26A*, 131.

(49) Lobana, T. S.; Rekha; Butcher, R. J.; Castineiras, A.; Bermejo, E.; Bharatam, P. V. *Inorg. Chem.* **2006**, *45*, 1535.

(50) Blanc, E.; Schwarzenbach, D.; Flack, H. D. *J. Appl. Crystallogr.* **1991**, *24*, 1035.

(51) Bruker, *SADABS, SAINT, SHELXTL and SMART*, Bruker AXS Inc., Madison, Wisconsin, SA, **2003**.

(52) Sheldrick, G. M. *Acta Crystallogr., Sect. A: Found. Crystallogr.* **2008**, *64*, 112.

(53) Krishnamoorthy, P.; Sathyadevi, P.; Cowley, A. H.; Butorac, R. R.; Dharmaraj, N. *Eur. J. Med. Chem.* **2011**, *46*, 3376.

(54) Dai, W. M.; Lai, K. W.; Wu, A.; Hamaguchi, W.; Lee, M. Y.; Zhou, L.; Ishii, A.; Nishimoto, S. *J. Med. Chem.* **2002**, *45*, 758.

(55) Mukhopadhyay, S.; Panda, P. K.; Behera, B.; Das, C. K.; Hassan, M. K.; Das, D. N.; Sinha, N.; Bissoyi, A.; Pramanik, K.; Maiti, T. K.; Bhutia, S. K. *Food Chem. Toxicol*. **2014**, *64*, 369.

(56) Mukhopadhyay, S.; Panda, P. K.; Das, D. N.; Sinha, N; Behera, B.; Maiti, T. K.; Bhutia, S. K. *Acta Pharmacol. Sin.* **2014**, *35*, 814.

(57) Lobana, T. S.; Bhatia, P. K.; Tiekink, E. R. T. *J. Chem. Soc., Dalton Trans.* **1989**, 749.

(58) Philip, V.; Suni, V.; Kurup, M. R. P.; Nethaji, M. *Polyhedron* **2006**, *25*, 1931.

(59) Sreekanth, A.; Kurup, M. R. P. *Polyhedron* **2003**, *22*, 3321.

(60) Lobana, T. S.; Kumari, P.; Hundal, G.; Butcher, R. J. *Polyhedron* **2010**, *29*, 1130.

(61) Datta, S.; Seth, D. K.; Butcher, R. J.; Bhattacharya, S. *Inorg. Chim. Acta* **2011**, *377*, 120.

(62) Leovac, V. M.; Bogdanović, G. A.; Jovanović, S.; Joksović, L.; Marković, V.; Joksović, M. D.; Denčić, S. M.; Isaković, A.; Marković, I.; Heinemann, F. W.; Trifunović, S.; Đalović, I. *J. Inorg. Biochem.* **2011**, *105*, 1413.

(63) Nirmala, M.; Manikandan, R.; Prakash, G.; Viswanathamurthi, P. *Appl. Organomet. Chem.* **2014**, *28*, 18.

(64) Chakraborty, P.; Adhikary, J.; Ghosh, B.; Sanyal, R.; Chattopadhyay, S. K.; Bauzá, A.; Frontera, A.; Zangrando, E.; Das, D. *Inorg. Chem.* **2014**, *53*, 8257.

(65) (a) Kowol, C. R.; Heffeter, P.; Miklos, W.; Gille, L.; Trondl, R.; Cappellacci, L.; Berger, W.; Keppler, B. K. *J. Biol. Inorg. Chem.* **2012**, *17*, 409. (b) Zhou, Y. H.; Tao, J.; Sun, D. L.; Chen, L. Q.; Jia, W. G.; Cheng, Y. *Polyhedron* **2015**, *85*, 849. (c) Naskar, S.; Naskar, S.; Figge, H. M.; Sheldrick, W. S.; Corbella, M.; Tercero, J.; Chattopadhyay, S. K. *Polyhedron* **2012**, *35***,** 77.

(66) (a) Mishra, D.; Naskar, S.; Drew, M. G. B.; Chattopadhyay, S. K. *Inorg. Chim. Acta* **2006**, *359*, 585. (b) Paul, P.; Seth, D. K.; Richmond, M. G.; Bhattacharya, S. *RSC Adv*. **2014**, *4*, 1432.

(67) Kumar, P.; Gorai, S.; Santra, M. K.; Mondal, B.; Manna, D.; *Dalton Trans.* **2012**, *41*, 7573.

(68) Patra, A. K.; Bhowmick, T.; Ramakumar, S.; Nethaji, M.; Chakravarty, A. R. *Dalton Trans*. **2008**, *48*, 6966.

(69) An, Y.; Liu, S. D.; Deng, S. Y.; Ji, L. N.; Mao, Z. W. *J. Inorg. Biochem.* **2006**, *100*, 1586.

(70) Banerjee, S.; Hussain, A.; Prasad, P.; Khan, I.; Banik, B.; Kondaiah, P.; Chakravarty, A. R. *Eur. J. Inorg. Chem.* **2012**, 3899.

(71) Li, L.; Guo, Q.; Dong, J.; Xu, T.; Li, J. *J. Photochem. Photobiol. B,* **2013**, *125*, 56.

(72) Sasmal, P. K.; Saha, S.; Majumdar, R.; De, S.; Dighe, R. R.; Chakravarty, A. R. *Dalton Trans.* **2010**, *39*, 2147.

(73) Avaji, P. G.; Kumar, C. H. V.; Patil, S. A.; Shivananda, K. N.; Nagaraju, C. *Eur. J. Med. Chem.* **2009**, *44*, 3552.

(74) Canelón, I. R.; Sadler, P. J. *Inorg. Chem.* **2013**, *52*, 12276.

(75) Casas, J. S.; García-Tasende, M. S.; Sordo, J. *Coord. Chem. Rev.* **2000**, *209*, 197.

(76) Ahmed, M.; Jamil, K. *Biol. Med*. **2011**, *3*, 60.

Chapter 4

Chemistry of oxido molybdenum(IV/VI) thiosemicarbazone complexes: Active centre of molybdenum oxotransferases

Chapter 4

Chemistry of oxido molybdenum(IV/VI) thiosemicarbazone complexes: Active centre of molybdenum oxotransferases

ABSTRACT:

Oxygen atom transfer (OAT) reactivity of dioxidomolybdenum(VI) complexes $[Mo^{(VI)}O_2L^{1-6}]$ (**1**–**6**) {4–(*p*–bromophenyl)thiosemicarbazone of salicylaldehyde (H_2L^1), 4–(*p*–X–phenyl)thiosemicarbazone of *o*–vanillin {where, X = F (H_2L^2) and X = Cl (H_2L^3) and X = OMe (H_2L^4)}, 4–(*p*–bromophenyl)thiosemicarbazone of 5–bromosalicylaldehyde (H_2L^5), and 4–(*p*–chlorophenyl)thiosemicarbazone of *o*–hydroxynaphthaldehyde (H_2L^6)} with PPh_3 have been investigated. The OAT reactions proceed through the formation of $OPPh_3$, which have been characterized by ^{31}P NMR. Dioxidomolybdenum(VI) complexes $[Mo^{(VI)}O_2L^{1/5/6}(DMSO)]$ (**1a, 5a** & **6a**), $[Mo^{(VI)}O_2L^{2/4}(H_2O)]$ (**2a** & **4a**), and $[Mo^{(VI)}O_2L^3(DMSO)]_4{\cdot}2DMSO$ (**3a**) and monooxidomolybdenum(IV) complexes $[Mo^{(IV)}OL^{1-6}(N–N)]$ (**7**–**12**) {where, N–N = 2,2'–bipyridyl or 1,10–phenanthroline} are reported as the product of substrate binding and oxygen atom transfer reactivity of dioxidomolybdenum(VI) complexes $[Mo^{(VI)}O_2L^{1-6}]$ (**1**–**6**) respectively. All the complexes have been spectroscopically charecterized. Molecular structures of some of the Mo(VI) (**1a**–**4a**) and Mo(IV) complexes (**7** and **9**–**11**) have been determined by single crystal X–ray crystallography. The catalytic activity of $Mo^{(VI)}$ complexes (**1a**–**6a**) have also been studied.

4.1. INTRODUCTION

Molybdenum participates in a wide range of metalloenzymes called molybdoenzymes, in which molybdenum forms a part of the active sites.[1,2] These enzymes utilize molybdenum as a cofactor that catalyses the transformation processes such as in sulphite oxidase,[3] xanthine oxidase,[4] and aldehyde oxidase.[5] Molybdenum(VI) complexes with thiosemicarbazones serving as ONS donor ligands have been regarded as excellent models for the molybdenum binding site of these enzymes.[6–9]

Molybdenum is found in a large class of enzymes capable of transferring an oxygen atom from or to a substrate referred to as mononuclear molybdoenzymes or oxotransferases. Oxygen atom transfer (OAT) processes, as well as oxidation processes, are important in nature and in chemical industry.[10] OAT chemistry has attracted considerable attention in recent years because of its relevance in biological processes mediated by molybdenum or tungsten *oxotransferases.*[11–13] It has been known that the presence of sulfur atoms coordinated to molybdenum is favourable for complexes of molybdenum to have oxotransfer activity, and many model compounds that mimic oxotransferases have been studied.[14–20] Molybdenum enzymes catalyze a number of such reactions. These oxotransferases contain oxido– (or dioxido)–molybdenum units additionally coordinated by sulfur atoms.[2,21] In order to understand the activity of oxotransferase molybdoenzymes, several attempts have been made to monitor the oxotransfer reaction of dioxidomolybdenum complexes to substrates such as PPh_3.[15] Oxidomolybdenum complexes have been isolated and characterized as end products of such reactions along with PPh_3O.[22] Some of these reactions have also been kinetically followed.[23]

In addition, molybdenum complexes are known for their catalytic applications in the oxidation[24–40] and oxidative bromination of organic substrates,[41–44] and the oxidation of sulfides.[45–48] Mo(VI) complexes are also known to be very active as epoxidation catalysts, generally in solution of an organic solvent, especially for neutral complexes[49] much as evidenced by number of publications.[32,37,39,45,50–57]

Our group have currently focused on dioxidomolybdenum(VI) complexes with ligands that mimic's the coordination environment of the metal ion in enzymes. Among them, tridentate ligands containing ONS donor atoms has attracted our interest. In this work, we describe the

synthesis of a series of *cis*–dioxidomolybdenum(VI) complexes $[Mo^{(VI)}O_2L^{1–6}]$ (**1**–**6**). Dioxidomolybdenum(VI) complexes $[Mo^{(VI)}O_2L^{1/5/6}(DMSO)]$ (**1a, 5a** & **6a**), $[Mo^{(VI)}O_2L^{2/4}(H_2O)]$ (**2a** & **4a**), and $[Mo^{(VI)}O_2L^{3}(DMSO)]_4 \cdot 2DMSO$ (**3a**) and monooxidomolybdenum(IV) complexes $[Mo^{(IV)}OL^{1–6}(N–N)]$ (**7**–**12**) {where, N–N = 2,2'–bipyridyl or 1,10–phenanthroline} are also reported as the product of substrate binding and oxygen atom transfer reactivity of dioxidomolybdenum(VI) complexes $[Mo^{(VI)}O_2L^{1–6}]$ (**1**–**6**) respectively. All the complexes have been spectroscopically charecterized. Molecular structures of some of the Mo(VI) (**1a**–**4a**) and Mo(IV) complexes (**7** and **9**–**11**) have been determined by single crystal X–ray crystallography. The catalytic activity (oxidation of styrene and cyclohexene) of $Mo^{(VI)}$ complexes (**1a**–**6a**) have also been studied.

4.2. EXPERIMENTAL SECTION

4.2.1. General methods and materials. All chemicals were purchased from commercial sources and used without further purification. Reagent grade solvents were dried and distilled prior to use. $[MoO_2(acac)_2]$ was prepared as described in the literature.[58] The thiosemicabazides were prepared from distilled substituted aniline by a known method reported earlier.[59] The ligands 4–(*p*–bromophenyl)thiosemicarbazone of salicylaldehyde (H_2L^1), 4–(*p*–X–phenyl)thiosemicarbazone of *o*–vanillin {where, X = F (H_2L^2) and X = Cl (H_2L^3) and X = OMe (H_2L^4)}, 4–(*p*–bromophenyl)thiosemicarbazone of 5–bromosalicylaldehyde (H_2L^5), and 4–(*p*–chlorophenyl)thiosemicarbazone of *o*–hydroxynaphthaldehyde (H_2L^6) were prepared by reported methods.[60,61] Elemental analyses were performed on a Vario ELcube CHNS Elemental analyzer. IR spectra were recorded on a Perkin–Elmer Spectrum RXI spectrometer. ^1H, ^{13}C and ^{31}P NMR spectra were recorded with a Bruker Ultrashield 400 MHz spectrometer using $SiMe_4$ as an internal standard. Electronic spectra were recorded on a Lamda25, PerkinElmer spectrophotometer. Electrochemical data were collected using PAR electrochemical analyzer and a PC–controlled potentiostat/galvanostat (PAR 273A) at 298 K in a dry nitrogen atmosphere. Cyclic voltammetry experiments were carried out with Pt working and auxiliary electrodes and Ag/AgCl as reference electrode. Mass spectra were recorded on a SQ–300 MS instrument operating in ESI mode.

4.2.2. Synthesis of dioxidomolybdenum(VI) complexes $[Mo^{(VI)}O_2L^{1–6}]$ (1–6). To a refluxing solution of ligand, $H_2L^{1–6}$ (1.0 mmol) in 30 mL of ethanol, $MoO_2(acac)_2$ (1.0 mmol) was added. The mixture was refluxed for 2 h and filtered. Dark brown coloured microcrystalline residue was obtained.

$[Mo^{(VI)}O_2L^1]$ (1): Yield: 78%. Anal. calc. for $C_{14}H_{10}BrMoN_3O_3S$: C, 35.31; H, 2.12; N, 8.82. Found: C, 35.35; H, 2.14; N, 8.85. Main IR peaks (KBr, cm^{-1}): 3261 ν(N(3)–H), 3012 *ν*(C(7)–H), 1597 s ν(C=C), 1512 m ν(C(7)=N(1)), 918 s, 899 s ν(Mo=O), 764 s ν(C(8)–S(1)). ^1H NMR (DMSO–d_6, 400 MHz) δ: 9.84 (s, 1H, –C(8)–N(3)H), 8.82 (s, 1H, –N(1)=C(7)H), 7.75–6.90 (m, 8H, C_6H_4). ^{13}C NMR (DMSO–d_6, 100 MHz) δ: 162.15, 160.43, 155.62, 153.57, 148.72, 139.32, 134.46, 133.77, 130.82, 124.36, 121.63, 121.22, 117.48, 115.12. ESI Mass (CH_3CN): *m/z* 477.07 (100%, $[M + H]^+$).

$[Mo^{(VI)}O_2L^2]$ (2): Yield: 75%. Anal. calc. for $C_{15}H_{12}FMoN_3O_4S$: C, 40.46; H, 2.72; N, 9.44. Found: C, 40.45; H, 2.70; N, 9.41. Main IR peaks (KBr, cm^{-1}): 3287 ν(N(3)–H), 3021 *ν*(C(7)–H), 1610 s ν(C=C), 1532 m ν(C(7)=N(1)), 922 s, 889 s ν(Mo=O), 776 s ν(C(8)–S(1)). ^{1}H NMR (DMSO–d_6, 400 MHz) δ: 9.86 (s, 1H, –C(8)–N(3)H), 8.80 (s, 1H, –N(1)=C(7)H), 7.82–6.78 (m, 7H, C_6H_4), 3.89 (s, 3H, OCH_3). ^{13}C NMR (DMSO–d_6, 100 MHz) δ: 171.41, 163.64, 158.35, 153.54, 149.33, 138.63, 134.56, 133.79, 130.24, 124.56, 121.33, 121.67, 117.65, 115.37, 58.85. ESI Mass (CH_3CN): *m/z* 468.15 (50%, $[M + Na]^+$); *m/z* 413 (100%, $[M–OCH_3]^+$).

$[Mo^{(VI)}O_2L^3]$ (3): Yield: 75%. Anal. calc. for $C_{15}H_{12}ClMoN_3O_4S$: C, 39.02; H, 2.62; N, 9.10. Found: C, 39.04; H, 2.60; N, 9.12. Main IR peaks (KBr, cm^{-1}): 3236 ν(N(3)–H), 3012 *ν*(C(7)–H), 1597 s ν(C=C), 1514 m ν(C(7)=N(1)), 917 s, 886 s ν(Mo=O), 783 s ν(C(8)–S(1)). ^{1}H NMR (DMSO–d_6, 400 MHz) δ: 9.79 (s, 1H, –C(8)–N(3)H), 8.65 (s, 1H, –N(1)=C(7)H), 7.67–6.34 (m, 7H, C_6H_4), 3.66 (s, 3H, OCH_3). ^{13}C NMR (DMSO–d_6, 100 MHz) δ: 169.67, 167.56, 163.87, 158.54, 155.76, 149.45, 147.34, 145.78, 141.67, 138.54, 135.77, 131.45, 126.76, 120.34, 55.87. ESI Mass (CH_3CN): *m/z* 462.19 (100%, $[M + H]^+$); 466.61(62%, $[M + 4H]^+$).

$[Mo^{(VI)}O_2L^4]$ (4): Yield: 73%. Anal. calc. for $C_{16}H_{15}MoN_3O_5S$: C, 42.02; H, 3.31; N, 9.19. Found: C, 42.05; H, 3.30; N, 9.21. Main IR peaks (KBr, cm^{-1}): 3289 ν(N(3)–H), 2996 *ν*(C(7)–H), 1589 s ν(C=C), 1526 m ν(C(7)=N(1)), 923 s, 894 s ν(Mo=O), 756 s ν(C(8)–S(1)). ^{1}H NMR (DMSO–d_6, 400 MHz) δ: 9.43 (s, 1H, –C(8)–N(3)H), 8.25 (s, 1H, –N(1)=C(7)H), 7.78–6.56 (m, 7H, C_6H_4), 3.87 (s, 3H, OCH_3), 3.56 (s, 3H, OCH_3). ^{13}C NMR (DMSO–d_6, 100 MHz) δ: 174.56, 168.45, 167.78, 160.34, 157.22, 150.67, 146.23, 142.54, 140.67, 135.76, 128.34, 122.43, 118.56, 112.89, 54.53, 51.42. ESI Mass (CH_3CN): *m/z* 457.49 (20%, $[M]^+$).

$[Mo^{(VI)}O_2L^5]$ (5): Yield: 78%. Anal. calc. for $C_{14}H_9Br_2MoN_3O_3S$: C, 30.29; H, 1.63; N, 7.57. Found: C, 30.28; H, 1.64; N, 7.55. Main IR peaks (KBr, cm^{-1}): 3224 ν(N(3)–H), 2964 *ν*(C(7)–H), 1585 s ν(C=C), 1523 m ν(C(7)=N(1)), 921 s, 882 s ν(Mo=O), 762 s ν(C(8)–S(1)). ^{1}H NMR (DMSO–d_6, 400 MHz) δ: 9.14 (s, 1H, –C(8)–N(3)H), 8.55 (s, 1H, –N(1)=C(7)H), 7.87–6.56 (m, 7H, C_6H_4). ^{13}C NMR (DMSO–d_6, 100 MHz) δ: 169.67, 158.52, 153.41, 150.34, 144.54, 140.56, 136.24, 132.74, 130.82, 128.15, 123.46, 120.37, 117.51, 113.56. ESI Mass (CH_3CN): *m/z* 557.42 (80%, $[M + 2H]^+$).

$[Mo^{(VI)}O_2L^6]$ (6): Yield: 72%. Anal. calc. for $C_{18}H_{12}ClMoN_3O_3S$: C, 44.88; H, 2.51; N, 8.72. Found: C, 44.92; H, 2.50; N, 8.71. Main IR peaks (KBr, cm^{-1}): 3267 ν(N(3)–H), 3011 *ν*(C(7)–H), 1586 s ν(C=C), 1523 m ν(C(7)=N(1)), 926 s, 878 s ν(Mo=O), 773 s ν(C(8)–S(1)). ^{1}H NMR

(DMSO–d_6, 400 MHz) δ: 9.28 (s, 1H, –C(8)–N(3)H), 8.63 (s, 1H, –N(1)=C(7)H), 7.63–6.55 (m, 10H, C_6H_4). ^{13}C NMR (DMSO–d_6, 100 MHz) δ: 169.52, 163.52, 162.52, 158.52, 156.36, 153.24, 146.56, 143.26, 140.26, 138.21, 135.36, 130.63, 125.42, 122.62, 120.76, 117.26, 113.56, 112.68. ESI Mass (CH_3CN): *m/z* 481.43 (100%, $[M]^+$).

4.2.3. Synthesis of dioxidomolybdenum(VI) complexes $[Mo^{(VI)}O_2L^{1/5/6}(DMSO)]$ (1a, 5a & 6a), $[Mo^{(VI)}O_2L^{2/4}(H_2O)]$ (2a & 4a), and $[Mo^{(VI)}O_2L^{3}(DMSO)]_4$·2DMSO (3a). Complexes **1a**–**6a** were obtained during recrystallization of **1**–**6** from DMSO.

$[Mo^{(VI)}O_2L^{1}(DMSO)]$ (1a): Yield: 73%. Anal. calc. for $C_{16}H_{16}BrMoN_3O_4S_2$: C, 34.67; H, 2.91; N, 7.58. Found: C, 34.65; H, 2.90; N, 7.60. Main IR peaks (KBr, cm^{-1}): 3271 ν(N(3)–H), 3018 *ν*(C(7)–H), 1598 s ν(C=C), 1504 m ν(C(7)=N(1)), 920 s, 896 s ν(Mo=O), 760 s ν(C(8)–S(1)). ^{1}H NMR (DMSO–d_6, 400 MHz) δ: 9.83 (s, 1H, –C(8)–N(3)H), 8.82 (s, 1H, –N(1)=C(7)H), 7.74–6.90 (m, 8H, C_6H_4), 2.54 (s, 6H, DMSO). ^{13}C NMR (DMSO–d_6, 100 MHz) δ: 161.55, 159.41, 155.60, 152.56, 147.76, 140.38, 134.74, 134.57, 131.83, 122.02, 121.50, 121.12, 118.58, 114.42, 50.34.

$[Mo^{(VI)}O_2L^{2}(H_2O)]$ (2a): Yield: 68%. Anal. calc. for $C_{15}H_{14}FMoN_3O_5S$: C, 38.89; H, 3.05; N, 9.07. Found: C, 38.85; H, 3.02; N, 9.10. Main IR peaks (KBr, cm^{-1}): 3395 *ν*(H_2O), 3285 *ν*(N(3)–H), 2968 *ν*(C(7)–H), 1603 s ν(C=C), 1516 m ν(C(7)=N(1)), 931 s, 887 s ν(Mo=O), 738 s ν(C(8)–S(1)). ^{1}H NMR (DMSO–d_6, 400 MHz) δ: 9.74 (s, 1H, –C(8)–N(3)H), 8.77 (s, 1H, –N(1)=C(7)H), 7.77–6.94 (m, 7H, C_6H_4), 3.78 (s, 3H, OCH_3). ^{13}C NMR (DMSO–d_6, 100 MHz) δ: 172.74, 163.51, 155.51, 147.67, 146.86, 143. 83, 143.74, 137. 75, 134.33, 127.54, 125.59, 124.76, 120.68, 118.47, 51.56.

$[Mo^{(VI)}O_2L^{3}(DMSO)]_4$·2DMSO (3a): Yield: 72%. Anal. calc. for $C_{72}H_{84}Cl_4Mo_4N_{12}O_{22}S_{10}$: C, 37.34; H, 3.66; N, 7.26. Found: C, 37.37; H, 3.68; N, 7.25. Main IR peaks (KBr, cm^{-1}): 3278 ν(N(3)–H), 3015 *ν*(C(7)–H), 1592 s ν(C=C), 1521 m ν(C(7)=N(1)), 916 s, 893 s ν(Mo=O), 778 s ν(C(8)–S(1)). ^{1}H NMR (DMSO–d_6, 400 MHz) δ: 9.81 (s, 1H, –C(8)–N(3)H), 8.79 (s, 1H, –N(1)=C(7)H), 7.78–6.97 (m, 7H, C_6H_4), 3.79 (s, 3H, OCH_3), 2.54 (s, 6H, DMSO). ^{13}C NMR (DMSO–d_6, 100 MHz) δ: 169.49, 167.35, 162.37, 158.23, 155.06, 148.98, 146.77, 144.58, 140.30, 137.67, 135.53, 131.47, 126.46, 120.96, 53.35, 48.27.

$[Mo^{(VI)}O_2L^{4}(H_2O)]$ (4a): Yield: 67%. Anal. calc. for $C_{16}H_{17}MoN_3O_6S$: C, 40.43; H, 3.60; N, 8.84. Found: C, 40.45; H, 3.62; N, 8.81. Main IR peaks (KBr, cm^{-1}): 3401 ν(H_2O), 3299 ν(N(3)–

H), 2978 *ν*(C(7)–H), 1591 s ν(C=C), 1517 m ν(C(7)=N(1)), 925 s, 895 s ν(Mo=O), 735 s ν(C(8)–S(1)). ^{1}H NMR (DMSO–d_6, 400 MHz) δ: 9.56 (s, 1H, –C(8)–N(3)H), 8.70 (s, 1H, –N(1)=C(7)H), 7.64–6.85 (m, 7H, C_6H_4), 3.78 (s, 3H, OCH_3), 3.72 (s, 3H, OCH_3). ^{13}C NMR (DMSO–d_6, 100 MHz) δ: 176.34, 172.45, 167.53, 160.43, 158.76, 150.88, 144.14, 142.46, 140.21, 135.54, 129.23, 123.52, 119.74, 113.45, 56.13, 50.24.

[$Mo^{(VI)}O_2L^5$(DMSO)] (5a): Yield: 68%. Anal. calc. for $C_{16}H_{15}Br_2MoN_3O_4S_2$: C, 30.35; H, 2.39; N, 6.64. Found: C, 30.38; H, 2.40; N, 6.65. Main IR peaks (KBr, cm^{-1}): 3211 ν(N(3)–H), 2915 *ν*(C(7)–H), 1594 s ν(C=C), 1554 m ν(C(7)=N(1)), 938 s, 892 s ν(Mo=O), 767 s ν(C(8)–S(1)). ^{1}H NMR (DMSO–d_6, 400 MHz) δ: 9.34 (s, 1H, –C(8)–N(3)H), 8.76 (s, 1H, –N(1)=C(7)H), 7.63–6.56 (m, 7H, C_6H_4), 2.53 (s, 6H, DMSO). ^{13}C NMR (DMSO–d_6, 100 MHz) δ: 168.63, 159.45, 154.72, 151.35, 144.74, 141.33, 135.56, 132.35, 130.54, 128.01, 123.65, 120.64, 117.87, 112.53, 52.67.

[$Mo^{(VI)}O_2L^6$(DMSO)] (6a): Yield: 71%. Anal. calc. for $C_{20}H_{18}ClMoN_3O_4S_2$: C, 42.90; H, 3.24; N, 7.50. Found: C, 42.92; H, 3.20; N, 7.51. Main IR peaks (KBr, cm^{-1}): 3282 ν(N(3)–H), 3013 *ν*(C(7)–H), 1589 s ν(C=C), 1512 m ν(C(7)=N(1)), 933 s, 887 s ν(Mo=O), 766 s ν(C(8)–S(1)). ^{1}H NMR (DMSO–d_6, 400 MHz) δ: 9.34 (s, 1H, –C(8)–N(3)H), 8.56 (s, 1H, –N(1)=C(7)H), 7.35–6.65 (m, 10H, C_6H_4), 2.53 (s, 6H, DMSO). ^{13}C NMR (DMSO–d_6, 100 MHz) δ: 168.53, 167.12, 165.53, 158.80, 156.35, 153.65, 146.34, 143.67, 140.64, 139.12, 136.57, 130.76, 126.36, 122.56, 120.65, 117.87, 113.77, 112.63, 56.32.

4.2.4. Synthesis of Mo^{IV} complexes [$Mo^{(IV)}OL^{1–6}$(N–N)] (7–12). To a refluxing solution of [$Mo^{(VI)}O_2L^{1–6}$] (**1**–**6**) (1.0 mmol) in 30 mL of degassed acetonitrile 1.5 mmol of PPh_3 was added followed by 1.0 mmol of (N–N) {coligand, (N–N) = 2,2'–bipyridyl (**7**, **10** & **11**) or 1,10–phenanthroline (**8**, **9** & **12**)}, and the solution was refluxed for 3 h. X–ray quality crystal of **7** and **9**–**11** were obtained from reaction mixture. {bipy = 2,2'–bipyridyl; phen = 1,10–phenanthroline}.

[$Mo^{(IV)}OL^1$(bipy)] (7): Yield: 78%. Anal. calc. for $C_{24}H_{18}BrMoN_5O_2S$: C, 46.77; H, 2.94; N, 11.36. Found: C, 46.75; H, 2.96; N, 11.37. Main IR peaks (KBr, cm^{-1}): 3322 ν(N(3)–H), 3041 *ν*(C(7)–H), 1598 s ν(C=C), 1540 m ν(C(7)=N(1)), 931 s ν(Mo=O), 753 s ν(C(8)–S(1)).

[Mo$^{(IV)}$OL^{2}(phen)] (8): Yield: 84%. Anal. calc. for $C_{27}H_{20}FMoN_5O_3S$: C, 53.21; H, 3.31; N, 11.49. Found: C, 53.25; H, 3.32; N, 11.51. Main IR peaks (KBr, cm^{-1}): 3315s ν(N(3)–H), 3053 *ν*(C(7)–H), 1586 s ν(C=C), 1502 m ν(C(7)=N(1)), 945 s ν(Mo=O), 740 s ν(C(8)–S(1)).

[Mo $^{(IV)}$OL^{3}(phen)] (9): Yield: 74%. Anal. calc. for $C_{27}H_{20}ClMoN_5O_3S$: C, 51.81; H, 3.22; N, 11.19. Found: C, 51.85; H, 3.20; N, 11.15. Main IR peaks (KBr, cm^{-1}): 3298 s ν(N(3)–H), 3012 *ν*(C(7)–H), 1586 s ν(C=C), 1512 m ν(C(7)=N(1)), 922 s ν(Mo=O), 746 s ν(C(8)–S(1)).

[Mo$^{(IV)}$OL^{4}(bipy)] (10): Yield: 76%. Anal. calc. for $C_{26}H_{23}MoN_5O_4S$: C, 52.26; H, 3.88; N, 11.72. Found: C, 52.25; H, 3.86; N, 11.75. Main IR peaks (KBr, cm^{-1}): 3286 s ν(N(3)–H), 2978 *ν*(C(7)–H), 1590 s ν(C=C), 1511 m ν(C(7)=N(1)), 941 s ν(Mo=O), 748 s ν(C(9)–S(1)).

[Mo$^{(IV)}$OL^{5}(bipy)] (11): Yield: 88%. Anal. calc. for $C_{24}H_{17}Br_2MoN_5O_2S$: C, 41.46; H, 2.46; N, 10.07. Found: C, 41.45; H, 2.42; N, 10.05. Main IR peaks (KBr, cm^{-1}): 3211 s ν(N(3)–H), 2976 *ν*(C(7)–H), 1589 s ν(C=C), 1516 m ν(C(7)=N(1)), 934 s, ν(Mo=O), 754 s ν(C(8)–S(1)).

[Mo$^{(IV)}$OL^{6}(phen)] (12): Yield: 85%. Anal. calc. for $C_{30}H_{20}ClMoN_5O_2S$: C, 55.78; H, 3.12; N, 10.84. Found: C, 55.75; H, 3.10; N, 10.81. Main IR peaks (KBr, cm^{-1}): 3311 s ν(N(3)–H), 3017 *ν*(C(7)–H), 1584 s ν(C=C), 1501 m ν(C(7)=N(1)), 928 s ν(Mo=O), 748 s ν(C(8)–S(1)).

4.2.5. X–ray crystallography. Single crystals of complexes were mounted on Bruker Smart APEX II CCD diffractometer (**1a**), Rigaku XtaLAB mini diffractometer (**2a**–**4a**), Bruker APEX II diffractometer (**7**, **9** and **11**) and Nonius Kappa CCD FR590 diffractometer (**10**) equipped with a graphite monochromator and a Mo Kα radiator (λ=0.71073 Å). Crystallographic data and details of refinement of **1a**–**4a** are given in **Table 4.1** and **7** and **9**−**11** are given in **Table 4.2**.The unit cell dimensions and intensity data were measured at 292(2) K for **1a**, 293(2) K for **2a** & **3a**, 100(2) K for **4a**, **9** & **11**, 105 K for **7** and, 130 K for **10**. The data were integrated and scaled using SAINT, SADABS within the APEX2 software package by Bruker.[62] Absorption corrections were applied using SADABS[63] and the structures were solved by direct methods using the program SHELXS−97[64] and refined using least squares with the SHELXL−97[64] software program. Hydrogen atoms were placed in geometrically idealised positions and constrained to ride on their parent atoms with C−H distances in the range 0.95−1.00 Å. The non–hydrogen atoms were refined anisotropically.

Table 4.1. Crystal data and refinement details of $[Mo^{(VI)}O_2L^1(DMSO)]$ (1a), $[Mo^{(VI)}O_2L^{2/4}(H_2O)]$ (2a & 4a), and $[Mo^{(VI)}O_2L^3(DMSO)]_4 \cdot 2DMSO$ (3a).

Compound	**1a**	**2a**	**3a**	**4a**
Formula	$C_{16}H_{16}BrMoN_3O_4S_2$	$C_{15}H_{14}FMoN_3O_5S$	$C_{72}H_{84}Cl_4Mo_4N_{12}O_{22}S_{10}$	$C_{16}H_{17}MoN_3O_6S$
M	554.29	463.29	2315.67	475.33
Crystal system	Monoclinic	Monoclinic	Monoclinic	Monoclinic
Space group	$P\,2_1/a$	$P\,2_1/c$	$C\,2/c$	$P\,2_1/c$
a(Å)	16.114(5)	15.082(15)	22.871(13)	16.002(11)
b(Å)	6.849(2)	13.711(13)	17.611(10)	13.425(6)
c(Å)	19.545(6)	10.399(10)	11.323(8)	10.581 (4)
α (°)	90	90	90	90
β (°)	107.847	93.938(7)	92.129(7)	93.767(7)
γ (°)	90	90	90	90
V(Å^3)	2053.3(11)	2145.3(4)	4557.3(5)	2268.2(2)
Z	4	4	2	4
D_{calc}(Mg.m^{-3})	1.793	1.434	1.688	1.392
F(000)	1096	928	2344	960
μ(Mo–Kα)(mm^{-1})	2.814	0.743	0.959	0.702
max./min.trans.	0.6313 / 0.5515	0.8778 / 0.8189	0.8313 / 0.8313	0.8960 / 0.8223
2θ(max)(°)	25.15	27.48	27.48	27.48
Reflections collected / unique	14246 / 3683 [R(int) = 0.1199]	4912 / 4912 [R(int) = 0.0293]	23695 / 5226 [R(int) = 0.0226]	5183 / 5183 [R(int) = 0.0254]
R_1[I>2σ(I)]	R1 = 0.0531, wR2 = 0.0905	R1 = 0.0332, wR2 = 0.0973	R1 = 0.0214, wR2 = 0.0548	R1 = 0.0285, wR2 = 0.0802
wR_2[all data]	R1 = 0.1287, wR2 = 0.1126	R1 = 0.0383, wR2 = 0.1003	R1 = 0.0233, wR2 = 0.0557	R1 = 0.0330, wR2 = 0.0829
S[goodness of fit]	0.971	1.076	1.052	1.083
min./max. res. (e.Å^{-3})	0.678 / –0.653	0.720 / –0.459	0.277 / –0.532	0.650 / –0.408

Table 4.2. Crystal data and refinement details of [$Mo^{(IV)}OL^{1,3-5}$(N–N)] (7, 9–11)

Compound	**7**	**9**	**10**	**11**
Formula	$C_{24}H_{18}BrMoN_5O_2S$	$C_{27}H_{20}ClMoN_5O_3S$	$C_{26}H_{23}MoN_5O_4S$	$C_{24}H_{17}Br_2MoN_5O_2S$
M	616.34	625.93	597.49	695.25
Crystal system	triclinic	Monoclinic	Monoclinic	Triclinic
Space group	$P\,\bar{1}$	$P\,2_1/n$	$P\,2_1/n$	$P\,\bar{1}$
a(Å)	9.965(6)	10.406(5)	10.505(4)	7.103(5)
b(Å)	10.537(6)	9.998(5)	10.549(4)	8.7250(7)
c(Å)	11.526(7)	24.028(12)	22.145(12)	19.151(16)
α (°)	101.490(3)	90	90	96.292(5)
β (°)	96.333(3)	93.926(3)	100.20(10)	92.914(5)
γ (°)	104.591(3)	90	90	91.650(5)
V($Å^3$)	1131.25(12)	2494.1(2)	2415.35(18)	1177.54(16)
Z	2	4	4	2
D_{calc}($Mg.cm^{-3}$)	1.809	1.667	1.643	1.961
F(000)	612	1264	1216	680
μ(Mo–Kα)(mm^{-1})	2.472	0.758	0.675	4.073
max./min.trans.	0.9295/0.9076	0.9850/0.9280	0.9356/0.8495	0.9604/ 0.8876
2θ(max)(°)	28.6	26.39	28.31	26.75
Reflections collected / unique	51409/5668 [R(int)=0.0415]	70158/5058 [R(int)=0.1008]	10989/5878 [R(int)=0.0586]	27997/4875 [R(int)=0.1318]
R_1[I>2σ(I)]	R1 = 0.0285, wR2 = 0.0556	R1 = 0.0478, wR2 = 0.0769	R1 = 0.0415, wR2 = 0.0881	R1 = 0.0626, wR2 = 0.1217
wR_2[all data]	R1 = 0.0384, wR2 = 0.0586	R1 = 0.0812, wR2 = 0.0860	R1 = 0.0753, wR2 = 0.0988	R1 = 0.1351, wR2 = 0.1454
S[goodness of fit]	1.075	1.058	0.950	1.008
min./max. res. ($e.Å^{-3}$)	0.543/–0.726	0.805/ –0.615	1.081/ –0.920	1.387/ –0.964

4.2.6. Substrate binding reactivity of $[Mo^{(VI)}O_2L^{1–6}]$ (1–6). Complexes (**1**–**6**) were recrystallized in DMSO leading to binding of substrate (solvent) to MoO_2L core, and yielding dark red crystals of $[Mo^{(VI)}O_2L^{1/5/6}(DMSO)]$ (**1a**, **5a** & **6a**), $[Mo^{(VI)}O_2L^{2/4}(H_2O)]$ (**2a** & **4a**), and $[Mo^{(VI)}O_2L^{3}(DMSO)]_4 \cdot 2DMSO$ (**3a**).

4.2.7. OAT reactivity studies

4.2.7.1. Oxo atom transfer to substrate: PPh_3. In a typical experiment, 1.0 mmol of $[Mo^{(VI)}O_2L^{1–6}]$ (**1**–**6**) was dissolved in 30 mL of degassed acetonitrile followed by addition of excess of PPh_3 and (N–N) {coligand, (N–N) = 2,2'–bipyridyl or 1,10–phenanthroline}. The solution was refluxed for 24 h. ^{31}P NMR spectra of the solution indicated selective formation of $OPPh_3$.

4.2.7.2. Oxo atom transfer from substrate: DMSO. The oxygen atom transfer from the substrate (DMSO) to the systems $[Mo^{(IV)}OL^{1–6}(N–N)]$ (**7**–**12**) has been studied spectrophotometrically.

4.2.8. Catalytic reactions

4.2.8.1. Oxidation of styrene. In a typical oxidation reaction, styrene (0.520 g, 5 mmol), aqueous 30% H_2O_2 (1.71 g, 15 mmol), catalyst (0.0010 g) and $NaHCO_3$ (0.126 g, 1.5 mmol) where mixed in 5 ml of CH_3CN. The reaction mixture was refluxed at 60°C for 4 h. The progress of the reaction was monitored by withdrawing samples at different time intervals and samples were extracted with n–hexane and then analysed quantitatively by gas chromatography. The effect of various parameters such as amount of catalyst, amount of oxidant, and solvent were checked to optimize the conditions for the best performance of the catalyst. The identity of the products was confirmed by GC–mass.

4.2.8.2. Oxidation of cyclohexene. Cyclohexene (0.41 g, 5 mmol), $NaHCO_3$ (0.126 g, 1.5 mmol) and 30% H_2O_2 (1.70 g, 15 mmol) were mixed in 5 ml of CH_3CN. Three different amounts of catalyst viz. 0.0005, 0.0010 and 0.0015 g as a function of time were added. The reaction mixture was refluxed at 60°C for 4 h. The identity of the products was confirmed as mentioned above.

4.3. RESULT AND DISSCUSSION

4.3.1. Dioxidomolybdenum(VI) complexes

4.3.1.1. Synthesis. Reaction of $MoO_2(acac)_2$ with ligands ($H_2L^{1–6}$) {4–(*p*–bromophenyl)thiosemicarbazone of salicylaldehyde (H_2L^1), 4–(*p*–X–phenyl)thiosemicarbazone of *o*–vanillin {where, X = F (H_2L^2) and X = Cl (H_2L^3) and X = OMe (H_2L^4)}, 4–(*p*–bromophenyl)thiosemicarbazone of 5–bromosalicylaldehyde (H_2L^5), and 4–(*p*–chlorophenyl)thiosemicarbazone of *o*–hydroxy naphthaldehyde (H_2L^6)} in the equimolar ratio in ethanol formed dark brown product of stoichiometry $[Mo^{(VI)}O_2L^{1–6}]$ (**1–6**), which when recrystallised in DMSO yielded dark red crystals of $[Mo^{(VI)}O_2L^{1/5/6}(DMSO)]$ (**1a**, **5a** & **6a**), $[Mo^{(VI)}O_2L^{2/4}(H_2O)]$ (**2a** & **4a**), and $[Mo^{(VI)}O_2L^3(DMSO)]_4{\cdot}2DMSO$ (**3a**) (**Scheme 4.1**). All the complexes are highly soluble in aprotic solvents, viz. DMF or DMSO and are sparingly soluble in alcohol, CH_3CN and $CHCl_3$.

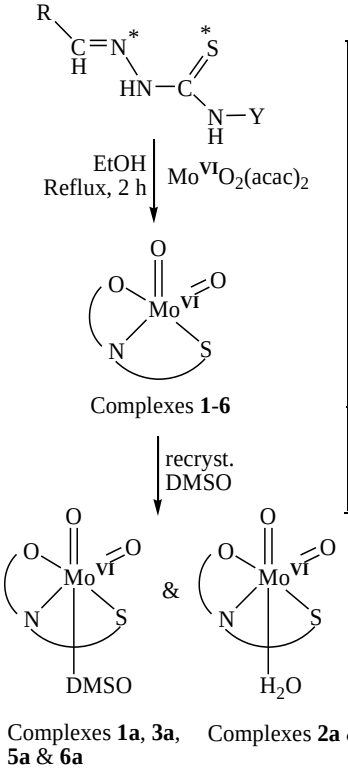

R	Y	Ligand	Complex
OH *	Br	H_2L^1	Complex **1**
OCH_3 OH *	F	H_2L^2	Complex **2**
	Cl	H_2L^3	Complex **3**
	OCH_3	H_2L^4	Complex **4**
Br OH *	Br	H_2L^5	Complex **5**
OH *	Cl	H_2L^6	Complex **6**

Scheme 4.1. Schematic diagram of ligands and synthetic pathways of dioxidomolybdenum(VI) complexes $[Mo^{(VI)}O_2L^{1–6})]$ (**1–6**), $[Mo^{(VI)}O_2L^{1/5/6}(DMSO)]$ (**1a**, **5a** & **6a**), $[Mo^{(VI)}O_2L^{2/4}(H_2O)]$ (**2a** & **4a**), and $[Mo^{(VI)}O_2L^3(DMSO)]_4{\cdot}2DMSO$ (**3a**).

4.3.1.2. Description of X–ray structure of dioxidomolybdenum(VI) complexes $[Mo^{(VI)}O_2L^1(DMSO)]$ (1a), $[Mo^{(VI)}O_2L^{2/4}(H_2O)]$ (2a & 4a), and $[Mo^{(VI)}O_2L^3(DMSO)]_4 \cdot 2DMSO$ (3a). The molecular structure and the atom numbering scheme for the complexes **1a**–**4a** are shown in **Figures 4.1–4.4** respectively. The relevant bond distances and angles are collected in **Table 4.3**. The coordination geometry around the molybdenum(VI) atom in **1a**–**4a** reveals a distorted octahedral environment with an NO_4S coordination sphere (**Scheme 4.1**). Each ligand molecule behaves as a dianionic tridentate one and bonded to the metal centre through the phenolate oxygen O(1), thiolate sulfur S(1) and the imine nitrogen N(1) forming a five membered and a six membered chelate ring with O(1)–Mo(1)–N(1) and S(1)–Mo(1)–N(1) bite angles of ~83.00(6)º and ~75.68(4)° respectively. In all the complexes, one of the two oxo group O(3) is located trans to the imine nitrogen N(1) in the same plane and the other oxo group O(2) is located in the axial plane along with the solvent molecule, DMSO (**1a** & **3a**) and H_2O (**2a** & **4a**).

We were unable to solve the structures of complexes **1**–**6** due to poor quality of crystals.

Table 4.3. Selected geometric parameters (Å, º) for $[Mo^{(VI)}O_2L^1(DMSO)]$ (1a), $[Mo^{(VI)}O_2L^{2/4}(H_2O)]$ (2a & 4a), and $[Mo^{(VI)}O_2L^3(DMSO)]_4 \cdot 2DMSO$ (3a)

	1	2	3	4
		Bond Distances		
Mo(1)–O(1)	1.932(5)	1.926(2)	1.929(1)	1.926(1)
Mo(1)–O(2)	1.699(5)	1.706(2)	1.703(1)	1.701(2)
Mo(1)–O(3)	1.701(5)	1.690(2)	1.707 (1)	1.698(2)
Mo(1)–O(4)	2.389(4)	2.342(2)	2.314(1)	2.319(2)
Mo(1)–N(1)	2.272(6)	2.266(2)	2.275(1)	2.289(2)
Mo(1)–S(1)	2.444(2)	2.426(7)	2.438(4)	2.417(6)
		Bond Angles		
O(2)–Mo(1)–O(3)	105.40(2)	105.41(1)	104.95(6)	105.21(9)
O(2)–Mo(1)–O(1)	97.50(2)	100.16(9)	98.15(6)	100.03(8)
O(3)–Mo(1)–O(1)	105.70(2)	104.05(9)	107.68(5)	103.70(7)
O(2)–Mo(1)–N(1)	92.30(2)	90.79(9)	91.12(5)	89.86(8)
O(3)–Mo(1)–N(1)	159.30(2)	160.30(1)	158.93(5)	161.90(8
O(1)–Mo(1)–N(1)	82.05(2)	83.52(7)	82.85(5)	83.00(6)
O(2)–Mo(1)–O(4)	169.10(2)	168.07(9)	169.92(5)	168.18(8)
O(3)–Mo(1)–O(4)	85.30(2)	86.42(1)	85.08(5)	86.59(8)
O(1)–Mo(1)–O(4)	77.03(2)	77.90(8)	77.48(5)	77.24(7)
N(1)–Mo(1)–O(4)	77.65(2)	77.31(8)	79.38(4)	78.43(6)
O(2)–Mo(1)–S(1)	99.05(2)	96.61(8)	97.32(4)	97.54(6)
O(3)–Mo(1)–S(1)	90.74(2)	91.06(8)	88.79(4)	92.15(6)
O(1)–Mo(1)–S(1)	152.59(1)	153.42(6)	153.53(4)	152.23(5)
N(1)–Mo(1)–S(1)	75.64(1)	75.74(5)	75.49(3)	75.68(4)
O(4)–Mo(1)–S(1)	82.75(1)	81.42(6)	83.66(3)	81.17(5)

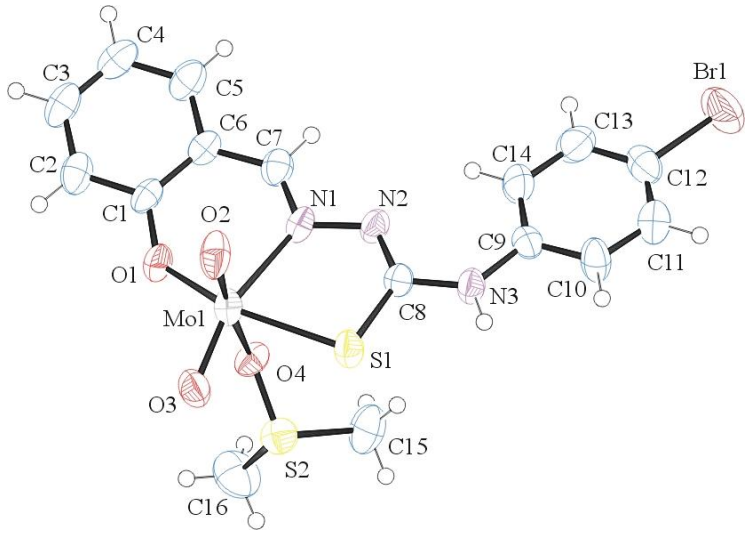

Figure 4.1. ORTEP diagram of $[Mo^{(VI)}O_2L^1(DMSO)]$ (**1a**) with atom labeling scheme.

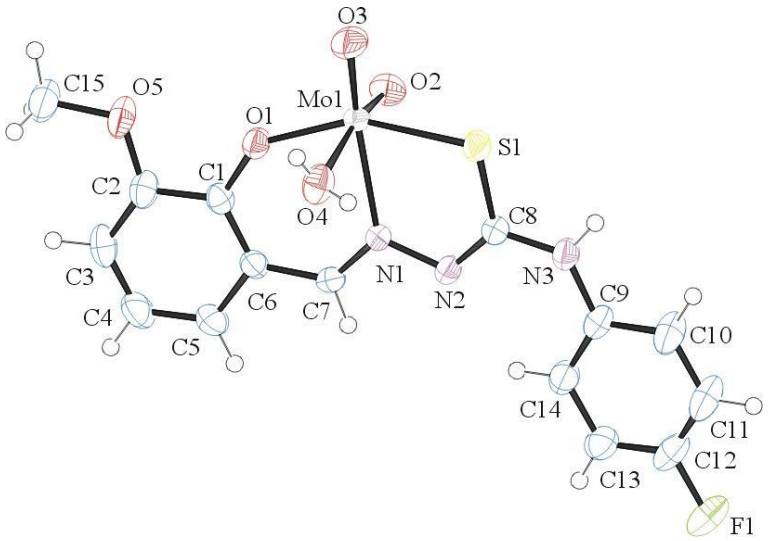

Figure 4.2. ORTEP diagram of $[Mo^{(VI)}O_2L^2(H_2O)]$ (**2a**) with atom labeling scheme.

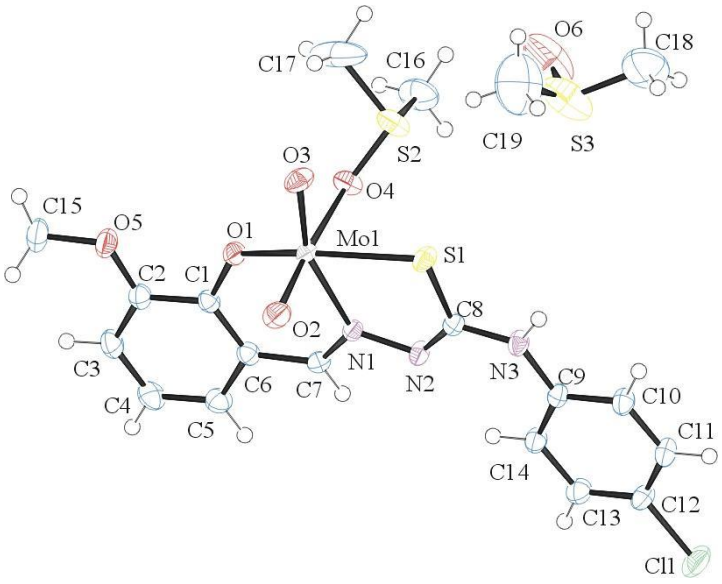

Figure 4.3. ORTEP diagram of asymmetric unit of $[Mo^{(VI)}O_2L^3(DMSO)]_4 \cdot 2DMSO$ (**3a**) with atom labeling scheme.

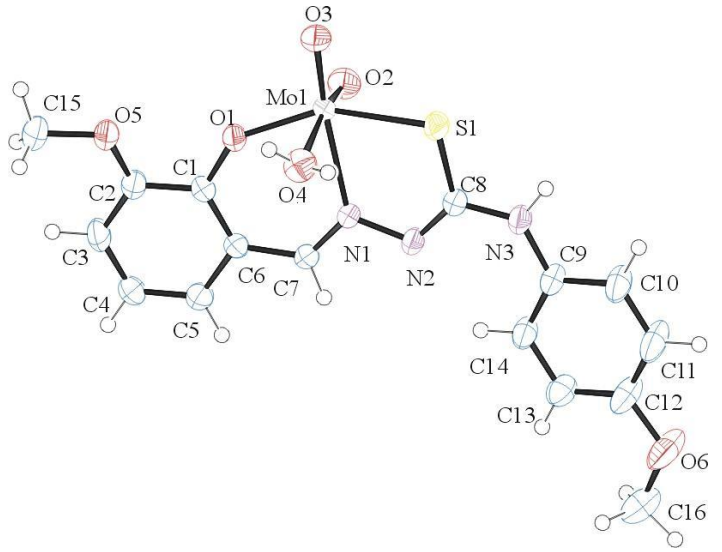

Figure. 4.4. ORTEP diagram of $[Mo^{(VI)}O_2L^4(H_2O)]$ (**4a**) with atom labeling scheme.

4.3.1.3. Spectral characteristics

4.3.1.3.1. IR spectroscopy. The infrared spectra of complexes (**1**–**6**) and (**1a**–**6a**), exhibits two strong absorptions in the range 938–878 cm^{-1}, beside typical ligand vibrations,[8,65] which are attributed to the symmetric and asymmetric ν(Mo=O) vibrations of the C_{2v} *cis*– MoO_2^{2+} groups, thus confirming the formation of mononuclear molybdenum(VI) complexes.[66] The detailed IR data has been included in the experimental section and **Figure 4.5(a)** depicts the representative spectra of $[Mo^{(VI)}O_2L^1]$ (**1**).

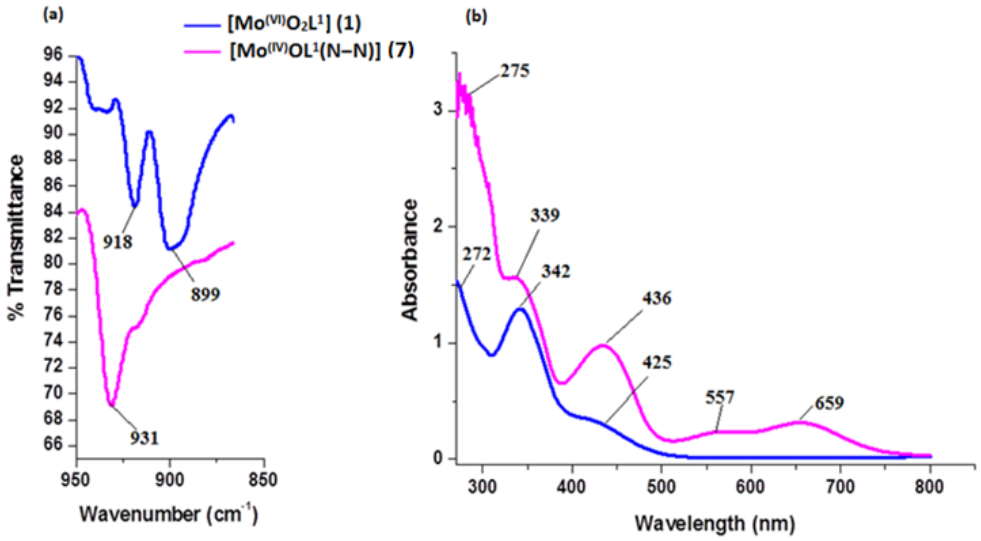

Figure 4.5. Overlay (a) IR spectra and (b) UV–Vis spectra of $[Mo^{(VI)}O_2L^1]$ (**1**) and $[Mo^{(IV)}OL^1(bipy)]$ (**7**).

4.3.1.3.2. UV–Vis spectroscopy. The electronic spectra of complexes (**1**–**6**) and (**1a**–**6a**) were recorded in CH_3CN and are listed in **Table 4.4**. **Figure 4.5(b)** depicts the representative UV–Vis spectra of $[Mo^{(VI)}O_2L^1]$ (**1**). Complexes (**1**–**6**) and (**1a**–**6a**) displays medium intensity band in 447–422 nm region and two strong absorptions in 346–243 nm range, which are assignable to ligand to molybdenum (pπ–dπ) charge transfer (LMCT) and intraligand transitions respectively.[67]

Table 4.4. Electronic spectra[a] for complexes $[Mo^{(VI)}O_2L^{1–6})]$ (1–6), $[Mo^{(VI)}O_2L^{1/5/6}(DMSO)]$ (1a, 5a & 6a), $[Mo^{(VI)}O_2L^{2/4}(H_2O)]$ (2a & 4a), and $[Mo^{(VI)}O_2L^{3}(DMSO)]_4 \cdot 2DMSO$ (3a).

Complex	λ_{max}/nm(ε/$dm^3mol^{-1}cm^{-1}$)
$[Mo^{(VI)}O_2L^1]$ (**1**)	272(16739), 342(14300), 425(3658)
$[Mo^{(VI)}O_2L^2]$ (**2**)	265(16366), 315(13896), 422(3589)
$[Mo^{(VI)}O_2L^3]$ (**3**)	278(15967), 345(14253), 447(3786)
$[Mo^{(VI)}O_2L^4]$ (**4**)	263(16636), 337(14654), 425(3677)
$[Mo^{(VI)}O_2L^5]$ (**5**)	278(16787), 335(14324), 426(3568)
$[Mo^{(VI)}O_2L^6]$ (**6**)	258(16746), 342(13877), 442(3578)
$[Mo^{(VI)}O_2L^1(DMSO)]$ (**1a**)	268(17072), 341(14323), 433(3370)
$[Mo^{(VI)}O_2L^2(H_2O)]$ (**2a**)	265(16341), 321(12543), 428(2789)
$[Mo^{(VI)}O_2L^3(DMSO)]_4 \cdot 2DMSO$ (**3a**)	264(17534), 346(13535), 436(5422)
$[Mo^{(VI)}O_2L^4(H_2O)]$ (**4a**)	274(16432), 328(14212), 442(3856)
$[Mo^{(VI)}O_2L^5(DMSO)]$ (**5a**)	270 (16322), 343(13648), 439(3922)
$[Mo^{(VI)}O_2L^6(DMSO)]$ (**6a**)	243(16429), 338(13768), 437(3425)

[a]In CH_3CN solution.

4.3.1.3.3. NMR spectroscopy. The NMR spectra (^1H and ^{13}C) of the dioxidomolybdenum(VI) complexes (**1**–**6**) and (**1a**–**6a**) were recorded using DMSO–d_6. The ^1H NMR spectrum exhibits two singlets in the range 9.86–8.25 ppm due to NH (–C(8)–N(3)H) and CH (–N(1)=C(7)–H) groups respectively. Signals for aromatic protons found as multiplets, in 7.87–6.34 ppm. The detailed NMR data of all the ligands and their corresponding Mo(VI) complexes have been included in the experimental section. The representative ^1H NMR spectrum of ligand H_2L^1 and its corresponding Mo^{VI} complexes $[Mo^{(VI)}O_2L^1]$ (**1**) and $[Mo^{(VI)}O_2L^1(DMSO)]$ (**1a**) is shown in **Figures 4.6**–**4.8** respectively.

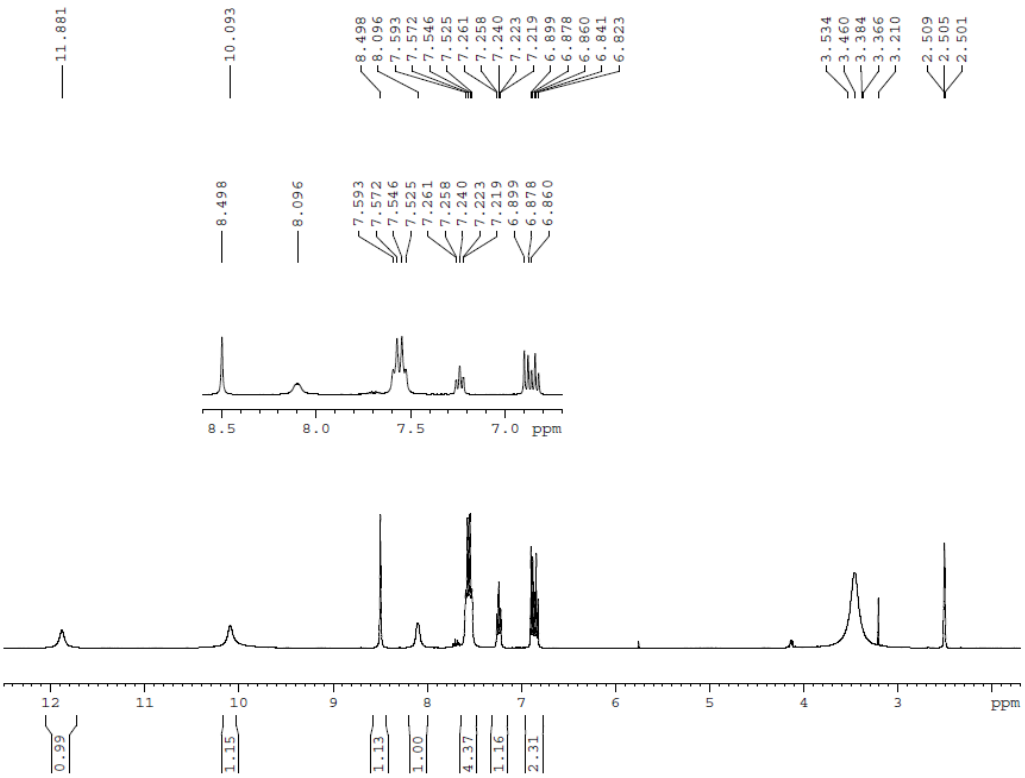

Figure 4.6. ^{1}H NMR spectra of ligand H_2L^1.

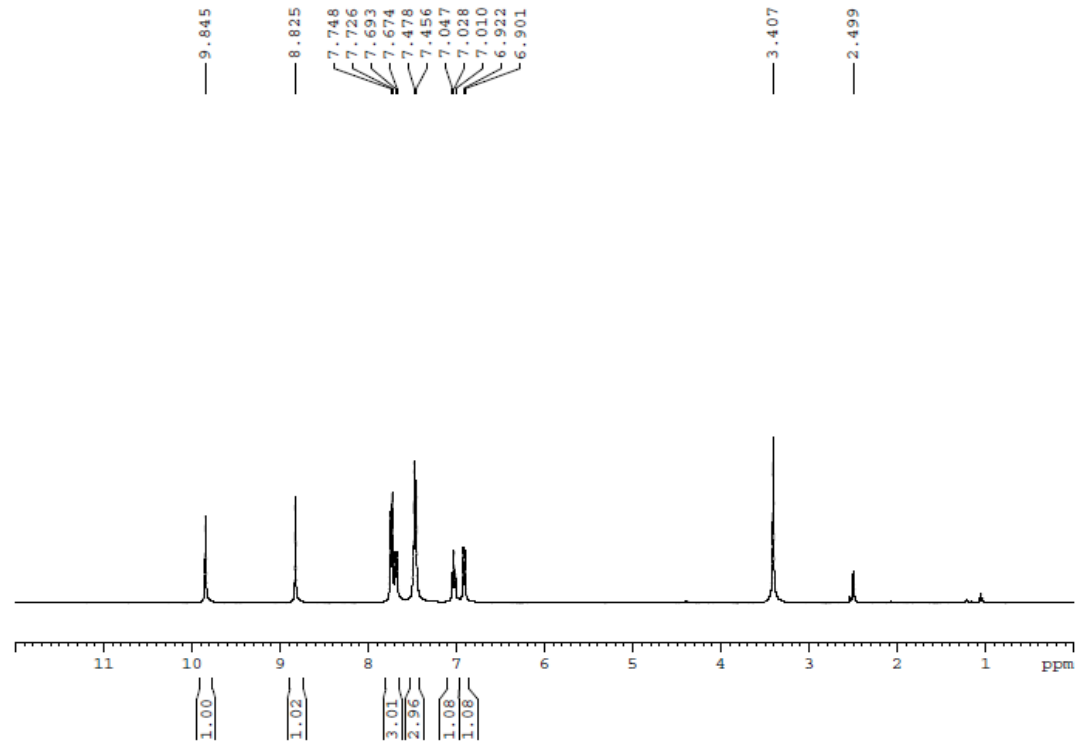

Figure 4.7. ^{1}H NMR spectra of complex $[Mo^{(VI)}O_2L^1]$ (**1**).

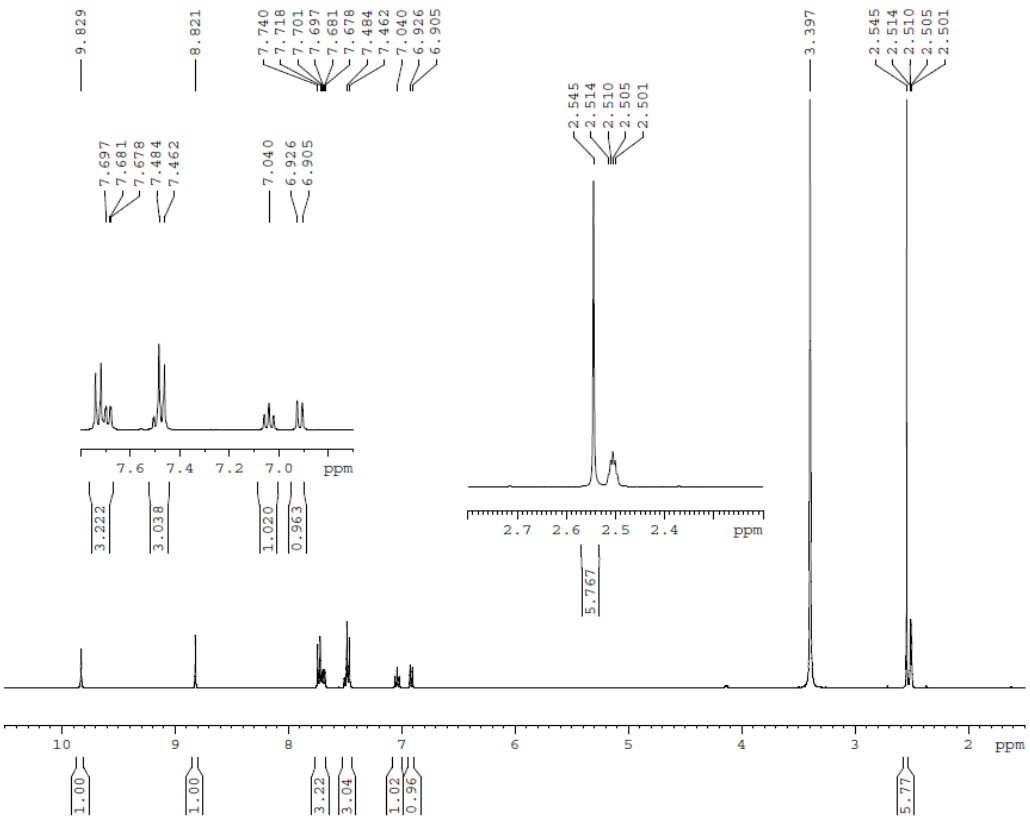

Figure 4.8. ^{1}H NMR spectra of complex [$Mo^{(VI)}O_2L^1$(DMSO)] (**1a**) in DMSO–d_6.

4.3.1.3.4. ESI mass spectroscopy. ESI mass spectra of **1**−**6** have been recorded in CH_3CN solution. Mass spectral analysis for **1**−**6** shows peaks at *m/z* 477.07 $[M + H]^+$, *m/z* 468.15 $[M + Na]^+$, *m/z* 462.19 $[M + H]^+$, *m/z* 457.49 $[M]^+$, *m/z* 557.42 $[M + 2H]^+$.and *m/z* 481.43 $[M]^+$ respectively. The detailed ESI mass data have been included in the experimental section.

4.3.1.4. Electrochemical properties. The electrochemical properties of **1a**–**6a** were examined in CH_3CN solution (0.1 M TEAP) by cyclic voltammetry using a platinum working electrode, platinum auxiliary electrode and an Ag/AgCl reference electrode. The potential data are listed in **Table 4.5** and **Figure 4.9** depicts the representative voltammogram of [$Mo^{(VI)}O_2L^2(H_2O)$] (**2a**). The voltammogram pattern is similar for **1a**–**6a**, which includes two irreversible reduction processes within the potential window –0.71 to –0.66 V and –0.92 to –0.85 V corresponding to metal centered reduction from $Mo^{(VI)/}Mo^{(V)}$ and $Mo^{(V)/}Mo^{(IV)}$ respectively.[68] The redox properties of **1**–**6** were also examined, and the results matched well with the above.

Table 4.5. Cyclic voltammetric[a] results for complexes $[Mo^{(VI)}O_2L^{1/5/6}(DMSO)]$ (1a, 5a & 6a), $[Mo^{(VI)}O_2L^{2/4}(H_2O)]$ (2a & 4a), and $[Mo^{(VI)}O_2L^{3}(DMSO)]_4 \cdot 2DMSO$ (3a)

Complex	Potentials (V) versus Ag/AgCl	
	$Mo^{(VI)}/Mo^{(V)}$	$Mo^{(V)}/Mo^{(IV)}$
	E_{pc}	E_{pc}
$[Mo^{(VI)}O_2L^{1}(DMSO)]$ (**1a**)	–0.66	–0.87
$[Mo^{(VI)}O_2L^{2}(H_2O)]$ (**2a**)	–0.71	–0.92
$[Mo^{(VI)}O_2L^{3}(DMSO)]_4 \cdot 2DMSO$ (**3a**)	–0.70	–0.92
$[Mo^{(VI)}O_2L^{4}(H_2O)]$ (**4a**)	–0.68	–0.85
$[Mo^{(VI)}O_2L^{5}(DMSO)]$ (**5a**)	–0.66	–0.87
$[Mo^{(VI)}O_2L^{6}(DMSO)]$ (**6a**)	–0.70	–0.88

[a]In CH_3CN at a scan rate 100 mV/s. E_{pc} is cathodic peak potentials vs. Ag/AgCl, respectively.

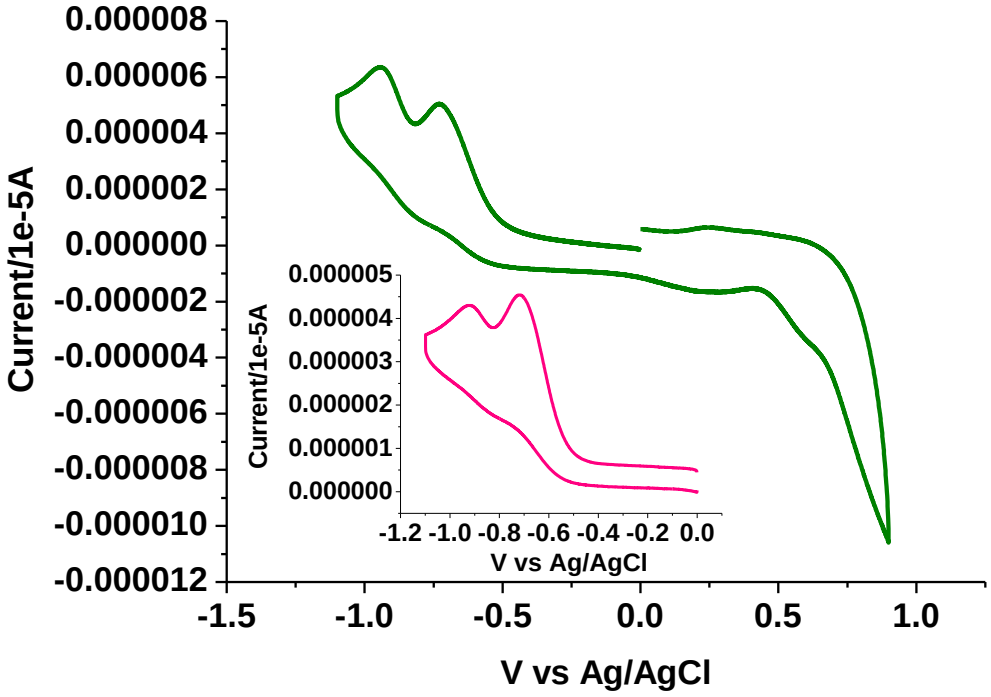

Figure 4.9. Cyclic voltammogram of $[Mo^{(VI)}O_2L^{2}(H_2O)]$ (**2a**).

4.3.1.5. Substrate binding reactivity of $[Mo^{(VI)}O_2L^{1-6}]$ (1–6). $[Mo^{(VI)}O_2L^{1-6}]$ (**1–6**) were recrystallized in DMSO yielding dark red crystals of $[Mo^{(VI)}O_2L^{1/5/6}(DMSO)]$ (**1a, 5a** & **6a**), $[Mo^{(VI)}O_2L^{2/4}(H_2O)]$ (**2a** & **4a**), and $[Mo^{(VI)}O_2L^{3}(DMSO)]_4 \cdot 2DMSO$ (**3a**) (**Scheme 4.1**). This can be considered as a substrate–binding reaction of the MoO_2L core when a solvent molecule (substrate) binds to the distorted square–pyramidal MoO_2L moiety forming a distorted octahedral species (**Eq. (1)**). This reaction reminds us of the substrate binding property of molybdoenzymes.[67b]

$$\mathbf{MoO_2L + Solv \rightleftharpoons MoO_2L(Solv)} \qquad \textbf{Eq. (1)}$$

Where, Solv: DMSO (1a, 3a, 5a & 6a) and H_2O (2a & 4a)

4.3.1.6. OAT reactivity studies

4.3.1.6.1. Oxo atom transfer to substrate: PPh_3. The assessment of oxygen atom transfer from $[Mo^{(VI)}O_2L^{1-6}]$ (**1–6**) to PPh_3 (**Scheme 4.2, Eq. (2)**) has been performed in acetonitrile in the presence of excess of the triphenylphosphine (PPh_3) and (N–N) {coligand, (N–N) = 2,2'–bipyridyl or 1,10–phenanthroline} in N_2 atmosphere. The reaction has been monitored by the gradual appearance of $OPPh_3$ (27 ppm) as probed by ^{31}P NMR. The ^{31}P NMR spectrum of the solution after 24 h displays signals for $OPPh_3$ and residual PPh_3. The representative ^{31}P NMR spectra showing the gradual conversion of PPh_3 to $OPPh_3$ by $[Mo^{(VI)}O_2L^{6}]$ (**6**) is given in **Figure 4.10**. In a control experiment, without adding complex only trace amounts of $OPPh_3$ were detected after 24 h due to phosphine reacting with atmospheric oxygen.

$$\mathbf{MoO_2L + PPh_3 \underset{N\text{-}N}{\overset{N_2,\ CH_3CN}{\rightleftharpoons}} MoOL(N\text{-}N) + OPPh_3} \qquad \textbf{Eq. (2)}$$

Where, N-N: 2,2'-bipyridyl or 1,l0-phenanthroline

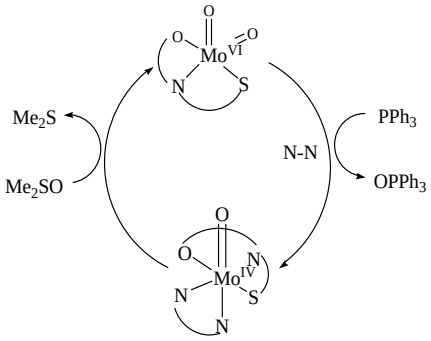

Scheme 4.2. Schematic diagram for OAT reactions.

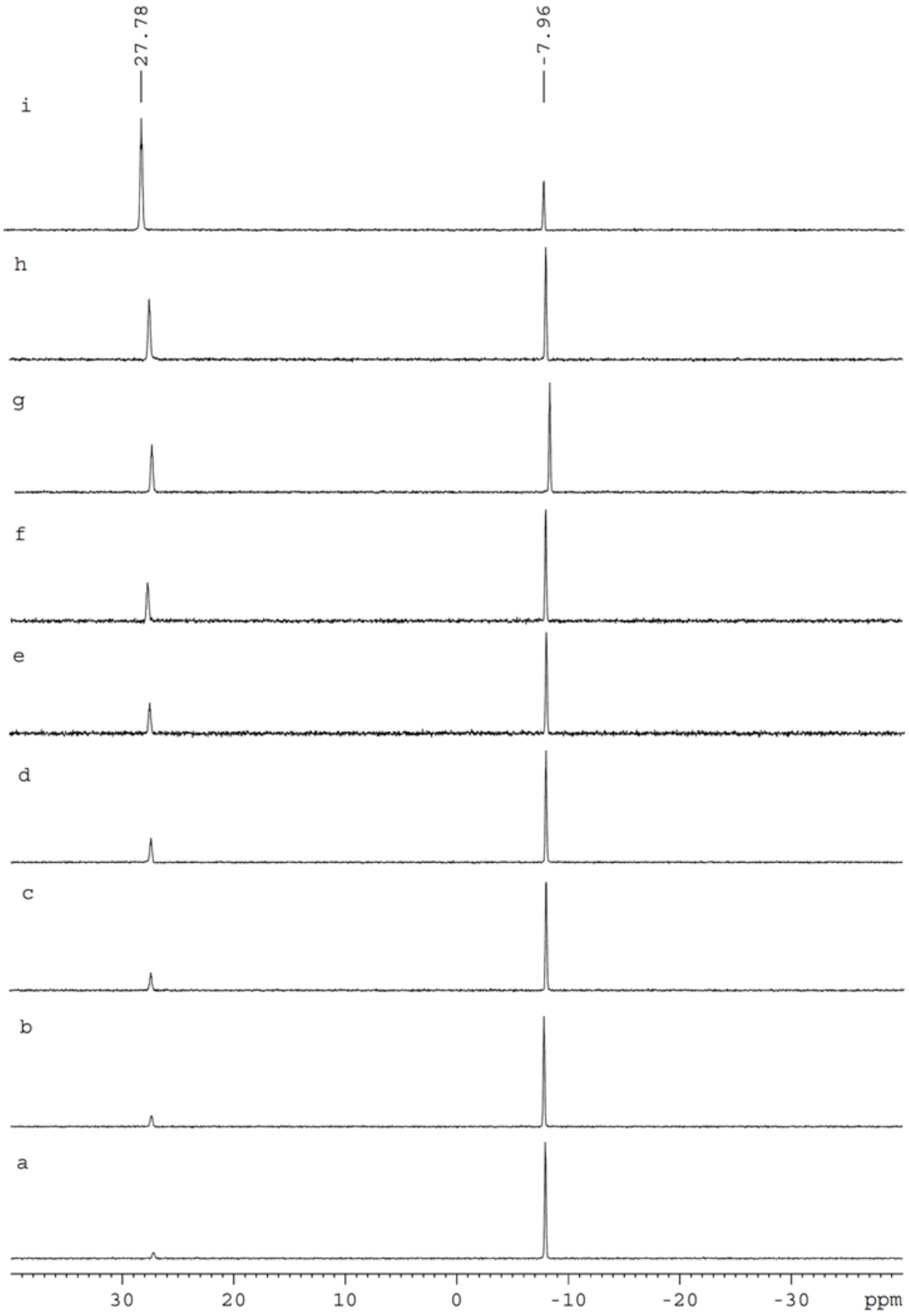

Figure 4.10. ^{31}P NMR spectra showing the gradual conversion of PPh_3 to $OPPh_3$ in a system containing initially 1 mmol $[Mo^{(VI)}O_2L^6]$ (**6**) with excess Ph_3P and 1,10–phenanthroline in degassed CH_3CN at (a) 0 h; (b) 1 h; (c) 2 h; (d) 3 h; (e) 4 h; (f) 5 h; (g) 6 h; (h) 7 h; (i) 24 h.

4.3.1.6.2. Oxo atom transfer from substrate: DMSO. The oxygen atom transfer from the substrate DMSO to the system $[Mo^{(IV)}OL^{1-6}(N–N)]$ (**7–12**) (**Scheme 4.2**) has been studied spectrophotometrically in DMSO solution. The parent complexes $[Mo^{(IV)}OL^{1-6}(N–N)]$ (**7–12**) exhibits a low–energy bands at ~640 to 550 nm and an intense band at ~430 nm. On addition of DMSO to $[Mo^{(IV)}OL^{1-6}(N–N)]$ (**7–12**), the intensity of these bands is found to decrease gradually. The bands due to d–d transition at ~640 to 550 nm finally disappear within 30 min, and a new the intensity of band, at ~350 nm increases. This observation clearly indicates the transfer of an oxygen atom from DMSO (Me_2SO) to the MoO^{2+} core, leading to the formation of MoO_2^{2+} and Me_2S species (**Eq. (3)**). The representative time dependent UV–Vis spectra of $[Mo^{(IV)}OL^1(bipy)]$ (**7**) in DMSO is given in **Figure 4.11**. The formation of Me_2S was confirmed by its characteristic odour.

$$\mathbf{MoOL(N\text{-}N) + DMSO \rightleftharpoons MoO_2L + Me_2S} \qquad \textbf{Eq. (3)}$$

Where, N-N: 2,2'-bipyridyl or 1,l0-phenanthroline

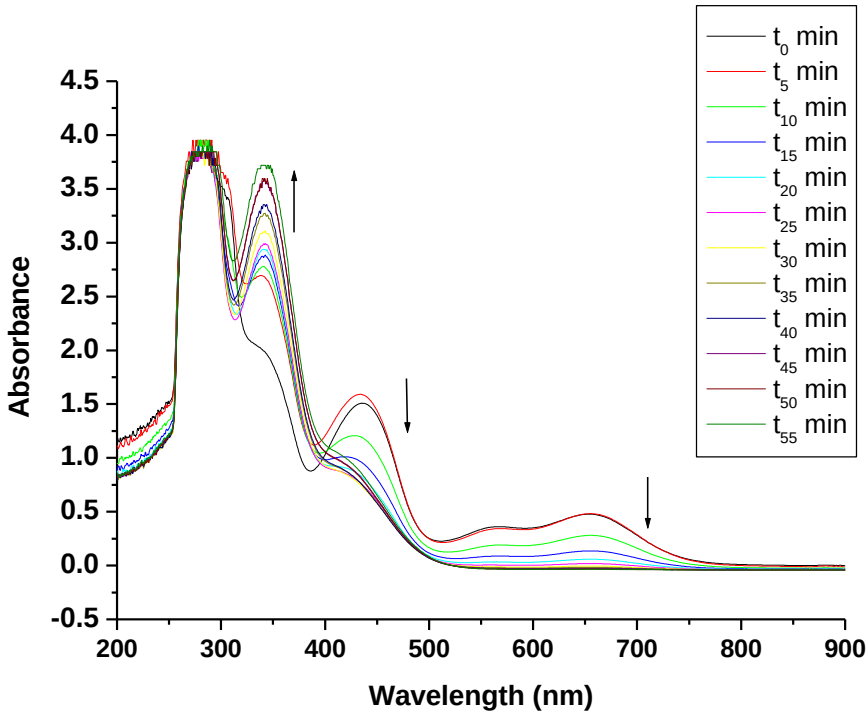

Figure 4.11. Time dependent UV–Vis spectra of $[Mo^{(IV)}OL^1(bipy)]$ (**7**) in DMSO showing the gradual vanish of d–d peak.

4.3.2. Monooxidomolybdenum(IV) complexes

4.3.2.1. Synthesis. Monooxidomolybdenum(IV) complexes $[Mo^{(IV)}OL^{1-6}(N–N)]$ (**7**–**12**) were synthesized by the reduction of dioxidomolybdenum(VI) complexes $[Mo^{(VI)}O_2L^{1-6}]$ (**1**–**6**) with PPh_3 in presence of 2,2'–bipyridyl or 1,10–phenanthroline in N_2 atmosphere. The detailed synthetic methods of complexes (**7**–**12**) are illustrated in **Scheme 4.3**. All the complexes are highly soluble in aprotic solvents, viz. DMF or DMSO and are sparingly soluble in alcohol, CH_3CN and $CHCl_3$.

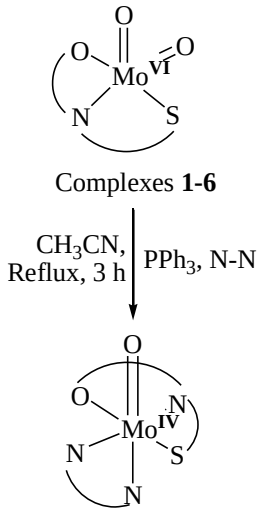

N-N: 2,2'-bipyridyl; 1,l0-phenanthroline

Scheme 4.3. Schematic diagram of synthetic pathways of monooxidomolybdenum(IV) complexes $[Mo^{(IV)}OL^{1-6}(N–N)]$ (**7**–**12**).

4.3.2.2. Description of X–ray structure of monooxidomolybdenum(IV) complexes $[Mo^{(IV)}OL^{1,3-5}(N–N)]$ (7 and 9−11). The atom numbering scheme for the complexes **7** and **9**−**11** are given in **Figures 4.12**−**4.15** with the relevant bond distances and angles collected in **Table 4.6**. The structure shows that the thiosemicarbazone ligand (L^{2-}) is coordinated to metal center in the expected tridentate fashion (**Scheme 4.3**), forming a six and a five membered chelate ring with O(1)–Mo(1)–N(1) and S(1)–Mo(1)–N(1) bite angles of ~86.82(7)º and ~78.81(5)° respectively. The bidentate co−ligands 2,2'−bipyridyl (**7**, **10** & **11**) and 1,10–phenanthroline (**9**) are coordinated to the metal center via N(4) and N(5). The cental metal is coordinated to one

oxido group O(2). Thus the complexes form monooxido Mo^{IV} complex with distorted octahedral geometry, where the equatorial positions are occupied by the thiolate sulfur S(1), the phenolate oxygen O(1) and the imino nitrogen N(1) of ligand and pyridyl nitogen N(4) of the coligand and the axial positions are occupied by the oxido oxygen O(2) and pyridyl nitogen N(5).

Table 4.6. Selected geometric parameters (Å, º) for $[Mo^{(IV)}OL^{1,3-5}(N–N)]$ (7 and 9−11).

	7	**9**	**10**	**11**
		Bond Distances		
Mo(1)–O(1)	2.067(2)	2.055(2)	2.077(2)	2.070(5)
Mo(1)–N(1)	2.135(2)	2.138(3)	2.136(2)	2.129(7)
Mo(1)–S(1)	2.390(6)	2.389(1)	2.401(8)	2.358(2)
Mo(1)–N(4)	2.172(2)	2.177(3)	2.199(2)	2.248(7)
Mo(1)–N(5)	2.314(2)	2.334(3)	2.304(2)	2.265(6)
Mo(1)–O(2)	1.685(2)	1.679(3)	1.685(2)	1.686(5)
		Bond Angles		
O(2)–Mo(1)–O(1)	104.71(8)	106.19(1)	104.60(9)	108.50(2)
O(2)–Mo(1)–N(1)	104.96(8)	103.74(1)	104.89(1)	95.10(2)
O(1)–Mo(1)–N(1)	86.82(7)	85.68(1)	86.10(8)	84.30(2)
O(2)–Mo(1)–N(4)	89.67(8)	88.18(1)	87.50(9)	81.10(2)
O(1)–Mo(1)–N(4)	85.76(7)	86.65(1)	87.79(8)	99.90(2)
N(1)–Mo(1)–N(4)	164.88(7)	167.25(1)	167.23(9)	175.00(2)
O(2)–Mo(1)–N(5)	160.02(8)	159.46(1)	157.52(1)	150.00(3)
O(1)–Mo(1)–N(5)	78.14(7)	76.54(1)	78.69(8)	74.30(2)
N(1)–Mo(1)–N(5)	94.90(7)	96.75(1)	97.49(9)	114.80(2)
N(4)–Mo(1)–N(5)	70.68(7)	71.53(1)	70.28(9)	69.20(2)
O(2)–Mo(1)–S(1)	101.53(6)	102.03(1)	101.66(7)	106.32(2)
O(1)–Mo(1)–S(1)	152.57(6)	150.24(9)	152.07(6)	142.30(2)
N(1)–Mo(1)–S(1)	78.81(5)	78.58(9)	78.08(6)	78.70(2)
N(4)–Mo(1)–S(1)	102.32(5)	103.66(9)	102.78(6)	99.25(2)
N(5)–Mo(1)–S(1)	79.95(5)	80.40(9)	80.71(6)	82.72(2)

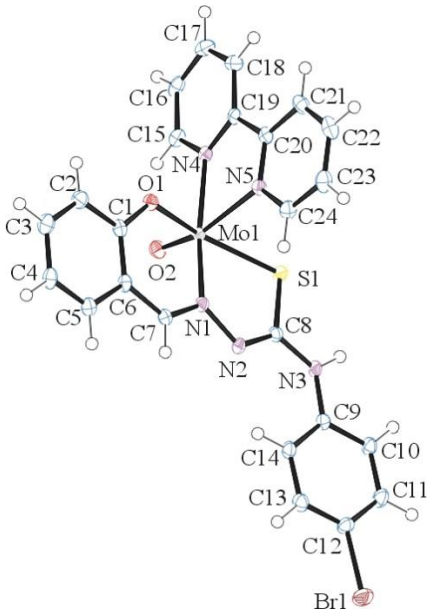

Figure 4.12. ORTEP diagram of [$Mo^{(IV)}OL^{1}$(bipy)] (**7**) with atom labeling scheme.

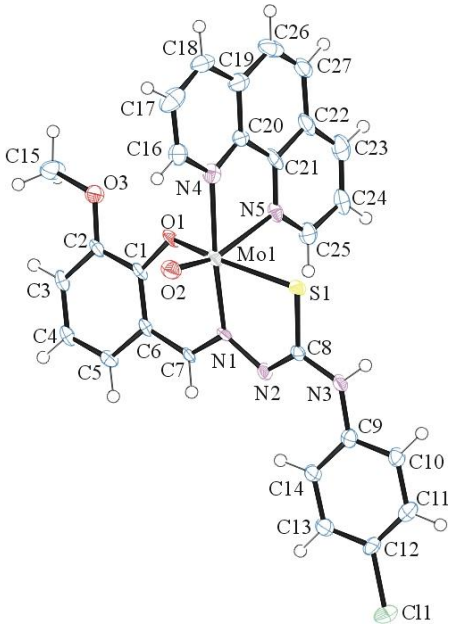

Figure 4.13. ORTEP diagram of [$Mo^{(IV)}OL^{3}$(phen)] (**9**) with atom labeling scheme.

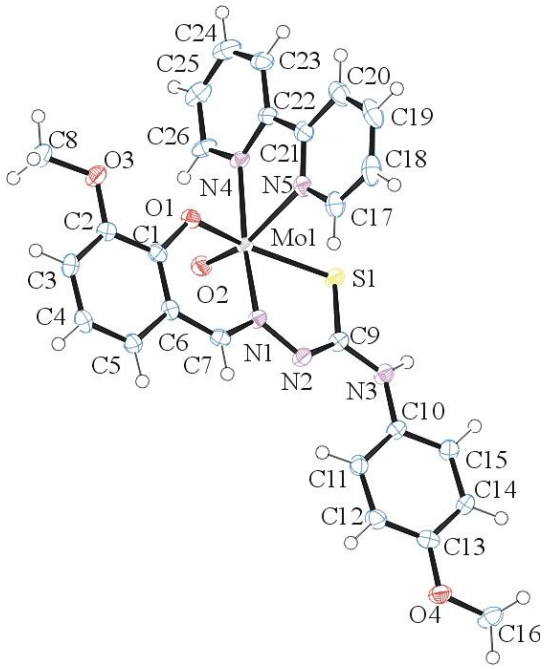

Figure 4.14. ORTEP diagram of [$Mo^{(IV)}OL^4$(bipy)] (**10**) with atom labeling scheme.

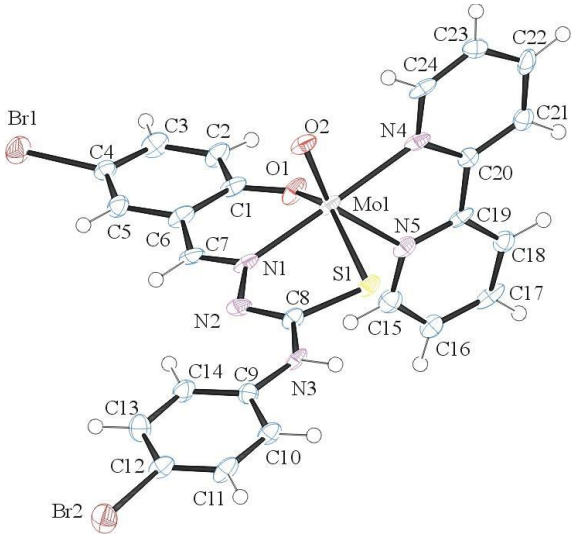

Figure 4.15. ORTEP diagram of [$Mo^{(IV)}OL^5$(bipy)] (**11**) with atom labeling scheme.

4.3.2.3. Spectral characteristics

4.3.2.3.1. IR spectroscopy. In contrast to Mo^{VI} complexes the IR spectra of complexes $[Mo^{(IV)}OL^{1-6}(N–N)]$ (**7**–**12**) shows only one strong absorption in the range 945–922 cm^{-1}, which indicates the presence of single ν(Mo=O) vibration.[69] The detailed IR data has been included in the experimental section. **Figure 4.5(a)** depicts the representative spectra of $[Mo^{(IV)}OL^{1}(bipy)]$ (**7**).

4.3.2.3.2. UV–Vis spectroscopy. $[Mo^{(IV)}OL^{1-6}(N–N)]$ (**7**–**12**) were found to display several absorption in the range 659–260 nm. The electronic data are listed in **Table 4.7**. The low energy charge transfer bands in the range 659–517 nm were observed due to d–d transition.[67] The medium intensity band in 462–414 nm region and two strong absorptions in 347–260 nm range are assignable to ligand to molybdenum (pπ–dπ) charge transfer (LMCT) and intraligand transitions, respectively. **Figure 4.5(b)** depicts the representative UV–Vis spectra of **7**.

Table 4.7. Electronic spectra[a] for complexes $[Mo^{(IV)}OL^{1-6}(N–N)]$ (7–12)

Complex	λ_{max}/nm(ε/$dm^3mol^{-1}cm^{-1}$)
$[Mo^{(IV)}OL^{1}(bipy)]$ (**7**)	275(40062), 339(19229), 436(12080), 557(2958), 659(3821)
$[Mo^{(IV)}OL^{2}(phen)]$ (**8**)	260(41234), 320(20131), 427(12545), 574(2675), 647(3921)
$[Mo^{(IV)}OL^{3}(phen)]$ (**9**)	274(40663), 345(19854) 462(12245), 523(2642), 634(3643)
$[Mo^{(IV)}OL^{4}(bipy)]$ (**10**)	278(41722), 347(19524), 415(13266), 517(2854), 641(3425)
$[Mo^{(IV)}OL^{5}(bipy)]$ (**11**)	264(40568), 328(18568), 421(13235), 534(2960), 635(3545)
$[Mo^{(IV}OL^{6}(phen)]$ (**12**)	262(42621), 342(16612), 414(12554), 542(2645), 652(3736)

[a]In CH_3CN solution

4.3.2.4. Electrochemical properties. The electrochemical properties of **7**–**12** were examined in CH_3CN solution (0.1 M TEAP) by cyclic voltammetry using a platinum working electrode, platinum auxiliary electrode and an Ag/AgCl reference electrode. The potential data are listed in **Table 4.8** and **Figure 4.16** depicts the representative voltammogram of $[Mo^{(IV)}OL^{1}(bipy)]$ (**7**). The voltammogram pattern of **7**–**12** includes both oxidation and reduction process. In the anodic region, an quasi reversible single electron wave at $E^{a}_{1/2}$ values within the potential window 0.71

to 0.66 V is assigned to the oxidation of $Mo^{(IV)}/Mo^{(V)}$.[68a,68b,70] In the cathodic region $Mo^{(IV)}$ is reduced to $Mo^{(III)}$ showing an irreversible single electron wave within the potential window –1.38 to –1.32 V.[68a,68b,70]

Table 4.8. Cyclic voltammetric[a] results for complexes $[Mo^{(IV)}OL^{1–6}(N–N)]$ (7–12)

Complex	Potentials (V) versus Ag/AgCl	
	$Mo^{(IV)}/Mo^{(V)}$	$Mo^{(IV)}/Mo^{(III)}$
	$E^{a}_{1/2}(\Delta E^{a}_{p})$	E_{pc}
$[Mo^{(IV)}OL^{1}(bipy)]$ (**7**)	0.70(103)	–1.38
$[Mo^{(IV)}OL^{2}(phen)]$ (**8**)	0.71(98)	–1.32
$[Mo^{(IV)}OL^{3}(phen)]$ (**9**)	0.66(82)	–1.32
$[Mo^{(IV)}OL^{4}(bipy)]$ (**10**)	0.71(76)	–1.38
$[Mo^{(IV)}OL^{5}(bipy)]$ (**11**)	0.69(69)	–1.36
$[Mo^{(IV}OL^{6}(phen)]$ (**12**)	0.68(74)	–1.33

[a]In CH_3CN at a scan rate 100 mV/s. $E_{1/2} = (E_{pa} + E_{pc})/2$, where E_{pa} and E_{pc} are anodic and cathodic peak potentials vs. Ag/AgCl, respectively. $\Delta E_P = E_{pa} - E_{pc}$.

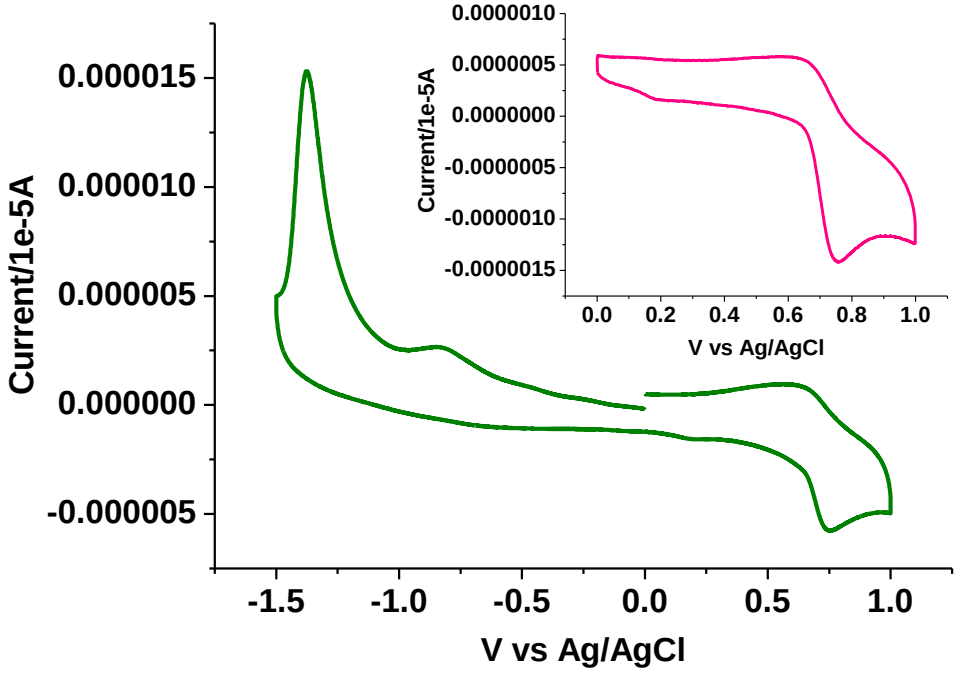

Figure 4.16. Cyclic voltammogram of $[Mo^{(IV)}OL^{1}(bipy)]$ (**7**).

4.3.3. Catalytic activity studies

4.3.3.1. Oxidation of styrene. Oxidation of styrene catalyzed by molybdenum complexes have been reported, where H_2O_2 has been used as oxidant in the presence of $NaHCO_3$.[71] Oxidation of styrene, catalyzed by dioxidomolybdenum(VI) complexes using aqueous 30% H_2O_2 as oxidant did not proceed. However, in the presence of $NaHCO_3$ the catalytic oxidation process was activated and gave two products namely, styrene oxide and phenyl acetaldehyde (**Scheme 4.4**). Such $NaHCO_3$ assisted oxidation of styrene has been reported in the literature and gave only one product, styrene oxide.[72–74]

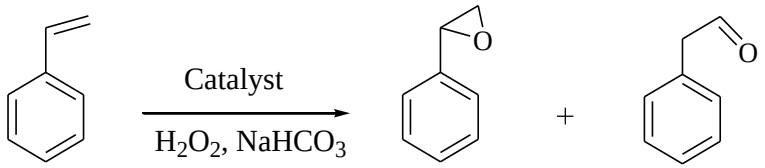

Scheme 4.4. Oxidation of styrene with H_2O_2.

$[Mo^{(VI)}O_2L^1(DMSO)]$ (**1a**) was considered as a representative catalyst to optimize the reaction conditions for the maximum oxidation of styrene, by studying five different parameters *viz.* the effect of amount of oxidant, amount of catalyst, amount of $NaHCO_3$, solvent and temperature of the reaction mixture in detail. The effect of oxidant was studied considering styrene:aqueous 30% H_2O_2 in the molar ratios of 1:3, 1:4 and 1:5, where the mixture of styrene (0.520 g, 5 mmol), catalyst (0.0010 g), $NaHCO_3$ (0.126 g, 1.5 mmol) and oxidant were taken in 5 ml of CH_3CN and the reaction was carried out at 60°C. As illustrated in entries no. 2, 6 and 7 of **Table 4.9**, the percent conversion of styrene improved from 77.7% to 92.5% on increasing the styrene to oxidant ratio from 1:3 to 1:4 but on further increment of ratio (1:5) there is no remarkable improvement in conversion, suggesting that 1:4 (styrene:H_2O_2) molar ratio is sufficient enough to perform the reaction with good conversion. Similarly, for three different amounts viz. 0.0005, 0.0010 and 0.0015 g of catalyst at styrene to H_2O_2 molar ratio of 1:4 under above reaction conditions, 0.0010 g catalyst gave 92.5% conversion while 0.0005 g gave 79% and 0.0015 g catalyst improved the conversion only slightly (93.4%) (entries no. 1, 2 and 3 of **Table 4.9**). The amount of $NaHCO_3$ has played significant role on the conversion of styrene and best conversion was obtained with 1.5 mmol of $NaHCO_3$ (entries no. 2, 4 and 5 in **Table 4.9**). In the absence of $NaHCO_3$ there was no conversion of substrate. Amongst three different temperatures of 40, 50 and 60°C for the fixed operating condition of styrene (0.52 g, 5 mmol), H_2O_2 (2.27 g, 20 mmol),

$[Mo^{(VI)}O_2L^1(DMSO)]$ (**1a**) (0.0010 g), $NaHCO_3$ (0.126, 1.5 mmol) and CH_3CN (5 ml), running the reaction at 60°C gave much better conversion (entries no. 2, 10 and 11 of **Table 4.9**).Variation in the volume of CH_3CN (5, 7 and 10 ml) was also studied (entries no. 2, 8 and 9 of **Table 4.9**) and it was observed that 5 ml of CH_3CN was sufficient enough to get good transformation of styrene while running the reaction at 60°C under above reaction conditions. Thus, all reaction conditions as concluded above (i.e. styrene (0.52 g, 5 mmol), H_2O_2 (2.27 g, 20 mmol), $[Mo^{(VI)}O_2L^1(DMSO)]$ (**1a**) (0.0010 g), $NaHCO_3$ (0.126, 1.5 mmol), CH_3CN (5 ml) and reaction temperature 60°C) were considered essential and applied for the maximum transformation of styrene into a mixture of oxidation products. **Table 4.9** and **Figure 4.17** summarize all the conditions and conversions obtained under a particular set of conditions.

The conversion of styrene and the selectivity of different reaction products using $[Mo^{(VI)}O_2L^1(DMSO)]$ (**1a**) as catalyst under the optimized reaction conditions (entry no. 2 of **Table 4.9**) have been analyzed as a function of time and are presented in **Figure 4.18** and **Table 4.10**. Thus, under the optimized reaction conditions, the selectivity of the two oxidation products varies in the order: styrene oxide (98.6%)> phenyl acetaldehyde (1.4%). Complexes $[Mo^{(VI)}O_2L^{1-6}(DMSO)]$ (**1a**–**6a**) follow same order of the selectivity of products with almost same conversion. Blank reaction under above reaction conditions gave 30% conversion.

Table 4.9. Conversion of styrene (0.520 g, 5 mmol) using [$Mo^{(VI)}O_2L^1$(DMSO)] (1a) as catalyst in 4 h of reaction time under different reaction conditions

Entry No.	Catalyst [g]	H_2O_2 [g(mmol)]	$NaHCO_3$ [g(mmol)]	CH_3CN [ml]	Temp. (^oC)	Conv. [%]
1	0.0005	2.27 (20)	0.126 (1.5)	5	60	79
2	0.0010	2.27 (20)	0.126 (1.5)	5	60	92.5
3	0.0015	2.27 (20)	0.126 (1.5)	5	60	93.4
4	0.0010	2.27 (20)	0.084 (1.0)	5	60	72
5	0.0010	2.27 (20)	0.168 (2.0)	5	60	93.6
6	0.0010	1.70 (15)	0.126 (1.5)	5	60	77.7
7	0.0010	2.83 (25)	0.126 (1.5)	5	60	96
8	0.0010	2.27 (20)	0.126 (1.5)	7	60	72.8
9	0.0010	2.27 (20)	0.126 (1.5)	10	60	48
10	0.0010	2.27 (20)	0.126 (1.5)	5	50	75.5
11	0.0010	2.27 (20)	0.126 (1.5)	5	40	51.7

Table 4.10. Oxidation of styrene, TOF and product selectivity using (1a–6a) as catalyst

Catalyst	TOF [h^{-1}][a]	Conv. [%]	Selectivity [%][b]	
			phac	so
[$Mo^{(VI)}O_2L^1$(DMSO)] (**1a**)	642	92.5	1.4	98.6
[$Mo^{(VI)}O_2L^2(H_2O)$] (**2a**)	600	96	1.3	98.7
[$Mo^{(VI)}O_2L^3$(DMSO)]$_4$·2DMSO (**3a**)	676	92	0.8	99.2
[$Mo^{(VI)}O_2L^4(H_2O)$] (**4a**)	586	94	0.9	99.1
[$Mo^{(VI)}O_2L^5$(DMSO)] (**5a**)	651	93.8	1.1	98.9
[$Mo^{(VI)}O_2L^6$(DMSO)] (**6a**)	647	93	0.6	99.4
Blank reaction	–	30	3	97

[a]TOF values calculated at 4 h of reaction time.

[b]so:styrene oxide; phac: phenyl acetaldehyde.

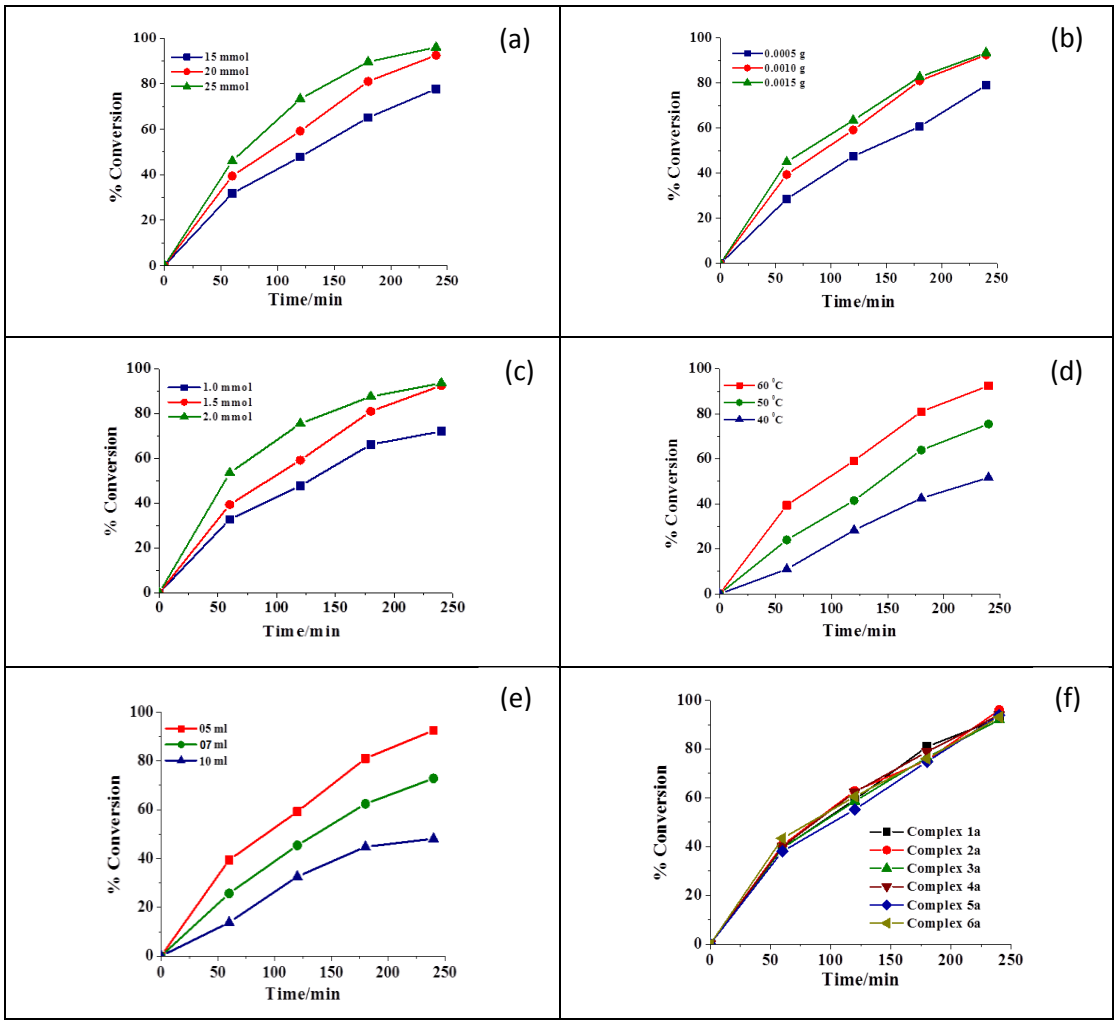

Figure 4.17. (a) Effect of oxidant amount on the oxidation of styrene. Reaction condition: styrene (0.520 g, 5 mmol), catalyst (0.0010 g), $NaHCO_3$ (0.126 g, 1.5 mmol), temperature 60°C and acetonitrile (5 ml). (b) Effect of catalyst amount on the oxidation of styrene. Reaction conditions: styrene (0.520 g, 5 mmol), 30% H_2O_2 (2.27 g, 20 mmol), $NaHCO_3$ (0.126 g, 1.5 mmol), temperature 60°C and acetonitrile (5 ml). (c) Effect of $NaHCO_3$ amount on the oxidation of styrene. Reaction condition: styrene (0.520 g, 5 mmol), catalyst (0.0010 g), 30% H_2O_2 (2.27 g, 20 mmol), temperature 60°C and acetonitrile (5 ml). (d) Effect of temperature on the oxidation of styrene. Reaction conditions: styrene (0.520 g, 5 mmol), 30% H_2O_2 (2.27 g, 20 mmol), $NaHCO_3$ (0.126 g, 1.5 mmol), catalyst (0.0010 g) and acetonitrile (5 ml). (e) Effect of solvent amount on the oxidation of styrene. Reaction conditions: styrene (0.520 g, 5 mmol), 30% H_2O_2 (2.27 g, 20 mmol), $NaHCO_3$ (0.126 g, 1.5 mmol), catalyst (0.0010 g) and temperature 60°C. (f) Plot showing conversion of all metal complexes.

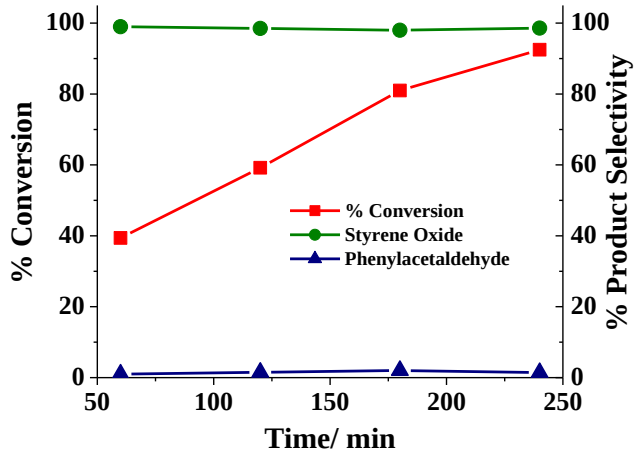

Figure 4.18. Plot showing conversion and product selectivity as a function of time.

4.3.3.2. Oxidation of cyclohexene. Oxidation of cyclohexene, catalyzed by dioxidomolybdenum(VI) complexes using aqueous 30% H_2O_2 as oxidant in the presence of $NaHCO_3$ gave one product namely, cyclohexene oxide (**Scheme 4.5**).

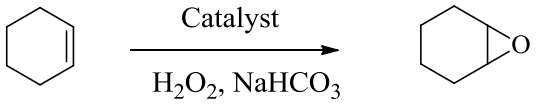

Scheme 4.5. Oxidation of cyclohexene with H_2O_2.

$[Mo^{(VI)}O_2L^1(DMSO)]$ (**1a**) was considered as a representative catalyst for the oxidation of cyclohexene by H_2O_2 in presence of $NaHCO_3$. In order to achieve optimum reaction conditions, the effect of catalyst considering three different amounts viz. 0.0005, 0.0010 and 0.0015 g as a function of time was studied for the fixed amount of cyclohexene (0.41 g, 5 mmol), $NaHCO_3$ (0.126 g, 1.5 mmol) and 30% H_2O_2 (1.70 g, 15 mmol) in 5 ml of CH_3CN and reaction was carried out at 60°C and results are illustrated in **Figure 4.19(a)** (entries no. 1, 2 and 3 of **Table 4.11**). It is clear from the plot that 0.0005 gave 81% conversion of the substrate whereas 0.0010 g and 0.0015 g of catalyst gave 93% and 95% out of these 0.0010 g was the best one to obtain a maximum of 93% conversion of cyclohexene. For the effect of oxidant three different cyclohexene to aqueous 30% H_2O_2 molar ratios viz. 1:2, 1:3 and 1:4 were considered for the

fixed amount of cyclohexene (0.41 g, 5 mmol), $NaHCO_3$ (0.126 g, 1.5 mmol) and catalyst (0.0010 g) in 5 ml of CH_3CN and reaction was carried out at 60°C. As presented in entries no. 2, 6 and 7 of **Table 4.11** and **Figure 4.19(b)**, a maximum of 63.6% conversion was obtained at a cyclohexene to H_2O_2 molar ratio of 1:2 in 4 h of reaction time. This conversion reached 93% on increasing this ratio to 1:3 while 1:4 ratios improve the conversion slightly (99%). Under the operating conditions as fixed above i.e. cyclohexene (0.41 g, 5 mmol), 30% H_2O_2 (1.70 g, 15 mmol), $NaHCO_3$ (0.126 g, 1.5 mmol) in 5 ml of CH_3CN. We have also optimized the amount of $NaHCO_3$ (entries no. 1, 4 and 5), the amount of solvent (acetonitrile, entries no. 1, 8 and 9) and temperature (entries no. 1, 10 and 11) of the reaction and found that 1.5 mmol of $NaHCO_3$, 5 ml of solvent and 60°C reaction temperature were sufficient enough to obtain 93% conversion under above reaction conditions. **Table 4.11** and **Figure 4.19** summarize all the conditions and conversions obtained under a particular set of conditions. No conversion of substrate in the absence of $NaHCO_3$ was obtained. Blank reaction under above reaction conditions gave 32% conversion.

Oxidation of cyclohexene, TOF and selectivity of cyclohexene oxide using different dioxidomolybdenum(VI) complexes as catalyst is given in **Table 4.12**.

Table 4.11. Conversion of cyclohexene (0.410g, 5 mmol) using $[Mo^{(VI)}O_2L^1(DMSO)]$ (1a) as catalyst in 4 h of reaction time under different reaction conditions

Entry No.	Catalyst [g (mmol)]	H_2O_2 [g (mmol)]	$NaHCO_3$ [g (mmol)]	CH_3CN [ml]	Temp. (^oC)	Conv. [%]
1	0.0005	1.70 (15)	0.126 (1.5)	5	60	81
2	0.0010	1.70 (15)	0.126 (1.5)	5	60	93
3	0.0015	1.70 (15)	0.126 (1.5)	5	60	95
4	0.0010	1.70 (15)	0.084 (1.0)	5	60	78.4
5	0.0010	1.70 (15)	0.168 (2.0)	5	60	95.2
6	0.0010	1.14 (10)	0.126 (1.5)	5	60	63.6
7	0.0010	2.27 (20)	0.126 (1.5)	5	60	99
8	0.0010	1.70 (15)	0.126 (1.5)	7	60	76.5
9	0.0010	1.70 (15)	0.126 (1.5)	10	60	43.6
10	0.0010	1.70 (15)	0.126 (1.5)	5	50	71.3
11	0.0010	1.70 (15)	0.126 (1.5)	5	40	42.2

Table 4.12. Oxidation of cyclohexene, TOF and selectivity of cyclohexene oxide using 1a–6a as catalyst

Catalyst	TOF $[h^{-1}]^a$	Conv. [%]	Selectivity [%]
$[Mo^{(VI)}O_2L^1(DMSO)]$ (**1a**)	646	93	100
$[Mo^{(VI)}O_2L^2(H_2O)]$ (**2a**)	579	92.7	100
$[Mo^{(VI)}O_2L^3(DMSO)]_4 \cdot 2DMSO$ (**3a**)	705	96	100
$[Mo^{(VI)}O_2L^4(H_2O)]$ (**4a**)	593	95	100
$[Mo^{(VI)}O_2L^5(DMSO)]$ (**5a**)	664	95.6	100
$[Mo^{(VI)}O_2L^6(DMSO)]$ (**6a**)	670	96.4	100
Blank reaction	–	32	100

[a] TOF values calculated at 4 h of reaction time.

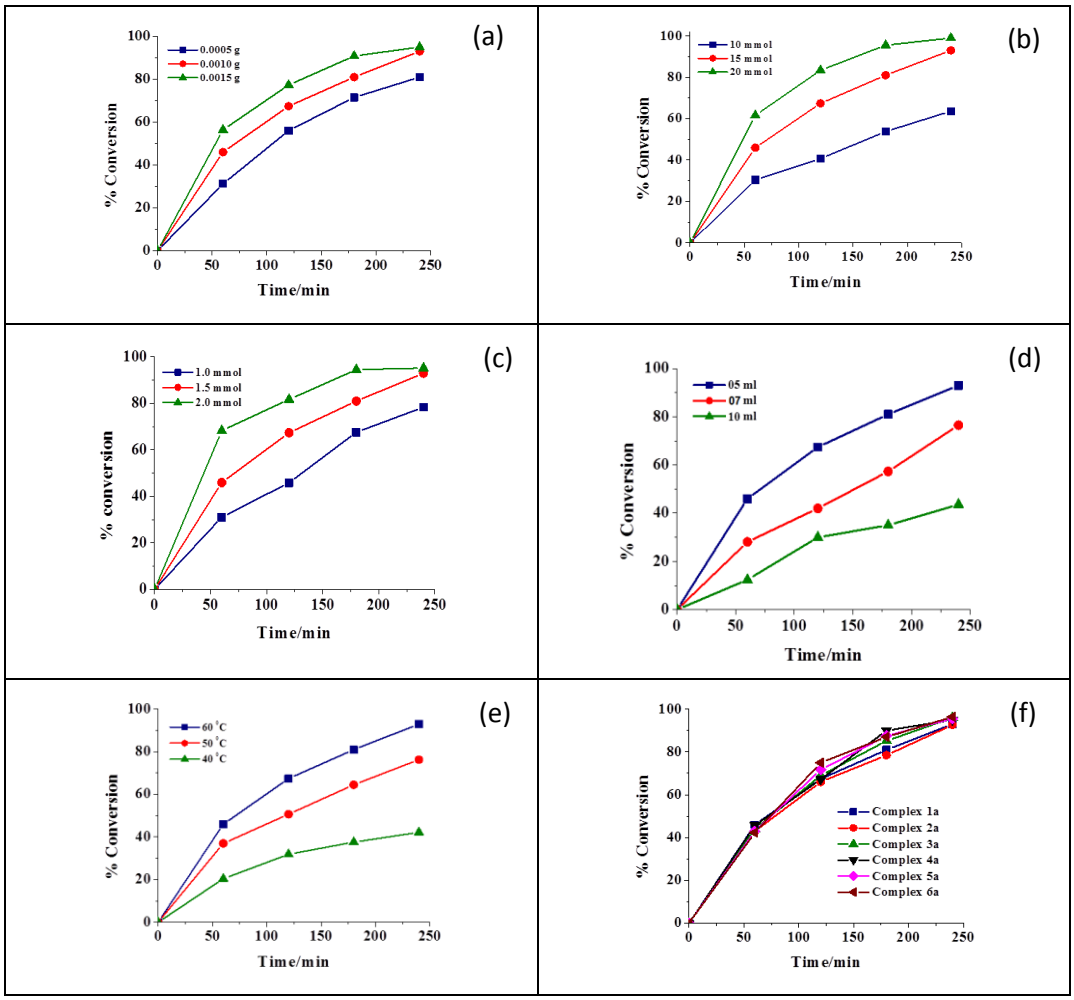

Figure 4.19. (a) Effect of catalyst amount on the oxidation of cyclohexene. Reaction conditions: cyclohexene (0.410 g, 5 mmol), 30% H_2O_2 (1.70 g, 15 mmol), $NaHCO_3$ (0.126 g, 1.5 mmol), temperature 60°C and acetonitrile (5 ml). (b) Effect of oxidant amount on the oxidation of cyclohexene. Reaction condition: cyclohexene (0.410 g, 5 mmol), catalyst (0.0010 g), $NaHCO_3$ (0.126 g, 1.5 mmol), temperature 60°C and acetonitrile (5 ml). (c) Effect of $NaHCO_3$ amount on the oxidation of cyclohexene. Reaction condition: cyclohexene (0.410 g, 5 mmol), catalyst (0.0010 g), 30% H_2O_2 (1.70 g, 15 mmol), temperature 60°C and acetonitrile (5 ml). (d) Effect of solvent amount on the oxidation of cyclohexene. Reaction conditions: cyclohexene (0.410 g, 5 mmol), 30% H_2O_2 (1.70 g, 15 mmol), $NaHCO_3$ (0.126 g, 1.5 mmol), catalyst (0.0010 g) and temperature 60°C (e) Effect of temperature on the oxidation of cyclohexene. Reaction conditions: cyclohexene (0.410 g, 5 mmol), 30% H_2O_2 (1.70 g, 15 mmol), $NaHCO_3$ (0.126 g, 1.5 mmol), catalyst (0.0010 g) and acetonitrile (5 ml). (f) Plot showing conversion of all metal complexes.

4.3.3.3. Reactivity of complexes with H_2O_2. Dioxidomolybdenum(VI) complexes react with H_2O_2 to give the corresponding oxido–peroxido complexes. The generation of such species has been established in DMSO by electronic absorption spectroscopy. In a typical reaction, 20 ml of ca. 3.6×10^{-5} M solution of $[Mo^{(VI)}O_2L^1(DMSO)]$ (**1a**) was treated with one drop portion of 30% aqueous H_2O_2 (0.260 g, 2.3 mmol) dissolved in 5 ml of DMSO and the resultant spectroscopic changes are presented in **Figure 4.20**. The bands at 312 nm and 343 nm increases while 267 and 420 nm bands decrease their intensity considerably. These changes indicate the interaction of $[Mo^{(VI)}O_2L^1(DMSO)]$ (**1a**) with H_2O_2 and formation of oxido–peroxido species.[43]

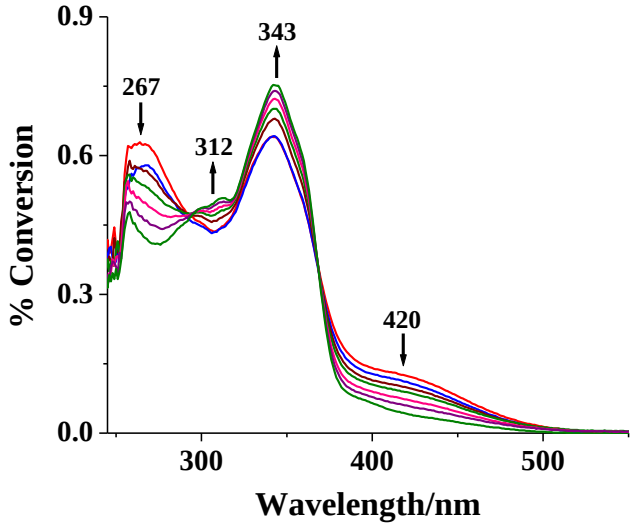

Figure 4.20. UV–Vis spectral changes observed during titration of complex **1a** with H_2O_2. The spectra were recorded after successive additions of 1–drop portion of 30% H_2O_2 (2.3 mmol) dissolved in 5 ml of DMSO to 20 ml of 3.6×10^{-5} M solution of complex **1a** in DMSO.

4.4. CONCLUSION

(a) Dioxidomolybdenum(VI) complexes $[Mo^{(VI)}O_2L^{1–6}]$ (**1**–**6**), of thiosemicarbazone ligands are reported.

(b) Dioxidomolybdenum(VI) complexes $[Mo^{(VI)}O_2L^{1/5/6}(DMSO)]$ (**1a, 5a** & **6a**), $[Mo^{(VI)}O_2L^{2/4}(H_2O)]$ (**2a** & **4a**), and $[Mo^{(VI)}O_2L^{3}(DMSO)]_4.2DMSO$ (**3a**) and monooxidomolybdenum(IV) complexes $[Mo^{(IV)}OL^{1–6}(N–N)]$ (**7**–**12**) {where, N–N = 2,2'–bipyridyl or 1,10–phenanthroline} are also reported as product of substrate binding and oxygen atom transfer reactivity respectively of precursor dioxidomolybdenum(VI) complexes $[Mo^{(VI)}O_2L^{1–6}]$ (**1**–**6**) respectively.

(c) All the Mo(VI) and Mo(IV) complexes have been charecterized by physicochemical techniques. Molecular structures of some of the Mo(VI) (**1a**–**4a**) and Mo(IV) complexes (**7** and **9**–**11**) have been determined by single crystal X–ray crystallography.

(d) The assessment of oxygen atom transfer from $[Mo^{(VI)}O_2L^{1–6}]$ (**1**–**6**) to PPh_3 has been monitored by the gradual appearance of $OPPh_3$ (27 ppm) as probed by ^{31}P NMR.

(e) The oxygen atom transfer from the substrate DMSO to the system $[Mo^{(IV)}OL^{1–6}(N–N)]$ (**7**–**12**) has been studied spectrophotometrically in DMSO solution.

(f) The catalytic activity (oxidation of styrene and cyclohexene) of $Mo^{(VI)}$ complexes (**1a**–**6a**) have been studied.

4.5. REFERENCES

(1) Mrndel, R. R.; Bittner, F. *Biochim. Biophys. Acta, Mol. Cell Res.* **2006**, *1763*, 621.

(2) Brondino, C. D.; Romao, M. J.; Moura, I.; Moura, J. J. G. *Curr. Opin. Chem. Biol*. **2006**, *10*, 109.

(3) D'Errico, G.; Salle, A. D.; Cara, F. L.; Rossi, M.; Cannio, R. *J. Bacteriol*. **2006**, *188*, 694.

(4) Harrison, R. *Free Radic. Biol. Med*. **2002**, *33*, 774.

(5) Pryde, D. C. *J. Med. Chem*. **2010**, *53*, 8441.

(6) Ngan, N. K.; Lo, K. M.; Wong, C. S. R. *Polyhedron* **2012**, *33*, 235.

(7) Quintal, S.; Matos, J.; Fonseca, I.; Félix, V.; Drew, M. G. B.; Trindade, N.; Meireles, M.; Calhorda, M. J. *Inorg. Chim. Acta* **2008**, *361*, 1584.

(8) Seena, E. B.; Kurup, M. R. P. *Polyhedron* **2007**, *26*, 3595.

(9) Vrdoljak, V.; Dilovic, I.; Rubcic, M.; Pavelic, S. K.; Kralj, M.; Calogovic, D. M.; Piantanida, I.; Novak, P.; Rozman, A.; Cindric, M. *Eur. J. Med. Chem*. **2010**, *45*, 38.

(10) (a) Choi, E. Y.; Stockert, A. L.; Leimkuhler, S.; Hill, R. *J. Inorg. Biochem*. **2004**, *98*, 841. (b) Rees, D. C.; Hu, Y.; Kisker, C.; Schindelin, H. *J. Chem. Soc., Dalton Trans*. **1997**, 3909. (c) Xiao, Z.; Bruck, M. A.; Enemark, J. H.; Young, C. G.; Wedd, A. G. *Inorg. Chem*. **1996**, *35*, 7508. (d) Pietsch, M. A.; Hall, M. B. *Inorg. Chem*. **1996**, *35*, 1273. (e) Topich, J.; Lyon III, J. T. *Inorg. Chem*. **1984**, *23*, 3202;

(11) Hille, R. *Chem. Rev.* **1996**, *96*, 2757.

(12) Johnson, M. K.; Rees, D. C.; Adams, W. W. *Chem. Rev.* **1996**, *96*, 2817.

(13) Hille, R. *Eur. J. Inorg. Chem.* **2006**, 1913.

(14) Holm, R. H. *Chem. Rev*. **1987**, *87*, 1401 references therein.

(15) Holm, R. H. *Coord. Chem. Rev*. **1990**, *100*, 183 references therein.

(16) Kollar, J. *Am. Chem. Soc. Div. Petr. Chem. Prepr*. **1978**, *23*, 106.

(17) Sheldon, R. A.; Kochi, J. K. *Metal Catalyzed Oxidation of Organic Compounds*, Academic, New York, **1981**.

(18) Mimoun, H. *J. Mol. Catal*. **1980**, *7*, 1.

(19) Bottomley, F.; Sutin, L. *Adv. Organomet. Chem*. **1988**, *28*, 339.

(20) Arzoumanian, H. *Bull. Soc. Chim. Belg*. **1991**, *100*, 717.

(21) (a) Mendel, R. R. *Dalton Trans*. **2005**, 3404. (b) McMaster, J.; Enemark, J. H. *Curr. Opin. Chem. Biol.* **1998**, *2*, 109. (c) Majumdar, A.; Sarkar, S. *Coord. Chem. Rev*. **2011**, *255*, 1039. (d) Hille, R.; Nishino, T.; Bittner, F. *Coord. Chem. Rev*. **2011**, *255*, 1179.

(22) (a) Rana, A.; Dinda, R.; Ghosh, S. P.; Blake, A. J. *Polyhedron* **2003**, *22*, 3075. (b) Pramanik, N. R.; Ghosh, S. P.; Raychaudhuri, T. K.; Ray, S.; Butcher, R. J.; Mandal, S. S. *Polyhedron* **2004**, *23*, 1595.

(23) Unoura, K.; Abiko, Y.; Yamazaki, A.; Kato, Y.; Coomber, D. C.; Fallon, G. D.; Nakahara, K.; Bond, A. M. *Inorg. Chim. Acta* **2002**, *333*, 41.

(24) Farahani, M. M.; Farzaneh, F.; Ghandi, M. *Catal. Commun*. **2007**, *8*, 6.

(25) Farahani, M. M.; Farzaneh, F.; Ghandi, M. *J. Mol. Catal. A: Chem*. **2006**, *248*, 53.

(26) Ambroziak, K.; Pelech, R.; Milchert, E.; Dziembowska, T.; Rozwadowski, Z. *J. Mol. Catal. A: Chem.* **2004**, *211*, 9.

(27) Sui, Y.; Zeng, X.; Fang, X.; Fu, X.; Xiao, Y.; Chen, L.; Li, M.; Cheng, S. J. *Mol. Catal. A: Chem.* **2007**, *270*, 61.

(28) Zhao, J.; Zhou, X.; Santos, A. M.; Herdtweck, E.; Romao, C. C.; Kuhn, F. E. *Dalton Trans.* **2003**, 3736.

(29) Zhou, X.; Zhao, J.; Santos, A. M.; Kuhn, F. E. *Naturforsch* **2004**, *59b*, 1223.

(30) Sobczak, J. M.; Ziolkowski, J. J. *Appl. Catal. A* **2003**, *248*, 261.

(31) Bagherzadeh, M.; Latifi, R.; Tahsini, L.; Amani, V.; Ellern, A.; Woo, L. K. *Polyhedron* **2009**, *28*, 2517.

(32) Rezaeifard, A.; Sheikhshoaie, I.; Monadi, N.; Alipour, M. *Polyhedron* **2010**, *29*, 2703.

(33) Pisk, J.; Agustin, D.; Vrdoljak, V.; Poli, R. *Adv. Synth. Catal*. **2011**, *353*, 2910.

(34) Pisk, J.; Prugovečki, B.; Matković–Čalogović, D.; Poli, R.; Agustin, D.; Vrdoljak, V. *Polyhedron* **2012**, *33*, 441.

(35) Judmaier, M. E.; Holzer, C.; Volpe, M.; Mosch–Zanetti, N. C. *Inorg. Chem.* **2012**, *51*, 9956.

(36) Lei, X.; Chelamalla, N. *Polyhedron* **2013**, *49*, 244.

(37) Maurya, M. R. *Curr. Org. Chem*. **2012**, *16*, 73.

(38) Maurya, M. R.; Arya, A.; Adao, P.; Pessoa, J. C. *Appl. Catal. A: Gen*. **2008**, *351*, 239. (39) Hu, Z.; Fu, X.; Li, Y. *Inorg. Chem. Commun*. **2011**, *14*, 497.

(40) Bhatia, R. K.; Rao, G. N. *J. Mol. Catal. A: Chem*. **1997**, *121*, 171.

(41) Maurya, M. R.; Kumar, U.; Manikandan, P. *Dalton Trans*. **2006**, 3561.

(42) Boruah, J. J.; Das, S. P.; Borah, R.; Gogoi, S. R.; Islam, N. S. *Polyhedron* **2013**, *52*, 246.

(43) Pasayat, S.; Dash, S. P.; Roy, S.; Dinda, R.; Maurya, M. R.; Kaminsky, W.; Patil, Y. P.; Nethaji, M.; Dhaka, S. *Polyhedron* **2014**, *67*, 1.

(44) Maurya, M. R.; Dhaka, S.; Avecilla, F. *Polyhedron* **2014**, *67*, 145.

(45) Jeyakumar, K.; Chand, D. K. *J. Chem. Sci*. **2009**, *121*, 111.

(46) Bagherzadeh, M.; Haghdoost, M. M.; Amini, M.; Derakhshandeh, P. G. *Catal. Commun*. **2012**, *23*, 14.

(47) Chakravarthy, R. D.; Suresh, K.; Ramkumar, V.; Chand, D. K. *Inorg. Chim. Acta* **2011**, *376*, 57.

(48) Sheikhshoaie, I.; Rezaeifard, A.; Monadi, N.; Kaafi, S. *Polyhedron* **2009**, *28*, 733.

(49) (a) Reis, P. M.; Gamelas, C. A.; Brito, J. A.; Saffon, N.; Gomez, M.; Royo, B. *Eur. J. Inorg. Chem.* **2011**, *5*, 666. (b) Dinoi, C.; Ciclosi, M.; Manoury, E.; Maron, L.; Perrin, L.; Poli, R. *Chem. Eur. J*. **2010**, *16*, 9572. (c) Jorgensen, K. A. *Chem. Rev*. **1989**, *89*, 431.

(50) Herbert, M.; Montilla, F.; Galindo, A. *J. Mol. Catal. A: Chem*. **2011**, *338*, 111.

(51) Gunyara, A.; Betzb, D.; Dreesb, M.; Herdtweck, E.; Kuhna, F. E. *J. Mol. Catal. A: Chem.* **2010**, *331*, 117.

(52) Maurya, M. R.; Sikarwar, S.; Manikandan, P. *Appl. Catal. A* **2006**, *315*, 74.

(53) Burke, A. J. *Coord. Chem. Rev*. **2008**, *252*, 170.

(54) Jain, K. R.; Herrmann, W. A.; Kuhn, F. E. *Coord. Chem. Rev*. **2008**, *252*, 556.

(55) Gupta, K. C.; Sutar, A. K. *Coord. Chem. Rev*. **2008**, *252*, 1420.

(56) Frederic, B. *Coord. Chem. Rev*. **2003**, *236*, 71.

(57) Syamal, A.; Maurya, M. R. *Coord. Chem. Rev*. **1989**, *95*, 183.

(58) Chen, G. J. J.; McDonald, J. W.; Newton, W. E. *Inorg. Chem.* **1976**, 15, 2612.

(59) Part 1: Ghosh, S.; Purohit, S. *Indian J. Chem., Sect. A: Inorg., Bio–inorg., Phys., Theor. Anal. Chem.* **1987**, *26A*, 131.

(60) Saswati; Dinda, R.; Schmiesing, C. S.; Sinn, E.; Patil, Y. P.; Nethaji, M.; Stoeckli–Evans, H.; Acharyya, R. *Polyhedron* **2013**, *50*, 354.

(61) Lobana, T. S.; Rekha; Butcher, R. J.; Castineiras, A.; Bermejo, E.; Bharatam, P. V; *Inorg. Chem.* **2006**, *45*, 1535.

(62) Bruker (**2007**) APEX2 (Version 2.1–4), SAINT (version 7.34A), SADABS (version 2007/4), BrukerAXS Inc, Madison, Wisconsin, USA.

(63) Bruker, *SADABS, SAINT, SHELXTL and SMART*, Bruker AXS Inc., Madison, Wisconsin, SA, **2003**.

(64) Sheldrick, G. M. *Acta Crystallogr., Sect. A: Found. Crystallogr.* **2008**, *64*, 112.

(65) (a) Pramanik, N. R.; Ghosh, S.; Raychaudhuri, T. K.; Drew, M. G. B.; Mandal, T. K.; Mandal, S. S. *Inorg. Chim. Acta* **2012**, *383*, 60.

(66) Stelzig, L.; Kötte S.; Krebs, B. *J. Chem. Soc., Dalton Trans*. ***1998***, *2921*.

(67) (a) Dinda, R.; Sengupta, P.; Ghosh, S.; Figge, H. M.; Sheldrick, W. S. *Dalton Trans.* **2002**, 4434. (b) Dinda, R.; Sengupta, P.; Ghosh, S.; Sheldrick, W. S. *Eur. J. Inorg. Chem*. **2003**, 363.

(68) (a) Purohit, S.; Koley, A. P.; Prasad, L. S.; Manoharan, P. T.; Ghosh, S. *Inorg.* Chem. **1989**, *28*, 3735. (b) Boyd, I. W.; Spence, J. T. *Inorg. Chem.* **1982**, *21*, 1602. (c) Kaul, B. B.; Enemark, J. H.; Merbs, S. L.; Spence, J. T. *J. Am. Chem. Soc.* **1985**, *107*, 2885.

(69) Nemykin, V. N.; Basu, P. *Inorg. Chem*. **2005**, *44*, 7494.

(70) Oku, H.; Ueyama, N.; Kondo, M.; Nakamura, A. *Inorg. Chem.* **1994**, *33*, 209.

(71) Bagherzadeh, M.; Aminia, M.; Parastar, H.; Jalali–Heravi, M.; Ellern, A.; Woo, L. K. *Inorg. Chem. Commun*. **2012**, *20*, 86.

(72) Maiti, S. K.; Dinda, S.; Banerjee, S.; Mukherjee, A. K.; Bhattacharyya, R. *Eur. J. Inorg. Chem.* **2008**, 2038.

(73) Lane, B. S.; Vogt, M.; DeRose, V. J.; Burgess, K. *J. Am. Chem. Soc*. **2002**, *124*, 11946.

(74) Richardson, D. E.; Yao, H.; Frank, K. M.; Bennett, D. A. *J. Am. Chem. Soc*. **2000**, *122*, 1729.

Chapter 5

Synthesis, reactivity and structural characterization of oxidovanadium(IV/V) complexes: Methylation of aliphatic hydrocarbon by dimethyl sulfoxide

Chapter 5

Synthesis, reactivity and structural characterization of oxidovanadium(IV/V) complexes: Methylation of aliphatic hydrocarbon by dimethyl sulfoxide

ABSTRACT

The synthesis and characterization of an oxidovanadium(IV) [$V^{IV}O(L)(acac)$] (**1**) and two dioxidovanadium(V) [$V^{V}O_2(L')$] (**2**) and [$V^{V}O_2(L)$] (**2a**) complexes of {(4–(*p*–fluorophenyl)thiosemicarbazone) of pyridine–2–aldehyde} (HL) is described in the present study. The oxidovanadium(IV) species [$V^{IV}O(L)(acac)$] (**1**) was synthesized in usual way by the reaction of metal precursor $VO(acac)_2$ with thiosemicarbazone ligand (HL) in refluxing ethanol. The recrystallization of [$V^{IV}O(L)(acac)$] (**1**) in DMF, CH_3CN or EtOH gave the same product *i.e.* dioxidovanadium(V) complex [$V^{V}O_2(L)$] (**2a**), whereas [$V^{V}O_2(L')$] (**2**) was synthesized during recrystallization of [$V^{IV}O(L)(acac)$] (**1**) in DMSO where the original ligand (HL) is transformed to a rearranged new ligand (HL'). The ligand in complex **1** is found to undergo methylation at the carbon centre attached to imine nitrogen in presence of DMSO and transformed to the corresponding dioxidovanadium(V) species through *in situ* reaction. The synthesized ligand and the metal complexes were characterized by elemental analysis, IR, UV–Vis, NMR and EPR spectroscopy. Molecular structures of complex **1** [$V^{IV}O(L)(acac)$] and complex **2** [$V^{V}O_2(L')$] have been determined by single crystal X–ray crystallography. Complexes **1** & **2** show *in vitro* insulin mimetic activity against insulin responsive L6 myoblast cells, with complex **1** being more potent, is comparable to insulin at 100 μM concentration, while complex **2** has considerable insulin mimetic activity. In addition, the *in vitro* antiproliferative activity of the complexes **1** & **2** against the MCF–7 and Vero cell lines were also assayed.

5.1. INTRODUCTION

Coordination chemistry of vanadium has attracted increasing interest, due to its biological properties,[1–5] and for the use of oxidovanadium complexes as oxidation and oxo transfer catalysis,[6,7] and potential medicinal applications.[8,9] Vanadium is one of the trace bio-elements existing in the human body, its complexes have been found to present antibacterial, antitumor, insulin-enhancing and antiparasitic effects.[10–13] Vanadium complexes could also suppress the growth and spread of existing tumors by inhibiting tumor cell proliferation, inducing apoptosis and limiting the invasion and metastatic potential of neoplastic cells.[13–15] Inorganic vanadyl and vanadate, as well as some vanadium(IV)/(V) complexes, are influential insulin mimics.[16] The discovery of the *in vivo* insulin mimesis per os of oxidovanadates(V),[17] the oxidovanadium(IV) precursor, vanadyl sulfate,[18] and the much more potent bis(maltolato)-oxidovanadium(IV) (BMOV)[19] encourages the explore of vanadium complexes having application in the treatment of type II diabetes.[20,21] Thus different approaches have been attempted to develop orally active vanadium containing insulin enhancing agents.[22]

Multidentate ligands with donor functionalities including combinations of oxygen, sulfur and nitrogen have been used to mimic relevant biological molecules that vanadium ions may interact with. Thiosemicarbazone is an important class of N, S donor ligands which have considerable pharmacological interest, due to their significant antibacterial, antiviral, antimalarial, antileprotic, antitumor and anticancer activities.[23–26] Metal complexes of thiosemicarbazone ligands have shown variable bonding properties and structural diversity, along with promising biological implications and ion sensing abilities.[25,27–34]

Here we report the formation of a dioxidovanadium(V) complex $[V^{V}O_2(L')]$ (**2**) of (4–(*p*–fluorophenyl)thiosemicarbazone) of pyridine–2–aldehyde (HL). The whole reaction takes place in two steps, first of which is the formation of oxidovanadium(IV) complex $[V^{IV}O(L)(acac)]$ (**1**), which slowly oxidises to the dioxidovanadium(V) complex $[V^{V}O_2(L')]$ (**2**) in presence of DMSO. The change in coloration of the complex (from green to orange) and UV–Vis data fully supports the observation.

Recrystallization of the crude green complex $[V^{IV}O(L)(acac)]$ (**1**) in DMSO interestingly methylates the C(8)–imine carbon which is confirmed by the X–ray crystal data of

dioxidovanadium(V) complex $[V^{V}O_2(L')]$ (**2**). This interesting observation lead us to repeat the experiment in different other solvents like DMF, CH_3CN, EtOH but surprisingly the methylation took place only in DMSO, and instead of $[V^{V}O_2(L')]$ (**2**), $[V^{V}O_2(L)]$ (**2a**) was prepared.

Thus the methylation of the imine carbon in DMSO may be attributed to the methylene transfer from the methylsulfinyl radical anion resulting from the oxidation of the $[V^{IV}O(L)(acac)]$ (**1**). The radical anion rapidly converts to a methyl sufinyl carbanion ($CH_3SOCH_2^-$) which is a unique methylating ylide and known to methylate olefin and aromatic systems.[35]

The synthesized ligand and the metal complexes were characterized by elemental analysis, IR, UV–Vis, NMR and EPR spectroscopy. Molecular structures of complex **1** $[V^{IV}O(L)(acac)]$ and complex **2** $[V^{V}O_2(L')]$ have been determined by single crystal X–ray crystallography. Complexes **1** & **2** show *in vitro* insulin mimetic activity against insulin responsive L6 myoblast cells, with complex **1** being the most potent, is comparable to insulin at 100 µM concentration, while the complex **2** has considerable insulin mimetic activity. In addition, the *in vitro* antiproliferative activity of complexes **1** & **2** against MCF–7 and Vero cell lines were also assayed.

5.2. EXPERIMENTAL SECTION

5.2.1. General methods and materials. $[VO(acac)_2]$ was prepared as described in the literature.[36] Reagent grade solvents were dried and distilled prior to use. All other chemicals were reagent grade, available commercially and used as received. HPLC grade DMSO and CH_3CN was used for spectroscopic and electrochemical studies and ethanol, methanol were used for synthesis of ligands and metal complexes. Commercially available TEAP (tetra ethyl ammonium perchlorate) was properly dried and used as a supporting electrolyte for recording cyclic voltammograms of the complexes. Elemental analyses were performed on a Vario ELcube CHNS Elemental analyzer. IR spectra were recorded on a Perkin-Elmer Spectrum RXI spectrometer. ^1H and ^{13}C NMR spectra were recorded with a Bruker Ultrashield 400 MHz spectrometer using $SiMe_4$ as an internal standard. Electronic spectra were recorded on a Lamda25, PerkinElmer spectrophotometer. Electrochemical data were collected using PAR Versastat-II instrument driven by E-chem software (PAR) at 298 K in a dry nitrogen atmosphere. Cyclic voltammetry experiments were carried out with Pt working and auxiliary electrodes and Ag/AgCl as reference electrode. X-band EPR measurements were performed on a JEOL JES-FA 200 and Bruker EMX EPR Spectrometer.

5.2.2. Synthesis of ligand (HL). The thiosemicabazide was prepared from distilled *p*–fluoroaniline by a known method reported earlier.[37] Schiff base ligand, 4–(*p*–fluorophenyl)thiosemicarbazone of pyridine–2–aldehyde was prepared in 80–90% yield, by stirring equimolar ratio of the thiosemicabazide with pyridine–2–aldehyde in methanol medium by standard procedures.[38] The resulting compound was filtered, washed thoroughly with methanol and dried over fused $CaCl_2$. **HL**: Yield: 85%. Anal. calc. for $C_{13}H_{11}N_4SF$: C, 56.92; H, 4.04; N, 20.42. Found: C, 56.95; H, 4.00; N, 20.41. Main IR peaks (KBr, cm^{-1}): 3311 s ν(N(1)–H), 2967 s ν(N(2)–H), 2825 m *ν*(C(8)–H), 1638 s ν(C=C), 836 s ν(C(7)–S(1)). ^1H NMR (DMSO–d_6, 400 MHz) δ: 12.08 (s, 1H, N(1)H), 10.29 (s, 1H, N(2)H), 8.59 (s, 1H, C(8)H), 8.58–7.20 (m, 8H, C_6H_4). ^{13}C NMR (DMSO-d_6, 100 MHz) δ: 177.25, 161.46, 159.05, 153.58, 149.82, 143.62, 136.98, 135.77, 128.86, 128.77, 124.76, 121.12, 115.37.

5.2.3. Synthesis of complex [$V^{IV}O$(L)(acac)] (1). To a solution of HL (0.274 g, 0.100 mmol) in hot ethanol, $VO(acac)_2$ (0.265 g, 1.0 mmol) was added. The mixture was refluxed for 2 h, yielding dark green colored crystalline residue of the complex. **[$V^{IV}O$(L)(acac)]** (**1**): Yield: 75%. Anal. calc. for $C_{18}H_{17}FN_4VO_3S$: C, 49.21; H, 3.90; N, 12.75. Found: C, 49.24; H, 3.87; N, 12.73. Main IR peaks (KBr, cm^{-1}): 3317 s ν(N(1)–H), 1602 s ν(C=C), 949 s ν(V=O), 762 s ν(C(7)–S(1)).

5.2.4. Synthesis of complex [$V^{V}O_2$(L´)] (2). The dark green crystalline residue of [$V^{IV}O$(L)(acac)] (**1**) was dissolved in DMSO for recrystallization and allowed to evaporate at room temperature. Reddish brown colored crystals of the complex were obtained from DMSO after 1–2 weeks. **[$V^{V}O_2$(L´)] (2):** Yield: 65%. Anal. calc. for $C_{14}H_{12}FN_4VO_2S$: C, 45.41; H, 3.27; N, 15.13. Found: C, 45.43; H, 3.25; N, 15.16. Main IR peaks (KBr, cm^{-1}): 3268 s ν(N(1)–H), 1604 s ν(C=C), 937, 925 s ν(V=O), 765 s ν(C(7)–S(1)). ^{1}H NMR (DMSO–d_6, 400 MHz) δ: 10.20 (s, 1H, N(1)H), 8.72–7.18 (m, 8H, C_6H_4), 2.66 (s, 3H, C(8)H_3). ^{13}C NMR (DMSO-d_6, 100 MHz) δ: 154.34, 153.80, 143.72, 141.34, 137.23, 130.68, 129.12, 126.94, 125.35, 122.48, 122.40, 115.88, 115.65, 67.87.

5.2.5. Synthesis of complex [$V^{V}O_2$(L)] (2a). The dark green crystalline residue of [$V^{IV}O$(L)(acac)] (**1**) was dissolved in EtOH for recrystallization and allowed to evaporate at room temperature. Yellow colored residue of the complex was obtained after few days. **[$V^{V}O_2$(L)] (2a):** Yield: 70%. Anal. calc. for $C_{13}H_{10}FN_4VO_2S$: C, 43.83; H, 2.83; N, 15.73. Found: C, 43.80; H, 2.85; N, 15.76. Main IR peaks (KBr, cm^{-1}): 3256 s ν(N(1)–H), 2834 m ν(C(8)–H), 1589 s ν(C=C), 934, 922 s ν(V=O), 775 s ν(C(7)–S(1)). ^{1}H NMR (DMSO–d_6, 400 MHz) δ: 10.29 (s, 1H, N(1)H), 8.79 (s, 1H, C(8)H), 8.78–7.16 (m, 8H, C_6H_4). ^{13}C NMR (DMSO-d_6, 100 MHz) δ: 166.16, 160.28, 159.10, 156.73, 150.24, 149.31, 138.11, 137.27, 125.45, 119.96, 119.88, 116.29, 116.06.

[$V^{IV}O$(L)(acac)] (**1**) when recrystallized in CH_3CN and DMF gave similar results as **2a**.

5.2.6. X–ray crystallography. The structure of both the complexes **1** & **2**, were measured at room temperature on an Agilent Technologies SuperNova Dual CCD with an Atlas detector fitted with Mo Kα radiation (λ = 0.71073 Å) to θ_{max} = 27.5°. Data processing and absorption correction were accomplished with CrysAlis PRO.[39] The structure was solved by direct methods with SHELXS–97[40] and refinement anisotropic displacement parameters, C–bound hydrogen atoms in the riding model approximation and a weighting scheme of the form $w = 1/[\sigma^2(F_o^2) + (0.059P)^2 + 3.139\ P]$ for $P = (F_o^2 + 2F_c^2)/3$) was on F^2 by means of SHELXL-97.[40] Crystallographic data and final refinement details are given in **Table 5.1**. The ORTEP plots of the complexes were drawn with ORTEP–3 for Windows[41] at the 50% probability level and the remaining crystallographic figures were drawn with DIAMOND[42] using arbitrary spheres. Data manipulation and interpretation were with WinGX[41] and PLATON.[43]

Table 5.1. Crystal and refinement data of $[V^{IV}O(L)(acac)]$ (1) and $[V^{V}O_2(L')]$ (2)

Compound	**1**	**2**
Formula	$C_{18}H_{17}FN_4VO_3S$	$C_{14}H_{12}FN_4VSO_2$
M	439.36	370.28
Crystal system	Triclinic	Monoclinic
Space group	*P* ī	*C*2/*c*
a(Å)	9.9204(13)	19.600(3)
b(Å)	13.6766(15)	14.7000(8)
c(Å)	14.9965(19)	14.922(2)
α (°)	68.292(11)	90.00
β (°)	84.254(11)	134.83(3)
γ (°)	89.768(10)	90.00
V(Å^3)	1879.7(4)	3049.1(17)
Z	2	8
D_{calc}(g.cm^{-3})	1.554	1.613
F(000)	1.904	1.613
μ(Mo-Kα)(mm^{-1})	0.784	0.812
Reflections collected / unique	11536 / 3211	11673 / 3449
R_1[I>2σ(I)]	0.062, 0.134	0.050, 0.118
wR_2[all data]	0.086, 0.151	0.090, 0.143
S[goodness of fit]	1.56	1.01
min./max. res. (e.Å^{-3})	–0.31, 0.45	–0.27, 0.41

5.2.7. *In vitro* Glucose uptake assay on L6 myotubes. L6 myoblast were cultured in DMEM containing 10% FBS and penicillin (100 U/ml) and streptomycin (100 µg/ml) in a humidified 5% CO_2 incubator at 37°C. To differentiate to myotubes, the myoblast cells ($5x10^4$) were seeded in 24 well plates in DMEM containing 2% FBS. The myoblast cells ($5x10^4$) were grown for 11 days in 0.4 ml of 2% FBS/DMEM to allow the formation of myotubes. The medium was changed every 2 days. On the 11^{th} day, the cells were washed and incubated in Kreb's bicarbonate buffer (KRBB) for 2 h. Myotubes were then further cultured in KRBB containing 25 mM glucose along with 25, 50, 100 µM of vanadium compounds ($[V^{IV}O(L)(acac)]$ (**1**), $[V^{V}O_2(L')]$ (**2**) and $VO(acac)_2$) for 4 h, respectively. The insulin (2 µM) was taken as positive control.[44] The residual glucose in the buffer aliquots remaining in each well after 4 h was estimated using hexokiase method by Randox autoanalyser.

5.2.8. Cell culture. MCF–7 and Vero cells were obtained from National Centre of Cell Science (NCCS), Pune, India and were maintained in minimal essential medium supplemented with 10% fetal bovine serum, penicillin-streptomycin solution and incubated at 37°C in 5% CO_2 and 95% humidified incubator

5.2.9. Cytotoxicity studies. The effect of the drugs on the cancer cell viability was studied using MTT dye reduction assay by measuring the optical density at 595 nm using micro plate reader spectrophotometer. After the cells were grown for 24 h to a subconfluent state (~ 60–70%), the cells were treated with different concentrations of complexes $[V^{IV}O(L)(acac)]$ (**1**) and $[V^{V}O_2(L')]$ (**2**) (5, 50, 100, 200 µM) in culture medium. The samples were tested in triplicates. After 24, 48 and 72 h the effect of the compound on cell viability was examined by MTT (thiazolyl blue tetrazolium bromide) test. Optical density was measured at 595 nm using automatic microplate reader.

5.2.10. DAPI staining. DAPI (4′,6–diamidino–2–phenylindole dihydrochloride) staining was performed to see the morphology of the nuclei after treatment. The cells were grown in the 96–well plate. After reaching approximately 90% confluency, the cells were treated with complexes $[V^{IV}O(L)(acac)]$ (**1**) and $[V^{V}O_2(L')]$ (**2**) at different concentrations (5, 50 100, 200 µM) and were incubated for 24, 48 and 72 h. Cells were observed with inverted fluorescence microscope after treatment to check for morphological changes, during cell death. Then the cells were washed twice with 1 x PBS and 3.7% of paraformaldehyde was added and incubated for 15 min. After

that the cells were again washed twice with PBS and treated with 0.2% triton–X 100 and 2% BSA in PBS for 30 seconds. Again the cells were washed twice with PBS and DAPI was added and kept for 30 min in dark. Finally the cells were washed twice with PBS and imaged under fluorescence microscope (FLoiD, Life technologies).

5.3. RESULTS AND DISCUSSION

5.3.1. Synthesis. Scheme 5.1 illustrates the synthesis of dioxidovanadium(V) complex, $[V^{V}O_2(L')]$ (**2**) of ligand HL {(4–(*p*–fluorophenyl)thiosemicarbazone) of pyridine–2–aldehyde}. The whole reaction takes place in two steps, first of which is the formation of monooxidovanadium(IV) complex, $[V^{IV}O(L)(acac)]$ (**1**) which slowly oxidizes to the dioxidovanadium(V) complex $[V^{V}O_2(L')]$ (**2**) (containing rearranged ligand HL´) in presence of DMSO. The same process when repeated in different other solvents like DMF, CH_3CN and EtOH doesn't leads to the rearrangement of the ligand and corresponding dioxidovanadium(V) complex $[V^{V}O_2(L)]$ (**2a**) is formed. The spectroscopic data were consistent with the X–ray structures of **1** & **2**. The purity of these compounds was further confirmed by elemental analyses. All the complexes were soluble in MeOH, CH_3CN, DMF and DMSO.

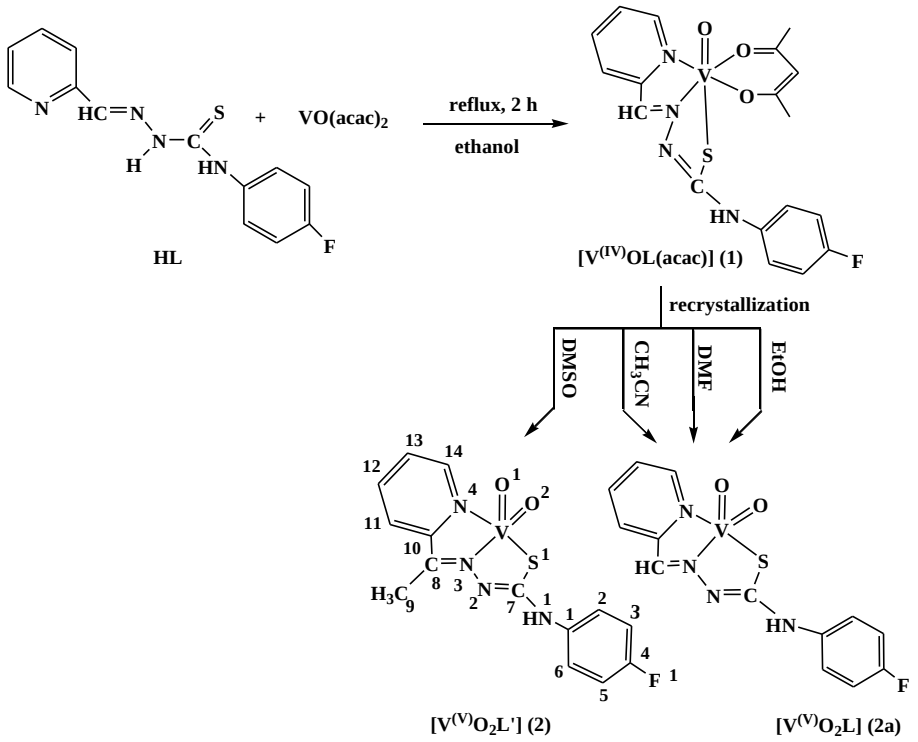

Scheme 5.1. Schematic representation of ligand (HL) and synthesis of variable valence vanadium complexes $[V^{IV}O(L)(acac)]$ (**1**), $[V^{V}O_2(L')]$ (**2**) and $[V^{V}O_2(L)]$ (**2a**).

5.3.2. Spectral characteristics

5.3.2.1. IR spectroscopy. The IR spectrum of the ligand exhibits bands due to ν(N(1)–H) and ν(N(2)–H) moieties in 3311–2967 cm^{-1} region, however the complexes **1**, **2** & **2a** do not exhibit, ν(N(2)–H) band. Thus it reveals that the ligand coordinates to the metal centre in the anionic form. The sharp band at 836 cm^{-1} due to ν(C(7)–S(1)) stretching in the ligand is lowered to 775–762 cm^{-1} in the complexes, indicating participation of the thione sulfur in the coordination.[45] The presence of a strong sharp band at 949 cm^{-1} in complex **1** shows the presence of monooxido (V=O), whereas two peaks in the range 937–922 cm^{-1} in complexes **2** & **2a** are assigned to dioxido (V=O) stretching.[46] **Figure 5.1** shows the IR spectra of complexes **1** and **2**. The IR data are summarized in **Table 5.2**.

Table 5.2. IR and electronic spectra for complexes 1, 2 & 2a

Complex	V−O str,[a] cm^{-1}	UV−vis[b] λ_{max}, nm (ϵ, $M^{-1}cm^{-1}$)
$[V^{IV}O(L)(acac)]$ (**1**)	949	252 (19216), 410 (10521), 586 (7893), 762 (6567)
$[V^{V}O_2(L')]$ (**2**)	937, 925	256 (18968), 431 (8500)
$[V^{V}O_2(L)]$ (**2a**)	934, 922	260 (17564), 428 (8134)

[a]In KBr pellet. [b]In CH_3OH.

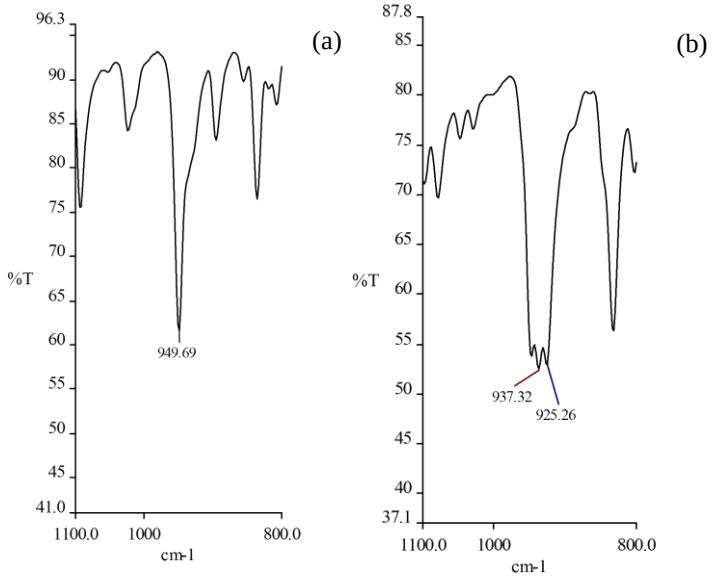

Figure 5.1. FTIR spectra of complexes $[V^{IV}O(L)(acac)]$ (**1**) (a) and $[V^{V}O_2(L')]$ (**2**) (b) showing (V=O) stretching.

5.3.2.2. UV−Vis spectroscopy. The electronic spectra of the complexes (**1**, **2** & **2a**) were recorded using CH_3OH solution. In all the complexes two strong absorptions are observed in the wavelength range 431–252 nm. The lower energy absorptions at 431–410 nm are ascribable to the ligand to metal charge transfer transitions[46a] whereas the higher energy absorptions are likely to be due to ligand centered transitions.[46b] Two weak absorptions at 762 nm and 586 nm were observed for **1** (V^{IV} complex), which are assigned to d−d transitions.[47,48] The UV−Vis data are summarized in **Table 5.2**. Electronic absorption spectra of complexes **1** & **2** are shown in **Figure 5.2**.

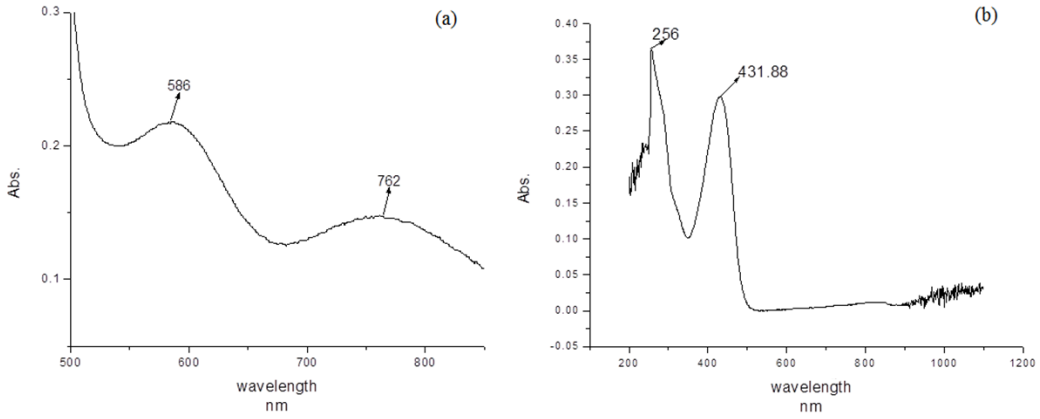

Figure 5.2. Electronic absorption spectra of complexes $[V^{IV}O(L)(acac)]$ (**1**) (a) and $[V^{V}O_2(L')]$ (**2**) (b).

5.3.2.3. NMR spectroscopy. The ^1H NMR spectra of the free ligand (**Figure 5.3**) and its corresponding dioxidovanadium(V) complexes $[V^{V}O_2(L')]$ (**2**) (**Figure 5.4**) and $[V^{V}O_2(L)]$ (**2a**) (**Figure 5.5**) were recorded in DMSO-d_6. The spectrum of the free ligand exhibits two singlets in the range 12.08 to 10.29 ppm due to two NH groups {N(1)H & N(2)H}, whereas in the spectra of the complexes **2** and **2a** there is only one peak in the range 10.29 to 10.20 ppm for one NH group{N(1)H} indicating coordination of the ligand to the metal center in anionic form. The peak due to C(8)H appears as singlet at 8.59 ppm for ligand and at 8.79 ppm for **2a**. The presence of a methyl peak at 2.66 ppm in the spectra of the complex $[V^{V}O_2(L')]$ (**2**) and absence of C(8)H peak indicates the methylation at imine carbon C(8) and formation of a new ligand. The detailed NMR data has been included in the experimental section.

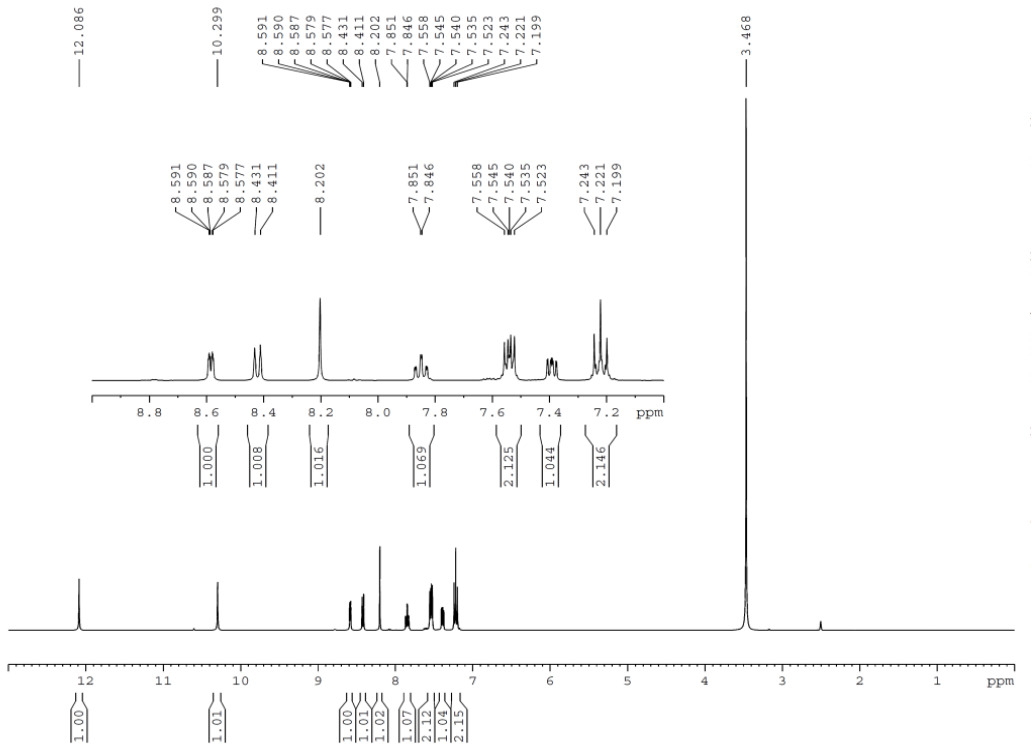

Figure 5.3. NMR spectra of ligand HL.

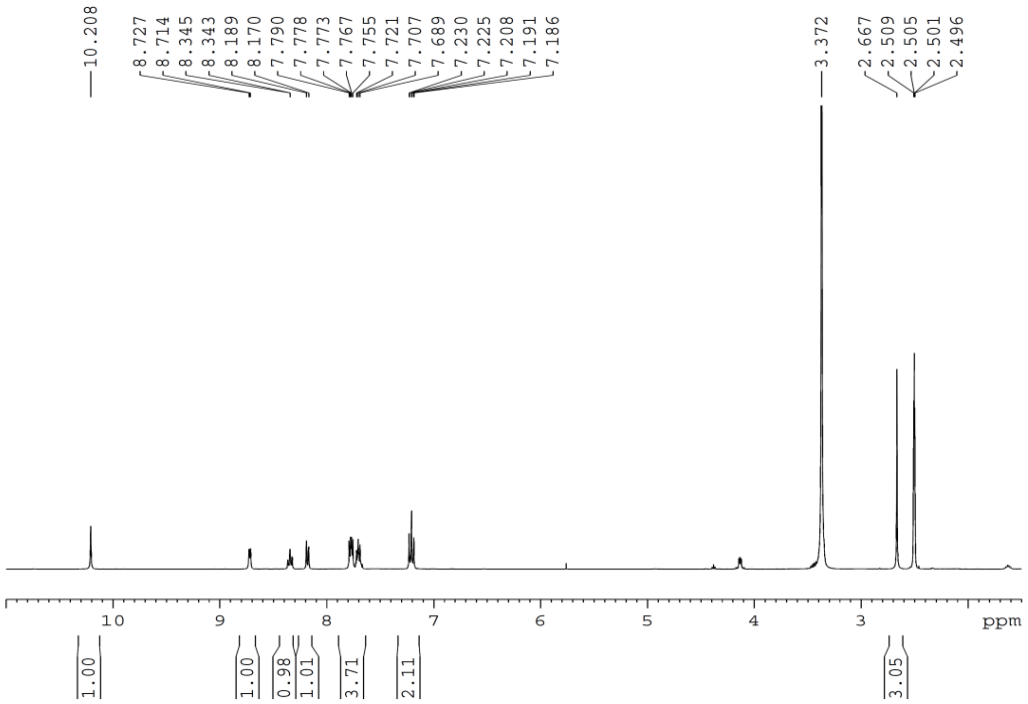

Figure 5.4. NMR spectra of complex [$V^{V}O_2$(L´)] (**2**).

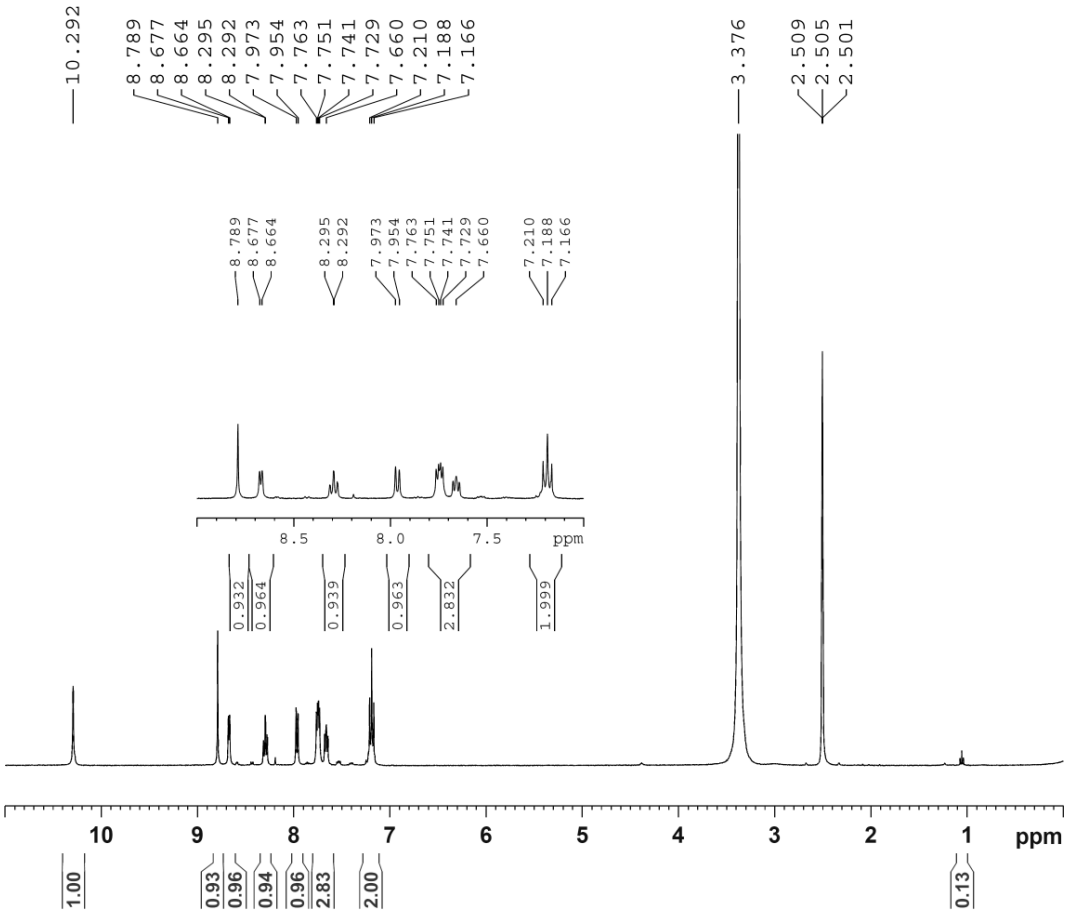

Figure 5.5. NMR spectra of complex $[V^{V}O_2(L)]$ (**2a**).

5.3.3. Electrochemical properties. The electrochemical properties of complexes **1** & **2** were examined in CH_3CN solution (0.1 M TEAP) by cyclic voltammetry using a platinum working electrode, platinum auxiliary electrode, and Ag/AgCl reference electrode. The potential data are listed in **Table 5.3**. The voltammogram pattern for complex **1** includes both oxidation and reduction processes (**Figure 5.6(a)**). Redox couple at $E_{1/2}$ value 0.62 V corresponds to V^{IV}/V^{V} oxidation, whereas $E_{1/2}$ value at –1.13 V corresponds to V^{IV}/V^{III} reduction couple. The voltammogram pattern for complex **2** includes only a quasi-reversible redox couple at $E_{1/2}$ value –0.73 V corresponding to V^{V}/V^{IV} reduction (**Figure 5.6(b)**). The redox property of complex **2a** was also examined, and the result matched well with that of complex **2**.

Table 5.3. Cyclic voltammetric[a] results for complexes $[V^{IV}O(L)(acac)]$ (1) (a) and $[V^{V}O_2(L')]$ (2) at 298 K

Complex	Potentials (V) versus Ag/AgCl		
	V^{IV}/V^{V}	V^{IV}/V^{III}	V^{V}/V^{IV}
	$E^{a}_{1/2}(\Delta E^{a}_{P})$	$E^{c}_{1/2}(\Delta E^{c}_{P})$	$E^{c}_{1/2}(\Delta E^{c}_{P})$
$[V^{IV}O(L)(acac)]$ (**1**)	0.62(450)	–1.13(200)	–
$[V^{V}O_2(L')]$ (**2**)	–	–	–0.73(120)

[a]In CH_3CN at a scan rate 100 mV/s. $E_{1/2} = (E_{pa} + E_{pc})/2$, where E_{pa} and E_{pc} are anodic and cathodic peak potentials vs. Ag/AgCl, respectively. $\Delta E_P = E_{pa} - E_{pc}$.

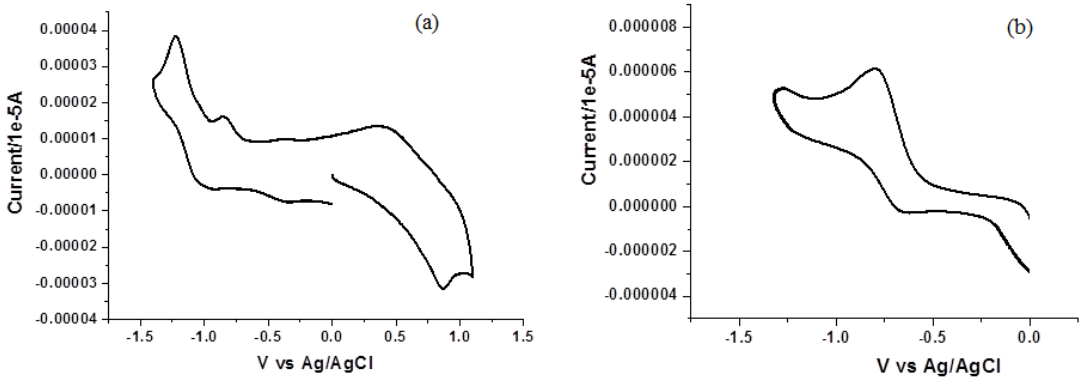

Figure 5.6. Cyclic voltammogram of the complexes $[V^{IV}O(L)(acac)]$ (**1**) (a) and $[V^{V}O_2(L')]$ (**2**) (b).

5.3.4. EPR spectroscopy. X–band EPR spectra of [$V^{IV}O(L)(acac)$] **1**, was recorded in CH_2Cl_2 solution in room temp. The spectrum of the complex [$V^{IV}O(L)(acac)$] is shown in **Figure 5.7**, which reveals well–resolved 8-line isotropic signals, characteristic of a mononuclear vanadium complex with nuclear spin (^{51}V, I = 7/2). The data are listed in **Table 5.4**.

Table 5.4. X-band EPR data for complex 1 at 300 K

Complex	g	A x 10^{-4} cm^{-1}
[$V^{IV}O(L)(acac)$] (**1**)	1.973	83.2

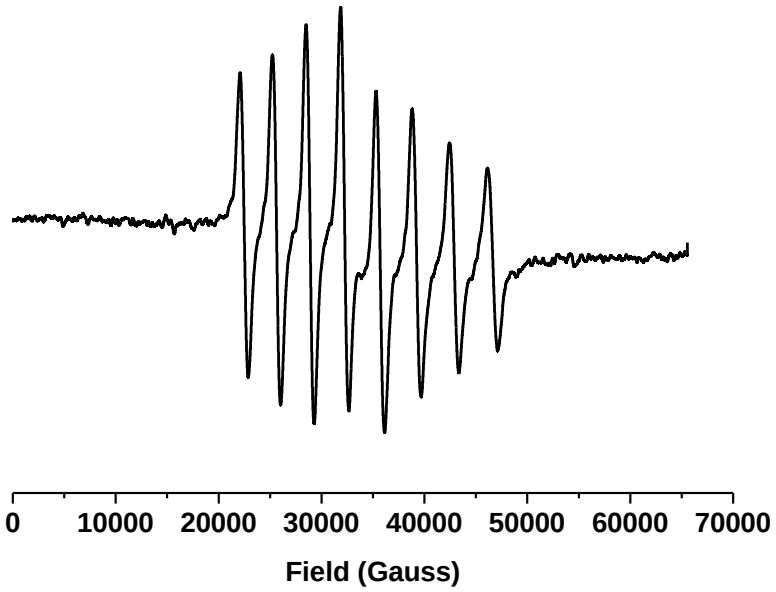

Figure 5.7. Room temperature solution X–band EPR spectrum in CH_2Cl_2 of complex [$V^{IV}O(L)(acac)$] (**1**). Instrument settings: power, -0.009 dB; modulation, 100 kHz; sweep center, 2500G; sweep time, 120s; sweep width, 2500G.

5.3.5. Structure. The structure of complexes [$V^{IV}O(L)(acac)$] (**1**) and [$V^{V}O_2(L')$] (**2**) were elucidated by X-ray crystallography.

5.3.5.1. Description of X-ray structures of [$V^{IV}O(L)(acac)$] (1). The atom numbering scheme for the complex **1** is given in **Figure 5.8**. The structure shows that the thiosemicarbazone ligand (L^{-1}) is coordinated to vanadium in the expected tridentate fashion (**Scheme 5.1**), forming two five-membered chelate rings with S(1)–V(1)–N(3) and N(3)–V(1)–N(4) bite angles. The coligand acetyl acetone group is coordinated in bidentate fashion forming a six membered ring. Thus the complex forms a monooxido distorted V(IV) octahedral structure with pyridyl nitrogen N(4), the imino nitrogen N(3), and the thiolate sulfur S(1) atom, together with acac oxygen O(2), constitute the basal plane and oxido oxygen O(1) and acac oxygen O(3) in the axial position. This is preliminary X–ray report of complex **1**, so we could not include the bond parameters.

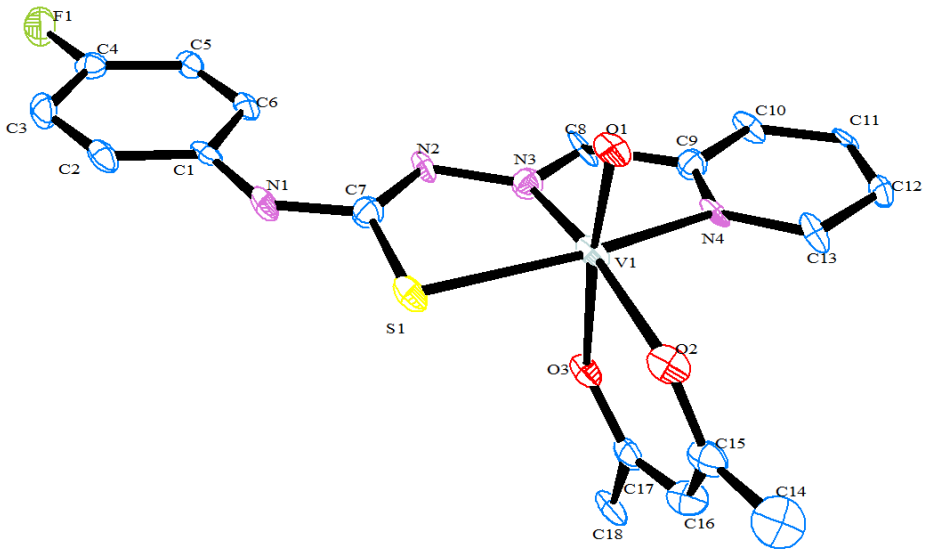

Figure 5.8. A view of the molecular structure of [$V^{IV}O(L)(acac)$] (**1**).

5.3.5.2. Description of X-ray structures of [$V^{V}O_2$(L´)] (2). A view of the molecular structure of **2** is shown in **Figure 5.9** and selected geometric parameters are collected in **Table 5.5**. The [$V^{V}O_2$(L´)] atom is bonded to the S, N, N-donors of the uninegative tridentate ligand and two oxido atoms. The length of the C–S bond (1.730(3) Å) suggests that the ligand is coordinating as a thiolate, a conclusion supported by the short C(7)–N(2) (1.305(4) Å) and C(8)–N(3) (1.306(4)) bonds. The $VSCN_2$ and VNC_2N five-membered chelate rings are each planar, having r.m.s. deviations of 0.0175 and 0.0149 Å, respectively, and form a dihedral angle of 2.6(1)°. The pyridyl ring forms dihedral angles of 4.26(17)° and 4.0(5)° with the adjacent chelate ring and terminal fluorobenzene ring, respectively, indicating that the entire molecule is approximately planar. The N_2O_2S donor set defines a highly distorted coordination geometry as seen in the value of the trigonality index, $\tau = 0.43$, which is intermediate between square pyramidal ($\tau = 0.0$) and trigonal bipyamdial ($\tau = 1.0$).[49] To a first approximation, the observed molecular structure of [$V^{V}O_2$(L´)] matches that reported for the *N*-bound methyl derivative which differs in geometric parameters. In the latter the V–S (2.3759(9) Å), V–O (1.631(2) Å) and N(3)–C(8) (1.323(4) Å) bond lengths are marginally longer than in [$V^{V}O_2$(L´)].[50] Also, the coordination geometry is closer to square pyramidal ($\tau = 0.22$).

In the crystal packing, supramolecular chains aligned along the *a*-axis and with a zig-zag topology are formed through N–H…O hydrogen bonding (**Figure 5.9(a)**; details of the intermolecular interactions are given in the caption). Chains are consolidated into the three-dimensional architecture by a combination of C–H…O (involving the other oxido–O atom) and C–H…π interactions as well as π…..π stacking between pyridyl and benzene rings. Of particular interest is the presence of the C–H….π interactions as the π-system is defined by the $VSCN_2$ chelate ring. Such C–H… π (chelate) synthons are gaining increasing recognition in the crystallographic literature, including for rings that contain sulfur.[51] Globally, the structure can be described in terms of columns of molecules parallel to the *c*-axis connected by N–H…O and C–H…O interactions; a view of the unit cell contents is shown in **Figure 5.10(b)**.

Table 5.5. Selected geometric parameters (Å, °) for [$V^{V}O_2$(L´)] (2)

Atoms	Parameter	Atoms	Parameter
V–S(1)	2.365(1)	V–O(1)	1.607(2)
V–O(2)	1.596(3)	V–N(3)	2.143(3)
V–N(4)	2.086(3)	C(7)–S(1)	1.730(3)
C(7)–N(2)	1.305(4)	N(2)–N(3)	1.374(4)
C(8)–N(3)	1.306(4)		
S(1)–V–O(1)	101.93(1)	S(1)–V–O(2)	98.93(1)
S(1)–V–N(4)	77.58(7)	S(1)–V–N(4)	151.34(1)
O(1)–V–O(2)	110.14(2)		

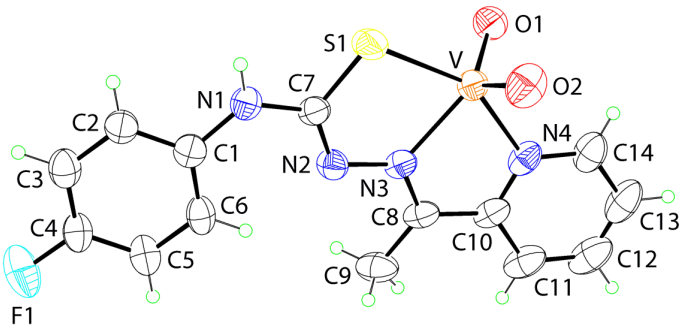

Figure 5.9. A view of the molecular structure of [$V^{V}O_2$(L´)] (**2**); one of the disorder components has been omitted for reasons of clarity.

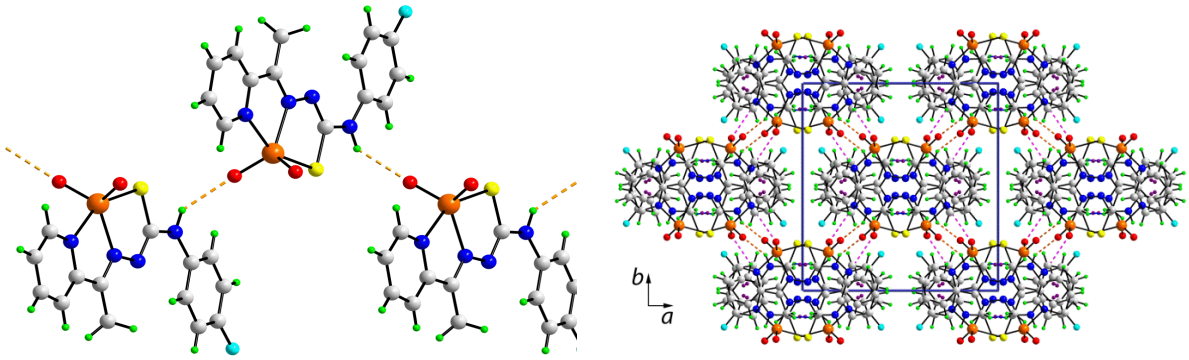

(a) (b)

Figure 5.10. (a) A view of the supramolecular zig–zag chain mediated by N–H…O hydrogen bonding and orientated along [1 0 1]. (b) A view in projection down the *c*-axis of the unit cell contents for **2**. The N–H...O [N1–H1...O1^{i} = 2.22(4) Å, N1...O1^{i} = 2.959(4) Å, angle at H1 = 142(3)° for symmetry operation *i*: -½+*x*, ½-*y*, -½+*z*], C–H...O [C11–H11a...O2^{ii} = 2.47 Å, C11...O2^{ii} = 3.173(5) Å, angle at H11a = 133° for *ii*: 1½-*x*, ½+*y*, 1½-*z*], C–H...π[C9–H9b... π(VSCN$_2$)^{iii} = 2.77 Å, C9... π(VSCN$_2$)^{iii} = 3.647(5) Å, angle at H9b = 152° for *iii*: 1–*x*, 1–*y*, 1–*z*] and π....π [Cg(C1-C6)...Cg(N4,C10-C14)^{iii} = 3.514(7) Å] interactions are shown as orange, pink, blue, and purple dashed lines, respectively.

5.3.6. *In Vitro* insulin mimetic activity. Vanadium compounds are known to have insulin mimetic effect.[52] In this study [$V^{IV}O(L)(acac)$] (**1**) and [$V^{V}O_2(L')$] (**2**) were tested for their insulin mimetic potential in an *in vitro* glucose uptake assay. In L6 myotubes, a cell line of skeletal muscle origin, glucose uptake in response to insulin stimulation plays a key role in the whole body glucose homeostasis. Glucose transporter (GLUT) 4 is the major glucose transporter of muscle exquisitely regulated by insulin through posttranslational events.[53] The L6 myotubes differentiated from L6 myoblast have the ability to respond to insulin via insulin receptor signaling and translocation of Glut 4 to the plasma membrane. The hyperglycemic condition was created in cell culture by incubating the cells in 25 mM glucose. In the present experiment, at 100 µM concentration **1** showed glucose uptake stimulating activity in the myotubes which was found to be comparable to that of 2 µM of insulin. Therefore, it can be concluded that complex **1** mimic's insulin action possibly via insulin receptor signaling with translocation of Glut 4 to the plasma membrane (**Figure 5.11**). Complex **2** at 100 µM concentration also showed considerable insulin mimetic activity compared to insulin, whereas $VO(acac)_2$ showed negligible insulin mimetic activity at the concentrations tested. In case of **1**, the enhancement of the insulin mimetic activity, with respect to **2**, might be related to the difference in the oxidation state of the complexes as vanadium(IV) complexes have been already established as anti diabetic drugs.[18,19]

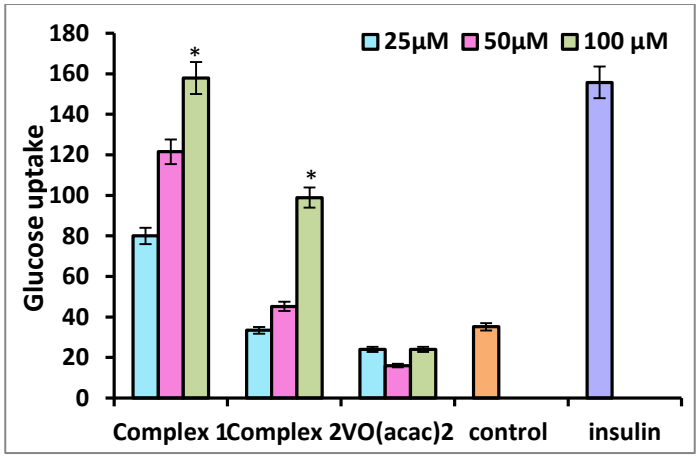

Figure 5.11. Effect of complexes (**1** & **2**) on glucose uptake in cultured L6 myotubes under high glucose conditions (25 mM Glucose). Three concentrations 25 µM, 50 µM and 100 µM were tested for each complex. The data is indicated as mean ± SEM (n=3). Student's t–Test was used where bars with asterisk show a significant difference (*P< .05) with respect to the untreated control.

5.3.7. Inhibition of cancer cell viability. In the present study antiproliferative efficacy of complexes **1** and **2** was assayed by determining the viability of MCF–7 and Vero cells using the MTT assay. The ligand, HL and $VO(acac)_2$ gave high IC_{50} values of >200 μM, whereas $[V^{IV}O(L)(acac)]$ (**1**) & $[V^{V}O_2(L')]$ (**2**) gave values in the range 23.15–115.62 μM for MCF–7 cells and 3.10–120.55 μM for Vero cells over a period of 72 h. Under similar conditions the IC_{50} values of standard drugs vincristine and cisplatin on MCF–7 cells were 1 μM and 10 μM respectively. The significant decrease in the inhibitory concentration for the ligand compared to the metal complex clearly indicates that incorporation of vanadium in the ligand environment has a marked effect on cytotoxicity. A possible explanation is that by coordination the polarity of the ligand and the central metal ion are reduced through the charge equilibration, which favors permeation of the complexes through the lipid layer of the cell membrane.[54,55] The present results are consistent with the observation that metal complexes can exhibit greater biological activities than the free ligand.[56]

Comparing the activity of the two complexes, the cytotoxic activity of $[V^{IV}O(L)(acac)]$ (**1**) is greater than $[V^{V}O_2(L')]$ (**2**) which is reflected from their IC_{50} values with dose dependency illustrated in **Figure 5.12** and **Table 5.6**, which can be correlated with the difference in the oxidation states of the complexes as oxidovanadium(IV) complexes are known to have enhance bioactivity that oxidovanadium(V) complexes.

Table 5.6. IC_{50} (μM) in both MCF–7 and Vero cell lines for complexes 1 and 2

Cytotoxicity on MCF–7 cells IC_{50} values (μM)					
$[V^{IV}O(L)(acac)]$ (**1**)			$[V^{V}O_2(L')]$ (**2**)		
24h	48h	72h	24h	48h	72h
28.49	26.34	23.15	115.62	90.61	84.04
Cytotoxicity on Vero cells IC_{50} values (μM)					
$[V^{IV}O(L)(acac)]$ (**1**)			$[V^{V}O_2(L')]$ (**2**)		
24h	48h	72h	24h	48h	72h
41.57	3.10	3.20	120.55	30.06	29.42

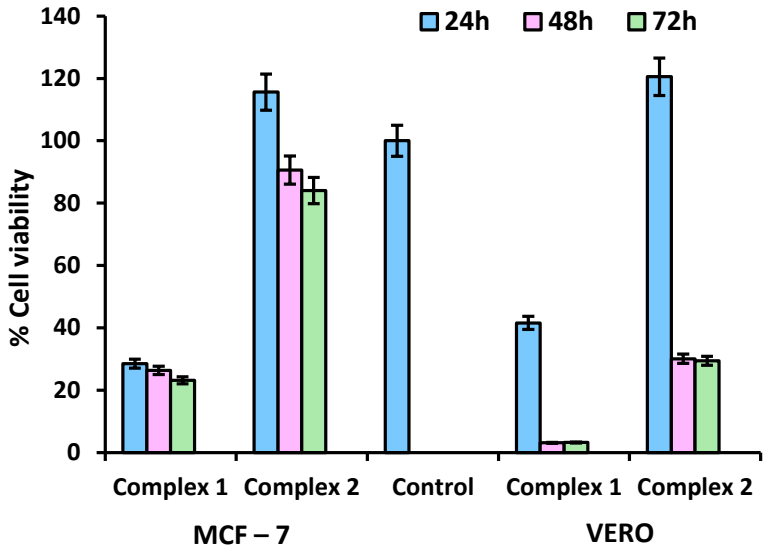

Figure 5.12. Effect of [$V^{IV}O(L)(acac)$] (**1**) and [$V^{V}O_2(L')$] (**2**) on cell viability and growth: MCF–7 and Vero cells were treated with different concentrations of the test compound for 24 h, 48 h & 72 h and then cell viability was measured by MTT assay. Data reported as the mean ± S.D. for *n* = 3 and compared against control (considered as 100% viability).

5.3.8. Nuclear staining assay. The mechanism of cell death due to the complexes (**1** & **2**) was checked by staining dying cells with DAPI. The density of the DAPI stained nuclei was used to check the live cells in different treatment groups. **Figure 5.13** shows images taken after DAPI staining in blue fluorescence at different concentrations of the complexes. It can be seen from the figure that the number of DAPI stained nuclei were reduced in treated wells with increasing concentrations of the complexes indicating the dose dependent cell death. **Figure 5.14** shows the grey scale images at different time points after the treatment with minimum toxic concentrations of the complexes. The distinct nuclear condensation, fragmentation was seen in treated cells compared to control cells.

(a) $[V^{IV}O(L)(acac)]$ (**1**)

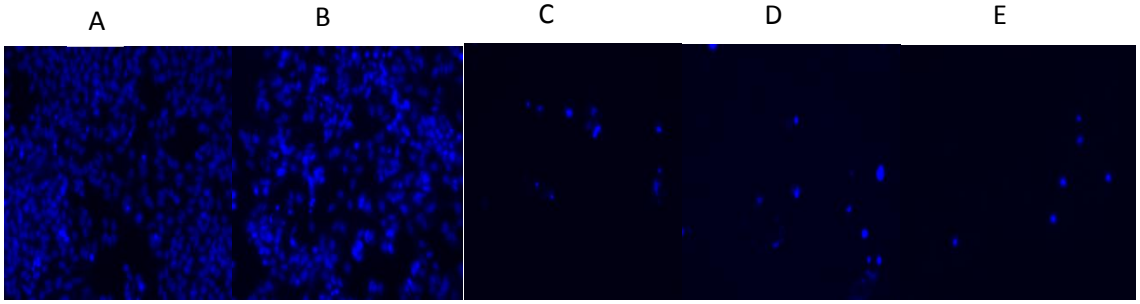

(b) $[V^{V}O_2(L')]$ (**2**)

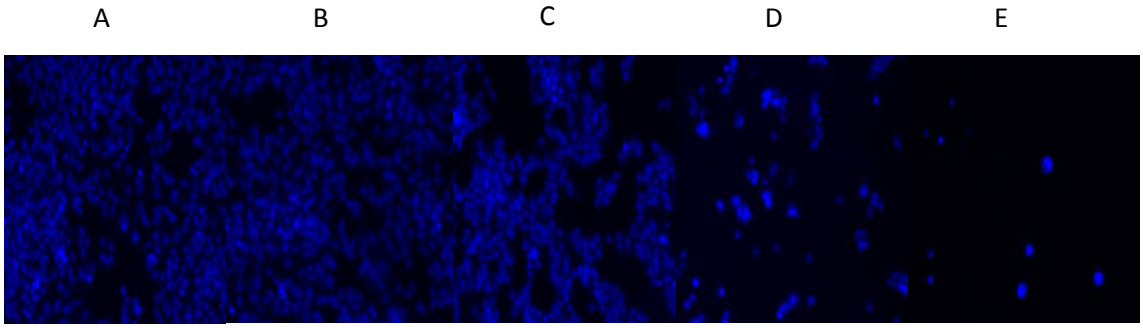

Figure 5.13 (a & b). Study of apoptosis by morphological changes in nuclei of MCF–7 cells: After treatment MCF–7 cells from control and treated group were fixed with 3.7% paraformaldehyde for 15 min, permeabilized with 0.1% Triton X–100 and 2% BSA and stained with 2 µg/ml DAPI for 30 min in the dark. The cells were then washed with PBS and examined by fluorescence microscopy (FloiD, Invitrogen). A–E (A–control, B–5 µM, C–50 µM, D–100 µM, E–200 µM) shows the decrease in cell density with increasing concentration of the drug compared to control.

(a) [$V^{IV}O(L)(acac)$] (**1**)

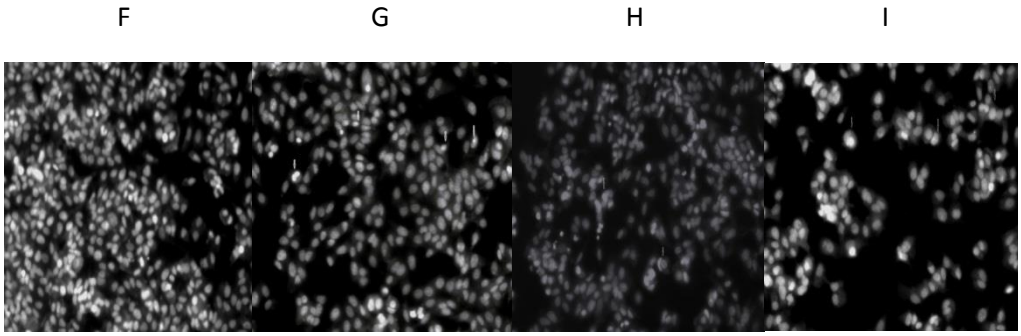

(b) [$V^{V}O_2(L')$] (**2**)

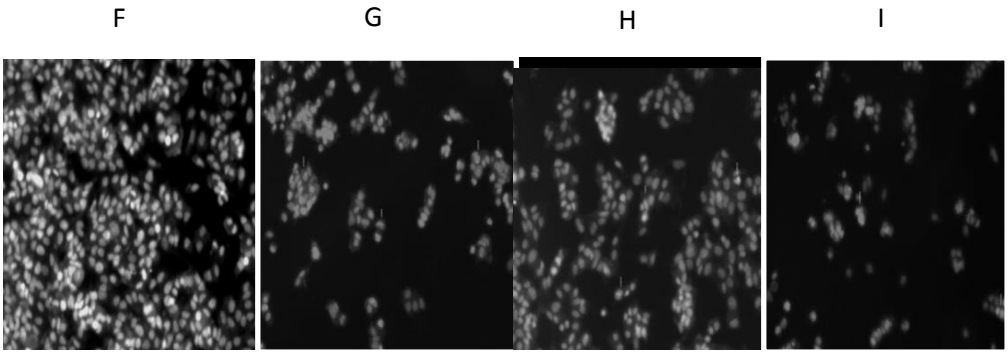

Figure 5.14 (a & b). F–I (F–control, G–24 h, H–48 h, I–72 h) shows the morphological changes in nuclei of MCF–7 with respect to treatment time on applying complexes (**1** and **2**) in comparison to control.

5.4. CONCLUSION

The syntheses and characterization of oxidovanadium(IV) complex [$V^{IV}O$(L)(acac)] (**1**) and two dioxidovanadium(V) complexes [$V^{V}O_2$(L')] (**2**) and [$V^{V}O_2$(L)] (**2a**) of {(4–(*p*–fluorophenyl)thiosemicarbazone) of pyridine–2–aldehyde} (HL) is reported. The oxidovanadium(IV) complex [$V^{IV}O$(L)(acac)] (**1**) is found to undergo methylation at the carbon centre attached to imine nitrogen of the ligand in presence of DMSO forming the dioxidovanadium(V) species[$V^{V}O_2$(L')] (**2**). The synthesized ligand and the metal complexes were characterized by elemental analysis, IR, UV–Vis, NMR and EPR spectroscopy. Molecular structures of complexes **1** & **2** have been determined by X–ray crystallography.

Complexes **1** & **2** show *in vitro* insulin mimetic activity against insulin responsive L6 myoblast cells, with complex **1** being the most potent, is comparable to insulin at 100 μM concentration, while **2** has considerable insulin mimetic activity. In addition, the *in vitro* antiproliferative activity of complexes **1** & **2** against the MCF–7 and Vero cell lines were also assayed.

5.5. REFERENCES

(1) *Vanadium Compounds, Chemistry, Biochemistry and Therapeutic Applications* (Eds.: A. Tracey, S.; Crans, D. C.), ACS Symp. Ser. 711, **1998**.

(2) *J. Inorg. Biochem.* **2000**, *80* (Special Issue on Biological Aspects of Vanadium; Guest Eds.: Rehder, D.; Conte, V.).

(3) *Vanadium and Its Role in Life* (vol. *31* of *Metal Ions in Biological Systems*; Eds: Sigel, H.; Sigel, A.), Marcel Dekker, New York, **1995**.

(4) Rehder, D. *Coord. Chem. Rev.* **1999**, *182*, 297.

(5) *Vanadium in the Environment* (Ed.: Nriagu, J. O.), Wiley, New York, **1998**.

(6) Hirao, T. *Chem. Rev.* **1997**, *97*, 2707.

(7) Arends, J. W. C. E.; Pellizon, M.; Sheldon, R. A. *Stud. Surf. Sci. Catal.* **1997**, *110*, 1031.

(8) Thompson, K. H.; McNeill, J. H.; Orvig, C. *Chem. Rev.* **1999**, *99*, 2561.

(9) Shechter, Y.; Li, J.; Meyerovitch, J.; Gefel, D.; Bruck, R.; Elberg, G.; Miller, D. S.; Shisheva, A. *Mol. Cell Biochem.* **1995**, *153*, 39.

(10) Xie, M. J.; Niu, Y. F.; Yang, X. D.; Liu, W. P.; Li, L.; Gao, L. H.; Yan, S. P.; Meng, Z. H. *Eur. J. Med. Chem.* **2010**, *45*, 6077.

(11) Mendes, I. C.; Botion, L. M.; Ferreira, A. V. M. *Inorg. Chim. Acta* **2009**, *362*, 414.

(12) Benítez, J.; Guggeri, L.; Tomaz, I.; Pesso, J. C.; Moreno, V.; Lorenzo, J.; Avilés, F. X.; Garat, B.; Gambino, D. *J. Inorg. Biochem.* **2009**, *103*, 1386.

(13) Lu, J.; Guo, H.; Zeng, X.; Zhang, Y.; Zhao, P.; Jiang, J.; Zang, L. *J. Inorg. Biochem*. **2012**, *112*, 39

(14) Benítez, J.; Becco, L.; Correia, I.; Leal, S. M.; Guiset, H.; Pessoa, J. C.; Tanco, S.; Escobar, P.; Moreno, V.; Garat, B.; Gambino, D. *J. Inorg. Biochem.* **2011**, *105*, 303.

(15) Maia, P. I. da S.; Pavan, F. R.; Leite, C. Q. F.; Lemos, S. S.; Sousa, G. F. de; Batista, A. A.; Nascimento, O. R.; Ellena, J.; Castellano, E. E.; Niquetf, E.; Deflon, V. M. *Polyhedron* **2009**, *28*, 398.

(16) (a) Wei, Y.; Zhang, C.; Zhao, P.; Yang, X.; Wang, K. *J. Inorg. Biochem.* **2011**, *105*, 1081. (b) Rehder, D.; Costa Pessoa, J.; Geraldes, C. F. G. C.; Kabanos, T.; Kiss, T.; Meier, B.; Micera, G.; Pettersson, L.; Rangel, M.; Salifoglou, A.; Turel, I.; Wang, D. *J. Biol. Inorg. Chem.* **2002**, *7*, 384. (c) Sutradhar, M.; Barman, T. R.; Mukherjee, G.; Kar, M.; Saha, S. S.; Drew, M. G. B.; Ghosh, S. *Inorg. Chim. Acta* **2011**, *368*, 13. (d) Saltiel, A. R.; Khan, C. R. *Nature* **2001**, *414*,

799. (e) Noblía, P.; Baran, E. J.; Otero, L.; Gambino, D. *Eur. J. Inorg. Chem*. **2004**, 322. (f) Nilsson, J.; Shteinman, A. A.; Rehder, D.; Nordlander, E. *J. Inorg. Biochem.* ***2011***, *105*, 1795. (g) Willsky, G. R.; Chi, L.-H.; Hu, Z.; Crans, D. C. *Coord. Chem. Rev.* **2011**, *255*, 2258. (h) Rehder, D. *Inorg. Chem. Commun*. **2003**, *6*, 604. (i) Islam, M. N.; Kumbhar, A. A.; Kumbhar, A. S.; Joshi, B. N. *Inorg. Chem.* **2010**, *49*, 8237. (j) Pillai, S. I.; Subramanian, S. P.; Kandaswamy, M. *Eur. J. Med. Chem*. **2013**, *63*, 109.

(17) (a) Shechter, Y.; Karlish, S. J. D. *Nature* **1980**, *284*, 556. (b) Heyliger, C. E.; Tahiliani, A. G.; McNeill, J. H. *Science* **1985**, *227*, 1474.

(18) Ramanadham, S.; Mongold, J. J.; Brownsey, R. W.; Cros, G. H.; McNeill, J. H. *Am. J. Physiol*. **1989**, *257*, 904.

(19) McNeill, J. H.; Yuen, V. G.; Hoveyda, H. R.; Orvig, C. *J. Med. Chem.* **1992**, *35*, 1489.

(20) Schecter, Y.; Meyerovitch, J.; Farfel, Z.; Sack, J.; Bar-Meir, S.; Amir, S.; Degani, H.; Karlish, S. J. D. *Vanadium in Biological Systems; Kluwer Academic Publishers: Norwell, MA*, **1990**; pp 129.

(21) Thompson, K. H.; McNeill, J. H.; Orvig, C. *Topics in Biological Chemistry: Metallopharmaceuticals; Springer-Verlag: Heidelberg*, **1999**; Vol. 2, pp 139.

(22) (a) Sakurai, H.; Fugono, J.; Yasui, H. *Mini-Rev. Med. Chem*. **2004**, *4*, 41. (b) Adachi, Y.; Yoshida, J.; Kodera, Y.; Katoh, A.; Takada, J.; Sakurai, H. *J. Med. Chem.* **2006**, *49*, 3251. (c) Melchior, M.; Thompson, K. H.; Jong, J. M.; Rettig, S. J.; Shuter, E.; Yuen, V. G.; Zhou, Y.; McNeill, J. H.; Orvig, C. *Inorg. Chem.* **1999**, *38*, 2288. (d) Yamaguchi, M.; Wakasugi, K.; Saito, R.; Adachi, Y.; Yoshikawa, Y.; Sakurai, H.; Katoh, A. *J. Inorg. Biochem*. **2006**, *100*, 260. (e) Crans, D. C.; Mahroof-Tahir, M.; Johnson, M. D.; Wilkins, P. C.; Yang, L.; Robbins, K.; Johnson, A.; Alfano, J. A.; Godzala, M. E.; Austin, L. T.; Willsky, G. R. *Inorg. Chim. Acta* **2003**, *356*, 365. (f) Karmaker, S.; Saha, T. K.; Yoshikawa, Y.; Yasui, H.; Sakurai, H. *J. Inorg. Biochem*. **2006**, *100*, 1535.

(23) Campbell, M. J. M. *Coord. Chem. Rev*. **1975**, *15*, 279.

(24) Padhye, S. B.; Kauffman, G. B. *Coord. Chem. Rev.* **1985**, *63*, 127.

(25) West, D. X.; Liberta, A. E.; Padhye, S. B.; Chikate, R. C.; Sonawane, P. B.; Kumbhar, A. S.; Yerande, R. G. *Coord. Chem. Rev.* **1993**, *123*, 49.

(26) Klayman, D. L.; Scovill, J. P.; Bartosevich, J. F.; Bruce, J. *J. Med. Chem.* **1983**, *26*, 39.

(27) Casas, J. S.; García-Tasende, M. S.; Sordo, J. *Coord. Chem. Rev*. **2000**, *209*, 197.

(28) Smith, D. R. *Coord. Chem. Rev*. **1997**, *164*, 575.

(29) Ainscough, E. W.; Brodie, A. M.; Ransford, J. D.; Waters, J. M. *J. Chem. Soc., Dalton Trans.* **1997**, 1251.

(30) Ali, M. A.; Mirza, A. H.; Hossain, A. M. S.; Nazimuddin, M. *Polyhedron* **2001**, *20*, 1045.

(31) Baldini, M.; Ferrari, M. B.; Bisceglie, F.; Pelosi, G.; Pinelli, S.; Tarasconi, P. *Inorg. Chem*. **2003**, *42*, 2049.

(32) Ferrari, M. B.; Bisceglie, F.; Pelosi, G.; Tarasconi, P.; Albertini, R.; Fava, G. G.; Pinelli, S. *J. Inorg. Biochem.* **2002**, *89*, 36.

(33) Ferrari, M. B.; Bisceglie, F.; Pelosi, G.; Albertini, P.; Dall'Aglio, P. P.; Bergamo, A.; Sava, G.; Pinelli, S. *J. Inorg. Biochem.* **2004**, *98*, 301.

(34) Saswati; Dinda, R.; Schmiesing, C. S.; Sinn, E.; Patil, Y. P.; Nethaji, M.; Evans, H. S.; Acharyya, R. *Polyhedron* **2013**, *50*, 354.

(35) Russel, G. A.; Weiner, S. A. *J. Org. Chem.* **1966**, 31, 248 and references herein.

(36) Rowe, R. A.; Jones, M. M. *Inorg. Synth.* **1957**, *5*, 113.

(37) Part 1: Ghosh, S.; Purohit, S. *Indian J. Chem., Sect. A: Inorg., Bio-inorg., Phys., Theor., Anal. Chem*. **1987**, *26A*, 131.

(38) Purohit, S.; Koley, A. P.; Prasad, L. S.; Manoharan, P. T.; Ghosh, S. *Inorg. Chem.* **1989**, *28*, 3735.

(39) *CrysAlis PRO. Agilent Technologies*, Yarnton, Oxfordshire, England, **2011**.

(40) Sheldrick, G. M. *Acta Cryst.* **2008**, *A64*, 112.

(41) Farrugia, L. J. *J. Appl. Cryst.* **2012**, *45*, 849.

(42) Brandenburg, K. DIAMOND. Crystal Impact GbR, Bonn, Germany, **2006**.

(43) Spek, A. L. *J. Appl. Crystallogr.* **2003**, *36*, 7.

(44) Ha, B. G.; Nagaoka, M.; Yonezawa, T.; Tanabe, R.; Woo, J. T.; Kato, H.; Chung, U.; Yakasaki, K. *J. Nutr. Biochem.* **2012**, *23*, 501.

(45) (a) Chattopadhyay, S. K.; Chattopadhyay, D.; Banerjee, T.; Kuroda, R.; Ghosh, S. *Polyhedron* **1997**, *16*, 1925. (b) Pérez-Rebolledo, A.; Mendes, I. C.; Speziali, N. L.; Bertani, P.; Resende, J. M.; Carvalho Alcôntara, A. F. de; Beraldo, H. *Polyhedron* **2007**, *26*, 1449.

(46) (a) Dinda, R.; Sengupta, P.; Ghosh, S.; Mak, T. C. W. *Inorg. Chem.* **2002**, *41*, 1684. (b) Dinda, R.; Sengupta, P.; Sutradhar, M.; Mak, T. C. W.; Ghosh, S. *Inorg. Chem.* **2008**, *47*, 5634.

(47) Lewis, N. A.; Liu, F.; Holder, A. A. *Eur. J. Inorg. Chem.* **2012**, 664.

(48) Ballhausen, C. J.; Gray, H. B. *Inorg. Chem.* **1962**, *1*, 111.

(49) Addison, A. W.; Rao, T. N.; Reedijk, J.; Rijn, J.; Verschoor, G. C. *J. Chem. Soc. Dalton Trans*. **1984**, 1349.

(50) Maia, P. I. da S.; Pavan, F. R.; Leite, C. Q. F.; Lemos, S. S.; de Sousa, G. F.; Batista, A. A.; Nascimento, O. R.; Ellena, J.; Castellano, E. E.; Niquet, E. *Polyhedron* **2009**, *28*, 398.

(51) (a) Milčič, M. K.; Medaković, V. B.; Sredojević, D. N.; Juranić, N. O.; Zarić, S. D. *Inorg. Chem*. **2006**, *45*, 4755. (b) Tiekink, E. R. T.; Zukerman-Schpector, J. *Chem. Commun.* **2011**, *47*, 6623. (c) Tiekink, E. R. T. in *Crystal engineering. in Supramolecular Chemistry: from Molecules to Nanomaterials*, Steed, J. W.; Gale, P. A. (eds). John Wiley & Sons Ltd, Chichester, UK, **2012**, pp. 2791.

(52) Islam, M. N.; Kumbhar, A. A.; Kumbhar, A. S.; Zeller M.; Butcher, R. J.; Dusane, M. B.; Joshi, B. N. *Inorg Chem.* **2010**, *49*, 8237.

(53) Ishiki, M.; Klip, A. *Endocrinology* **2005**, *146*, 5071.

(54) Ramadan, A. M. *J. Inorg. Biochem.* **1997**, *65*, 183.

(55) Avaji, P. G.; Kumar, C. H. V.; Patil, S. A.; Shivananda, K. N.; Nagaraju, C. *Eur. J. Med. Chem.* **2009**, *44*, 3552.

(56) Rosu, T.; Pahontu, E.; Pasculescu, S.; Georgescu, R.; Stanica, N.; Curaj, A.; Popescu, A.; Leabu, M. *Eur. J. Med. Chem*. **2010**, *45*, 1627.

Chapter 6

Zinc(II) complexes as functional models of phosphatases: Synthesis, structure and characterization

Chapter 6

Zinc(II) complexes as functional models of phosphatases: Synthesis, structure and characterization

ABSTRACT

4–(*p*–methoxyphenyl)thiosemicarbazone of *o*–hydroxynapthaldehyde (H_2L^1), 4–(*p*–methoxyphenyl)thiosemicarbazone of benzoyl pyridine (HL^2) and 4–(*p*–chlorophenyl)thiosemicarbazone of *o*–vanillin (H_2L^3) and their dimeric Zn(II) complexes $[\{ZnL^1(DMSO)\}_2]\cdot 3DMSO$ (**1**), $[\{ZnL^2Cl\}_2]$ (**2**), and a novel tetrameric Zn(II) complex $[(Zn_2L^3)_2(\mu\text{–}OAc)_2(\mu_3\text{–}O)_2]$ (**3**) are reported. The synthesized ligands and their zinc complexes were characterized by elemental analysis, NMR, IR and UV–Vis spectroscopy. Molecular structures of all the complexes (**1**–**3**) have been determined by single crystal X–ray crystallography.

6.1. INTRODUCTION

Metal complexes of d^{10} system constitute an especially attractive topic in view of their differences with regard to their chemical and biological behavior. Zn(II) is an essential metal ion because of its presence in certain metalloenzymes,[1,2] while Cd(II) and Hg(II), present in the environment are toxic.[3]

Zn(II) ions, as a cofactor are part of over 300 enzymes (carbonic anhydrases, zinc proteinases, histone deacetylases, alkaline phosphatases, alcohol dehydrogenases, aminopeptidases, etc.), which are involved in metabolic processes of living organisms: viruses, bacteria, plants and animals.[2,4–10] Zinc is cytoprotective and suppresses apoptotic pathways; it has a specific function as a neuromodulator in addition to its other typical cellular functions.[11–13] Some of the Zn(II) complexes of thiosemicarbazone have been considered as agents with antitumor activity against some of the human cancer cell lines.[14]

Thiosemicarbazones have been extensively studied due to their biological properties, analytical applications and their interesting chemical and structural properties towards metal ions.[15–17] The biological properties of thiosemicarbazone complexes are often related to metal ion. The lipophilicity, which is related to the tendency of a molecule to be transported through biological membranes, can be modified by coordination. The metal in the complex has its own influence in enhancing the overall activity of the complex compared to the free ligand through a synergic effect.[18,19]

Zn(II) ion has either a structural or catalytic role in several proteins.[20] It has been recognized as an important cofactor in biological molecules, either as a structural template in protein folding or as a Lewis acid catalyst that can readily adopt 4–, 5– or 6–coordination.[21] Therefore, it is a challenging area of research to get compounds which are able to form stable complexes with Zn(II), thiosemicarbazone ligands could be well appropriate for this purpose.

Considering these facts and as a continuation of our ongoing research on the study of pharmacological and catalytic properties[22] of transition metal complexes, we report the synthesis and characterization of two new Zn(II) dimeric complexes $[\{ZnL^1(DMSO)\}_2]\cdot 3DMSO$ (**1**) and $[\{ZnL^2Cl\}_2]$ (**2**), and a novel tetranuclear zinc(II) complex $[(Zn_2L^3)_2(\mu\text{–}OAc)_2(\mu_3\text{–}O)_2]$ (**3**). The

physical and structural characteristics of the complexes suggest that they may be considered as functional model of phosphatase enzyme.

6.2. EXPERIMENTAL SECTION

6.2.1. General methods and materials. All chemicals were purchased from commercial sources and used without further purification. Reagent grade solvents were dried and distilled prior to use. The thiosemicabazides were prepared from distilled substituted aniline by a known method reported earlier.[23] Elemental analyses were performed on a Vario ELcube CHNS Elemental analyser. IR spectra were recorded on a Perkin–Elmer Spectrum RXI spectrometer. Electronic spectra were recorded on a Lamda25, PerkinElmer spectrophotometer. ^{1}H and ^{13}C spectra were recorded with a Bruker Ultrashield 400 MHz spectrometer using $SiMe_4$ as an internal standard.

6.2.2. Synthesis of ligands. The ligands 4–(*p*–methoxyphenyl)thiosemicarbazone of *o*–hydroxynapthaldehyde (H_2L^1), 4–(*p*–methoxyphenyl)thiosemicarbazone of benzoyl pyridine (HL^2) and 4–(*p*–chlorophenyl)thiosemicarbazone of *o*–vanillin (H_2L^3) were prepared by reported methods.[22c,24] To the stirring solution of the substituted thiosemicabazide, required aldehyde was added in equimolar ratio in methanol medium and the mixture was stirred for 2 h. The resulting compound was filtered, washed thoroughly with methanol and dried over fused $CaCl_2$.

H_2L^1: Yield: 86%. Anal. calc. for $C_{19}H_{17}N_3SO_2$: C, 64.94; H, 4.88; N, 11.96. Found: C, 64.95; H, 4.86; N, 11.95. Main IR peaks (KBr, cm^{-1}): 3432 s ν(O(1)–H), 3128 s ν(N(1)–H), 2996 s ν(N(2)–H), 2831 m *ν*(C(8)–H), 1621 s ν(C=C), 1539 s ν(C(8)=N(3)), 815 s ν(C(7)=S(1)). ^{1}H NMR (DMSO–d_6, 400 MHz) δ: 11.70 (s, 1H, –C(18)–O(1)H), 10.01 (s, 1H, –C(7)–N(1)H), 9.21 (s, 1H, –C(7)–N(2)H), 8.45 (s, 1H, –N(3)=C(8)H), 7.90–6.93 (m, 10H, C_6H_4), 3.74 (s, 3H, OCH_3). ^{13}C NMR (DMSO–d_6, 100 MHz) δ: 176.63, 157.40, 157.04, 143.92, 133.03, 132.50, 132.16, 129.24, 128.55, 128.28, 127.60, 123.99, 122.83, 119.03, 113.91, 113.71, 112.64, 110.13, 55.70.

HL^2: Yield: 86%. Anal. calc. for $C_{20}H_{18}N_4SO$: C, 66.28; H, 5.01; N, 15.46. Found: C, 66.25; H, 5.02; N, 15.41. Main IR peaks (KBr, cm^{-1}): 3165 s ν(N(1)–H), 2961 s ν(N(2)–H), 2837 m *ν*(C(8)–H), 1637 s ν(C=C), 1510 s ν(C(8)=N(3)), 832 s ν(C(7)=S(1)). ^{1}H NMR (DMSO–d_6, 400 MHz) δ: 9.53 (s, 1H, –C(7)–N(1)H), 9.01 (s, 1H, –C(7)–N(2)H), 7.44–6.85 (m, 13H, C_6H_4), 3.71 (s, 3H, OCH_3). ^{13}C NMR (DMSO–d_6, 100 MHz) δ: 180.65, 180.21, 175.46, 171.45, 156.99,

156.65, 149.04, 141.32, 138.15, 133.51, 132.59, 131.06, 128.71, 127.23, 126.66, 126.22, 124.65, 114.09, 113.68, 55.65.

H_2L^3: Yield: 86%. Anal. calc. for $C_{15}H_{14}N_3SO_2Cl$: C, 53.65; H, 4.20; N, 12.51. Found: C, 53.68; H, 4.18; N, 12.50. Main IR peaks (KBr, cm^{-1}): 3421 s ν(O(1)–H), 2988 s ν(N(1)–H), 2867 s ν(N(2)–H), 2752 m *ν*(C(8)–H), 1614 s ν(C=C), 1531 s ν(C(8)=N(3)), 839 s ν(C(7)=S(1)). ^{1}H NMR (DMSO–d_6, 400 MHz) δ: 11.85 (s, 1H, –C(14)–O(1)H), 10.07 (s, 1H, –C(7)–N(1)H), 9.35 (s, 1H, –C(7)–N(2)H), 8.52 (s, 1H, –N(3)=C(8)H), 7.68–6.77 (m, 7H, C_6H_4), 3.82 (s, 3H, OCH_3). ^{13}C NMR (DMSO–d_6, 100 MHz) δ: 175.73, 147.90, 146.22, 145.56, 140.40, 138.04, 129.27 127.93, 127.74, 127.36, 120.45, 119.04, 118.45, 113.09, 55.87.

6.2.3. Synthesis of Zn(II) complexes. $Zn(OAc)_2·2H_2O$ (**1** & **3**) or $ZnCl_2$ (**2**) (1.0 mmol) was added to 20 ml of hot ethanolic solution of the ligand $H_{1–2}L^{1–3}$ (1.0 mmol), and the contents were refluxed for 2 h. The resulting yellow solution was filtered and slow evaporation of the filtrate over 4–5 days produced light yellow crystalline product. X–ray quality crystals of complex **1** were obtained by slow evaporation from DMSO.

[{ZnL^1(DMSO)}$_2$]·3DMSO (1): Yield: 74%. Anal. calc. for $C_{48}H_{60}N_6O_9S_7Zn_2$: C, 47.25; H, 4.96; N, 6.89. Found: C 47.28; H, 4.92; N, 6.87. Main IR peaks (KBr, cm^{-1}): 3048 m *ν*(N(1)–H), 2863 m *ν*(C(8)–H), 1595 s *ν*(C=C), 1507 s *ν*(–C(8)=N(3)), 743 s ν(C(7)–S). ^{1}H NMR (DMSO–d_6, 400 MHz) δ: 9.32 (s, 1H, –C(7)–N(1)H), 8.63 (s, 1H, –N(3)=C(8)H), 8.06–6.83 (m, 10H, C_6H_4), 3.71 (s, 3H, OCH_3), 2.54 (s, 3H, DMSO). ^{13}C NMR (DMSO–d_6, 100 MHz) δ: 167.02, 162.24, 159.35, 157.53, 153.95, 150.32, 145.43, 135.80, 134.68, 132.34, 130.34, 129.00, 127.19, 126.24, 121.35, 119.95, 115.46, 113.91, 55.55, 49.06.

[{ZnL^2Cl}$_2$] (2): Yield: 77%. Anal. calc. for $C_{40}H_{34}Cl_2N_8O_2S_2Zn_2$: C, 51.96, H, 3.71, N, 12.12. Found: C, 51.94, H, 3.74, N, 12.15. Main IR peaks (KBr, cm^{-1}): 3318 m *ν*(N(1)–H), 1592 s *ν*(C=C), 1503 s *ν*(–C(8)=N(3)), 792 s ν(C(7)–S). ^{1}H NMR (DMSO–d_6, 400 MHz) δ: 9.54 (s, 1H, –C(7)–N(1)H), 8.00–6.54 (m, 13H, C_6H_4), 3.65 (s, 3H, OCH_3). ^{13}C NMR (DMSO–d_6, 100 MHz) δ: 154.72, 154.34, 149.77, 147.58, 147.05, 140.96, 134.94, 133.26, 129.77, 129.56, 129.15, 128.86, 125.63, 125.45, 123.97, 122.30, 121.97, 113.57, 113.45, 55.53.

$[(Zn_2L^3)_2(\mu\text{–}OAc)_2(\mu_3\text{–}O)_2]$ (3): Yield: 63%. Anal. calc. for $C_{34}H_{30}Cl_2N_6O_{10}S_2Zn_4$: C, 37.84, H, 2.80, N, 7.79. Found: C, 37.81, H, 2.84, N, 7.76. Main IR peaks (KBr, cm^{-1}): 3024 m ν(N(1)–H), 2761 m ν(C(8)–H), 1590 s ν(C=C), 1533 s ν(–C(8)=N(3)), 810 s ν(C(7)–S). ^{1}H NMR (DMSO–d_6, 400 MHz) δ: 8.92 (s, 1H, –C(7)–N(1)H), 8.43 (s, 1H, –N(3)=C(8)H), 7.84–6.35 (m, 7H, C_6H_4), 3.69 (s, 3H, OCH_3), 2.06 (s, 6H, OAc). ^{13}C NMR (DMSO–d_6, 100 MHz) δ: 168.86, 165.78, 156.77, 141.13, 140.51, 132.76, 130.12, 128.68, 128.44, 125.27, 124.21, 121.36, 121.22, 121.05, 56.51, 28.80, 25.36.

6.2.4. X–ray crystallography. Single crystals of complexes were mounted on a SuperNova diffractometer (Agilent) (**1**) with a CCD detector and Cu–K_α radiation and Bruker Smart Apex II diffractometer (**2** and **3**) equipped with a graphite monochromator and a Mo Kα radiator (λ) 0.71073 Å. Crystallographic data and details of refinement are given in **Table 6.1**. The unit cell dimensions and intensity data were measured at 100(2) K for **1** and 297(2) K for **2** and **3**. The intensity data were corrected for Lorentz, polarization and absorption effects. Absorption corrections were applied using SADABS[25] and the structures were solved by direct methods using the program SHELXS–97[26] and refined using least squares with the SHELXL–97[26] software program. Hydrogens were either found or placed in calculated positions and isotropically refined using a riding model. The non–hydrogen atoms were refined anisotropically.

Table 6.1. Crystal and refinement data of complexes [{ZnL^1(DMSO)}$_2$]·3DMSO (1), [{ZnL^{2}Cl}$_2$] (2) and [(Zn$_2$L^3)$_2$(μ–OAc)$_2$(μ$_3$–O)$_2$] (3)

Compound	**1**	**2**	**3**
Formula	$C_{48}H_{60}N_6O_9S_7Zn_2$	$C_{40}H_{34}Cl_2N_8O_2S_2Zn_2$	$C_{34}H_{30}Cl_2N_6O_{10}S_2Zn_4$
M	1220.29	924.51	1079.14
Crystal system	monoclinic	triclinic	triclinic
Space group	*P* 2$_1$/*c*	*P* ī	*P* ī
a(Å)	14.477 (6)	11.969(9)	12.225(2)
b(Å)	15.959(7)	13.427(10)	12.823(2)
c(Å)	23.632(8)	14.197(11)	13.848(2)
α (°)	90.00	75.202(5)	70.957(10)
β (°)	97.8659(3)	65.407(4)	80.706(10)
γ (°)	90.00	83.354(5)	80.579(10)
V(Å^3)	5408.76(4)	2006.0(3)	2011.05(6)
Z	4	2	2
D_{calc}(g.cm^{-3})	1.499	1.531	1.782
F(000)	2536	944	1084
μ(Mo–Kα)(mm^{-1})	4.104	1.480	2.657
2θ(max)(^{o})	71.98	20.90	22.03
Reflections collected / unique	10657 / 9711	56236 / 4233	57117 / 4932
R_1[I>2σ(I)]	R1 = 0.0461 wR2 = 0.137	R1 = 0.0361, wR2 = 0.078	R1 = 0.0414, wR2 = 0.090
wR_2[all data]	R1 = 0.049 wR2 =0.142	R1 = 0.059, wR2 = 0.088	R1 = 0.086, wR2 = 0.1068
S[goodness of fit]	1.100	1.002	1.007
max. / min. res. (e.Å^{-3})	1.404 and –0.842	0.387 and –0.341	0.402 and –0.408

6.3. RESULTS AND DISCUSSION

6.3.1. Synthesis. Reaction of $Zn(OAc)_2{\cdot}2H_2O$ (**1** & **3**) or $ZnCl_2$ (**2**) with 4–(*p*–methoxyphenyl)thiosemicarbazone of *o*–hydroxynapthaldehyde (H_2L^1), 4–(*p*–methoxyphenyl)thiosemicarbazone of benzoyl pyridine (HL^2) and 4–(*p*–chlorophenyl)thiosemicarbazone of *o*–vanillin (H_2L^3) in equimolar ratio in ethanol medium yielded light yellow coloured dimeric complexes $[\{ZnL^1(DMSO)\}_2]{\cdot}3DMSO$ (**1**), $[\{ZnL^2Cl\}_2]$ (**2**) and tetrameric complex $[(Zn_2L^3)_2(\mu\text{–}OAc)_2(\mu_3\text{–}O)_2]$ (**3**). NMR spectra were consistent with the X–ray structures. The purity of these compounds was further confirmed by elemental analyses. The synthetic methods of all the complexes are illustrated in **Scheme 6.1**. All the complexes were soluble in MeOH, MeCN, DMF and DMSO, and were stable in both solid and solution phases.

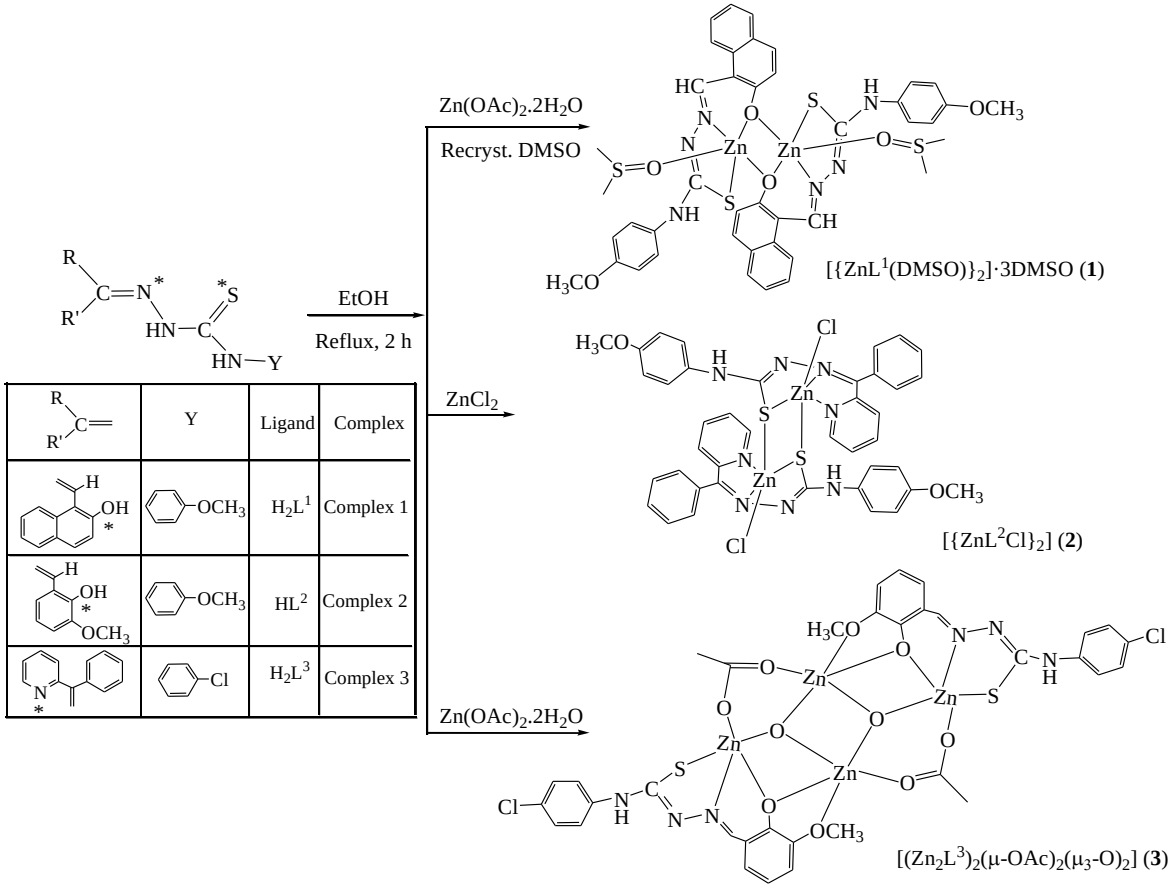

R, R'	Y	Ligand	Complex
	$-OCH_3$	H_2L^1	Complex 1
	$-OCH_3$	HL^2	Complex 2
	$-Cl$	H_2L^3	Complex 3

Scheme 6.1. Schematic representation of ligands $H_{1–2}L^{1–3}$ and synthetic pathways of their corresponding Zn(II) complexes $[\{ZnL^1(DMSO)\}_2]{\cdot}3DMSO$ (**1**), $[\{ZnL^2Cl\}_2]$ (**2**) and $[(Zn_2L^3)_2(\mu\text{–}OAc)_2(\mu_3\text{–}O)_2]$ (**3**).

6.3.2. Structure. The observed elemental analysis (C, H, N) data of all the complexes (**1**–**3**) are consistent with their composition. In order to authenticate the molecular structure of the complexes, the molecular structures have been determined by X–ray crystallography.

6.3.2.1. Description of X–ray structure of [{ZnL^1(DMSO)}$_2$]·3DMSO (1). The structure of the binuclear Zn(II) complex [{ZnL^1(DMSO)}$_2$]·3DMSO is illustrated in **Figure 6.1** and selected bond parameters are collected in **Table 6.2(a)**. Compound **1** contains three DMSO molecules as solvent of crystallization. The structure contains two identical units of ZnL^1(DMSO). In other words, the dimeric Zn(II) species is formed by the dimerisation of two ZnL^1(DMSO) units bridged by two reciprocal coordinated phenolate oxygen atom of the individual ZnL^1(DMSO) unit. Each zinc atom is coordinated by phenolate oxygen O(1)/O(4), imine nitrogen N(3)/N(6) and thiolate sulfur S(1)/S(3) of the thiosemicarbazone moiety and O(3)/O(6) of DMSO group. The length of metal coordinated bonds (Zn(1)−S(1)/S(3) and Zn(1)−N(3)/N(6)) is usual like similar systems reported earlier.[27] The bond angles are also in conformity with a distorted square pyramidal structure around the zinc centers. The phenolate oxygen O(1), the imine nitrogen N(3), and the thiolate sulfur S(1) atom, along with bridging oxygen O(4), constitute the basal plane and O(3) of DMSO in the axial position around the Zn(1) center. Similar orientation was observed for Zn(2) center also. The bond lengths in the basal plane agree with those found in Zn(II) complexes containing thiosemicarbazones as binegative tridentate ligand.[27]

Table 6.2(a). Selected geometric parameters (Å, º) for [{ZnL[1](DMSO)}$_2$]·3DMSO (1)

Bond Distances			
Zn(1)–S(1)	2.337(6)	Zn(1)–O(3)	2.039(2)
Zn(1)–N(3)	2.077(2)	Zn(1)–O(4)	2.072(2)
Zn(1)–O(1)	2.040(2)		
Bond Angles			
O(3)–Zn(1)–O(1)	102.08(7)	O(4)–Zn(1)–N(3)	148.68(7)
O(3)–Zn(1)–O(4)	96.37(7)	O(3)–Zn(1)–S(1)	105.00(5)
O(1)–Zn(1)–O(4)	75.81(6)	O(1)–Zn(1)–S(1)	152.88(5)
O(3)–Zn(1)–N(3)	111.83(7)	O(4)–Zn(1)–S(1)	102.50(5)
O(1)–Zn(1)–N(3)	84.89(7)	N(3)–Zn(1)–S(1)	83.68(5)

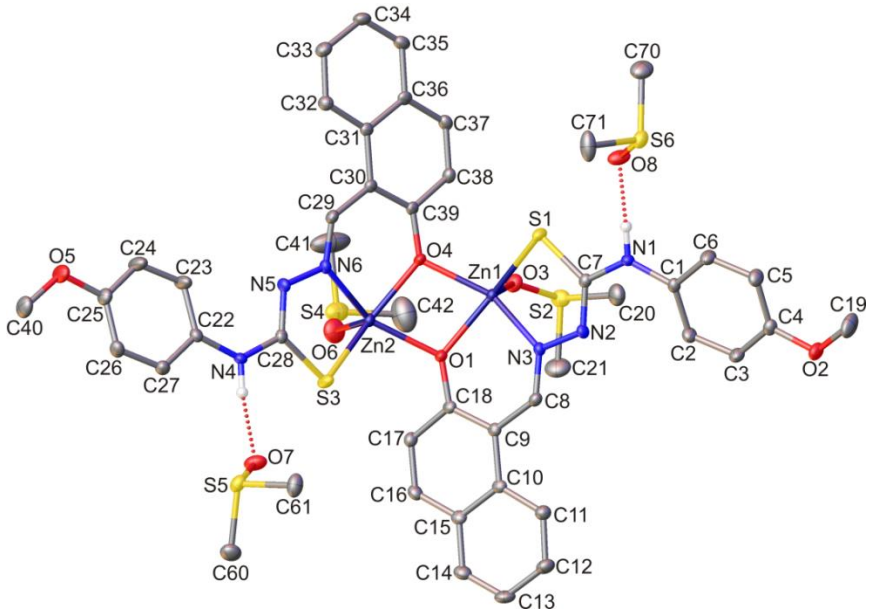

Figure 6.1. ORTEP diagram of [{ZnL[1](DMSO)}$_2$]·3DMSO (**1**) with atom labeling scheme.

6.3.2.2. Description of X–ray structures of [{ZnL^{2}Cl}$_2$] (2). The structure of the binuclear Zn(II) complex [{ZnL^{2}Cl}$_2$] is illustrated in **Figure 6.2** and selected bond parameters are collected in **Table 6.2(b)**. The structure contains two identical units of ZnL^{2}Cl. In other words, the dimeric Zn(II) species is formed by the dimerisation of two ZnL^{2}Cl units bridged by two reciprocal coordinated thiolate sulfur atoms of the individual ligand unit. Each zinc atom is coordinated by a pyridyl nitrogen N(4)/N(8), imine nitrogen N(3)/N(7) and thiolate sulfur S(1)/S(2) of the thiosemicarbazone moiety and a chlorine atom Cl(1)/Cl(2). The length of metal coordinated bonds (Zn(1)−S(1)/S(2) and Zn(1)−N(3)/N(7)) is usual like similar systems reported earlier.[27] The bond angles are also in conformity with a distorted square pyramidal structure around the zinc centers. The pyridyl nitrogen N(4), the imine nitrogen N(3), and the thiolate sulfur S(1) atom, together with chlorine Cl(1) atom, constitute the basal plane around Zn(1), and the bridging thiolate sulfur S(2) in the axial position. The coordination around Zn(2) is similar to Zn(1).

Table 6.2(b). Selected geometric parameters (Å, º) for [{ZnL^{2}Cl}$_2$] (2)

Bond Distances			
Zn(1)–N(3)	2.123(4)	Zn(1)–N(4)	2.135(4)
Zn(1)–Cl(1)	2.222(2)	Zn(1)–S(1)	2.477(1)
Zn(1)–S(2)	2.488(2)		
Bond Angles			
N(3)–Zn(1)–N(4)	75.27(2)	N(3)–Zn(1)–Cl(1)	145.66(1)
N(4)–Zn(1)–Cl(1)	100.35(1)	N(3)–Zn(1)–S(1)	78.31(1)
N(4)–Zn(1)–S(1)	153.58(1)	Cl(1)–Zn(1)–S(1)	101.32(6)
N(3)–Zn(1)–S(2)	108.12(1)	N(4)–Zn(1)–S(2)	95.12(1)
Cl(1)–Zn(1)–S(2)	106.19(7)	S(1)–Zn(1)–S(2)	93.17(5)

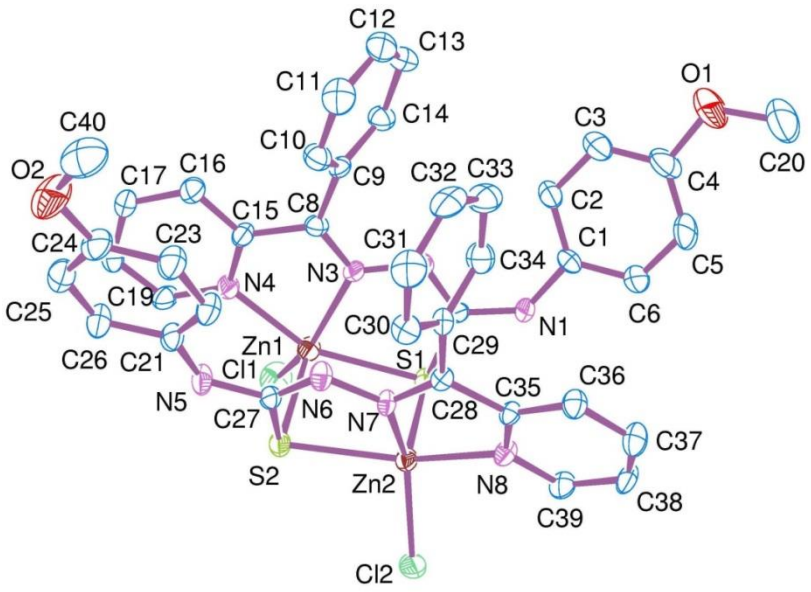

Figure 6.2. ORTEP diagram of [{ZnL^2Cl}$_2$] (**2**) with atom labeling scheme.

6.3.2.3. Description of X–ray structures of [$(Zn_2L^3)_2(\mu$–OAc$)_2(\mu_3$–O$)_2$] (3). The structure of the tetranuclear Zn(II) complex [$(Zn_2L^3)_2(\mu$–OAc$)_2(\mu_3$–O$)_2$] is illustrated in **Figure 6.3** and selected bond parameters are collected in **Table 6.2(c)**. The molecular structure of **3**, a centrosymmetric zinc tetramer, consists of two [$(Zn_2L^3)(\mu$–OAc$)(\mu_3$–O)] dimeric units, is built up by two chelating bidentate dianionic ligands (H_2L^3), two three–coordinate oxygen (μ_3–O) atoms and two bridging bidentate (ethoxide) chelators. Like complex **1** the ligands are coordinated to Zn center by phenolate oxygen of ligand O(1)/O(3), imine nitrogen N(3)/N(6) and thiolate sulfur S(1)/S(2) of the thiosemicarbazone moiety. The coordination geometry of Zn(1) is distorted square pyramidal formed by two oxygen atoms (one μ_3–O(10) and one phenolate O(1) atom from the ligand), imine nitrogen N(3) and thiolate sulfur S(1) of the ligands in the basal plane and one O(5) atom of the bridging acetate in the apical site. The coordination geometry of Zn(2) is also a distorted square pyramidal but it is formed by four oxygen atoms in the basal plane (one μ_3–O(10), one phenolate O(1) atom from the ligand, one O(8) atom of the bridging acetate and a methoxide O(2)–atom of the ligand) and one three coordinate oxygen μ_3–O(7) atom is in the apical site. Similar coordination is observed for Zn(3) and Zn(4) also. The length of all the metal coordinated bonds is usual like similar systems reported earlier.[27] The bond angles are also in conformity with a distorted square pyramidal structure around the zinc centers.[27]

Table 6.2(c). Selected geometric parameters (Å, º) for $[(Zn_2L^3)_2(\mu\text{–}OAc)_2(\mu_3\text{–}O)_2]$ (3)

Bond Distances			
Zn(1)–O(1)	2.016(4)	Zn(1)–O(5)	2.077(5)
Zn(1)–N(3)	2.081(5)	Zn(1)–O(10)	2.101(4)
Zn(1)–S(1)	2.289(2)	Zn(2)–O(8)	1.919(5)
Zn(2)–O(1)	1.923(4)	Zn(2)–O(7)	1.957(4)
Zn(2)–O(10)	2.200(4)	Zn(2)–O(2)	2.247(5)
Bond Angles			
O(1)–Zn(1)–O(5)	96.90(2)	O(1)–Zn(1)–N(3)	85.02(2)
O(5)–Zn(1)–N(3)	104.17(2)	O(1)–Zn(1)–O(10)	79.20(2)
O(5)–Zn(1)–O(10)	96.90(2)	N(3)–Zn(1)–O(10)	155.02(2)
O(1)–Zn(1)–S(1)	153.81(1)	O(5)–Zn(1)–S(1)	108.96(1)
N(3)–Zn(1)–S(1)	84.74(2)	O(10)–Zn(1)–S(1)	101.11(1)
O(8)–Zn(2)–O(1)	130.40(2)	O(8)–Zn(2)–O(7)	114.74(2)
O(1)–Zn(2)–O(7)	114.79(2)	O(8)–Zn(2)–O(10)	107.10(2)
O(1)–Zn(2)–O(10)	78.78(2)	O(7)–Zn(2)–O(10)	85.17(2)
O(8)–Zn(2)–O(2)	94.90(2)	O(1)–Zn(2)–O(2)	76.24(2)
O(7)–Zn(2)–O(2)	98.42(2)	O(10)–Zn(2)–O(2)	153.88(2)

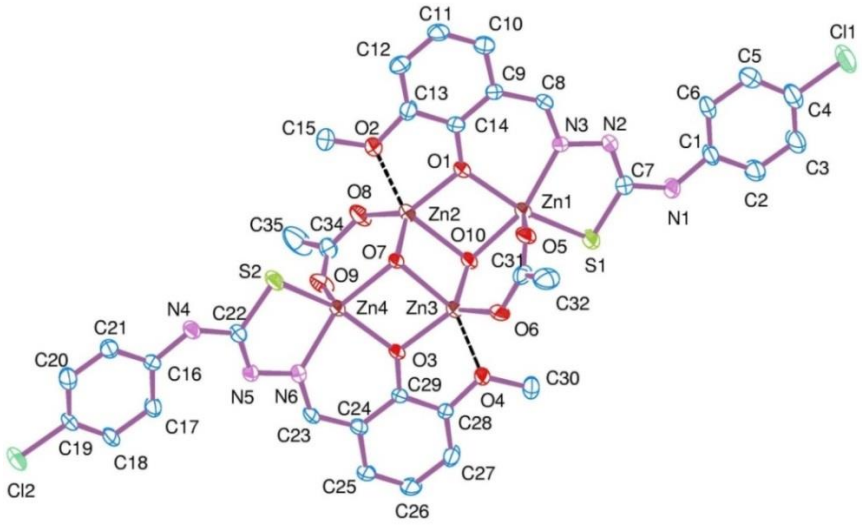

Figure 6.3. ORTEP diagram of $[(Zn_2L^3)_2(\mu\text{–}OAc)_2(\mu_3\text{–}O)_2]$ (**3**) with atom labeling scheme.

6.3.3. Spectral characteristics

6.3.3.1. IR spectroscopy. The IR spectra of all the complexes (**1**–**3**) showed the presence of *ν*(N–H) band in the range 3318–3024 cm^{-1} for –N(1)–H. The *ν*(C–H) band for **1** & **3** appeared in the range 2863–2761 cm^{-1} for –C(8)–H stretching. The peaks for ν(C=N) and ν(C=C) vibrational modes appeared in the range 1595–1503 cm^{-1}, while the thioamide bands ν(C–S) appeared in the range 810–743 cm^{-1} (compared to free ligands, 839–815 cm^{-1}).[22f] The detailed IR data has been included in the experimental section. The representative IR spectra of complex $[\{ZnL^2Cl\}_2]\cdot 3DMSO$ (**2**) is shown in **Figure 6.4**.

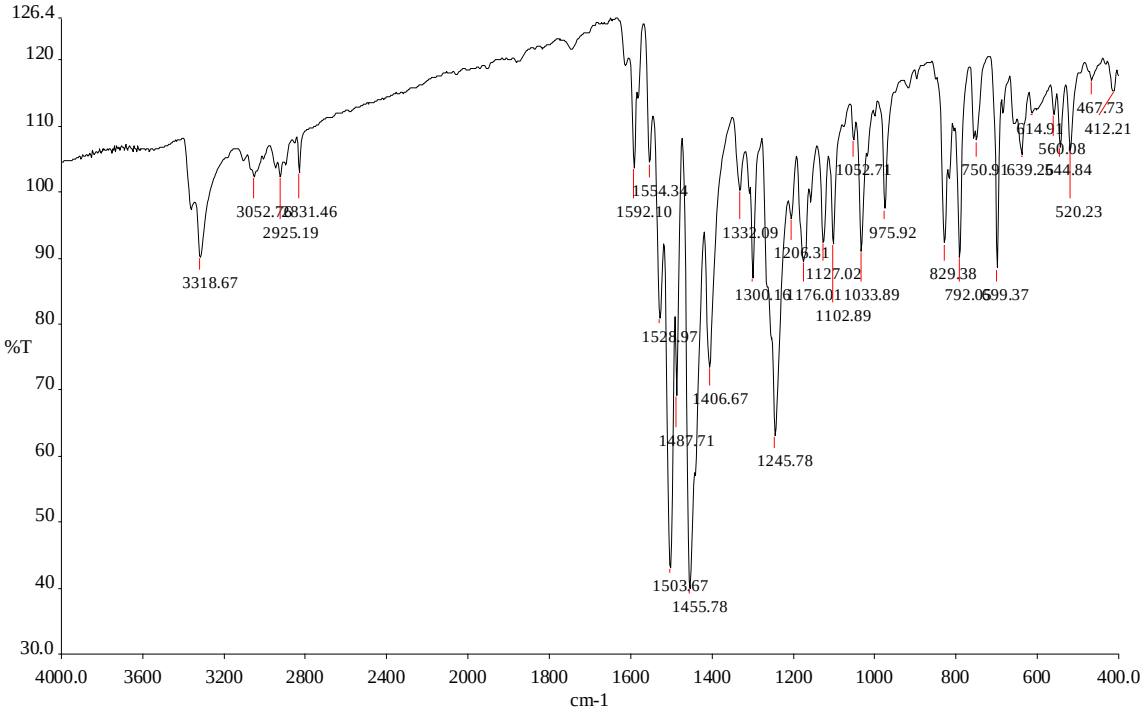

Figure 6.4. IR spectra of $[\{ZnL^2Cl\}_2]\cdot 3DMSO$ (**2**).

6.3.3.2. UV spectroscopy. The electronic spectra of all the complexes (**Table 6.3**) were recorded in methanol solutions. In the spectra of **1**–**3** three strong absorptions are observed in the wavelength range 453–255 nm. The lower energy absorptions at around 453–422 nm are ascribable to metal to ligand charge transfer transitions whereas the higher energy absorptions are likely to be due to ligand centered transitions.[28] The representative electronic absorption spectra of $[\{ZnL^2Cl\}_2]$ (**2**) is shown in **Figure 6.5**.

Table 6.3. Electronic spectra for complexes $[\{ZnL^1(DMSO)\}_2]\cdot 3DMSO$ (1), $[\{ZnL^2Cl\}_2]$ (2) and $[(Zn_2L^3)_2(\mu\text{–}OAc)_2(\mu_3\text{–}O)_2]$ (3) in CH_3OH

Complex	λ_{max}/nm (ε/dm^{3}mol^{-1} cm^{-1})
$[\{ZnL^1(DMSO)\}_2]\cdot 3DMSO$ (**1**)	268(41042), 333(26629), 422(33670)
$[\{ZnL^2Cl\}_2]$ (**2**)	265(16388), 338(12425), 425(6666)
$[(Zn_2L^3)_2(\mu\text{–}OAc)_2(\mu_3\text{–}O)_2]$ (**3**)	255(12022), 310(18411), 357(10943), 453(9770)

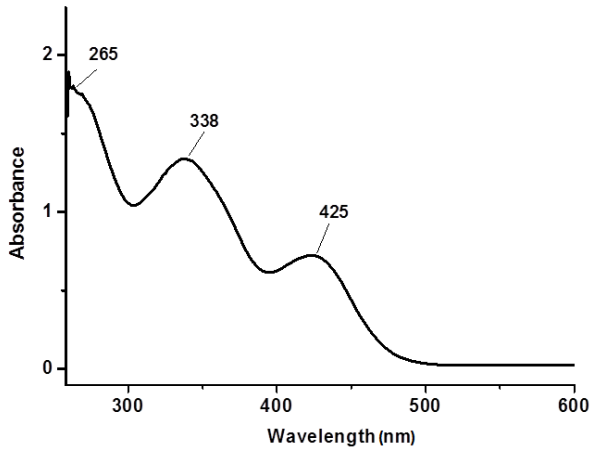

Figure 6.5. Electronic spectra of $[\{ZnL^2Cl\}_2]$ (**2**).

6.3.3.3. NMR spectroscopy. The NMR spectra (^{1}H and ^{13}C) of all the complexes and ligands were recorded in DMSO–d_6. The ^{1}H NMR spectrum of all the complexes (**1**–**3)** exhibits one singlet in the range 9.54–8.92 ppm due to NH (–C(7)–N(1)H), and one singlet in the range 8.63–8.43 ppm due to CH (–N(3)=C(8)H) for **1** & **3**. Signals for aromatic protons found as multiplets in 8.06–6.35 ppm range.[22f] The detailed NMR data has been included in the experimental section. The representative ^{1}H NMR spectra of ligand H_2L^3 and its corresponding Zn complex $[(Zn_2L^3)_2(\mu\text{–}OAc)_2(\mu_3\text{–}O)_2]$ (**3**) in DMSO–d_6 is shown in **Figures 6.6** and **6.7** respectively.

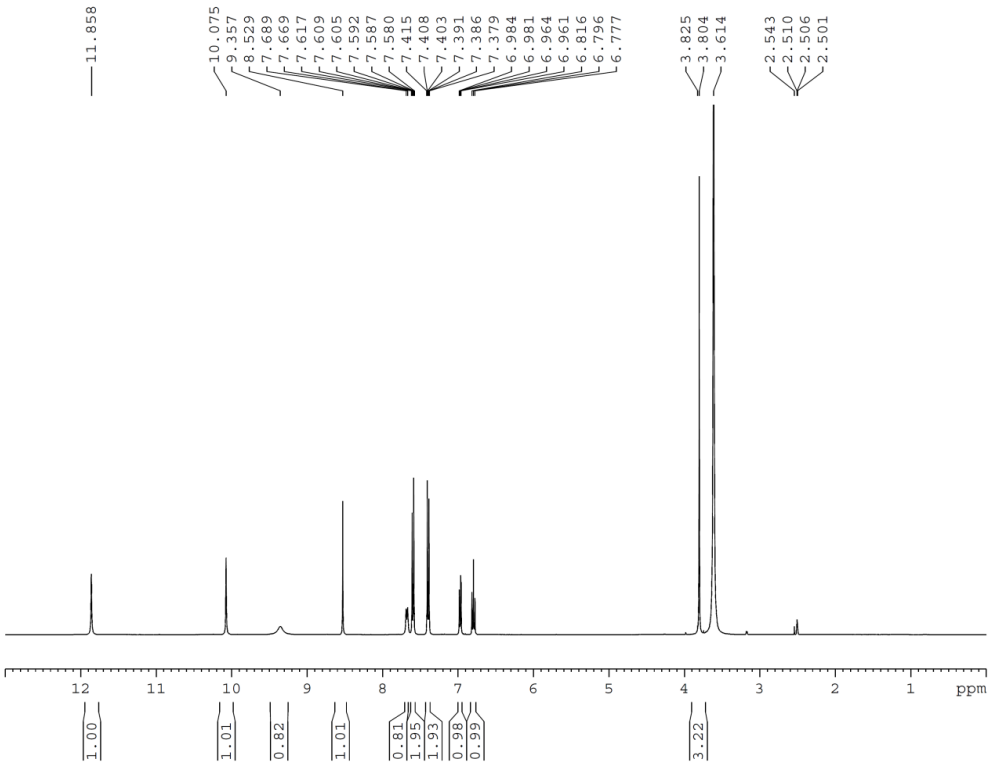

Figure 6.6. NMR spectra of ligand H_2L^3.

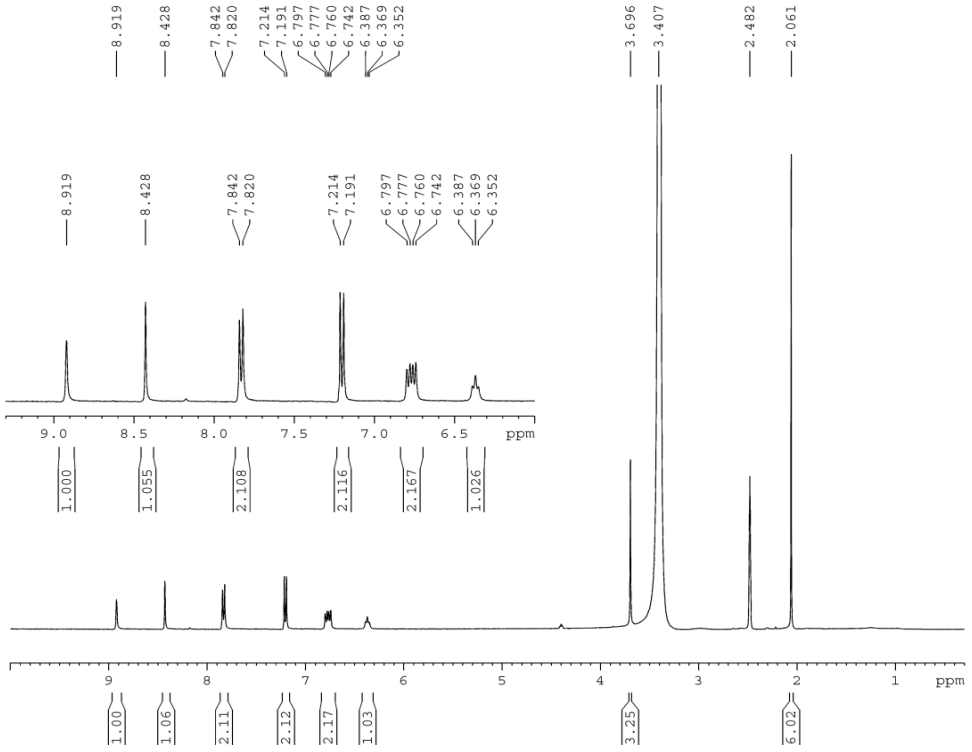

Figure 6.7. NMR spectra of $[(Zn_2L^3)_2(\mu\text{–}OAc)_2(\mu_3\text{–}O)_2]$ (**3**).

6.4. CONCLUSION

The syntheses and characterization of three new TSC ligands and their corresponding Zn(II) complexes $[\{ZnL^1(DMSO)\}_2]\cdot 3DMSO$ (**1**), $[\{ZnL^2Cl\}_2]$ (**2**) and $[(Zn_2L^3)_2(\mu\text{–}OAc)_2(\mu_3\text{–}O)_2]$ (**3**) have been reported. The synthesized ligands and the complexes were characterized by elemental analysis, NMR, IR and UV–Vis spectroscopy. Molecular structures of all the Zn(II) complexes (**1**–**3**) have been determined by single crystal X–ray crystallography. The spectroscopic data are in accordance with the X–ray structures. The physical and structural characteristics of the complexes suggest that they may be considered as functional model of phosphatase enzyme. Considering the future scope of work, the study of reactivity as biomimetic phosphate hydrolysis catalyst is under progress.

6.5. REFERENCES

(1) (a) Buchholz, R. R.; Etienne, M. E.; Dorgelo, A.; Mirams, R. E.; Smith, S. J.; Chow, S. Y.; Hanton, L. R.; Jameson, G. B.; Schenk, G.; Gahan, L. R. *Dalton Trans.* **2008**, 6045. (b) Chen, J.; Wang, X.; Zhu, Y.; Lin, J.; Yang, X.; Li, Y.; Lu, Y.; Guo, Z. *Inorg. Chem*. **2005**, *44*, 3422. (c) Wilcox, D. E. *Chem. Re*v. **1996**, *96*, 2435. (d) Horton, N. C.; Perona, J. J. *Nat. Struct. Biol*. **2001**, *8*, 290.

(2) Kimura, E.; Koike, T. *Adv. Inorg. Chem*. **1997**, *44*, 229.

(3) (a) Boening, D.W. *Chemosphere* **2000**, *40*, 1335. (b) Benoit, J. M.; Fitzgerald, W. F.; Damman, A. W. *Environ. Res*. **1998**, *78*, 118. (c) Clarkson, T. W.; Magos, L.; Myers, G. J.; *N. Engl. J. Med*. **2003**, *349*, 1731. (d) Burg, R. V. *J. Appl. Toxicol*. **1995**, *15*, 483. (e) Nolan, E. M.; Lippard, S. J. *Chem. Rev*. **2008**, *108*, 3443. (f) Hayes, A. W. *Principles and Methods of Toxicology* Philadelphia: CRC Press. **2007**, pp. 858.

(4) Kimura, E. *Pure Appl. Chem*. **1993**, *65*, 355.

(5) Kontogiorgis, C. A.; Papaioannou, P.; Hadjipavlou–Litina, D. J. *Curr. Med. Chem*. **2005**, *12*, 339.

(6) Scozzafava, A.; Supuran, C. J. *J. Med. Chem*. **2000**, *43*, 3677.

(7) Rubino, M. T.; Agamennone, M.; Campestre, C.; Fracchiolla, G.; Laghezza, A.; Loiodice, F.; Nuti, E.; Rossello, A.; Tortorella, P. *Chem. Med. Chem*. **2009**, *4*, 352.

(8) Chiu, Y. H.; Gabriel, G. J.; Canary, J. W. *Inorg. Chem.* **2005**, *44*, 40.

(9) Miller, T. A.; Witter, D. J.; Belvedere, S. J. *J. Med. Chem*. **2003**, *46*, 5097.

(10) Hase, C. C.; Finkelstein, R. A. *Microbiol. Mol. Biol. Rev*. **1993**, *57*, 823.

(11) Maret, W. *BioMetals* **2001**, *14*, 187.

(12) Walkup, G. K.; Burdette, S. C.; Lippard, S. J.; Tsien, R. Y. *J. Am. Chem. Soc*. **2000**, *122*, 5644.

(13) Hellmich, H. L.; Frederickson, C. J.; DeWitt, D. S.; Saban, R.; Parsley, M. O.; Stephenson, R.; Velasco, M.; Uchida, T.; Shimamura, M.; Prough, D. S. *Neurosci. Lett.* **2004**, *355*, 221.

(14) Demertzi, D. K.; Alexandratos, A.; Papageorgiou, A.; Yadav, P. N.; Dalezis, P.; Demertzis, M. A. *Polyhedron* **2008**, *27*, 2731.

(15) West, D. X.; Padhye, S. B.; Sonawane, P. B. *Struct. Bonding* **1991**, *76*, 1.

(16) Casas, J. S.; García-Tasende, M. S.; Sordo, J. *Coord. Chem. Rev.* **2000**, *209*, 197.

(17) Lobana, T. S.; Sharma, R.; Bawa, G.; Khanna, S. *Coord. Chem. Rev.* **2009**, *253*, 977.

(18) Iakovidou, Z.; Mioglou, E.; Mourelatos, D.; Kotsis, A.; Demertzis, M. A.; Papagoergiou, A.; Miller, J. R.; Demertzi, D. K. *Anticancer Drugs* **2001**, *12*, 65.

(19) Demertzi, D. K.; Demertzis, M. A.; Miller, J. R.; Papadopoulou, C.; Dodorou, C.; Filousis, G. *J. Inorg. Biochem*. **2001**, *86*, 555.

(20) Peariso, K.; Goulding, C. W.; Huang, S.; Matthews, R. G.; Penner–Hahn, J. E. *J. Am. Chem. Soc.* **1998**, *120*, 8410.

(21) Seena, E. B.; Kurup, M. R. P. *Spectrochim. Acta A* **2008**, *69*, 726.

(22) (a) Dash, S. P.; Pasayat, S.; Saswati; Dash, H. R.; Das, S.; Butcher, R. J.; Dinda, R. *Polyhedron* **2012**, *31*, 524. (b) Pasayat, S.; Dash, S. P.; Saswati; Majhi, P. K.; Patil, Y. P.; Nethaji, M.; Dash, H. R.; Das, S.; Dinda, R. *Polyhedron* **2012**, *38*, 198. (c) Saswati; Dinda, R.; Schmiesing, C. S.; Sinn, E.; Patil, Y. P.; Nethaji, M.; Stoeckli–Evans, H.; Acharyya, R. *Polyhedron* **2013**, *50*, 354. (d) Dash, S. P.; Pasayat, S.; Bhakat, S.; Roy, S.; Dinda, R.; Tiekink, E. R. T.; Mukhopadhyay, S.; Bhutia, S. K.; Hardikar, M. R.; Joshi, B. N.; Patil, Y. P; Nethaji, M. *Inorg. Chem.* **2013**, *52*, 14096. (e) Dash, S. P.; Panda, A. K.; Pasayat, S.; Dinda, R.; Biswas, A.; Tiekink, E. R. T.; Patil, Y. P.; Nethaji, M.; Kaminsky, W.; Mukhopadhyay, S.; Bhutia, S. K. *Dalton Trans.* **2014**, *43*, 10139. (f) Saswati; Chakraborty, A.; Dash, S. P.; Panda, A. K.; Acharyya, R.; Biswas, A.; Mukhopadhyay, S.; Bhutia, S. K.; Crochet, A.; Patil, Y. P.; Nethaji, M.; Dinda, R. *Dalton Trans*. **2015**, *44*, 6140. (g) Pasayat, S.; Dash, S. P.; Roy, S.; Dinda, R.; Dhaka, S.; Maurya, M. R.; Kaminsky, W.; Patil, Y. P.; Nethaji, M. *Polyhedron* **2014**, *67*, 1.

(23) Part 1: Ghosh, S.; Purohit, S. *Indian J. Chem., Sect. A: Inorg., Bio–inorg., Phys., Theor. Anal. Chem.* **1987**, *26A*, 131.

(24) Lobana, T. S.; Rekha; Butcher, R. J.; Castineiras, A.; Bermejo, E.; Bharatam, P. V. *Inorg. Chem.* **2006**, *45*, 1535.

(25) Bruker, *SADABS, SAINT, SHELXTL and SMART*, Bruker AXS Inc., Madison, Wisconsin, SA, **2003**.

(26) Sheldrick, G. M. *Acta Crystallogr., Sect. A: Found. Crystallogr.* **2008**, *64*, 112.

(27) Li, Y.; Yang, Z. Y.; Wu, J. C. *Eur. J. Med. Chem.* **2010**, *45*, 5692.

(28) Latheef, L.; Manoj, E.; Kurup, M. R. P. *Polyhedron* **2007**, *26*, 4107.

A Brief Resume of the Work Embodied in this Dissertation and Concluding Remark

A Brief Resume of the Work Embodied in this Dissertation and Concluding Remark

The aim of this dissertation was to explore in depth certain aspects of the chemistry of a series of variable valence transition metal (Ni, Cu, Mo, V & Zn) complexes of some selected tridentate ONS, NNS and monodentate S donor thiosemicabazone (TSC) ligands. Major emphasis was given to the structural and spectroscopic characterization of the synthesized complexes as well as their study of chemical, electrochemical, pharmacological and catalytic activities. Work described in **chapter 2-6** reveals the results of the attempts taken to fulfill all the objectives. The following chapter-wise summary of the work presented in this dissertation reveals the extent to which the above-mentioned objectives are fulfilled.

Chapter 2 deals with the syntheses and characterization of some mixed-ligand nickel(II) complexes {[Ni(L^1)(PPh_3)] (**1**); [Ni(L^1)(Py)] (**2**); [Ni(L^2)(PPh_3)]·DMSO (**3**); [Ni(L^2)(Imz)] (**4**), [Ni(L^3)(4–pic)] (**5**) and [{Ni(L^3)}$_2$(μ–4,4′–byp)]·2DMSO (**6**)} of the selected three thiosemicarbazones {4–(*p*–X–phenyl)thiosemicarbazone of salicylaldehyde} ($H_2L^{1–3}$), differing in the inductive effect of the substituent X (X = F, Br and OCH_3), in order to observe their influence, if any, on the redox potentials and biological activity of the complexes. All the synthesized ligands and the metal complexes were successfully characterized by elemental analysis, IR, UV–Vis, NMR spectroscopy and cyclic voltammetry. Molecular structures of four mononuclear (**1**–**3** and **5**) and one dinuclear (**6**) Ni(II) complexes have been determined by X–ray crystallography. The complexes have been screened for their antibacterial activity against *Escherichia coli and Bacillus*. Minimum inhibitory concentration of these complexes indicates compound **4** as the potential lead molecule for drug designing.

In ***Chapter 3*** 4–(*p*–X–phenyl)thiosemicarbazone of napthaldehyde {where, X = Cl (HL^1) and X = Br (HL^2)}, thiosemicarbazone of quinoline–2–carbaldehyde (HL^3) and 4–(*p*–fluorophenyl)thiosemicarbazone of salicylaldehyde (H_2L^4) and their copper(I), {[Cu(HL^1)(PPh_3)$_2$Br]·CH_3CN (**1**) and [Cu(HL^2)(PPh_3)$_2$Cl]·DMSO (**2**)} and copper(II), {[($Cu_2L^3{}_2Cl$)$_2$(μ–Cl)$_2$]·2H_2O (**3**) and [Cu(L^4)(Py)] (**4**)} complexes are reported. The synthesized ligands and their copper complexes were successfully characterized by elemental analysis, cyclic voltammetry, NMR, ESI–MS, IR and UV–Vis spectroscopy. Molecular structures of all the Cu(I) and Cu(II) complexes have been determined by X–ray crystallography. All the complexes (**1**–**4**) were tested for their ability to exhibit DNA binding and cleavage activity. The complexes

effectively interact with CT–DNA possibly by groove binding mode, with binding constants ranging from $10^4 - 10^5$ M^{-1}. Among the complexes, **3** show highest chemical (60%) as well as photo-induced (80%) DNA cleavage activity against pUC19 DNA. Finally, the *in vitro* antiproliferative activity of all the complexes were assayed against the HeLa cell line. Some of the complexes proved to be as active as the clinically referred drugs, and the greater potency of **3** may be correlated with its aqueous solubility and the presence of quinonoidal group in the thiosemicarbazone ligand coordinated to the metal.

Chapter 4 describes oxygen atom transfer (OAT) reactivity of dioxidomolybdenum(VI) complexes $[Mo^{(VI)}O_2L^{1-6}]$ (**1**–**6**) {4–(*p*–bromophenyl)thiosemicarbazone of salicylaldehyde (H_2L^1), 4–(*p*–X–phenyl)thiosemicarbazone of *o*–vanillin {where, X = F (H_2L^2) and X = Cl (H_2L^3) and X = OMe (H_2L^4)}, 4–(*p*–bromophenyl)thiosemicarbazone of 5–bromosalicylaldehyde (H_2L^5), and 4–(*p*–chlorophenyl)thiosemicarbazone of *o*–hydroxynaphthaldehyde (H_2L^6)} with PPh_3. The OAT reactions proceed through the formation of $OPPh_3$, which have been characterized by ^{31}P NMR. Dioxidomolybdenum(VI) complexes $[Mo^{(VI)}O_2L^{1/5/6}(DMSO)]$ (**1a, 5a** & **6a**), $[Mo^{(VI)}O_2L^{2/4}(H_2O)]$ (**2a** & **4a**), and $[Mo^{(VI)}O_2L^3(DMSO)]_4 \cdot 2DMSO$ (**3a**) and monooxidomolybdenum(IV) complexes $[Mo^{(IV)}OL^{1-6}(N–N)]$ (**7**–**12**) {where, N–N = 2,2'–bipyridyl or 1,10–phenanthroline} are reported as the product of substrate binding and oxygen atom transfer reactivity of dioxidomolybdenum(VI) complexes $[Mo^{(VI)}O_2L^{1-6}]$ (**1**–**6**) respectively. All the complexes have been spectroscopically characterized. Molecular structures of some of the Mo(VI) (**1a**–**4a**) and Mo(IV) complexes (**7** and **9**–**11**) have been determined by single crystal X–ray crystallography. The catalytic activity of $Mo^{(VI)}$ complexes (**1a**–**6a**) have also been studied.

In ***chapter 5*** the synthesis and characterization of an oxidovanadium(IV) $[V^{IV}O(L)(acac)]$ (**1**) and two dioxidovanadium(V) $[V^VO_2(L')]$ (**2**) and $[V^VO_2(L)]$ (**2a**) complexes of {(4–(*p*–fluorophenyl)thiosemicarbazone) of pyridine–2–aldehyde} (HL) is described in the. The oxidovanadium(IV) species $[V^{IV}O(L)(acac)]$ (**1**) was synthesized in usual way by the reaction of metal precursor $VO(acac)_2$ with thiosemicarbazone ligand (HL) in refluxing ethanol. The recrystallization of $[V^{IV}O(L)(acac)]$ (**1**) in DMF, CH_3CN or EtOH gave the same product *i.e.* dioxidovanadium(V) complex $[V^VO_2(L)]$ (**2a**), whereas $[V^VO_2(L')]$ (**2**) was synthesized during recrystallization of $[V^{IV}O(L)(acac)]$ (**1**) in DMSO where the original ligand (HL) is transformed

to a rearranged new ligand (HL'). The ligand in complex **1** is found to undergo methylation at the carbon centre attached to imine nitrogen in presence of DMSO and transformed to the corresponding dioxidovanadium(V) species through *in situ* reaction. The synthesized ligand and the metal complexes were characterized by elemental analysis, IR, UV–Vis, NMR and EPR spectroscopy. Molecular structures of complex **1** [$V^{IV}O(L)(acac)$] and complex **2** [$V^{V}O_2(L')$] have been determined by single crystal X–ray crystallography. Complexes **1** & **2** show *in vitro* insulin mimetic activity against insulin responsive L6 myoblast cells, with complex **1** being more potent, is comparable to insulin at 100 μM concentration, while complex **2** has considerable insulin mimetic activity. In addition, the *in vitro* antiproliferative activity of the complexes **1** & **2** against the MCF–7 and Vero cell lines were also assayed.

In ***chapter 6*** 4–(*p*–methoxyphenyl)thiosemicarbazone of *o*–hydroxynapthaldehyde (H_2L^1), 4–(*p*–methoxyphenyl)thiosemicarbazone of benzoyl pyridine (HL^2) and 4–(*p*–chlorophenyl)thiosemicarbazone of *o*–vanillin (H_2L^3) and their dimeric Zn(II) complexes $[\{ZnL^1(DMSO)\}_2]\cdot 3DMSO$ (**1**), $[\{ZnL^2Cl\}_2]$ (**2**), and a novel tetrameric Zn(II) complex $[(Zn_2L^3)_2(\mu\text{–}OAc)_2(\mu_3\text{–}O)_2]$ (**3**) are reported. The synthesized ligands and their zinc complexes were characterized by elemental analysis, NMR, IR and UV–Vis spectroscopy. Molecular structures of all the complexes (**1**–**3**) have been determined by single crystal X–ray crystallography.

The author is very much aware of the fact that some portions of the work described in the present dissertation left scope for future work especially the phosphoesterase, pharmacological and catalytic studies. All the reported complexes can be used for the study of several other catalytic and bio activities. This dissertation also left scope for further qualitative improvement by the utilization of some relevant instrumental data, which could have been really helpful in arriving at completely unambiguous conclusions. As those instrumental facilities were not available to us, we were rather helpless. However, the above discussion on the entire work presented in **chapter 2-6** reveals that the aims and objectives of the present dissertation are mostly fulfilled.

List of Publications [Published in cited Journals (SCI)]

1) '*Synthesis, X-ray structure and in vitro cytotoxicity studies of Cu(I/II) complexes of thiosemicarbazone: Special emphasis on their interactions with DNA*', **Saswati**; Chakraborty, A.; Dash, S. P.; Panda, A. K.; Acharyya, R.; Biswas, A.; Mukhopadhyay, S.; Bhutia, S. K.; Crochet, A.; Patil, Y. P.; Nethaji M.; Dinda, R. *Dalton Trans*. **2015**, *44*, 6140.

2) '*Highly Stable Hexacoordinated Nonoxidovanadium(IV) Complexes of Sterically Constrained Ligands: Syntheses, Structure and Study of Antiproliferative and Insulin Mimetic Activity*', Dash, S. P.; Pasayat, S.; **Saswati**; Roy, S.; Dinda, R.; Tiekink, E. R. T.; Mukhopadhyay, S.; Bhutia, S. K.; Hardikar, M. R.; Joshi, B. N.; Patil Y. P.; Nethaji, M. *Inorg. Chem*. **2013**, *52*, 14096.

3) '*Mixed-ligand nickel(II) thiosemicarbazone complexes: Synthesis, characterization and biological evaluation*', **Saswati**; Dinda, R.; Schmiesing, C. S.; Sinn, E.; Patil, Y. P.; Nethaji, M.; Stoeckli-Evans, H.; Acharyya, R. *Polyhedron* **2013**, *50*, 354.

4) '*Mixed-ligand aroylhydrazone complexes of molybdenum: Synthesis, structure and biological activity*', Pasayat, S.; Dash, S. P.; **Saswati**; Majhi, P. K.; Patil, Y. P.; Nethaji, M.; Dash, H. R.; Das, S.; Dinda, R. *Polyhedron* **2012**, *31*, 198.

5) '*Oxovanadium(V) complexes incorporating tridentate aroylhydrazoneoximes: Synthesis, characterizations and antibacterial activity*', Dash, S. P.; Pasayat, S.; **Saswati**, Dash, H. R.; Das, S.; Butcher, R. J.; Dinda, R. *Polyhedron* **2012**, *38*, 524.

Bio-data

Saswati

Research Scholar

Department of Chemistry

National Institute of Technology, Rourkela

Rourkela-769008, Odisha, India

Research experience

a. Doctoral Research (July 2010 – Continuing)

Supervisor: Dr. Rupam Dinda, Department of Chemistry, National Institute of Technology Rourkela, Odisha, India.

Research area: Bio-Inorganic Chemistry

Analytical Techniques

Spectroscopy: Acquisition and analysis of ^{1}H, ^{13}C, ^{51}V NMR, ESI-Mass spectra. Recording and interpretation of GC-MS, FT-IR, UV-Vis spectra and cyclic voltammetry. Interpretation of X-ray crystal structure

X-Ray Crystallography Software: MERCURY & ORTEP

Education Profile

2003 Secondary (**10th)**, CBSE Board, Atomic Energy Central School, Jadugoda, Jharkhand, India

2005 Higher Secondary **(+2 Science)**, Atomic Energy Central School, Jadugoda, Jharkhand, India

2008 Graduation (**B.Sc. Hons. in Chemistry)**, S. B. Women's College, Cuttack, Utkal University, Odisha, India.

2010 Post graduation (**M.Sc. in Chemistry)**, Department of Chemistry, National Institute of Technology Rourkela, Odisha, India,

Honors and Fellowship

- Fellowship: CSIR SRF

Personal Profile

- Date of Birth 4^{th} September 1988
- Nationality Indian
- Permanent Address B/1/7 UCIL Housing Colony,
  Turamdih, Sundernagar,
  Jamshedpur, Jharkhand.
  India, 832107